UNIVERSIDADE D
COIMBRA

Pedro Daniel Rosete Bento

MULTILAYER MASSIVE MIMO AT MMWAVE FOR HIGH POWER AND SPECTRAL EFFICIENT COMMUNICATIONS

Tese no âmbito do Doutoramento em Engenharia Electrotécnica e de Computadores – Ramo de Especialização em Telecomunicações orientada pelo Professor Doutor Marco Alexandre Cravo Gomes e co-orientada pelo Professor Doutor Rui Miguel Henriques Dias Morgado Dinis e apresentada ao Departamento de Engenharia Electrotécnica e de Computadores da Faculdade de Ciências e Tecnologia.

Julho de 2019

Faculdade de Ciências e Tecnologia
da Universidade de Coimbra

MULTILAYER MASSIVE MIMO AT MMWAVE FOR HIGH POWER AND SPECTRAL EFFICIENT COMMUNICATIONS

Pedro Daniel Rosete Bento

Tese no âmbito do Doutoramento em Engenharia Electrotécnica e de Computadores – Ramo de Especialização em Telecomunicações orientada pelo Professor Doutor Marco Alexandre Cravo Gomes e co-orientada pelo Professor Doutor Rui Miguel Henriques Dias Morgado Dinis e apresentada ao Departamento de Engenharia Electrotécnica e de Computadores da Faculdade de Ciências e Tecnologia.

Julho de 2019

UNIVERSIDADE D
COIMBRA

This thesis is supported by the European Regional Development Fund (FEDER), through the Competitiveness and Internationalization Operational Program of the Portugal 2020 framework, Regional OP Centro (POCI-01-0145- FEDER-030588), Regional OP Lisboa (Lisboa-01-0145-FEDER-03058) and by FCT/MEC through national funds, under projects MASSIVE5G (SAICT-45-2017-02) and PES3N (2018-SAICT-45-2017-POCI-01-0145-FEDER-030629), by the project UID/EEE/50008/2019 and by the FCT PhD grant SFRH/BD/108522/2015.

À Heloísa e aos meus pais, pelo seu amor e apoio incondicional.

The problem is not the problem. The problem is your attitude about the problem.

- Jack Sparrow

All our dreams can come true, if we have the courage to pursue them.

- Walt Disney

Agradecimentos

Um trabalho como este não se consegue sem esforço, dedicação, querer e sacrifício, mas, principalmente, apoio. Foram muitos os que me ajudaram e a todos gostaria de deixar estas palavras de agradecimento.

Começo por agradecer ao Instituto de Telecomunicações, por me ter acolhido e por todos os meios materiais disponibilizados, e à Fundação para a Ciência e Tecnologia, por ter financiado em parte este trabalho.

Aos meus colegas de laboratório, pelo bom ambiente que sempre houve e disponibilidade que tinham para partilhar momentos de descontração, mas também momentos de discussão muitas vezes importantes para o seguimento dos trabalhos.

Um agradecimento aos Professores Rui Dinis e Vitor Silva pelas suas ideias e espírito crítico na avaliação dos resultados obtidos.

Ao Professor Marco Gomes, por desde sempre ter acreditado em mim e me ter chamado para este trabalho. Pela sua orientação e trabalho incansável. Sem ele teria sido impossível levar este trabalho a um bom porto.

Aos meus pais e à minha família que desde sempre estão ao meu lado, a apoiar-me e constantemente interessados nos meus resultados. Agradeço-lhes também, todas as oportunidades que desde criança me têm dado e que me tornaram naquilo que hoje sou.

À Heloísa, por todo o amor, paciência, apoio, dedicação, compreensão e carinho que demonstrou ao longo deste percurso em que não tive disponibilidade para lhe dar a atenção merecida.

A todos,

Muito Obrigado.

Abstract

The evolution from 4th Generation (4G) to 5th Generation (5G) wireless systems is driven by the expected huge growth in user bit rates and overall system throughput. This requires a substantial spectral efficiency increase, while maintaining or even improving power efficiency. To accomplish this, one needs new transmission techniques employing new technologies, with the most promising ones being millimeter Wave (mmWave) frequencies and massive Multiple-Input and Multiple-Output (m-MIMO).

We consider broadband mmWave transmission with high spectral and power efficiencies. We develop new signal processing schemes for a novel multilayer m-MIMO architecture with large antenna arrays that explores spatial multiplexing, beamforming and employs efficient amplification. To cope with time-dispersive effects associated to high data rate transmission over multipath channels while achieving high power efficiency, we propose the use of Single Carrier with Frequency Domain Equalisation (SC-FDE) schemes using high-level constellation sizes that are decomposed into Offset Quadrature Phase Shift Keying (OQPSK)-type signals and have quasi-constant envelope, allowing the use of amplification schemes based on multiple Non-Linear Amplifiers (NLAs). Upon reception, we address the uplink transmission case, and we propose a set of low complexity iterative equalisers for offset and non-offset modulations within the proposed multilayer m-MIMO architecture.

Keywords:

Wireless Communications, millimeter Wave (mmWave), massive Multiple-Input and Multiple-Output (m-MIMO), Frequency Domain Equalisation (FDE), Envelope Control, Offset constellations

Resumo

A evolução dos sistemas sem fios de 4ª geração (4G) para a 5ª geração (5G) é impulsionada pelo enorme crescimento esperado das taxas de dados dos utilizadores e na taxa de transferência global do sistema. Isso requer um aumento substancial da eficiência espectral, mantendo ou até melhorando a eficiência energética. Para isso, são necessárias novas técnicas de transmissão empregando novas tecnologias, sendo as mais promissoras as frequências de ondas milimétricas (**en:** mmWave) e sistemas massivos de múltipla entrada e múltipla saída (**en:** m-MIMO).

Neste trabalho é considerada a transmissão de banda larga nas ondas milimétricas com alta eficiência espectral e de potência. Desenvolvemos novos esquemas de processamento de sinal para uma nova arquitetura m-MIMO multicamada com grandes matrizes de antenas que exploram multiplexação espacial, formação de feixe (**en:** beamforming) e empregam amplificação eficiente. Para lidar com os efeitos dispersivos no domínio temporal associados à transmissão de alta taxa de dados nos canais multipercurso enquanto se obtém alta eficiência energética, propomos o uso de esquemas mono portadora com equalização no domínio da frequência (**en:** SC-FDE) usando constelações de tamanho elevado que são decompostas em sinais do tipo OQPSK e têm envolvente quase constante, permitindo o uso de esquemas de amplificação baseados em múltiplos amplificadores não lineares (**en:** NLA). Na recepção, abordamos o caso de ligação ascendente e propomos um conjunto de equalizadores iterativos de baixa complexidade para modulações com e sem offset dentro da arquitetura m-MIMO multicamada proposta.

Palavras-chave:

Comunicações sem fios, ondas milimétricas (**en:** mmWave), sistemas massivos de múltiplas entrada e múltipla saída (**en:** m-MIMO), Equalização no domínio da frequência, Controlo de envolvente, Constelações com offset

Contents

List of Figures

List of Tables

List of Acronyms

3G	3rd Generation
4G	4th Generation
5G	5th Generation
ADC	Analogue-to-Digital Converter
AM/AM	Amplitude Modulation/Amplitude Modulation
AM/PM	Amplitude Modulation/Phase Modulation
AoA	Angles of Arrival
APSK	Amplitude Phase-Shift Keying
AWGN	Additive White Gaussian Noise
BER	Bit Error Rate
BF	Beamforming
BPSK	Binary Phase Shift Keying
CP	Cyclic Prefix
DAC	Digital-to-Analogue Converter
DFT	Discrete Fourier Transform
EGC	Equal Gain Combining

FDE Frequency Domain Equalisation

FLOP Floating-point Operation

GMSK Gaussian Minimum Shift Keying

IB-DFE Iterative Block Decision Feedback Equalisation

IBO Input Back-Off

IDFT Inverse Discrete Fourier Transform

IoT Internet of Things

IQI In-phase Quadrature Interference

ISI Inter-Symbol Interference

KL Kullback-Leibler

LHS Left Hand Side

LLR Log-Likelihood Ratio

LST Layered Space-Time

LTE Long Term Evolution

LUT Look-Up Table

m-MIMO massive Multiple-Input and Multiple-Output

M**-OQAM** M-ary Offset Quadrature Amplitude Modulation

M**-QAM** M-ary Quadrature Amplitude Modulation

MFB Matched Filter Bound

MIMO Multiple-Input and Multiple-Output

mmWave millimeter Wave

MM Magnitude Modulation

MMSE Minimum Mean Squared Error

MPMM Multistage Polyphase Magnitude Modulation

MRC Maximum Ratio Combining

MSE Mean Squared Error

MSK Minimum Shift Keying

NF Nyquist pulse shaping Filter

NLA Non-Linear Amplifier

OBO Output Back-Off

OFDM Orthogonal Frequency Division Multiplexing

OQAM Offset QAM

OQPSK Offset Quadrature Phase Shift Keying

PA Power Amplifier

PAM Pulse Amplitude Modulation

PAPR Peak-to-Average Power Ratio

PDF Probability Density Function

PS Polar Scaling

PSK Phase Shift Keying

QAM Quadrature Amplitude Modulation

QPSK Quadrature Phase Shift Keying

RC Raised Cosine

RF Radio Front-end

RMM Ring-type Magnitude Modulation

RRC	Root Raised Cosine
RS	Rectangular Scaling
SC	Single Carrier
SC-FDE	Single Carrier with Frequency Domain Equalisation
SD	Spatial Diversity
SINR	Signal-to-Interference plus Noise Ratio
SISO	Single-Input and Single-Output
SM	Spatial Multiplexing
SNR	Signal-to-Noise Ratio
SSPA	Solid State Power Amplifier
ZF	Zero Forcing

List of Symbols

General Symbols

a_{fit} Curve fitting parameter between α and D_{KL}

A MM maximum admissible amplitude

$A_k^{(r,t)}$ Argument of the channel frequency response at the k-th frequency for the antenna pair (r,t)

$A_{(k,l)}^{(r,t)}$ Argument of the channel frequency response at the (k,l)-th frequency for the antenna pair (r,t)

b_{fit} Curve fitting parameter between α and D_{KL}

$b_{n_p}^{(m)}$ Polar representation (i.e., ± 1) of the m-th bit associated to the n_p-th symbol of the constellation

$\bar{b}_n^{(t,m,i-1)}$ Polar representation of the m-th estimated bit of the n-th transmitted symbol by the t-th transmitter at iteration $i-1$

$b_{n_p}^{eq(i)}$ i-th polar component of s_{n_p}

$B_k^{(t,t,i)}$ Feedback equalisation coefficient at frequency k and iteration i for the antenna pair (t,t)

B_z -3 dB bandwidth

d Distance between BF antennas

d_n MM distortion added to s_n

$\tilde{d_n}$ Projection of d_n in the direction that produces a symbol error detection

D_{KL} KL divergence

E_b Energy per information bit

E_s Energy per information symbol

f_c Carrier frequency

f_{X_n} PDF of the distribution X_n

F_k Feedforward equalisation coefficient at the k-th frequency

$F_k^{(t,r,i)}$ Feedforward equalisation coefficient at frequency k and iteration i for the antenna pair (t,r)

$F_{(k,l)}^{(t,r,i)}$ Feedforward equalisation coefficient at a rate L/T_s for frequency k and iteration i for the antenna pair (t,r)

g_i i-th complex coefficient of constellation polar decomposition

$G(.)$ AM/AM conversion function

$\mathfrak{G}$ Alphabet containing the polar form of all constellation symbols

$\mathfrak{G}^{(I)}$ Alphabet containing the polar form of in-phase components

$\mathfrak{G}^{(Q)}$ Alphabet containing the polar form of quadrature components

h_τ Continuous time domain channel impulse response

$h_\tau^{(r,t)}$ Channel response between transmitting antenna t and receiving antenna r

H_k Frequency response of the channel at the k-th frequency

$H_k^{(r,t)}$ Channel frequency response at the k-th frequency for the antenna pair (r,t)

$H_k^{(r_u,r_b,t)}$ Channel frequency response at the k-th frequency between the t-th transmission antenna and the r_b-th antenna in the r_u group

$H_{k'}^{(r,t)}$ Channel frequency response at a rate L/T_s for the k'-th frequency for the antenna pair (r,t)

(I) In-phase component

$J_k^{(i)}$ Lagrange function to minimise the MSEs of all transmitters at iteration i and frequency k

L Oversampling factor

$\bar{m}$ Average of MM factors, i.e., $\bar{m}{=}\mathbb{E}\left[m_n\right]$

m_n Time-varying real non-negative MM factor applied to s_n

$m_n^{(I)}$ Time-varying real non-negative MM factor applied to $s_n^{(I)}$

$m_n^{(Q)}$ Time-varying real non-negative MM factor applied to $s_n^{(Q)}$

M Number of constellations points

n_{n_z} Zero-mean complex AWGN noise added to x_n

$n_{n_z}^{(I)}$ In-phase component of the zero-mean complex AWGN noise added to x_n

$n_{n_z}^{(Q)}$ Quadrature component of the zero-mean complex AWGN noise added to x_n

n_τ Continuous time domain AWGN noise

N_0 Power spectral density of the zero-mean complex AWGN noise

N_b Number of BF antennas in a group at the transmitter

N_{block} Block size, i.e., number of symbols in each block

N_{ch_clu} Number of clusters

N_p Number of polar components

N_k Noise component at the k-th frequency

$N_k^{(r)}$ Noise component of the r-th antenna at the k-th frequency

$N_{k'}^{(r)}$ Noise component at oversampling rate L/T_s of the r-th antenna at the k'-th frequency

N_R Number of reception antennas

N_{ray} Number of multipath components

N_{ray_clu} Number of multipath components, i.e., rays, in each cluster

N_T Number of transmission antennas

N_u Number of data streams

p_{amp} Parameter control of the AM/AM characteristic curve in SSPA model

p_n Discrete time domain pulse shaping filter

$p_{n'}$ Sampled version of the pulse shaping filter at the rate L/T_s

p_τ Continuous time domain pulse shaping filter

P_b^{MFB} Bit error probability employing MFB

$\bar{P}_b^{\text{MFB}}$ Average bit error probability employing MFB for all transmission antennas

P_e Bit error probability for an uncoded M-PSK transmission over the AWGN channel

$\bar{P}_e$ Average bit error probability for an uncoded M-PSK transmission over time-dispersive channels

P_e^{MM} Bit error probability for an uncoded MM M-PSK transmission over the AWGN channel

$\tilde{P}_e^{\text{MM}}$ Bit error probability obtained by simulation for an uncoded MM M-PSK transmission over the AWGN channel

$\bar{P}_e^{\text{MM}}$ Average bit error probability for an uncoded MM M-PSK transmission over time-dispersive channels

P_f Frequency domain pulse shaping filter

P_{in} PA's input power

$P_{in,avg}$ Average power of the input signal

$P_{in,sat}$ Input power at the saturation point of the PA

$P_{k'}$ N_{block}-size DFT of $p_{n'}$

$P_{\text{MFB}}^{(t)}$ Bit error probability employing MFB for the t-th transmission antenna

P_{out} PA's output power

$P_{out,avg}$ Average power of the output signal

$P_{out,sat}$ Output power at the saturation point of the PA

P_{PC} PA's power consumption

(Q) Quadrature component

R_b Number of BF antennas in a group at the receiver

R_u Number of low correlated antenna groups with SM purposes

s_n n-th complex modulated symbol of the transmitted discrete data block

$s_n^{(I)}$ In-phase component of the n-th complex modulated symbol of the transmitted discrete data block

$s_n^{(Q)}$ Quadrature component of the n-th complex modulated symbol of the transmitted discrete data block

s_{n_p} Symbol of an $\sqrt{M}$-PAM constellation

$s_n^{(t)}$ Symbol transmitted by the t-th antenna composed by in-phase $\left(s_n^{(t,I)}\right)$ and quadrature $\left(s_n^{(t,Q)}\right)$ components

s'_n n-th MM complex modulated symbol of the transmitted discrete data block

$\hat{s}_n^{(t,i-1)}$ Hard decision of $s_n^{(t)}$ at iteration $i-1$.

$\bar{s}_n^{(t,i-1)}$ Soft decision of $s_n^{(t)}$ at iteration $i-1$.

$\breve{s}_{n'}^{(t)}$ Symbol $s_n^{(t)}$ at oversampling rate L/T_s composed by in-phase $\left(s_{n'}^{(t,I)}\right)$ and quadrature $\left(s_{n'}^{(t,Q)}\right)$ components

$S_k^{(t)}$ N_{block}-size DFT of $s_n^{(t)}$ composed by in-phase $\left(S_k^{(t,I)}\right)$ and quadrature $\left(S_k^{(t,Q)}\right)$ components

S'_k Discrete MM symbol transmitted at the k-th frequency

$\tilde{S}'_k$ Estimation of the discrete MM symbol transmitted at the k-th frequency

$\hat{S}_k^{(t,i-1)}$ N_{block}-size DFT of $\hat{s}_n^{(t,i-1)}$ at iteration $i-1$.

$\bar{S}_k^{(t,i-1)}$ N_{block}-size DFT of $\bar{s}_n^{(t,i-1)}$ at iteration $i-1$.

$\breve{S}_{k'}^{(t)}$ N_{block}-size DFT of $\breve{s}_{n'}^{(t)}$ composed by in-phase $\left(S_{k'}^{(t,I)}\right)$ and quadrature $\left(S_{k'}^{(t,Q)}\right)$ components

T_s Symbol's duration

x_n Discrete time domain transmitted signal

x'_n MM time domain transmitted signal

$x_n^{(t)}$ n-th symbol of the discrete block transmitted by the t-th antenna

$\breve{x}_{n'}^{(t)}$ Sampled version of $\breve{x}_{\tau}^{(t)}$ at a rate L/T_s

x_{sat} PA's saturation level

x_{τ} Continuous time domain transmitted signal

x_{τ}^{PA} PA's input signal

$\breve{x}_{\tau}^{(t)}$ Complex equivalent baseband signal transmitted by the t-th antenna

$X_k^{(t)}$ Discrete symbol transmitted by the t-th antenna at the k-th frequency

$\breve{X}_{k'}^{(t)}$ N_{block}-size DFT of $\breve{x}_{n'}^{(t)}$

y_n Discrete time domain received signal

$y_n^{(r)}$ n-th sample of the discrete symbol received by the r-th antenna

y_{τ} Continuous time domain received signal

y_{τ}^{PA} PA's output signal

Y_k Received signal at the k-th frequency

$Y_k^{(r)}$ Discrete symbols received by the r-th antenna at the k-th frequency

$Y_{k'}^{(r)}$ Discrete symbols received at oversampling rate L/T_s by the r-th antenna at the k'-th frequency

Greek Symbols

α Correction weighting factor of the MM distortion

α_0 PA's gain

$\alpha_i^{(r,t)}$ Gain of the selective path i for the antenna pair (r,t)

$\alpha_i^{(r_u,r_b,t)}$ Path gain of i-th ray created by the t-th transmission antenna when reaches the r_b-th antenna in the r_u group

β RC or RRC filter's roll-off

$\beta_{n_p}^{(m)}$ Binary representation (i.e., 0 or 1) of the m-th bit associated to the n_p-th symbol of the constellation

$\beta_n^{(t,m,i-1)}$ Binary representation of the m-th estimated bit of the n-th transmitted symbol by the t-th transmitter at iteration $i-1$

δ_n Discrete Dirac delta signal

$\Delta_k^{(t,i-1)}$ Zero-mean quantisation error of the symbol transmitted by the t-th transmitter at frequency k and iteration $i-1$

ε Very small difference between delays of the rays in the same cluster

η PA's power efficiency

$\overline{\eta}$ PA's time average power efficiency

η_{PAE} PA's power-added efficiency

η_{PSE} PA's power supply efficiency

γ Signal-to-Noise Ratio

$\gamma_{m,i}$ m-th bit of the binary representation of i-th polar component of s_{n_p}

$\kappa^{(t,t)}$ Normalisation coefficient for the t-th antenna

λ Wavelength

$\lambda_k^{(i)}$ Lagrange multiplier at iteration i and frequency k

$\lambda_n^{(t,m,i-1)}$ LLR associated with $\bar{b}_n^{(t,m,i-1)}$

μ Number of bits representing an M-QAM constellation point, i.e., $\log_2(M)$

μ_p Number of bits representing an $\sqrt{M}$-PAM constellation point , i.e., $\log_2(\sqrt{M})$

$\mathbf{\Omega}_k^{(i)}$ Sum of the MSEs of all transmitters at iteration i and frequency k

$\Omega_k^{(t,i)}$ MSE of the t-th transmitter at iteration i and frequency k

ϕ Characterising angle of the distance between M-PSK symbols

ϕ_τ^{PA} Phase of the PA's input signal

$\Phi(.)$ AM/PM conversion function

$\Psi_a^{(m)}$ Subset of $\mathfrak{G}$ containing a symbol s with $\beta_n^{(t,m,i-1)} = a$

$\rho^{(t,i-1)}$ Correlation factor of the t-th transmitter at iteration $(i-1)$

$\overline{\rho}^{(t,i-1)}$ Average correlation factor of the t-th transmitter at iteration $(i-1)$

$\rho_n^{(I)}$ Reliability of the in-phase component of the estimate of the n-th transmitted symbol by the t-th transmitter at iteration $i-1$

$\rho_n^{(Q)}$ Reliability of the quadrature component of the estimate of the n-th transmitted symbol by the t-th transmitter at iteration $i-1$

$\rho_n^{(t,i-1)}$ Reliability of one component of the estimate of the n-th transmitted symbol by the t-th transmitter at iteration $i-1$

$\rho_n^{(t,m,i-1)}$ Reliability of the m-th estimated bit of the n-th transmitted symbol by the t-th transmitter at iteration $i-1$

ρ_u Correlation factor between two r_u groups

σ_d^2 MM distortion power

$\left(\sigma_{\text{LLR}}^2\right)^{(i-1)}$ LLR's variance at iteration $i-1$

σ_{MSE}^2 Variance of complex MSE

$\sigma_{n_z}^2$ Complex AWGN noise power

$\sigma^2_{s_n}$ Signal power

$\sigma^2_{s'_n}$ MM signal power

τ Temporal index

τ_c Delay of the first ray of the c-th cluster

τ_i Delay of selective path i

θ_c AoA associated to the c-th cluster

$\Theta_{k'}$ Time-shifting factor of DFT

Matrix Symbols

$\mathbf{A}_k$ Matrix of $\mathbf{H}_k$ phases with size $N_R \times N_T$

$\mathbf{A}_{(k,l)}$ Matrix of $\mathbf{H}_{(k,l)}$ phases with size $N_R \times N_T$

$\mathbf{B}_k^{(i)}$ Feedback equalisation coefficients matrix at frequency k and iteration i with size $N_T \times N_T$

$\mathbf{B}_{(k,l)}^{(i)}$ Feedback equalisation coefficients matrix at a rate L/T_s at frequency (k,l) and iteration i with size $N_T \times N_T$

$\mathbf{E}_{(k,l)}$ Feedforward equalisation coefficients matrix without pulse shaping at a rate L/T_s for frequency (k,l) with size $N_T \times N_R$

$\mathbf{E}_{(k,l)}^{(i)}$ Feedforward equalisation coefficients matrix without pulse shaping at a rate L/T_s for frequency (k,l) and iteration i with size $N_T \times N_R$

$\mathbf{F}_k$ Feedforward equalisation coefficients matrix at frequency k with size $N_T \times N_R$

$\mathbf{F}_k^{(i)}$ Feedforward equalisation coefficients matrix at frequency k and iteration i with size $N_T \times N_R$

$\mathbf{F}_{k'}^{(i)}$ or $\mathbf{F}_{(k,l)}^{(i)}$ Feedforward equalisation coefficients matrix at a rate L/T_s for frequency k' and iteration i with size $N_T \times N_R$

$\mathbf{g}$ Vector of constellation coefficients

$\mathbf{H}_\tau$ Matrix of continuous time domain channel impulse responses or channel information matrix

$\mathbf{H}_k$ Channel matrix of dimensions $N_R \times N_T$ at the k-th frequency

$\mathbf{H}_{k'}$ or $\mathbf{H}_{(k,l)}$ Channel matrix of dimensions $N_R \times N_T$ at a rate L/T_s for the k'-th frequency

$\mathbf{H}_{k'}^{eq}$ or $\mathbf{H}_{(k,l)}^{eq}$ Equivalent channel matrix of dimensions $N_R \times N_T$ at a rate L/T_s for the k'-th frequency

$\mathbf{I}_W$ Identity matrix with size W

$\mathbf{n}_\tau$ Vector of continuous time domain AWGN noise

$\mathbf{N}_k$ Vector of N_R noise components at the k-th frequency

$\mathbf{N}_{k'}$ or $\mathbf{N}_{(k,l)}$ Vector of N_R noise components at a rate L/T_s for the k'-th frequency

$\mathbf{s}$ Vector of the constellation symbols of an $\sqrt{M}$-PAM constellation

$\tilde{\mathbf{s}}_n^{(i-1)}$ Vector of the time domain estimations of the n-th transmitter symbol at iteration $i-1$

$\widetilde{\mathbf{S}}_k^{(i)}$ Vector of the estimation of the N_T transmitted symbols at frequency k and iteration i

$\hat{\mathbf{S}}_k^{(i-1)}$ Vector of the hard decisions of the N_T transmitted symbols at frequency k and iteration $i-1$

$\overline{\mathbf{S}}_k^{(i-1)}$ Vector of the average symbol values of the N_T transmitters conditioned to the output of the equaliser at frequency k and iteration $i-1$

$\check{\mathbf{S}}_{k'}$ Frequency-domain vector of N_T transmitted symbols at a rate L/T_s for the k'-th frequency

$\breve{\mathbf{S}}_{(k,l)}^{(i-1)}$ Frequency-domain vector of soft decisions of N_T transmitted symbols at a rate L/T_s for the (k,l)-th frequency at iteration $i-1$

$\widetilde{\check{\mathbf{S}}}_{k'}$ Frequency-domain vector of estimations of N_T transmitted symbols at a rate L/T_s for the k'-th frequency

$\widetilde{\check{\mathbf{S}}}_{(k,l)}^{(i)}$ Frequency-domain vector of estimations of N_T transmitted symbols at a rate L/T_s for the (k,l)-th frequency at iteration i

$\mathbf{W}$ Hadamard matrix with dimensions $\sqrt{M} \times \sqrt{M}$

$\mathbf{x}_\tau$ Vector of continuous time domain transmitted signals

$\mathbf{X}_k$ Vector of N_T transmitted signals at the k-th frequency

$\widetilde{\mathbf{X}}_k$ Vector containing the estimation of the N_T transmitted signals in the frequency domain

$\check{\mathbf{X}}_{k'}$ Frequency-domain vector of N_T transmitted signals at a rate L/T_s for the k'-th frequency

$\mathbf{y}_\tau$ Vector of continuous time domain received signals

$\mathbf{Y}_k$ Vector of N_R received signals at the k-th frequency

$\mathbf{Y}_{k'}$ or $\mathbf{Y}_{(k,l)}$ Vector of N_R received signals at a rate L/T_s for the k'-th frequency

$\boldsymbol{\alpha}_{N_R \times N_{ray}}$ Gain matrix of dimensions $N_R \times N_{ray}$ for clustered channel

$\boldsymbol{\Delta}_k^{(i-1)}$ Vector of the zero-mean quantisation errors of the N_T transmitted symbols at frequency k and iteration $i-1$

$\boldsymbol{\kappa}$ Normalisation diagonal matrix with size $N_T \times N_T$

$\boldsymbol{\Lambda}_k^{(i)}$ Inverse matrix with size $N_T \times N_T$ used to obtain $\mathbf{F}_k^{(i)}$

$\boldsymbol{\Lambda}_{(k,l)}^{(i)}$ Inverse matrix with size $N_T \times N_T$ used to obtain $\mathbf{F}_{(k,l)}^{(i)}$

$\boldsymbol{\varrho}^{(i-1)}$ Diagonal matrix of the correlation factors at iteration i with size $N_T \times N_T$

$\overline{\boldsymbol{\varrho}}^{(i-1)}$ Diagonal matrix of the average correlation factors at iteration i with size $N_T \times N_T$

$\boldsymbol{\tau}^{(t)}$ Vector of the delays linked to the t-th transmission antenna

$\boldsymbol{\theta}^{(t)}$ Vector of the AoA linked to the t-th transmission antenna

Common Operators

$\mapsto$ Maps to

$\mathbf{A}^*$ Complex conjugated matrix of $\mathbf{A}$

$\mathbf{A}^T$ Transposed matrix of $\mathbf{A}$

$\mathbf{A}^H$ Transposed and complex conjugated matrix (Hermitian) of $\mathbf{A}$

$\mathbb{E}[.]$ Expectation operator

$\nabla_Z(W)$ Gradient of W with respect to Z

$Q(.)$ Gaussian Q-function

$\mathrm{Tr}(\mathbf{A})$ Trace of matrix $\mathbf{A}$

$\Upsilon(.)$ Function denoting average in L defined by (5.17)

1 Introduction

1.1 Scope and Motivation

The evolution towards the next wireless communications systems (5th Generation (5G) and beyond) faces multiple challenges. These new systems should be able to cope with applications as diverse as Internet of Things (IoT), autonomous driving cars, remote surgery or augmented reality while improving the data rate and the availability of the previous generations [1]. In fact, it is expected a massive growth in user bit rates (a 10 to 100 times increase) and overall system throughput (about a 1000 times increase) [2], which means the need of a substantial spectral efficiency increase. At the same time, the power efficiency should be maintained or even improved, not only to have greener communications but also to cope with the billions of sensors that will populate every place, that will require long battery lifetimes [1, 3]. To accomplish these requirements, one needs to employ new transmission techniques, with the most promising ones being based on the massive Multiple-Input and Multiple-Output (m-MIMO) concept, together with the transmission at millimeter Wave (mmWave) frequencies [3, 4].

The adoption of mmWave transmission is interesting not only due to the vast bandwidth available, but also because of their small wavelength. In fact, with the wavelengths contained in the range of 1 to 10 millimetres, the antennas become smaller, allowing small-sized transmitters and receivers with a very high number of antenna elements and, therefore, enabling m-MIMO implementations. In its turn, m-MIMO can be used to explore Spatial Multiplexing (SM) and Beamforming (BF) gains, enabling the service of multiple users with high bit-rates while reducing interference and/or increasing coverage [5]. However, mmWave frequencies present considerable challenges regarding propagation (high propagation free-space path losses, small diffraction effects and almost total absorption losses due to obstacles) and implementation difficulties, both at the analogue and digital domains (e.g., Digital-to-Analogue Converter (DAC) and Analogue-to-Digital Converter (ADC) design, efficient amplification, signal processing requirements for equalisation and user separation, etc.), which can be particularly challenging for m-MIMO systems [6]. Besides that, power and spectral efficiencies could be conflicting, and different techniques must be employed to achieve each one of them, which makes a significant challenge to combine them with success.

One way to increase the spectral efficiency is by employing dense and large constellations, such as 64-Quadrature Amplitude Modulation (QAM) or 256-QAM. However, not only larger constellations have higher power requirements, but also the corresponding signals have larger envelope fluctuations, requiring the use of linear amplifiers with higher back-off, which further reduces the power amplifier efficiency. By employing single carrier schemes at uplink, such as Single Carrier with Frequency Domain Equalisation (SC-FDE) [7, 8], instead of the commonly used Orthogonal Frequency Division Multiplexing (OFDM) schemes [9, 10], we can reduce the amplifier's back-off, improving amplification efficiency. This is mainly because SC-FDE signals have lower envelope fluctuations than OFDM schemes based on similar constellations. Nonetheless, SC-FDE signals still present substantial envelope fluctuations and a relatively high Peak-to-Average Power Ratio (PAPR), especially for large constellations and/or when the signals are filtered to have compact spectrum. This means that a quasi-linear amplifier is required (e.g., a class A or B amplifier), which are more difficult to implement and have much lower amplification efficiency than strongly non-linear amplifiers (such as class D amplifiers). PAPR reduction using Magnitude Modulation (MM) techniques [11, 12] and linear amplification schemes based on the use of multiple ideally grossly Non-Linear Amplifiers (NLAs) [13] could be one solution to improve the power efficiency of the system. Another solution is the decomposition of the large

constellations into a sum of Binary Phase Shift Keying (BPSK), Quadrature Phase Shift Keying (QPSK) or Offset Quadrature Phase Shift Keying (OQPSK) components [14, 15] that present a reduced dynamic range and can be separately amplified without distortion (or with reduced distortion) by different NLAs [16], allowing a more efficient amplification while maintaining the same spectral efficiency.

To tackle the effects of the transmitter's impairments (e.g. non-linear amplification distortion, MM distortion or correlation between antenna elements) and the multipath characteristics of the mmWave channel, as well as, to perform user separation, Iterative Block Decision Feedback Equalisation (IB-DFE) can be used. IB-DFE receivers [8] present good results, but with some problems yet, such as poor performance with offset modulations due to the interference between in-phase and quadrature components [17]. Moreover, when performing digital processing, they become too complex for m-MIMO schemes since they require matrix inversions for each subcarrier and each iteration. Hence, there is a need to develop receivers that do not require matrix inversions, while still able to achieve good performance.

At last, although the previously mentioned techniques have already been very well studied, it should be mentioned that their combination with m-MIMO at mmWave is not trivial, and there are still some problems to solve at power amplification and signal processing levels. In that sense, we propose a new multilayer multi-user m-MIMO architecture at mmWave bands using SC-FDE schemes for uplink scenarios, with a generic representation presented in Fig. 1.1.

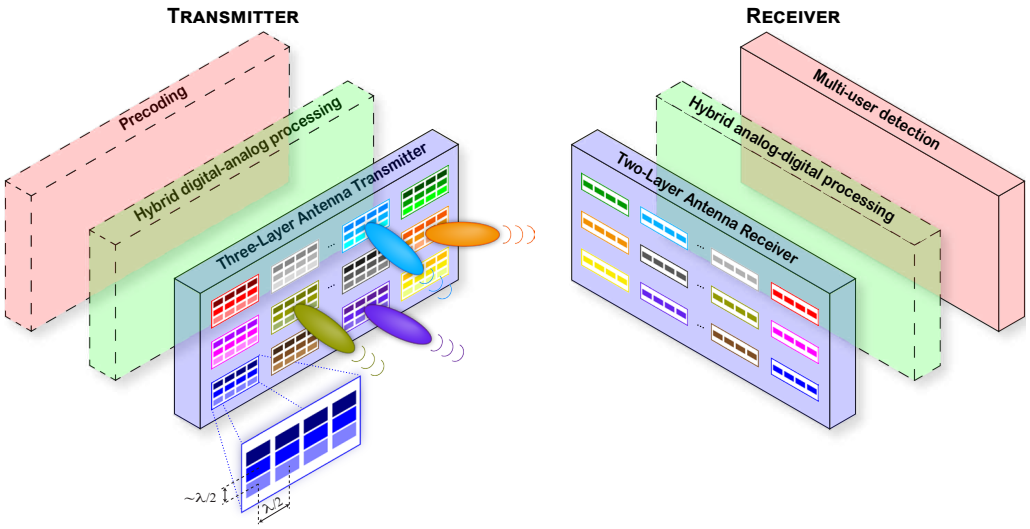

Figure 1.1 Generalised multi-user m-MIMO architecture at mmWave bands for SC-FDE schemes.

1.2 Objectives

The goal of this thesis is to design and evaluate transceivers with reduced complexity and high efficiency that are suitable for broadband wireless communications at mmWave frequencies targeting future 5G wireless communications systems deployment. To achieve it, the objectives of this thesis are:

1. Design a mmWave m-MIMO system using large and dense constellations, Nyquist filtering close to the minimum band for high spectral efficiency, and signals with low envelope fluctuations for high power efficiency while maintaining low complexity.

2. Design a transmitter able to deal with large constellations by splitting them as a sum of OQPSK-type signals with a reduced dynamic range.

3. Design of low complexity receivers using Frequency Domain Equalisation (FDE) that tackle the effects of offset constellations, the transmitter's impairments (e.g. correlation between antenna elements), the multipath characteristics of the mmWave channel and, most important, able to separate SM's data streams.

4. Performance evaluation and optimisation of the proposed techniques, theoretically and by simulation.

1.3 Outline

This thesis is organised into 6 chapters: Introduction, Fundamental Concepts, A new multilayer MIMO architecture at mmWave bands, Iterative receivers for m-MIMO, m-MIMO with offset constellations and Conclusions and Future Work. Following, a brief summary of each chapter's contents is presented:

- *Chapter 2 - Fundamental Concepts*

  The fundamental concepts to build the new proposed architecture are presented. mmWave and m-MIMO are the key technologies to the next generation systems. To build systems based on these concepts, we study channels models, including the channel model proposed for this thesis and presented in [18], band limit transmission, amplification and linear equalisers. This study is the starting point to the understanding of our new architecture.

- *Chapter 3 - A new multilayer MIMO architecture at mmWave bands*

  A multilayer massive MIMO architecture for broadband mmWave communications is proposed [19–22] and its benefits and challenges are explained. It can employ highly-efficient, low-cost saturated amplifiers with any constellation, even large QAM constellations or other dense constellations with high spectral efficiency. Different approaches to improve the power efficiency of the system are addressed: MM techniques and decomposition of high level constellations. Also, for MM, a Bit Error Rate (BER) analysis is performed for both flat fading and time-dispersive channel scenarios, resulting in simpler formulas to evaluate systems where MM is used to improve the power amplifier's efficiency [23].

- *Chapter 4 - Iterative receivers for m-MIMO*

  Frequency domain iterative detection schemes based on Maximum Ratio Combining (MRC) and Equal Gain Combining (EGC) concepts, which do not require matrix inversions, and suitable for m-MIMO systems employing SC-FDE modulations are proposed [18]. The operation at mmWave allows the use of m-MIMO schemes with hundreds of antennas. Since the channel matrix dimensions grow with the number of antennas, conventional Multiple-Input and Multiple-Output (MIMO) detection schemes can become too complex as the number of antennas is increased, namely due to the need to invert high dimension matrices. For this reason, m-MIMO schemes should employ simple techniques to separate data streams that avoid matrix inversions inherent to conventional MIMO receivers. Performance results show that low complexity techniques can approach the Matched Filter Bound (MFB) with just a few iterations, even with significant correlation between different antenna elements.

- *Chapter 5 - m-MIMO with offset constellations*

  Receivers for offset constellations are developed. Offset constellations designed to have either an almost constant envelope or being decomposed as the sum of constant-envelope signals, allow the use of strongly non-linear power amplifiers, improving system's power efficiency. Receivers for these type of signals have been developed in [17, 24], but only for Single-Input and Single-Output (SISO) schemes. Here, this previous work is extended, giving rise to conventional IB-DFE and pragmatic receivers for MIMO schemes. Moreover, new MRC and EGC based receivers are proposed to lower the complexity of the equalisation process. These new receivers are designed and evaluated in [25], where it is also

shown that low complexity receivers can have excellent performance/complexity trade-off in m-MIMO scenarios, making them particularly interesting for future wireless systems operating at mmWave bands.

1.4 Research contributions

The research of this thesis has resulted in 1 patent application, 3 journal articles and 10 articles in proceedings of international conferences with the achievement of the following contributions:

- A new multilayer m-MIMO architecture at mmWave bands that results in 1 patent applications, submitted in the USA and in Portugal, and 3 international conference articles.

    1. P. Bento, P. Carvalho, R. Dinis, M. Gomes, and V. Silva, "Transmission method with double directivity," USA PPP USPTO 15 330 968 (Pending), Jan, 2015
    2. P. Bento, P. Carvalho, R. Dinis, M. Gomes, and V. Silva, "Método de Transmissão com dupla directividade," Portugal PPP PT 108 149A, Jan, 2015
    3. R. Dinis, P. Montezuma, P. Bento, M. Gomes, and V. Silva, "A multi-antenna technique for mm-wave communications with large constellations and strongly nonlinear amplifiers," in *Microwave Conf. (GeMiC), 2015 German*, Mar 2015, pp. 284–287
    4. R. Dinis, P. Montezuma, P. Bento, M. Gomes, and V. Silva, "A Massive MIMO Architecture for Highly Efficient mm-Wave Communications with Saturated Amplifiers," in *International Conf. on Electronics, Information, and Communication*, Jan 2015
    5. R. Dinis, P. Carvalho, P. Bento, M. Gomes, and V. Silva, "Linear Amplification with Multiple Amplifiers and Antennas," in *IASTED International Conf. on Modelling, Identification and Control - MIC*, vol. 1, February 2016, pp. 1–5

- Low complexity receivers for offset constellations in m-MIMO scenarios at mmWave bands, resulting in 2 journal articles, one of them as first author, and 1 in an international conference. In the conference article, it was also presented the channel model proposed for this thesis.

    6. P. Bento, A. Pereira, R. Dinis, M. Gomes, and V. Silva, "Low complexity equalisers for offset constellations in massive MIMO schemes," *IEEE Access*, June 2019

7. A. P. S. Silva, P. Bento, M. Gomes, R. Dinis, and V. Silva, "Complexity Analysis of FDE Receivers for Massive MIMO Block Transmission Systems," *IET Communications*, vol. 13, pp. 1762–1768, July 2019
8. P. Bento, A. Pereira, R. Dinis, M. Gomes, and V. Silva, "Frequency-Domain Detection without Matrix Inversions for mmWave Communications with Correlated Massive MIMO Channels," in *2017 IEEE 85th Vehicular Technology Conference (VTC Spring)*, June 2017, pp. 1–5

- A simple BER expression for MM signals in both flat fading and time-dispersive channel scenarios, that results in 1 journal article as first author. Moreover, the study of MM also results in another 2 international conference articles about a ring-type MM suitable for offset signals.

9. P. Bento, A. Pereira, M. Gomes, R. Dinis, and V. Silva, "Simplified and accurate BER analysis of magnitude modulated M-PSK signals," *IET Communications*, vol. 13, pp. 1443–1448, June 2019
10. A. Simões, P. Bento, M. A. C. Gomes, R. Dinis, and V. Silva, "Efficient LINC Amplification for 5G Through Ring-type Magnitude Modulation," in *IEEE GC 2015 Workshop on Mobile Commun. in Higher Frequency Bands (MCHFB) (GC'15 - Workshop - MCHFB)*, San Diego, USA, Dec. 2015
11. A. Simoes, P. Bento, M. Gomes, R. Dinis, and V. Silva, "Ring-Type Magnitude Modulation for OQPSK: Enabling NL-Amplification of Spectral Efficient Signals," in *2016 IEEE 83rd Vehicular Technology Conference (VTC Spring)*, May 2016, pp. 1–5

- A study of meta-heuristics to optimise beamforming on the detection of multiple users in wireless systems, that results in 1 international conference article.

12. P. Bento, C. H. Antunes, M. Gomes, R. Dinis, and V. Silva, "Beamforming Optimization for Multiuser Wireless Systems Using Meta-Heuristics," in *2016 IEEE 84th Vehicular Technology Conference (VTC-Fall)*, Sep. 2016, pp. 1–5

- The development of low complexity receivers for MIMO systems was also done for multi carrier systems, but not explored in this document, resulting in 3 international conference articles.

13. A. Pereira, P. Bento, M. Gomes, R. Dinis, and V. Silva, “Iterative MRC and EGC Receivers for MIMO-OFDM Systems,” in *2018 IEEE 87th Vehicular Technology Conference (VTC Spring)*, June 2018, pp. 1–4

14. A. Pereira, P. Bento, M. Gomes, R. Dinis, and V. Silva, “TIBWB-OFDM: A Promising Modulation Technique for MIMO 5G Transmissions,” in *2018 IEEE 88th Vehicular Technology Conference (VTC-Fall)*, Aug 2018, pp. 1–5

15. A. Pereira, P. Bento, M. Gomes, R. Dinis, and V. Silva, “MIMO Time-Interleaved Block Windowed Burst OFDM with Iterative Frequency Domain Equalization,” in *2018 15th International Symposium on Wireless Communication Systems (ISWCS)*, Aug 2018, pp. 1–6

2

Fundamental Concepts

The evolution of wireless system communications leads to new challenges. From the 4th Generation (4G) to the 5th Generation (5G), these challenges are related to multiple capabilities presented in Fig. 2.1 [34]. This diagram makes clear that 5G systems are supposed to have much higher capacity and spectral efficiency requirements than current systems. Many techniques are independently emerging to fulfil these requirements, with the mmWave communications alongside m-MIMO and small-cell (pico and femto) deployment being expected to be a crucial part of 5G systems [2, 3]. Therefore, in this chapter, it will be presented the fundamental concepts that will be used in the design of the new architecture proposed in this thesis. First, a brief description of mmWave bands' features is presented. Then, MIMO concepts [4, 5] are studied, followed by the description of channel types. Also, band limited transmission, as well as, amplification topics are described. Finally, some linear equalisers are presented. This previous knowledge provides a valuable starting basis to tackle the different degrees of freedom for achieving conflicting requirements on mmWave, as high spectral and power efficiency, and affordable complexity.

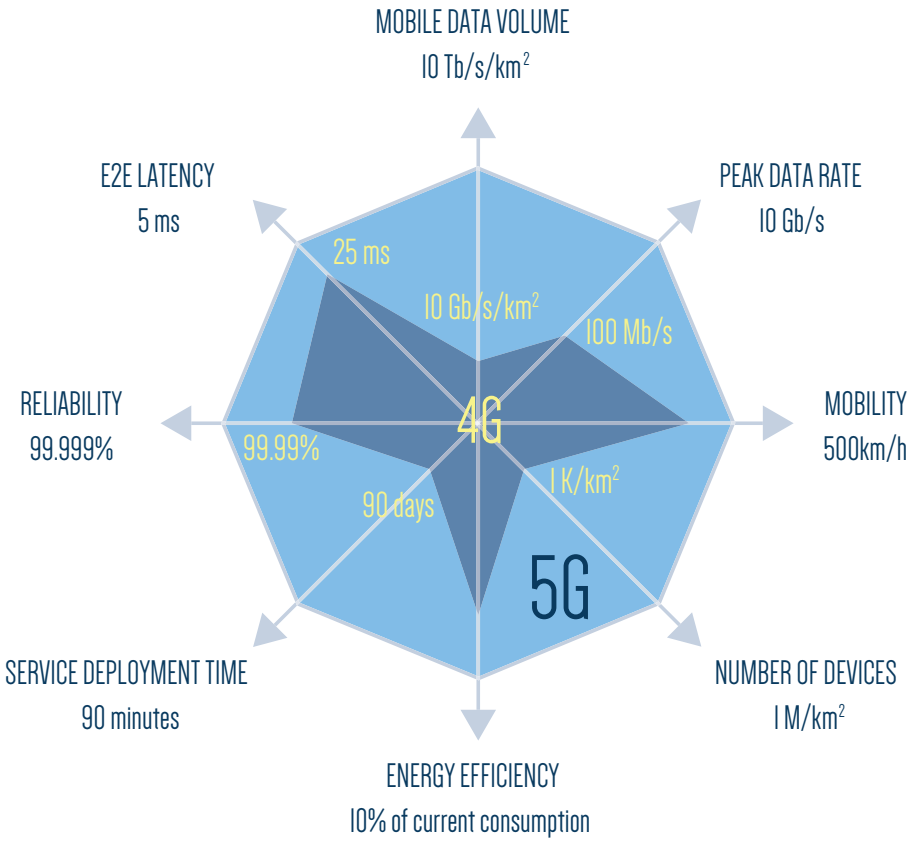

Figure 2.1 Comparison diagram of 4G and 5G capabilities [34].

2.1 Millimeter Wave

The transmission of broadband wireless signals using mmWave bands, i.e., frequencies in 30 GHz to 300 GHz range, is motivated by the wide available spectrum and the small wavelengths that allows the use of m-MIMO techniques. At mmWave bands, available spectrum can be 10x to 100x larger than in the actual operating frequencies below 10 GHz [2, 3, 35]. This increase depends on the bands considered. If one looks at 28, 38 and 72 GHz bands alone (bands being considered for cellular traffic), one can see over of 10 GHz of available spectrum, while above 100 GHz it can almost reach hundreds of GHz. Thus, comparing these values with the spectrum of less than 1 GHz actually allocated for all the world's cellphones, it may be concluded that the achievement of higher data rates desired by consumers in the next generation wireless communication systems is possible. Observing Fig. 2.2 that represents the radio spectrum of the United States (but it is similar for other countries) [35], one can see that all the bandwidth of actual wireless systems fits, in fact, into the unlicensed 60 GHz band (shaded areas have similar spectrum).

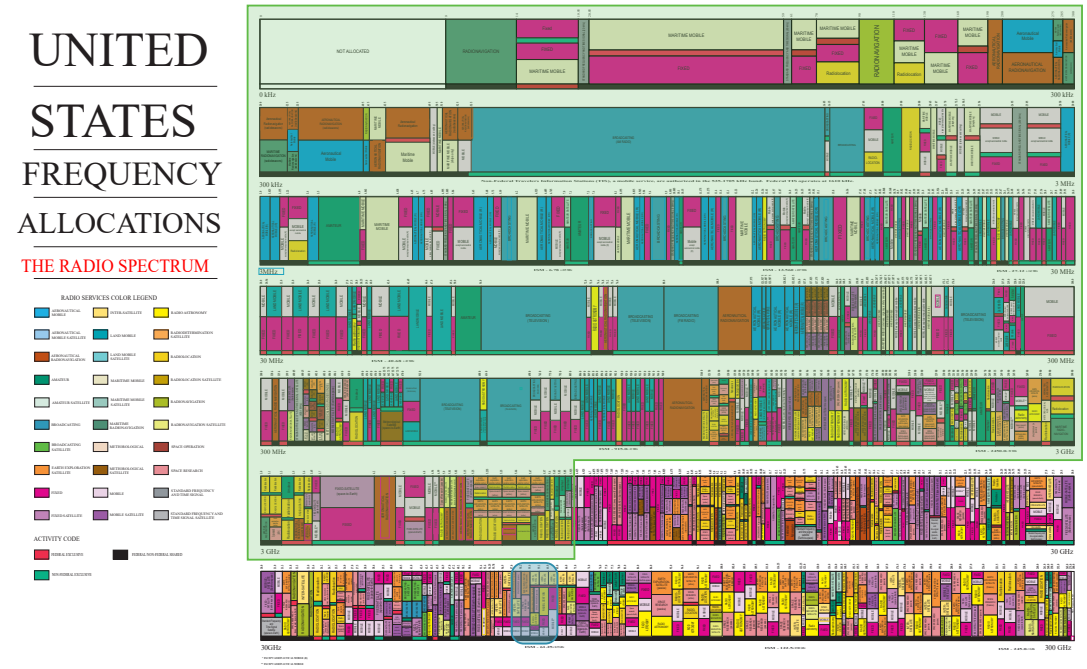

Figure 2.2 Wireless spectrum used by commercial systems in the USA. Each row represents a decade in frequency. Other countries in the world have similar spectrum allocations [36].

Although the first mmWave communication system was developed in 1895 [37], mmWave transmission only became attractive in the last decade with the advancements and price reduction of integrated mmWave analogue circuits, baseband digital memory and processors. Hence, mmWave wireless communications are currently being seen as alternatives to wired connections in data centres and as replacement of wired interconnects on chips, as well as, vehicular, cellular and aerospace applications [35].

However, mmWave transmission presents relevant problems like high free-space path losses, minimal diffraction effects and huge losses due to obstacles' absorption [2, 35]. These problems occur because the wavelengths at mmWave frequencies are so small that most objects in the physical environment are enormous relative to them. Also, the molecular constituency of air and water plays a significant role in the free space distances achievable, as well as, the weather, such as rain or snow. Therefore, depending on the frequency, the free space loss will vary as shown in Fig. 2.3. For indoor scenarios, things like moving objects, the presence of people, room dimension or furniture can influence the signal. Fortunately, one can use highly directional multiple elements antennas to overcome some of this limitations constraints [4, 35], as will be seen later. Because of these differences between different frequency bands, some of them (marked with yellow dotted

bubbles), look especially promising for next generation cellular systems since they have a low free space attenuation, while others (marked with green dashed bubbles) with higher free space losses, look suitable for short-range networks enabling highly frequency reuse [2, 35].

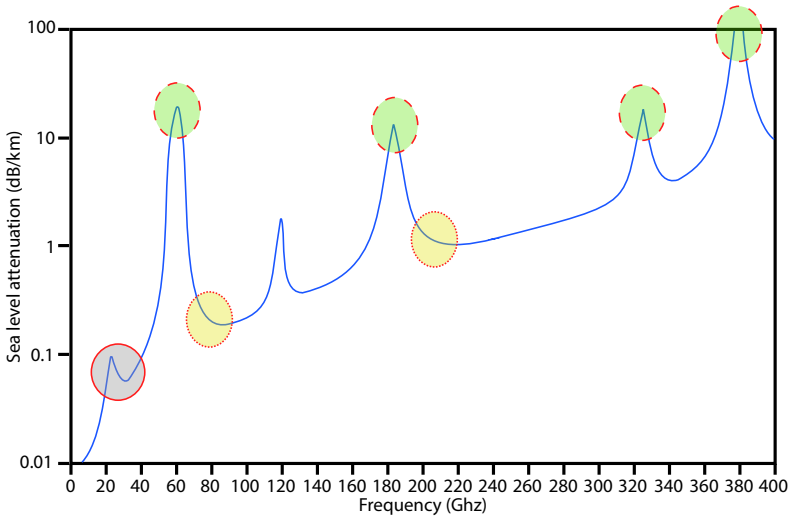

Figure 2.3 Attenuation of free space propagation due to absorption in the air at sea level across the frequency spectrum. The grey solid bubble shows the small attenuation in the air for current wireless networks, while other bubbles show interesting attenuation characteristics that can be exploited at mmWave [35].

Nonetheless, it should be mentioned that some of mmWave apparently impairments, such as high free-space path losses, minimal diffraction effects and huge losses due to obstacles' absorption, can in fact be used as advantages due to some sort of existing symbiosis between mmWave and the use of m-MIMO techniques and small-cell networks [38]. On the one hand, mmWave small wavelengths allow small-sized transceivers with a large number of antenna elements [35, 38], enabling m-MIMO schemes that can be leveraged by either using SM and/or BF [4] as will be explained in section 2.2. On the other hand, due to the increased path loss, mmWave signals have limited range, allowing higher frequency reuse, which leverages the deployment of small cells networks [2]. Moreover, the high reflection effects can be used to improve coverage.

2.2 MIMO concepts

Multiple-Input and Multiple-Output (MIMO) is a technique first presented in the 90s [39] that use multiple antennas at the transmitter and the receiver in order to achieve significant gains in capacity, coverage and/or reliability [5]. Due to its powerful performance-enhancing capabilities,

it has rapidly gained in popularity over the past decade. These capabilities come from:

- *Spatial Diversity (SD)* - used to fight against fading channels, improving the quality and reliability of reception through the use of redundancy in the system. For this purpose, multiple copies (ideally independent) of the signal are transmitted by different antennas to the receiver, with each one of the receiver's antennas receiving the contributions from all transmitter's antennas. These multiple replicas improve the probability of at least one copy of the signal reaches the receiver without suffering deep fades while enables the use of efficient equalisation techniques that explore the diversity of the system through the proper combination of the received copies [7]. The spatial diversity order of the system is defined as the number of independent links between the transmitter and the receiver, i.e., $N_T \times N_R$, with N_T and N_R being the transmitter's and receiver's antennas, respectively. It is straightforward to conclude that, the higher is the spatial diversity order, the more reliable is the system.

- *Spatial Multiplexing (SM)* - SM techniques add an additional degree of freedom to explore MIMO systems, both at serving a single or more users, where throughput gains can be achieved through diversity by transmitting simultaneously and in parallel different bit streams on the same Radio Front-end (RF) channel through different antennas [4]. Therefore, the SM gain is less than or equal to $\min\{N_T, N_R\}$, limited by the rank of the channel matrix. For SM to work well, the correlation between different channels should be low enough to allow efficient user/stream separation, both when this separation is performed at the transmitter side (through precoding techniques [6]) or the receiver side (through equalisation techniques [7, 40]). SM is particularly interesting for the implementation of m-MIMO schemes at mmWave bands with multiple users.

- *Beamforming (BF)* - BF [4, 5] results from the coherent combination of multiple signals transmitted/received by multiple antennas to increase the receive Signal-to-Interference plus Noise Ratio (SINR) at the desired receivers while minimising it for undesired receivers. The system becomes more robust to noise, leading to an improvement in the coverage and the range of the wireless network.

  At the transmitter, BF is performed sending the same information on each antenna, but with a variation in the amplitude and/or the phase in the signal of each antenna. With this variation,

the radiation pattern of the overall antenna array can be shaped and directed depending on the number of antenna elements, as shown in Fig. 2.4.

In a receiver employing BF, determining the phase of hundreds of antenna elements at receiver arrays to ensure the quality of communication, i.e. with a high SINR, can become a very difficult problem to solve. A possible solution is the use of meta-heuristics as we showed in [30].

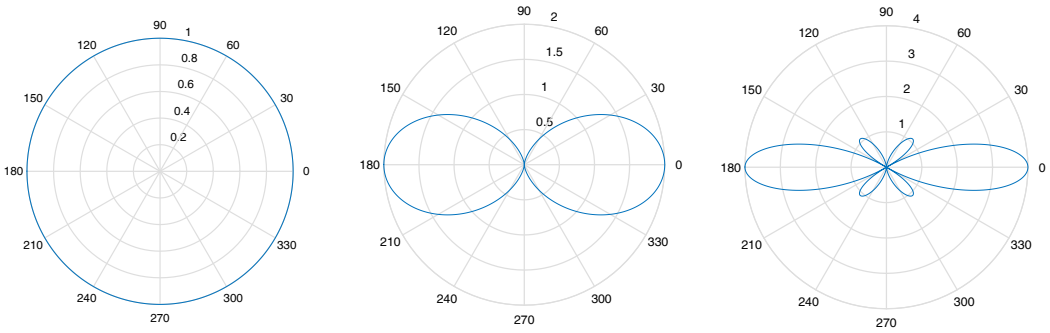

(a) (b) (c)

Figure 2.4 Comparison of the radiation pattern obtained with different number of antennas when performing BF: (a) 1 isotropic antenna (no BF); (b) 2 antennas; (c) 4 antennas. Note that as more the antennas, more directive is the main lobe.

Although all these benefits are usually not exploited simultaneously, some combinations of them can improve the capacity, coverage and/or reliability of the network depending on the intended goals. Therefore, systems using MIMO are being recommended to use in the present, e.g. Wi-Fi, 3rd Generation (3G) and 4G [5], and future wireless communications, such as 5G [4, 19, 21, 22]. Furthermore, the use of mmWaves in 5G systems, allows the use of m-MIMO schemes (i.e. hundreds of antennas in both sides) with huge SM and BF gains, as mentioned before.

2.2.1 SISO *vs.* MIMO

First of all, the differences between SISO and MIMO systems and their advantages and drawbacks should be understood. While a SISO system can be represented as in Fig. 2.5, a MIMO system with two links is represented as shown in Fig. 2.6. As at receivers arrive signals from all the transmitters, it is clear that the maximum bit rate of the overall system can be bigger in MIMO than in SISO systems, when similar channels and links are considered.

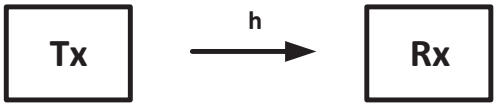

Figure 2.5 Representation of a SISO channel.

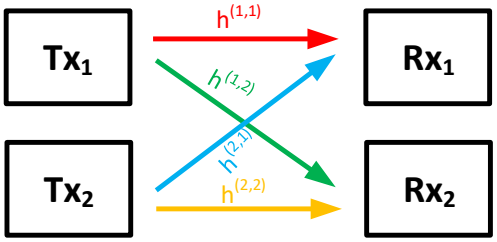

Figure 2.6 Representation of a MIMO channel.

If a narrowband frequency flat fading channel without time dispersion is considered, the continuous time domain signal at the SISO receiver for a specified instant [41] is given by

$$y_\tau = h_\tau * x_\tau + n_\tau \,, \tag{2.1}$$

where x_τ and y_τ are, respectively, the continuous time transmitted and the received signals, h_τ is the channel impulse response, n_τ is the Additive White Gaussian Noise (AWGN) and '$*$' denotes the convolution operator. While for MIMO, the equivalent representation is given by

$$\mathbf{y}_\tau = \mathbf{H}_\tau * \mathbf{x}_\tau + \mathbf{n}_\tau \,, \tag{2.2}$$

where $\mathbf{y}_\tau$ and $\mathbf{x}_\tau$ are column vectors containing the signals at the receivers and the transmitters, respectively, $\mathbf{n}_\tau$ is the channel noise vector, and $\mathbf{H}_\tau = h_\tau^{(r,t)}$ is a matrix with all the time domain channel responses between each pair of transmitting and receiving antennas, where $h_\tau^{(r,t)}$ denotes the channel response between transmitting antenna t and receiving antenna r. $\mathbf{H}_\tau$ is also called channel information matrix.

Both in SISO and MIMO, if the channel response is known, it is easy to obtain an estimation of the transmitted signal from the received signal. Unfortunately, real channels contain a combination of noise, multipath propagation, selective frequency fading, scattering or Doppler shifts, as well as,

the transmitted signals' power decreases with the distance travelled [5, 42]. These phenomenons could become more problematic for MIMO than for SISO due to the number of transmitting signals, that increases the complexity of the channel information matrix. On the other hand, these effects allow the exploitation of diversity, increasing the channel capacity and obtaining better performance [5, 41].

2.2.2 MIMO challenges at mmWave bands

By combining small cells with m-MIMO systems, one could employ directional BF to boost the received power signal to offset mmWave considerable propagation losses and increase cell coverage and/or accommodate a large number of co-channel users (multi-user m-MIMO), by reducing inter-cell interference while granting high frequency reuse [3, 4, 43]. The beams can also be steered in various directions to exploit reflections and scattering from objects for maximal signal strength while coherently aligning the received waveforms [44].

Although the usage of mmWave is particularly suitable for the implementation of m-MIMO, there are issues preventing easy scalability of the designs of conventional MIMO. It is not practical to associate an RF chain with every antenna element and perform all the processing in the digital domain when the number of antennas is very high [4, 6]. The need for high resolution and power consuming ADCs per RF chain at the receiver side increases the power consumption [6, 38]. Moreover, the optimum design of multi-user m-MIMO systems is too complicated since it involves operations with huge matrices. Therefore, some grouping will be needed with part of the BF performed at the RF level using analogue phase shifters and/or variable gain amplifiers [6, 45].

Furthermore, in order to system support SM and BF, precoding can be used [6, 35, 46]. Precoding means that multiple BF vectors are used, one for each stream to be transmitted [35]. As BF is performed in both analogue and digital domain, hybrid precoding must be used [6, 35], with some of the precoding being performed in digital and some performed in analogue.

2.3 Channel Models

In this section, the MIMO channel models used in this work to evaluate SC-FDE schemes, such as the one illustrated in Fig. 1.1, are presented. The channel models will be defined in the frequency domain given that within the multilayer m-MIMO architecture proposed in this work, the equalisation techniques developed are carried in that domain.

Assuming a block-based transmission and a sampling rate of $1/T_s$, where T_s is the symbol's duration, the block of discrete symbols transmitted by the t-th antenna is $\{x_n^{(t)}; n{=}0, \ldots, N_{block}{-}1\}$, and the block of discrete symbols received by the r-th antenna becomes $\{y_n^{(r)}; n{=}0, \ldots, N_{block}{-}1\}$. Then, applying a Discrete Fourier Transform (DFT) of N_{block} points, the following signals are obtained

$$\mathbf{X}_k{=}\left[X_k^{(1)} \ldots X_k^{(N_T)}\right]^T \text{ with } \{X_k^{(t)}; k{=}0, \ldots, N_{block}{-}1\}{=}\text{DFT}\{x_n^{(t)}; n{=}0, \ldots, N_{block}{-}1\} \quad (2.3)$$

and

$$\mathbf{Y}_k{=}\left[Y_k^{(1)} \ldots Y_k^{(N_R)}\right]^T \text{ with } \{Y_k^{(r)}; k{=}0, \ldots, N_{block}{-}1\}{=}\text{DFT}\{y_n^{(r)}; n{=}0, \ldots, N_{block}{-}1\} \quad (2.4)$$

The received frequency domain signals in a MIMO scheme can be expressed by

$$\mathbf{Y}_k = \mathbf{H}_k \mathbf{X}_k + \mathbf{N}_k, \quad (2.5)$$

where $\mathbf{N}_k = [N_k^{(1)} \ldots N_k^{(N_R)}]^T$ denotes the discrete channel noise in the frequency domain and $\mathbf{H}_k$ is the $N_R \times N_T$ channel matrix for the k-th frequency, and it is represented by

$$\mathbf{H}_k = \begin{bmatrix} H_k^{(1,1)} & \cdots & H_k^{(1,N_T)} \\ \vdots & \ddots & \vdots \\ H_k^{(N_R,1)} & \cdots & H_k^{(N_R,N_T)} \end{bmatrix}. \quad (2.6)$$

2.3.1 Additive White Gaussian Noise (AWGN) model

The simplest channel model that can be considered is the AWGN one. The AWGN channel only adds Gaussian noise to the signal accordingly the Signal-to-Noise Ratio (SNR), i.e., there is no gain neither phase distortion introduced by the channel and $H_k^{(r,t)} = 1$ for every k and every pair (r,t). This model is mainly used for line of sight transmissions, but not for scenarios with reflections. However, mainly in SISO, it is very often used as benchmark in the comparison of methods or for validation of simulation results because its theoretical expressions are, in general, easy to obtain. For MIMO schemes with a similar number of transmission and reception antennas, it is not interesting because there is no diversity gain.

2.3.2 Time-dispersive model

A more interesting model for MIMO schemes is the time-dispersive one [47]. This kind of channels assumes that the transmitted signals suffer multipath propagation, i.e., the transmission is reflected or diffracted in different surfaces, originating many rays with different gains and delays. These features could attenuate a signal frequency or delay it until being undetectable or could amplify it in such a way that will surpass all the others, for this reason, it is also known as frequency selective channel. There are several models to describe a time-dispersive channel, and in this work, the chosen one [47] is characterised by

$$H_k^{(r,t)} = \sum_{i=1}^{N_{\text{ray}}} \alpha_i^{(r,t)} e^{-j2\pi k\tau_i}, \tag{2.7}$$

where N_{ray} is the number of multipath components, $\alpha_i^{(r,t)}$ is the gain of the selective path i for the antenna pair (r,t) and τ_i is the delay of selective path i.

2.3.3 mmWave clustered model

The propagation characteristics of mmWave channels combined with the high number of antennas presented in m-MIMO schemes make the models used for traditional MIMO in current frequency bands inaccurate. Therefore, in [18], we proposed a mmWave clustered model embodying SM and BF gains, following the idea of a channel with clusters presented in [48]. It is possible to integrate these gains due to the use of different antenna arrangements at the receiver. The antennas can be grouped in linear arrays of R_b antennas for BF purposes with high correlation indexes between them, or they can be arranged in R_u groups away from each other, allowing SM with low correlation between antennas and a more straightforward user separation. These two different arrangements can also be combined and used simultaneously as shown in Fig. 2.7.

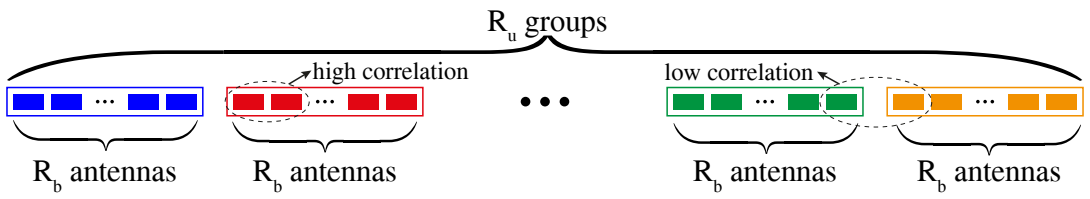

Figure 2.7 Example of the combination of two different arrangement of antennas in a horizontal plan.

This model assumes that the transmitter sends to the receiver a signal with unitary power,

that is split into N_{ray} multipath components. These components can be grouped in clusters of equal number of elements with similar delays and similar Angles of Arrival (AoA). Then, $N_{ray} = N_{ray\_clu} \times N_{ch\_clu}$, where N_{ray_clu} is the number of multipath components, i.e., rays, in each cluster and N_{ch_clu} is the number of clusters. Fig. 2.8 presents an example of a channel realisation following this model, where, for the sake of simplicity, only one transmission antenna is shown.

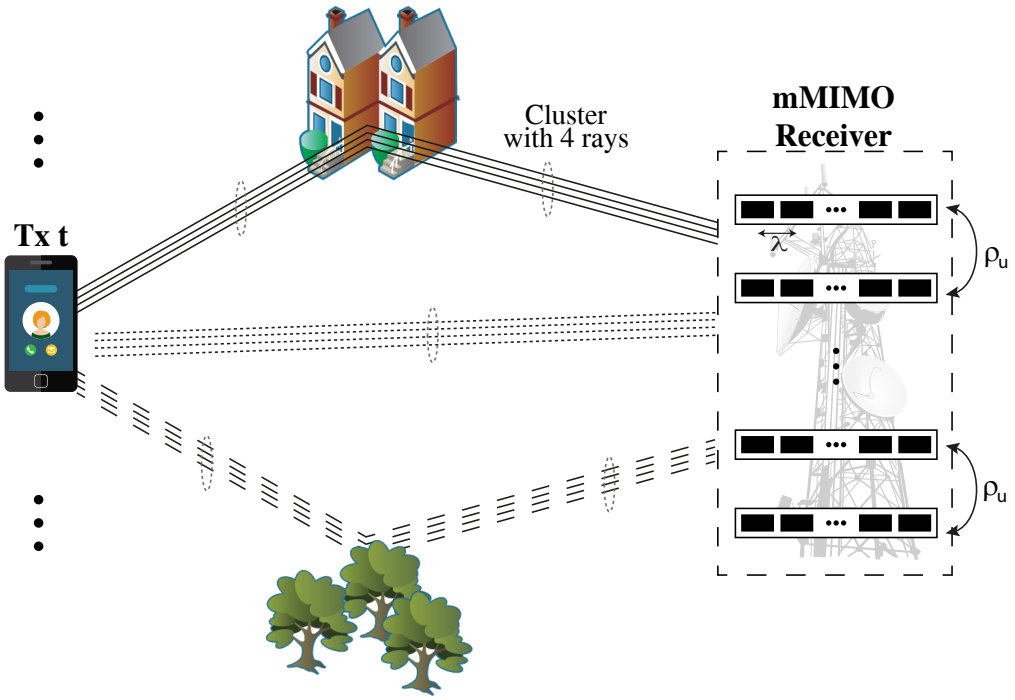

Figure 2.8 Example of one channel realisation following the clustered model considering one transmission antenna that produces $N_{ch\_clu} = 3$ clusters of $N_{ray\_clu} = 4$ multipath components each one.

Although the clusters are formed assuming similar delays and similar AoA for all rays, there are small differences between them. These differences can be neglected concerning AoA. Therefore, the AoA is defined by $\{\theta_c; c = 1, 2, \ldots, N_{ch\_clu}\}$, and the AoA vector linked to the t-th transmission antenna is defined by

$$\boldsymbol{\theta}^{(t)} = \Big[\underbrace{\theta_1^{(t)}, \ldots, \theta_1^{(t)}}_{N_{ray\_clu}}, \underbrace{\theta_2^{(t)}, \ldots, \theta_2^{(t)}}_{N_{ray\_clu}}, \ldots, \underbrace{\theta_{N_{ch\_clu}}^{(t)}, \ldots, \theta_{N_{ch\_clu}}^{(t)}}_{N_{ray\_clu}}\Big]^T_{(N_{ray} \times 1)} . \tag{2.8}$$

However, small differences in delays can significantly influence the performance of the receiver. In this case, it is considered that τ_c is the delay of the first ray of the c-th cluster and the

delay of the other rays within the cluster are linear related and can be computed based on affine function with parameter ε corresponding to the minimal difference between rays. Thus, the delay vector linked to the t-th transmission antenna is

$$\boldsymbol{\tau}^{(t)}=\left[\tau_1^{(t)},\tau_1^{(t)}+\varepsilon,\ldots,\tau_1^{(t)}+\left(N_{ray\_clu}-1\right)\varepsilon,\ldots,\tau_{N_{ch\_clu}}^{(t)},\tau_{N_{ch\_clu}}^{(t)}+\varepsilon,\ldots,\tau_{N_{ch\_clu}}^{(t)}+\left(N_{ray\_clu}-1\right)\varepsilon\right]^T_{(N_{ray}\times 1)}. \quad (2.9)$$

On the receiver side, it is assumed that there are N_R antennas arranged in R_u groups of R_b antennas. The R_u groups are away from each other assuring low correlation between them, and the R_b antennas compose a linear array for BF purpose having high correlation indexes between each other. To each one of these N_R antennas reaches N_{ray} rays, whose path-gain must be computed. Let $\alpha_i^{(r_u,r_b,t)}$ denotes the path gain of i-th ray created by the t-th transmission antenna when reaches the r_b-th antenna in the r_u group. Based on $\alpha_i^{(1,1,t)}$ modelled as a random complex gain that follows a normal distribution with power $P_{1,1}=1/N_{block}$, where $P_{1,1}$ is the normalised power of the first transmitted ray by the first transmission antenna, it is possible to compute all other path gains with low computational effort.

As in practice, it is not possible to ensure that the correlation between groups is zero because they are in the same space, the gain of the first antenna of each r_u group can be related to the gain of the first antenna of the other groups. Using the Bussgang theorem [49], $\alpha_i^{(r_u,r_b,t)}$ can be decomposed into two components: one related to $\alpha_i^{(1,1,t)}$ by the correlation factor between groups, ρ_u, and a random component. Thus, it is expressed by

$$\alpha_i^{(r_u,r_b,t)}=\alpha_i^{(1,1,t)}\times\rho_u+\mu_2, \quad (2.10)$$

where

$$\mu_2\sim N\left(P_{1,1}\times\left(1-|\rho_u|^2\right)\right). \quad (2.11)$$

It is assumed that ρ_u is the same between every two adjacent groups, i.e., ρ_u is constant.

Moreover, the gain of antennas within the same cluster can be computed using the equation of the array factor. Hence, the gain of antenna r_b at cluster r_u is given by

$$\alpha_i^{(r_u,r_b,t)}=\alpha_i^{(r_u,1,t)}\times e^{-j2\pi\frac{d}{\lambda}(r_b-1)\cos\theta_i^{(t)}}, \quad (2.12)$$

where d is the distance between the array elements and λ is the wavelength.

Finally, these gains produce a matrix $\boldsymbol{\alpha}_{N_R \times N_{ray}}$ and the channel impulse response for the k-th frequency between the antenna pair (r_u, r_b, t) is given by

$$H_k^{(r_u,r_b,t)} = \sum_{i=1}^{N_{ray}} \alpha_i^{(r_u,r_b,t)} e^{-j2\pi k \tau_i^{(t)}}. \tag{2.13}$$

The previous equations define one of the many possible ways to represent a mmWave channel combined with m-MIMO schemes, and it is the one used in in the further chapters for the BER performance comparison of the different proposed techniques.

2.4 Band limited transmission

Pulse shaping [47, 50] is usually required to limit the bandwidth of the signal to transmit to the available channel bandwidth and to make the spectrum go down quickly outside of the passband by reducing the amplitude of the sidelobes, thus avoiding/minimising the inter-channel interference. Nevertheless, the pulse shaping filter should respect the Nyquist criterion in order to prevent Inter-Symbol Interference (ISI) [47], i.e., at time instants multiples of the symbol period T_s, the pulse shaping impulse response should be zero. Many different pulses satisfy this criterion, and between them, an obvious choice is the rectangular pulse in the time domain, that ensures constant envelope signals for M-Phase Shift Keying (PSK) modulations but presents poor spectral characteristics due to their high sidelobes [50] of the *sinc* frequency response. Therefore, other options must be taken into account, such as the half-cosine, filtered half-cosine or raised cosine pulses [47, 50]. Fig. 2.9 presents the typical time impulse response of these windows, while their spectrum is shown in Fig. 2.10.

2.4.1 Half-cosine

A half-cosine pulse respecting the Nyquist criterion is defined as

$$p_\tau = \cos(\pi\tau/T_s), \quad |\tau| \leq \frac{T_s}{2}, \tag{2.14}$$

where T_s is the symbol period.

This kind of pulses is mostly used in Minimum Shift Keying (MSK) modulations [50], where the quadrature component is shifted, such as for OQPSK type signals. Even though they present

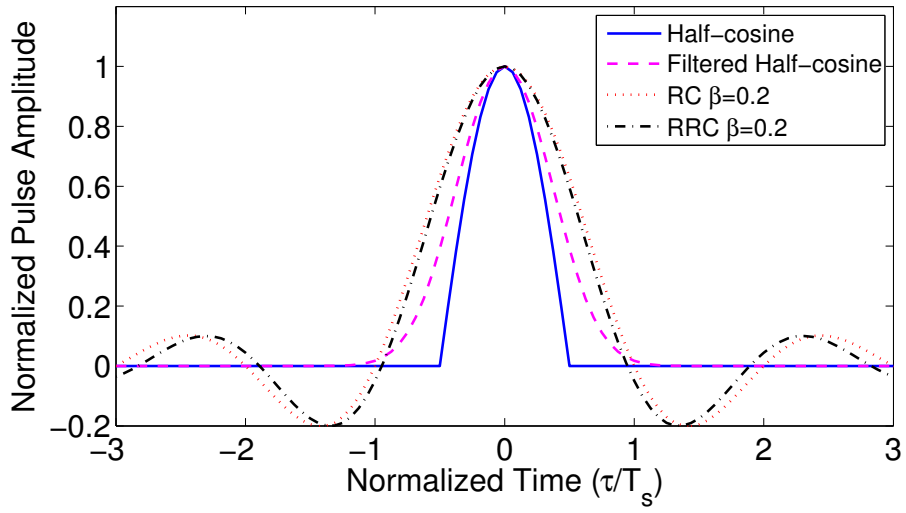

Figure 2.9 Comparison of the behaviour of several pulse shaping filters in the time domain.

a large bandwidth, as could be seen in Fig. 2.10, they are an acceptable choice for pulse shaping. This choice is supported by the achievement of constant or almost constant envelope signals, while the energy of their sidelobe is 10 dB lower than the rectangular pulse, improving the spectral efficiency without deteriorating the power efficiency.

2.4.2 Filtered Half-cosine

One hay to improve the half-cosine pulse is filtering it with a Gaussian filter expressed by

$$g_\tau = \frac{\sqrt{\pi}B_z}{\sqrt{-\ln\sqrt{0.5}}} e^{\pi^2\tau^2 B_z^2/(\ln\sqrt{0.5})}, \tag{2.15}$$

where B_z is the -3 dB bandwidth. Looking at Fig. 2.10, one could see that there is a reduction of almost 30 dB in energy of the main sidelobe while maintaining the constant envelope. Usually, it is used for Gaussian Minimum Shift Keying (GMSK) signals, presenting an attractive power efficiency and slightly improving the spectral efficiency [50], but still presenting bandwidth substantially above the minimum Nyquist band. Moreover, it does not respect the Nyquist criterion as could be observed in Fig. 2.9, requiring a powerful equalisation to mitigate ISI [50].

2.4.3 Raised Cosine

To improve spectral efficiency, one could employ a Nyquist pulse shaping Filter (NF) with bandwidth close to the minimum band using Raised Cosine (RC) or Root Raised Cosine (RRC)

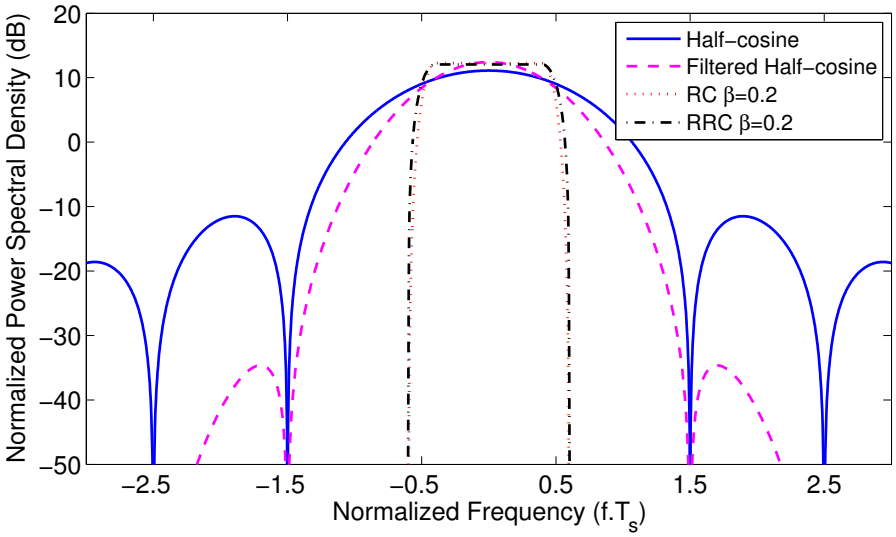

Figure 2.10 Comparison of the spectrum of several pulse shaping filters.

[47, 50, 51]. These pulses belongs to the same family, and they are designed in the frequency domain with characteristics depending on the roll-off factor β. In Figs. 2.9 and 2.10, it is possible to see an enormous bandwidth reduction, but with the cost of increased envelope fluctuations in the time domain of the filtered signal.

The frequency response of the RC pulse filter is expressed by

$$P_f = \begin{cases} T_s & 0 \leq |f| \leq (1-\beta)/2T_s \\ \frac{T_s}{2}\left(1 - \sin\frac{\pi T_s}{\beta}\left(f - \frac{1}{2T_s}\right)\right) & (1-\beta)/2T_s < |f| < (1+\beta)/2T_s \\ 0 & |f| \geq (1+\beta)/2T_s \end{cases}, \tag{2.16}$$

where β is the roll-off factor, i.e., the excess bandwidth considered with respect to the minimum Nyquist band, which is $1/2T_s$. The frequency response of the RRC pulse filter is obtained by applying a square root to the frequency response response of the RC, ensuring the Nyquist criterion at the reception when perfect matched filtering occurs [47, 50].

The roll-off factor can vary between 0 and 1, with zero corresponding to the ideal Nyquist filter rectangular pulse in the frequency domain and minimum bandwidth of $1/2T_s$. Therefore, β should be kept as lower as possible to improve the spectral efficiency. However, when β decreases, the power of the sidelobes of the filter impulse response increases. This leads to an increase of the envelope fluctuations of the filtered signal by the pulse shaping filter, and consequently of the

signal's PAPR and also to a decrease of performance in case of synchronisation errors [50]. In this way, the main contribution for high PAPR on the transmitted signal comes from the pulse shaping filter.

2.5 Amplification

In a transmitter system, the last stage is a RF module that is responsible for amplifying and sending the signal. To have a reliable system, the RF module must have high spectral and power efficiencies, as well as high linearity in order to ensure a low distortion of the transmitted signal, which results in a low BER at the receiver [13].

2.5.1 Power Amplifier's Efficiency

The main stage of the transmitter's RF is the Power Amplifier (PA) whose linearity requirements critically affect the power efficiency of the system. The better the linearity of the amplifier the lower is its efficiency. These two parameters are linked to the nature of the signal to transmit (particularly to the signal's PAPR) and are not independent of each other. Therefore, choosing the PA class and its operating point must be a compromise between power efficiency and linearity.

There are many classes of linear amplifiers, each one with different characteristics. The linear classes are A, AB and B. These classes are defined according to the conduction angle, i.e., the number of degrees of linearity. Amplifiers of class A have a conduction angle of 2π, which represents high linearity. However, they are the least efficient with a maximum power efficiency of 25% [52]. As mentioned earlier, the higher the linearity, the lower the efficiency. Class B has a conduction angle of π and class AB a conduction angle in $]\pi, 2\pi[$ [52] and, therefore, they are more power efficient. Besides these three classes, there are others, like C and D, that are strongly non-linear but presenting high power efficiency with values above 80% [53]. Due to the high non-linearities that they introduce in the system, they are not so attractive for communication systems. However, if signals with constant envelope are used, these classes of amplifiers could be employed.

A typical input-output characteristic of a PA is illustrated in Fig. 2.11. In order to maximise the efficiency of the PA, the operation point must be as close as possible to the saturation level [13]. However, near this point, PAs have a non-linear behaviour characterised by the 1dB compression point. In this point, the gain of the amplifier is reduced by 1dB concerning the output power

saturation level.

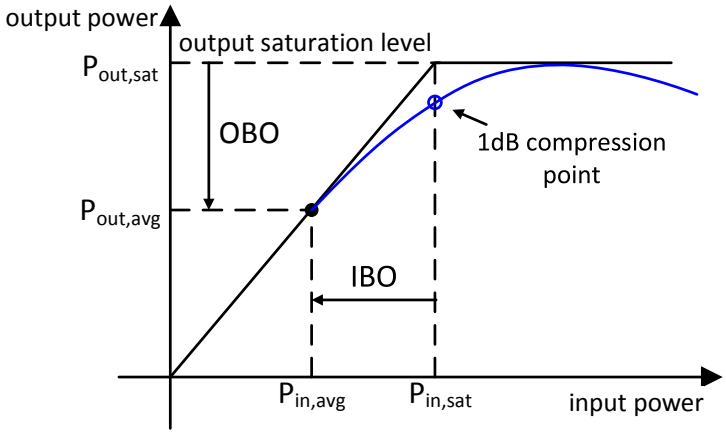

Figure 2.11 Input-output power characteristic of a PA.

As signals with high PAPR can drive the PA into a non-linear region, the PA must be operated with some amount of Input Back-Off (IBO) to shift the operating point to a linear region as it is shown in Fig. 2.11. The IBO is the ratio between the input power at the saturation point of the PA, $P_{in,sat}$, and the average power of the input signal, $P_{in,avg}$ [54], and it is given in decibels by

$$\text{IBO} = 10\log_{10}\left(\frac{P_{in,sat}}{P_{in,avg}}\right) . \tag{2.17}$$

Similarly, an Output Back-Off (OBO) is defined as the ratio between the output power at the saturation point of the PA, $P_{out,sat}$, and the average power of the output signal, $P_{out,avg}$, and it is given in decibels by

$$\text{OBO} = 10\log_{10}\left(\frac{P_{out,sat}}{P_{out,avg}}\right) . \tag{2.18}$$

By proper adjust of the IBO and the OBO, it can be ensured that the amplified signal does not exceed the saturation level, i.e., the signal is not clipped. However, the use of back-off decreases the efficiency of the PA and, consequently, leads to significant energy losses.

The power efficiency of a PA, η, can be measured in two different ways: the power supply efficiency, η_{PSE}, and the power-added efficiency, η_{PAE} [54]. The first one is defined as the ratio between the output power, P_{out}, and the PA's power consumption, P_{PC}, i.e., as

$$\eta_{PSE} = \frac{P_{out}}{P_{PC}} . \tag{2.19}$$

However, η_{PSE} does not depend on the input power, and it is, therefore, an optimistic view of the efficiency of the PA. Alternatively, η_{PAE}, that takes into account the input power, P_{in}, and is defined by

$$\eta_{PAE} = \frac{P_{out} - P_{in}}{P_{PC}} \,, \tag{2.20}$$

is a more suitable measure.

Equations (2.19) and (2.20) are only valid for signals with constant envelope. For signals with a non-constant envelope, the time-average efficiency is

$$\overline{\eta} = \int_a^b \eta(\tau) dt, \tag{2.21}$$

with $[a, b)$ representing the interval where the signal is defined.

2.5.2 Peak-to-Average Power Ratio (PAPR)

To define the IBO it is necessary some kind of measure for the envelope fluctuations. Peak-to-Average Power Ratio (PAPR) is a standard measure with hundreds of works addressing its use and the ways to reduce it [55, 56]. If IBO is lower or equal to PAPR, it is ensured that the amplified signal will not suffer distortion on the amplification process.

The PAPR can be defined for both continuous time and discrete time signals and it is measured in the time domain. For a continuous time signal, PAPR of a symbol is defined as the ratio of the maximum instantaneous power to the average power [55, 56] and it is mathematically expressed as

$$PAPR(x_\tau) = \frac{\max\limits_{0 \leq \tau < T} |x_\tau|^2}{\frac{1}{T_s} \int\limits_0^{T_s} |x_\tau|^2 dt} \,, \tag{2.22}$$

where T_s is the symbol period.

In discrete time, the PAPR of a symbol is expressed as

$$PAPR(x_n) = \frac{\max\limits_{0 \leq n \leq N_{block}-1} |x_n|^2}{E\left[|x_n|^2\right]} \,. \tag{2.23}$$

If PAPR is limited to a certain level, envelope fluctuations will be limited too and it is possible to improve the amplifier's efficiency. Therefore, lots of research has been made to reduce PAPR [55, 56]. However, it should be taken into account, that PAPR reduction techniques in general

do not preclude the necessity of using linear amplification, although allowing for considerable improvement on the front-end power efficiency by considerably reducing amplifiers' back-off requirements [57]. In fact, the dynamic range of the envelope remains high because in general, the envelope runs from zero to its maximum value (note that a signal can have a very low PAPR, close to 0 dB, and still possess an extensive dynamic range, e.g. consider a signal that is "1" almost all time and goes to "0" with a very small probability). Therefore, the reduction of the dynamic range becomes vital and MM [11, 12, 58, 59] is one of the techniques that allows this reduction, as it will be seen ahead.

2.5.3 Power Amplifier Models

In the previous subsections, it was discussed the loss in efficiency at the PA upon the amplification of non-constant envelope signals. This loss occurs in order to prevent the introduction of non-linearities in the system that appear when leading the PA into saturation. Therefore, it is necessary to find a way to quantify non-linearities and reduce them. However, to study this problem, PAs' characteristics must be modelled.

Several mathematical models have been proposed to mimic the characteristics of the different non-linearities that the PA might introduce. In this work, the Solid State Power Amplifier (SSPA) model [60, 61] and the hard-limiter are studied.

Considering that the input of the PA is

$$x_\tau^{PA} = \left|x_\tau^{PA}\right| e^{j\phi_\tau^{PA}} , \tag{2.24}$$

where $\left|x_\tau^{PA}\right|$ and ϕ_τ^{PA} are the amplitude and the phase of the input signal, respectively, a PA is usually modelled by the functions Amplitude Modulation/Amplitude Modulation (AM/AM) conversion, $G(.)$, and the Amplitude Modulation/Phase Modulation (AM/PM) conversion, $\Phi(.)$, with the PA's output being given by

$$y_\tau^{PA} = G\left(\left|x_\tau^{PA}\right|\right) e^{j\left(\phi_\tau^{PA} + \Phi(|x_\tau^{PA}|)\right)} , \tag{2.25}$$

i.e., the gain $G(.)$ and the phase shift $\Phi(.)$ of the output signal depend on the envelope of the input, $\left|x_\tau^{PA}\right|$, and these functions model the non-linearities of the PA.

For the case of the SSPA [60] model,

$$G\left(\left|x_{\tau}^{PA}\right|\right) = \frac{\alpha_0 \left|x_{\tau}^{PA}\right|}{\left(1+\left(\frac{\left|x_{\tau}^{PA}\right|}{x_{sat}}\right)^{2p_{amp}}\right)^{1/2p_{amp}}}\,, \tag{2.26}$$

and

$$\Phi\left(\left|x_{\tau}^{PA}\right|\right) \approx 0\,, \tag{2.27}$$

where α_0 is the amplifier's gain, x_{sat} the saturation level of the PA and p_{amp} a parameter that controls the sharpness of the AM/AM characteristic curve as can be seen in Fig. 2.12.

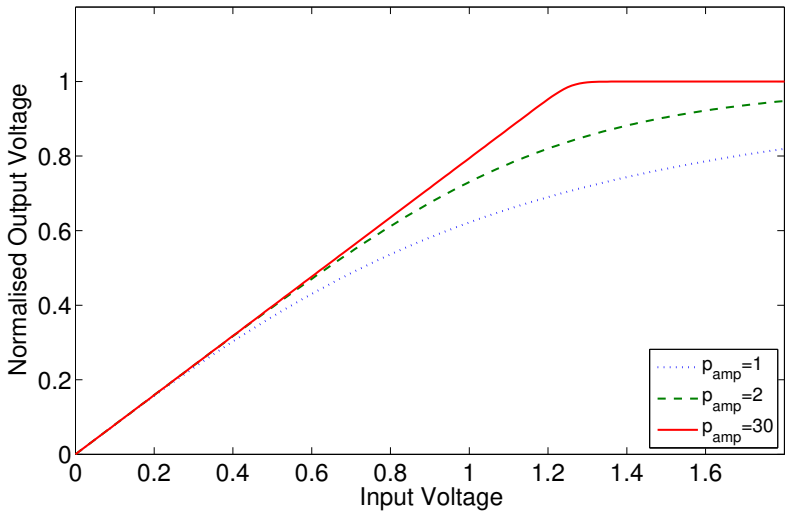

Figure 2.12 AM/AM curves for the SSPA model with different values of the sharpness parameter p_{amp}.

For the case of the hard-limiter model, the information contained in amplitude is lost, with the AM/AM characteristic becoming

$$G\left(\left|x_{\tau}^{PA}\right|\right) = \text{constant}. \tag{2.28}$$

The phase of the signal does not suffer distortion, with the AM/PM characteristic being also given by (2.27).

SSPA model is used in many communication scenarios [61, 62]. For that reason, it is a suitable choice when studying the effects of non-linearities and how to tackle them at the receiver, as it will be done in chapter 5. On the other hand, the hard-limiter represents the worst case scenario and it

will be used as a bound on the improvement of the system against non-linearities.

2.6 Linear equalisation for MIMO systems

The equalisation of MIMO and m-MIMO SC-FDE schemes should tackle different reception issues. These issues can result from multipath channels and/or multiple users in the system, which will cause interference between different replicas of the signal and/or different users, turning the signal separation for MIMO one of the major problems at the reception. However, by considering a MIMO system with a number of antennas at the receiver at least equal to the number employed at the transmitter (i.e. $N_T \leq N_R$), it is theoretically possible to separate the N_T different signals [7]. On flat frequency fading MIMO channels, the signal separation is quite simple [7], needing only to invert the channel matrix. Nevertheless, for frequency-selective channels, signal separation requires the implementation of more complex inter-antenna interference cancellation schemes [7, 63].

In that sense, receiver design for MIMO and m-MIMO SC-FDE schemes can follow different approaches. The most common is based on Zero Forcing (ZF) techniques [46, 50], although a better performance can be achieved using Minimum Mean Squared Error (MMSE) receivers [5, 46, 50]. However, both of these receivers require matrix inversions, which will be prohibitive in m-MIMO schemes due to the expected large matrix dimensions, setting the need for reduced-complexity receivers such as Maximum Ratio Combining (MRC) and Equal Gain Combining (EGC) [50, 64]. In this section, it is provided a brief description of conventional techniques for SC-FDE m-MIMO schemes, and also presented lower complexity approaches based on MRC and EGC concepts [50, 64].

2.6.1 Zero Forcing (ZF)

The ZF [46, 50] linear equaliser is one of the most known methods to perform equalisation and/or signal separation. It is a straightforward technique that uses the inverse of the channel frequency response or, in the case of the channel matrix being singular, it uses the Moore-Penrose pseudoinverse matrix. The equaliser filter, $\mathbf{F}_k$, is defined as

$$\mathbf{F}_k = \boldsymbol{\kappa} \left(\mathbf{H}_k^H \mathbf{H}_k \right)^{-1} \mathbf{H}_k^H, \tag{2.29}$$

with $\mathbf{H}_k^H$ being the hermitian matrix of $\mathbf{H}_k$ and $\boldsymbol{\kappa}$ a diagonal normalisation matrix chosen to ensure $\mathbf{F}_k\mathbf{H}_k^H \approx 1$.

Considering (2.5), the estimated signal $\widetilde{\mathbf{X}}_k$ is equal to

$$\widetilde{\mathbf{X}}_k = \mathbf{F}_k\mathbf{Y}_k = \mathbf{X}_k + \mathbf{F}_k\mathbf{N}_k. \tag{2.30}$$

Although ZF receiver allows perfect separation of different users, as well as ISI removal, it can cause severe noise enhancement, particularly when cancelling severe channel deep fades. Moreover, it requires matrix inversions whose dimensions can be very high in m-MIMO systems.

2.6.2 Minimum Mean Squared Error (MMSE)

An improved linear equaliser is based on the MMSE criterion, i.e., in the minimisation of the Mean Squared Error (MSE) [5, 46, 50]. Contrarily to ZF, this equaliser takes into account the SNR value upon reception, γ, producing better results when in the presence of frequency-selective channels.

Minimising the MSE[1] results in the coefficients of MMSE equaliser being given by

$$\mathbf{F}_k = \boldsymbol{\kappa}\left(\mathbf{H}_k{}^H\mathbf{H}_k + \frac{1}{\gamma}\mathbf{I}_{N_T}\right)^{-1}\mathbf{H}_k{}^H, \tag{2.31}$$

and the estimated signal $\widetilde{\mathbf{X}}_k$ is obtained by

$$\widetilde{\mathbf{X}}_k = \mathbf{F}_k\mathbf{Y}_k. \tag{2.32}$$

Although MMSE equaliser improves the system BER performance, it still requires matrix inversions.

2.6.3 Maximum Ratio Combining (MRC) and Equal Gain Combining (EGC)

As matrix inversions could be a problem in m-MIMO schemes, equalisers based on MRC and EGC concepts [50, 64] become simpler approaches than ZF or MMSE. Both techniques provide accurate approximations when $N_R/N_T \gg 1$ (i.e., for m-MIMO schemes) and the channels

[1] The minimisation problem is well documented in the literature and will not be presented here. However, in chapter 4 the IB-DFE equaliser based on the MMSE criterion will be described using a similar approach, with the first iteration corresponding to the linear MMSE.

between different transmit and receive antennas have a small correlation. In these conditions, in [64], it is shown that

$$\mathbf{H}_k^H \mathbf{H}_k \approx N_R \mathbf{I}_{N_R}, \tag{2.33}$$

where $\mathbf{I}_{N_R}$ is an identity matrix with size N_R. This approximation is on the base of the definition of the MRC equaliser. Therefore, the linear frequency domain equaliser/signal separation performing MRC at each frequency uses

$$\mathbf{F}_k = \boldsymbol{\kappa} \mathbf{H}_k^H. \tag{2.34}$$

For EGC equaliser, matrix $\mathbf{A}$ is obtained from $\mathbf{H}_k$, where the (r,t)-th element of $\mathbf{A}$ is given by

$$A_k^{(r,t)} = \frac{H_k^{(r,t)}}{|H_k^{(r,t)}|} = e^{j \arg\left(H_k^{(r,t)}\right)}, \tag{2.35}$$

i.e., they have absolute value 1 and phase identical to the corresponding element of the matrix $\mathbf{H}_k$, ensuring that the elements of the main diagonal of $\mathbf{A}_k^H \mathbf{H}_k$ are much bigger than the outside of the main diagonal. In this case, the linear frequency domain equaliser/signal separation performing EGC at each frequency uses

$$\mathbf{F}_k = \boldsymbol{\kappa} \mathbf{A}_k^H. \tag{2.36}$$

However, for both cases, the residual interference levels can still be substantial, especially for moderate values of N_R/N_T.

2.6.4 BER performance comparison for linear equalisers

In this subsection, a brief comparison of the previously presented equalisers is presented in order to show their potential. Three different MIMO scenarios are tested: all of them with 16 transmitters each one with 1 transmitting antenna and at the reception 64, 128 and 256 antennas have been used. The system employs SC-FDE transmission that uses a 4-QAM constellation with data blocks of size $N_{block} = 256$. Pulse shaping is not performed. Channel is assumed time-dispersive channel with four multipath components and it is also assumed that system employs a Cyclic Prefix (CP) longer than the maximum overall channel impulse response to effectively cancel ISI.

Fig. 2.13 makes clear that ZF and MMSE equalisers are the best option to deal with MIMO, even when the ratio between receiving and transmitting antennas is low. However, when there

is an increase in the number of antennas at the reception, not only MMSE and ZF improve their performance, as well as, MRC and EGC. This behaviour is expected because the approximations when defining these equalisers are made in the assumption of much more antennas at the receiver side. These results are particularly attractive for m-MIMO schemes. Based on them, in chapter 4, the equalisers herein presented will be used iteratively to improve their performance, with their iterative version being used in the proposed multilayer m-MIMO scheme.

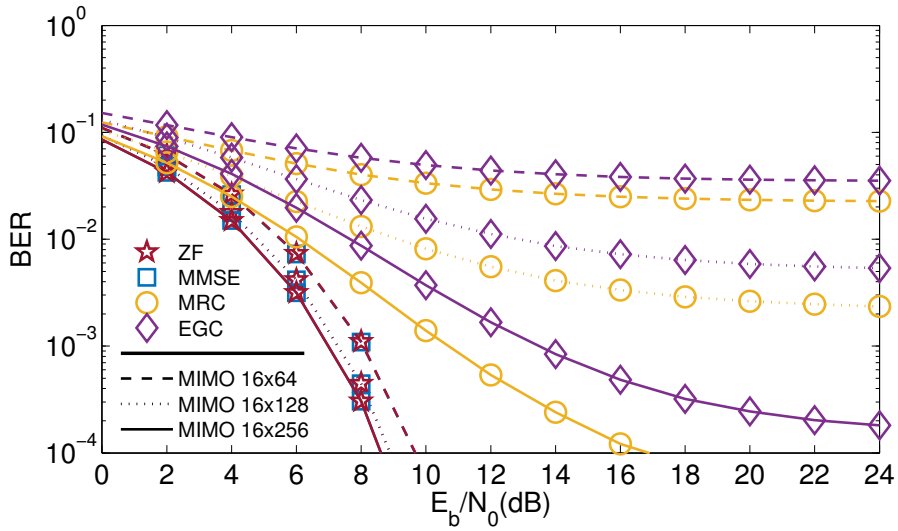

Figure 2.13 BER performance comparison for several linear equalisers in three different MIMO scenarios.

3

A new multilayer MIMO architecture at mmWave bands

In the next generation wireless communication systems, the demand for spectral and power efficient schemes is one of the main challenges. To achieve a high power efficiency, one needs low PAPR values, which means lower back-off in the operation of the PA [65]. For this reason, Single Carrier (SC) modulations, which usually have a lower PAPR than multi carrier ones, are preferred to be used in the uplink for wireless transmissions [66]. Moreover, to achieve a high spectral efficiency, large constellations combined with selective filtering are required. Nevertheless, SC modulations employed with large constellations still have high PAPR values, make them more sensitive to non-linearities in the PA. To improve the power efficiency of the system, decomposition of large constellations into OQPSK-type signals and/or envelope control techniques could be used.

In the present chapter, a new multilayer MIMO architecture at mmWave bands is proposed. This architecture allows the use of constellation decomposition and/or envelope control tech-

niques. The chapter starts with an overview of the architecture. Then, Magnitude Modulation (MM), an envelope control technique, is presented and a BER analysis is performed. Following, decomposition of large constellations is addressed and the chapter concludes with a detailed description of transmitter and receiver modules.

The work addressed in this chapter has resulted in one patent submitted in Portugal and in the USA [21, 22], one journal article [23] and five articles in international conferences [19, 20, 28, 29, 67].

3.1 A new multilayer m-MIMO scheme

The high bitrates, combined with large constellations (required for high spectral efficiencies) and mmWave bands means very high power requirements. Moreover, large bandwidths together with multipath propagation can lead to severely time-dispersive channels, especially when overall transmitter and receiver directivities are not high. Finally, although m-MIMO schemes are suitable for mmWave frequencies and allow substantial gains in terms of both power and spectral efficiency, its implementation might be too complex, both at the analogue and the digital domains, and sub-optimal implementations are required. To overcome these difficulties, we take advantage of state-of-the-art RF front-end technologies (including power amplifiers and antenna arrays) and we develop new digital signal processing schemes for the novel multilayer m-MIMO architecture depicted in Fig. 3.1. This new architecture is based on the following approach:

1. Adoption of large and dense constellations allowing high spectral efficiency with reduced power requirements for a given constellation size [68].

2. SC-FDE schemes to cope with severely time-dispersive channels [7, 15], with receivers designed taking into account signals' and mmWave channel characteristics [2, 17].

3. Multilayer m-MIMO schemes with up to three antenna layers at the transmitter [19–22], where:

    - 1st-layer is designed to efficiently amplify the different OQPSK-type components in which a given multilevel constellation can be decomposed [14, 15], by employing multiple Non-Linear Amplifiers (NLAs) and antennas, and with signals' combination performed at the wireless channel [16];

- 2nd-layer is used for BF purposes, to separate users, multipath components and/or increasing coverage;
- 3rd-layer is employed for SM, to allow multi-user support without directional constraints.

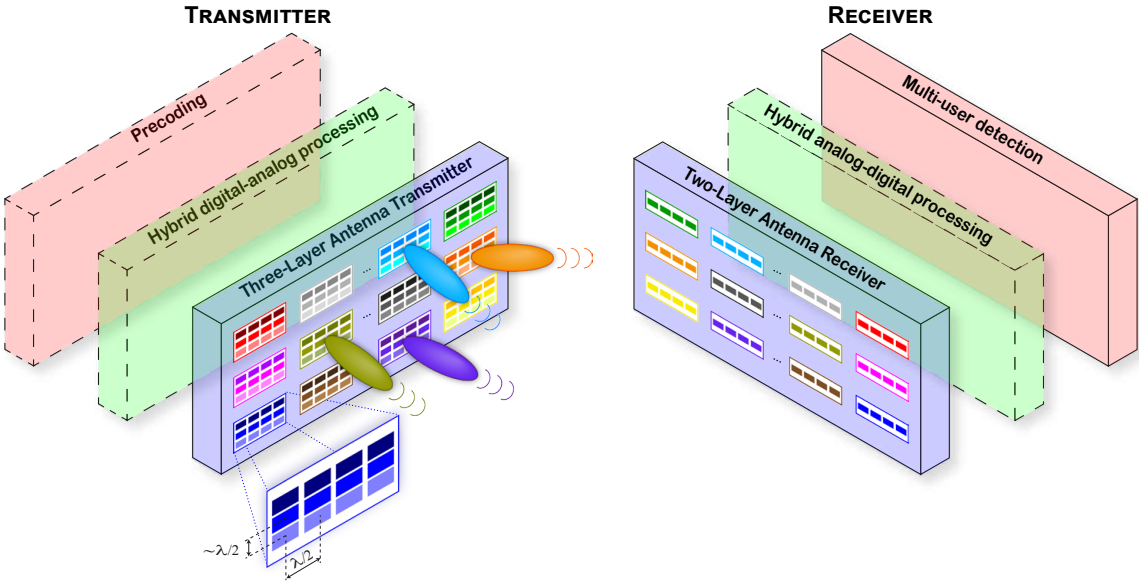

Figure 3.1 Proposed block diagram of the new multilayer m-MIMO architecture for mmWave bands with high power and spectral efficiencies.

This multilayer approach is a promising technique for mmWave bands, since the small wavelength allows a large number of antenna elements in a small space. However, it has important difficulties and challenges to be addressed.

First, large and dense constellations have high PAPR values, which reduces transmitter's power efficiency as discussed in chapter 2. There are two possible ways to fight against this phenomenon: the use of control envelope techniques, such as MM techniques [11, 12]; or decomposition into OQPSK components with quasi-constant envelope [14, 15] that are separately amplified. These both features will be addressed in the remaining of the chapter.

The second challenge is the fact that FDE design for offset modulations with SM is an open issue. We will develop appropriate FDE receivers based on the combination of pragmatic FDE implementations [17, 24] with IB-DFE based on multi-user detectors [7, 8]. This topic will be later addressed in chapters 4 and 5.

3.2 Magnitude Modulation (MM)

To limit the transmission band and improve spectral efficiency even of large constellations, one could employ a Nyquist pulse shaping Filter (NF) with bandwidth close to the minimum band (e.g., using RRC filtering), as mentioned early in section 2.4. Nevertheless, the signal components no longer have a constant envelope (although its envelope does not reach zero, it can still reach values of about $10\% \sim 20\%$ of the average, becoming sensitive to the non-linearities mentioned before, which precludes the use of NLAs). Hence, the main contribution for high PAPR on the transmitted signal comes from the pulse shaping filter (normally RRC). Taking this into account, the principle of MM [11, 12, 58, 59], illustrated in Fig. 3.2 and 3.3, can be used to control the signal's envelope at the output of pulse shaping filter. This is done by magnitude modulating, i.e., multiplying each complex modulated symbol s_n at the input of the bandwidth limiting pulse shaping filter by a time-varying real non-negative factor, m_n. The transmitted MM signal, x'_n, is thus given by

$$x'_n = p_n * \sum_k m_k s_k \delta_{n-kL} \ , \tag{3.1}$$

where p_n is the discrete pulse shaping impulse response, L is the oversampling rate at which the pulse shaping filter operates, δ_n denotes the discrete Dirac delta signal and '$*$' the discrete convolution.

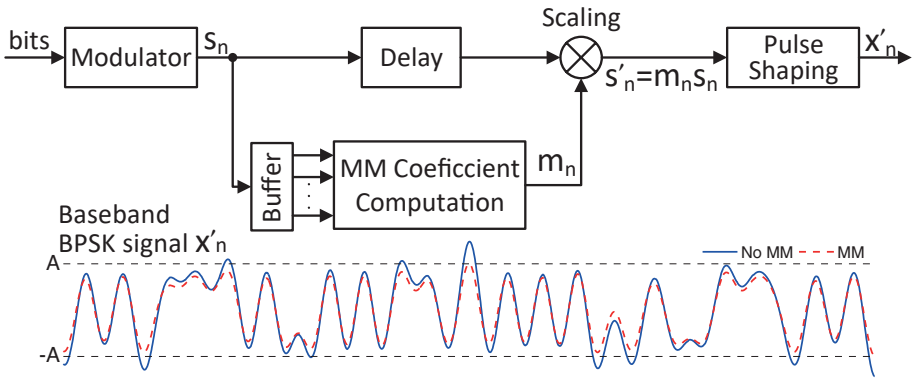

Figure 3.2 A generic block diagram of a transmitter performing MM and example of a BPSK signal to which MM was applied.

A maximum admissible amplitude, A, on the x'_n's envelope (i.e., to ensure $|x'_n| \leq A$) is usually set up according to the desired maximum allowed excursion that does not take the PA into saturation and reduces back-off, thus improving the transmitter's power efficiency. Each factor m_n is dependent on the limit A, the known impulse response of the pulse shaping filter, p_n, and the close

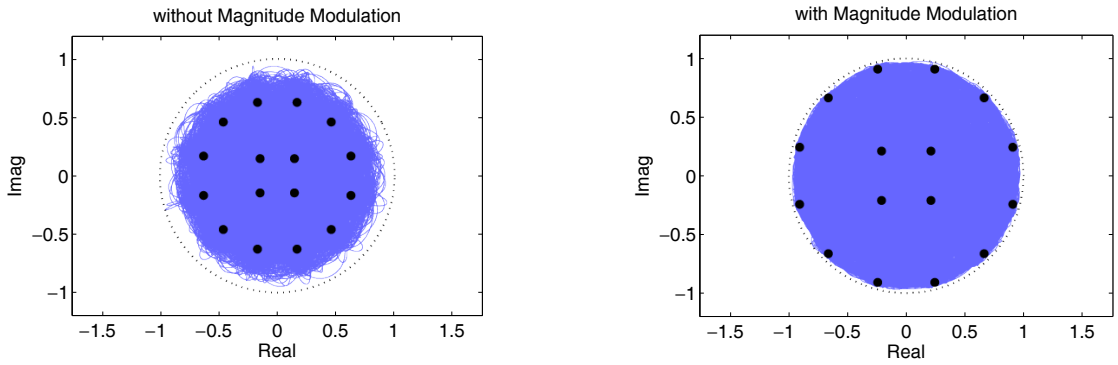

Figure 3.3 Example of a 16-Amplitude Phase-Shift Keying (APSK) constellation diagram with and without MM [69], where we can see that the outer envelope has been constrained.

symbol neighbours of s_n that manage to contribute (according to p_n's length) to the transmitted signal x'_n. MM factors can be computed either *a priori* for small size constellations with factors being stored in a Look-Up Table (LUT) [58, 70] for the various symbol combinations or they can be computed in real time by using the Multistage Polyphase Magnitude Modulation (MPMM) method that can be applied to any constellation size [11].

As can be seen in Fig. 3.2, MM smooth scales only the undesirable peaks, and since it acts before the pulse shaping it does not affect the spectral bandwidth, contrarily to conventional PAPR reduction techniques such as clipping. Moreover, by being able to considerably reduce the peak power while only causing a small decrease in the average power, the MM techniques lead to a considerable reduction in the PAPR and thus simplifying the power amplification procedure [65].

There are two approaches to perform MM scaling: Polar Scaling (PS) and Rectangular Scaling (RS). PS scales the amplitude of the complex symbol and the transmitted MM signal, x'_n, is given by (3.1). The RS approach scales in-phase and quadrature components of the signal, separately, and the transmitted MM signal, x'_n, in this case, becomes

$$x'_n = \left(\sum_k m_k^{(I)} s_k^{(I)} \delta_{n-kL}\right) * p_n + j \left(\sum_k m_k^{(Q)} s_k^{(Q)} \delta_{n-kL}\right) * p_n, \tag{3.2}$$

where the superscripts (I) and (Q) denote the in-phase and quadrature components, respectively.

However, MM may add some distortion to the signal. In the case of the PS approach, only the amplitude is affected, while when the RS approach is considered, not only the amplitude but also the phase could suffer some distortion. So even though RS approach can provide a more refined control of the envelope excursions than PS, since it has an additional degree of freedom, for the

sake of simplicity, in next subsections, only PS will be considered. This choice results from the fact that amplitude distortion by itself may not cause symbol errors, although it increases error sensitivity because symbols can become closer, as can be seen in Fig. 3.4. This figure shows the scatter plot of received MM symbols when subjected to AWGN noise, and it can be seen that clouds are elliptical instead of circular.

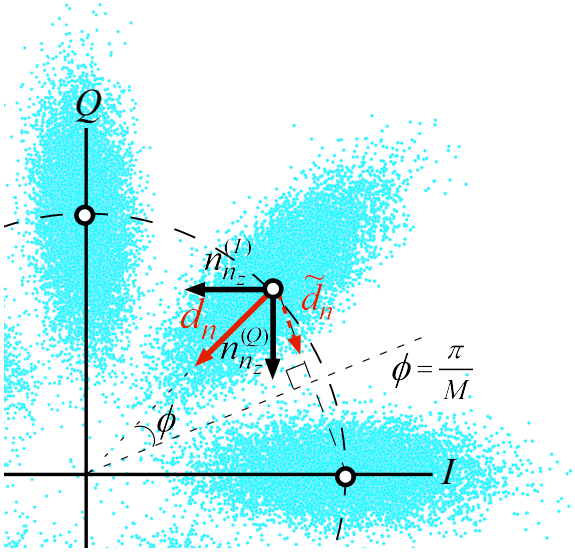

Figure 3.4 Example of a received MM PSK signal through the AWGN channel for a generic M-PSK transmission.

At last, it should be mentioned that these MM methods have only been designed to control the outer envelope. However, for OQPSK signals, the inner envelope could also be controlled, resulting in a ring shape as we have shown in [28, 29].

3.2.1 Simplified BER analysis of MM signals for the AWGN channel

This subsection is focused on the analytical study of M-PSK constellations combined with MM techniques in the AWGN channel. MM techniques can be employed [69, 70] to reduce envelope fluctuations of bandwidth limited signals, allowing for an enhanced power efficiency upon transmission. As will be discussed later, in section 3.4, PSK-type constellations combined with MM may be considered for the design of systems with high spectral and power efficiency for 5G and beyond, in particular within the structure of multilayer m-MIMO system architecture [19–22], presented in this thesis, for transmissions at mmWave wavelengths. To enable a performance evaluation of this new proposed MIMO architecture, a first step is required in the analytical easy assessment of MM PSK-type SISO transmission performance for different channels.

In [12] it was shown that MM factors, m_n, follow an extreme value distribution for PSK-type transmissions, and an analytical formula was derived for the BER performance at the AWGN channel. However, that formula is expressed by a cumbersome integral that is difficult to evaluate and also very hard to extend to other channel types. Also, it is shown in [12] that it is the correct modelling of the tail of MM factors' distribution that most influences the accuracy of any derived BER formula based on MM's distribution. Therefore, the use of a Gaussian approximation (while natural by the law of large numbers) is useful to obtain a simpler BER expression based on the Q-function.

In this subsection, a simplified analytical BER expression is developed. The use of Kullback-Leibler (KL) divergence, as it will be shown, allow us to measure in a simple way the divergence of the Gaussian approximation to the exact distribution of the MM factors, especially in the aforementioned tail zone. This fact allows to express the BER performance of M-PSK with MM in terms of the well-known Gaussian Q-function [51], which is straightforward to evaluate and, that can be applicable, not only, to the AWGN case, but also easily extendable to typical wireless selective channel, conditioned to the channel realisation [71], as will be seen in the next subsection.

System Characterisation

To perform the BER analysis of MM signals in the AWGN channel, a transceiver using the MM concept [58, 59] is considered. The input bit stream at the transmitter is mapped into an M-PSK constellation (with a Gray mapping and unitary symbol energy) with MM performed afterwards (implementing either the LUT-based or MPMM methods [11, 12, 58, 59]) giving rise to an MM sequence $s'_n = m_n s_n$. This sequence is filtered by the pulse shaping filter p_n, resulting in the envelope controlled signal x_n, as defined by (3.1). Only polar scaling MM is considered in order to avoid phase modulation effects (a problem for PSK transmissions). At the receiver, after perfect matched filtering, the signal is given by $y_n = s'_n + n_{n_z}$, where n_{n_z} is the zero-mean complex AWGN noise with power spectral density N_0, i.e., with variance $\sigma^2_{n_z} = \mathbb{E}\left[|n_{n_z}|^2\right] = N_0$ and $\mathbb{E}[\cdot]$ denotes the expectation operator.

Simplified analysis using a Gaussian approximation

To obtain a simplified expression for the BER of an uncoded M-PSK transmission using MM over the AWGN channel, we should first recall the non-MM case. The BER performance as a

function of the SNR, γ, is, in this case, approximated by (see, e.g., [51]),

$$P_e(\gamma) \simeq \frac{2}{\log_2(M)} Q\left(\sqrt{2\gamma}\sin\left(\frac{\pi}{M}\right)\right), \tag{3.3}$$

where $Q(.)$ is the Gaussian Q-function. The SNR is given by $\gamma{=}\sigma^2_{s_n}/\sigma^2_{n_z}$, with $\sigma^2_{s_n}{=}\mathbb{E}\left[|s_n|^2\right]{=}$ $=E_s{=}E_b\log_2(M)$[1], where E_s and E_b denote the energy per information symbol and per information bit, respectively, and M is the constellation size.

For the MM case, the received signal can be written as

$$y_n = s'_n + n_{n_z} = \bar{m}s_n + n_{n_z} + d_n, \tag{3.4}$$

where $\bar{m}s_n$ (with $\bar{m}{=}\mathbb{E}[m_n]$) is the average position of the constellation symbol after the MM procedure and d_n is the MM distortion defined as $d_n{=}s'_n{-}\bar{m}s_n$, having zero mean and power given by $\sigma^2_d = \mathbb{E}\left[|s'_n - \bar{m}s_n|^2\right]$.

Assuming a jointly Gaussian distribution of the total noise-distortion term, i.e., of $(n_{n_z}{+}d_n)$, when employing MM, the BER could be easily obtained from (3.3) with

$$\gamma{=}\frac{\mathbb{E}\left[|\bar{m}s_n|^2\right]}{\mathbb{E}\left[|n_{n_z}{+}d_n|^2\right]}. \tag{3.5}$$

However, to compute $\mathbb{E}\left[|n_{n_z}{+}d_n|^2\right]$, it should be noted that since MM polar scaling is considered, its distortion is of a rather particular type, being radial, i.e., $d_n = \pm|d_n|e^{j\arg\{s_n\}}$. Thus, the MM noise components applied to in-phase (I) and quadrature (Q) of s_n are highly correlated, giving rise to a total noise-distortion with an elliptical cloud shape as depicted in Fig. 3.4. Yet MM distortion is only relevant for BER analysis when it points in the direction that reduces the distance between symbols. This is also illustrated in Fig. 3.4, where vectors are used to represent d_n and the uncorrelated $n^{(I)}_{n_z}$ and $n^{(Q)}_{n_z}$ components of the AWGN, and the dashed vector $\tilde{d_n} = d_n\sin(\pi/M)$ corresponds to the projection of d_n in the direction that produces a symbol error detection[2]. The three components that could cause a symbol error, i.e., $n^{(I)}_{n_z}$, $n^{(Q)}_{n_z}$ and $\tilde{d_n}$, are independent, and

[1]The signal power is only equal to the symbol energy if T_s is considered unitary.

[2]MM increases sensitivity to noise only when the MM symbol s'_n approaches the centre of the constellation diagram. The distance from s'_n to the decision boundary between transmitted symbols (i.e., the bisectrix of angle ϕ in Fig. 3.4) measures this sensitivity to noise, and thus only the dashed line component $\tilde{d_n}$ of the MM distortion perpendicular to this decision boundary matters for the evaluation of the BER performance.

thus assuming that d_n follows a Gaussian distribution, it follows

$$\begin{aligned}\mathbb{E}\left[|n_{n_z}+d_n|^2\right] &= \mathbb{E}\left[|n_{n_z}^{(I)}\right] + \mathbb{E}\left[|n_{n_z}^{(Q)}\right] + \mathbb{E}\left[|\tilde{d_n}|^2\right] \\ &= \sigma_{n_z}^2 + \sigma_d^2 \sin^2(\pi/M). \end{aligned} \tag{3.6}$$

In fact, MM factors do not follow a Gaussian distribution, and therefore the added MM distortion does not follow it either, although they are close to one another as can be seen in Fig. 3.5. However, for low values of M (i.e., in the left tail zone of the distribution that is marked in Fig. 3.5), the Probability Density Function (PDF) of Gaussian distribution is lower than the MM histogram, resulting in underestimated BER results; this zone is more relevant for BER analysis because low values of m_n cause an increment in the noise sensitivity. Thus, for accurate BER results, one needs to evaluate the deviation shown by the MM distribution relative to the Gaussian distribution.

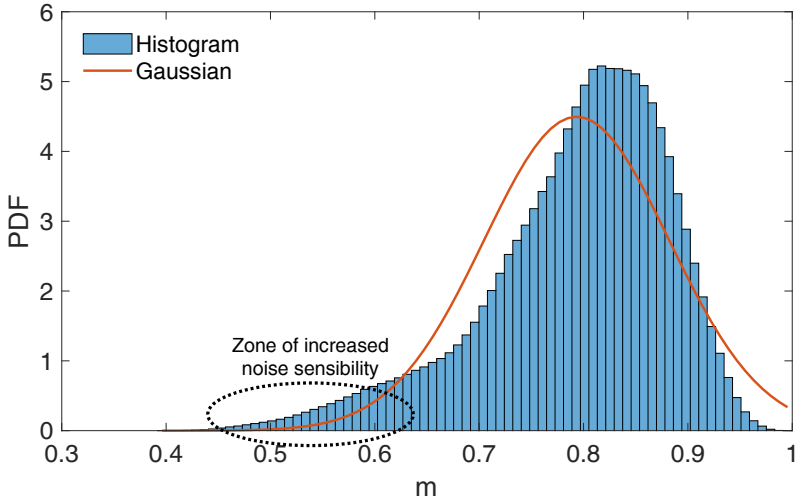

Figure 3.5 Histogram of MM factors of a system performing QPSK, using an RRC with roll-off β=0.2 and setting A=1, and the PDF of the Gaussian distribution with same mean and variance.

Measuring divergence of the MM factors' PDF from Gaussian approximation

One well-known way to measure the divergence between PDFs is the KL divergence [72], given by

$$D_{\mathrm{KL}}\left(X_1||X_2\right) = \int_{-\infty}^{+\infty} f_{X_1}(x) \log_2 \frac{f_{X_1}(x)}{f_{X_2}(x)} dx, \tag{3.7}$$

where f_{X_1} and f_{X_2} are the PDFs of the distributions X_1 and X_2, respectively. In this case, X_1 is the MM factors' distribution and X_2 is the Gaussian distribution with same mean and variance. Although (3.7) is in continuous form, it can be used in discrete form by replacing the Gaussian distribution by a similar discrete distribution (and replacing the integral by a sum), allowing a simple estimation of D_{KL}.

From D_{KL}, it is possible to define a correction weighting factor α in the MM distortion, i.e., the second term in (3.6), to obtain an accurate BER expression. Thus, for an M-PSK system with MM, the equation (3.3) with γ given by (3.5), becomes

$$P_e^{\text{MM}}(\gamma) \simeq \frac{2}{\log_2(M)} Q\left(\sqrt{\frac{2\bar{m}^2 E_s}{\sigma_{n_z}^2 + \alpha\sigma_d^2 \sin^2(\pi/M)}} \sin\left(\frac{\pi}{M}\right)\right). \tag{3.8}$$

Now, the key issue is how to relate D_{KL} to α. Although there is no straightforward relation between them, it is possible to define an optimisation problem, that expresses α as a simple function of D_{KL}. This approach makes the calculation of α, and also the analytical BER (given by (3.8)) straightforward , given just the simple computation of the D_{KL} of MM factors' PDF to the Gaussian approximation.

Optimising the correction factor

Different M-PSK constellations were considered to determine the relation between D_{KL} and α. One of them is 16-PSK, although it has low practical interest, it is only presented here to show that the method can be used for other M-PSK constellations. For all the cases, BER values were obtained by Monte Carlo simulation and then an optimisation problem was defined, where the maximum distance between these simulation values and the ones obtained by (3.8) was minimised. Log-likelihood between simulation and analytical BER was used as the distance metric, paying heed to the fact that BER is usually expressed in a $\log_{10}(\cdot)$ scale as a function of γ, and that optimisation should be guaranteed over a wide range of γ values for which BER may differ in several orders of magnitude. The optimisation problem is defined as

$$\min_{\boldsymbol{\alpha}} \max \left| \log_{10}\left(\frac{P_e^{\text{MM}}(\gamma)}{\tilde{P}_e^{\text{MM}}(\gamma)}\right)\right|, \tag{3.9}$$

subject to $\alpha \geq 1$, where $\tilde{P}_e^{\text{MM}}(\gamma)$ is the BER obtained by simulation for a given SNR, γ.

Solving this problem by varying the constellation size, the pulse shaping roll-off β and the

MM maximum admissible amplitudes A, provides the graphs in Fig. 3.6, where α is plotted as a function of D_{KL}. The depicted curves, suggested a logarithmic relation between α and D_{KL}, thus, following a curve fitting optimisation, it was found that α can be expressed quite accurately as

$$\alpha = a_{\mathrm{fit}} \log_{10} D_{\mathrm{KL}} + b_{\mathrm{fit}}, \tag{3.10}$$

with parameters presented in table 3.1.

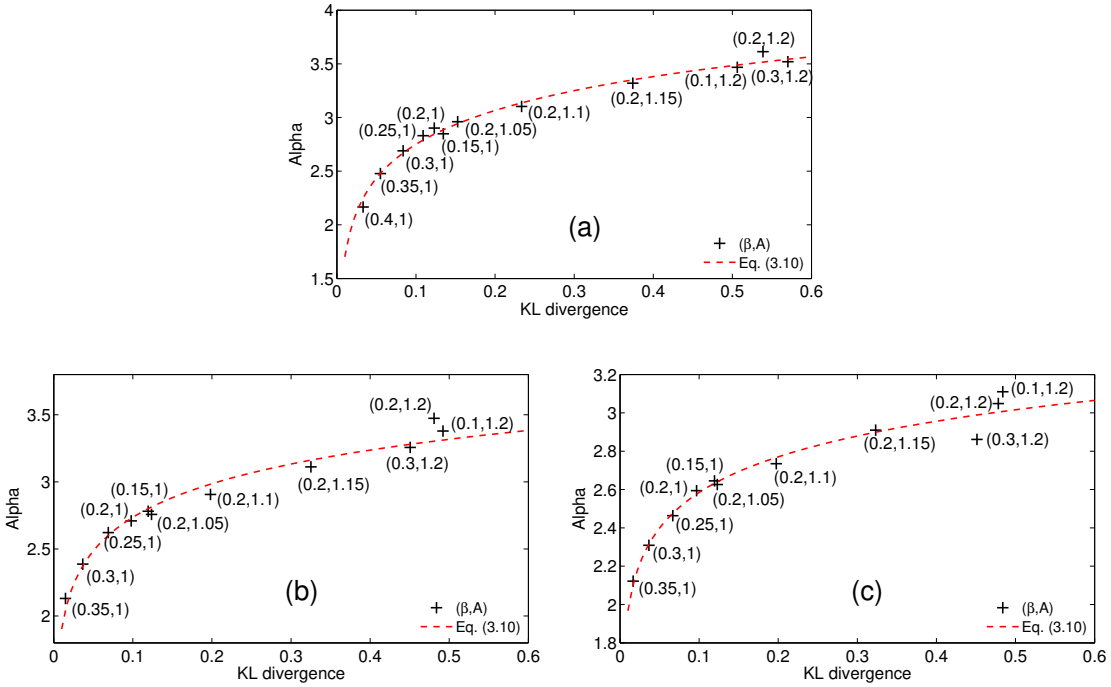

Figure 3.6 Relation between D_{KL} and α, for (a) QPSK, (b) 8-PSK and (c) 16-PSK constellations using several roll-off, β, and MM maximum admissible amplitude, A, values.

In brief, the BER performance of M-PSK with MM can be calculated straightforwardly using (3.8), after the simple computation of (3.7), followed by (3.10) to obtain α.

Table 3.1 Set-up parameters of equation (3.10).

	QPSK	**8-PSK**	**16-PSK**
$a_{\mathbf{fit}}$	1.048	0.8326	0.6174
$b_{\mathbf{fit}}$	3.798	3.568	3.202

Performance Results

Results given by (3.8) were compared with simulation ones, as well as with the ones obtained by the theoretical expression proposed in [12], for different M-PSK constellations and MM carried with 1-stage MPMM technique [11]. To test the robustness of the proposed approach, several cases that were not used in the optimisation problem were included; different values of pulse shaping roll-off ranging from 0.1 to 0.5 were considered, and the value A=1 was chosen for the MM maximum admissible amplitude to ensure a good envelope control, and A=1.2 was chosen where the effects of MM are reduced. The histogram of MM factors was used to compute D_{KL} through a numerical approximation of (3.7)[3], followed by determining α using (3.10) for the corresponding constellation.

Fig. 3.7 presents BER performance as a function of E_b/N_0 for the case of β=0.22, that is the typical value for Long Term Evolution (LTE) standard [73], and the stringent β=0.1, in order to show that (3.8) can be used in the analysis of future systems where β will become smaller. Fig. 3.7 shows that (3.8) is in fact very accurate for both tested configurations, and that, although simple to compute, it performs better than the previously proposed analytical BER expression [12], which, as seen in Fig. 3.7, underestimates the results obtained by Monte Carlo simulation.

Alternatively, in Fig. 3.8, BER is plotted as a function of the roll-off β for a given fixed E_b/N_0. For each constellation two values of E_b/N_0 were selected, corresponding to the points of BER= 10^{-3} and 10^{-4} shown in Fig. 3.7. In this case, too, the good fit between the analytical and simulation results bears out the accuracy of the parameters present in table 3.1.

3.2.2 BER analysis in time-dispersive channels

The BER analysis for time-dispersive channels becomes more relevant than AWGN one, mainly when SC modulations are used. For time-dispersive channels, SC is usually performed using a block-based transmission with FDE; SC signals samples are transmitted in blocks $\{s'_n : n{=}0, \cdots, N_{block}{-}1\}$ padded with an appropriate Cyclic Prefix (CP) longer than the length of the channel impulse response of the time dispersive channel. At the receiver, after CP removal, the unitary DFT is applied to the received signal block, and this is equalised in the frequency domain.

Let S'_k=DFT$\{s'_n\}$ denote the N_{block}-point unitary DFT of the transmitted block

[3]The integral (3.7) was approximated by a summation using the trapezoidal rule, based on a histogram with 75 bins within the range of the MM factors obtained.

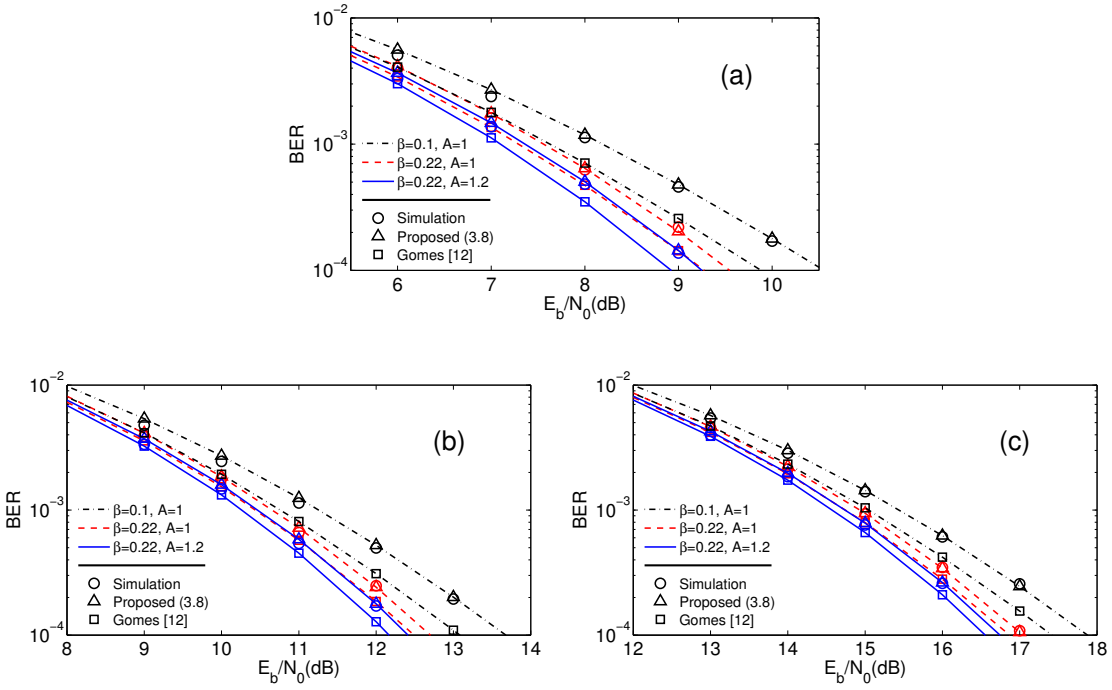

Figure 3.7 BER of (a) QPSK, (b) 8-PSK and (c) 16-PSK on the AWGN channel when using MM, 1-stage MPMM, different roll-off and MM maximum admissible amplitude values.

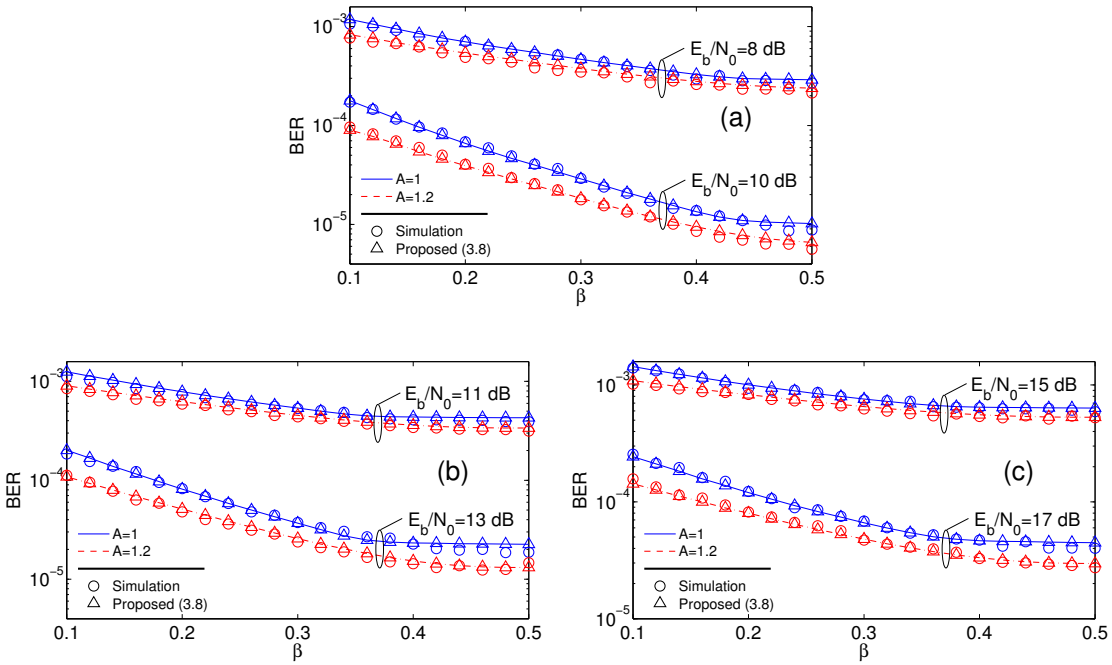

Figure 3.8 BER as a function of roll-off β, considering a fixed E_b/N_0, for (a) QPSK, (b) 8-PSK and (c) 16-PSK on the AWGN channel when using MM, 1-stage MPMM and different MM maximum admissible amplitude values.

$\{s'_n{:}n{=}0,\ldots,N_{block}{-}1\}$, and $\{H_k{:}k{=}0,\cdots,N_{block}{-}1\}$ the frequency response of the channel. The received signal at the k-th subcarrier can be written as

$$Y_k = H_k S'_k + N_k, \quad k{=}0,\cdots,N_{block}{-}1, \tag{3.11}$$

where N_k is the DFT of the AWGN noise component. Signal Y_k is then submitted to a linear MMSE equaliser that retrieves an estimation of the original S'_k obtained as

$$\tilde{S}'_k = F_k Y_k, \quad \text{with} \quad F_k = \left(H_k^* H_k + 1/\gamma\right)^{-1} H_k^*, \tag{3.12}$$

where H_k^* denotes the complex conjugate of H_k and γ the channel SNR.

Assuming that no MM is used, the BER can no longer be obtained from (3.3), because the noise power in $\tilde{S}'_k$ is not equal to $\sigma^2_{n_z}$ as in the AWGN channel and it is time-variant; there is always some residual interference resulting from the equalisation process. Thus, the BER also varies, and it is only possible to obtain a semi-theoretical BER average, $\bar{P}_e$, across channel realisations based on computation of the MSE [74], with $\bar{P}_e$ being given by

$$\bar{P}_e = \frac{2}{\log_2(M)} Q\left(\sqrt{\frac{2E_s}{\sigma^2_{\text{MSE}}}} \sin\left(\frac{\pi}{M}\right)\right), \tag{3.13}$$

where σ^2_{MSE} is the variance of complex MSE computed as

$$\sigma^2_{\text{MSE}} = \frac{1}{N} \sum_{k=0}^{N-1} \mathbb{E}\left[\left|\tilde{S}'_k - S'_k\right|^2\right]. \tag{3.14}$$

Following (3.11) and (3.12), it is straightforward to obtain a theoretical expression for MSE considering a certain channel realisation which is given by

$$\begin{aligned} \mathbb{E}\left[\left|\tilde{S}'_k - S'_k\right|^2\right] &= \mathbb{E}\left[\left|F_k S'_k H_k + F_k N_k - S'_k\right|^2\right] \\ &= \left|F_k H_k - 1\right|^2 \sigma^2_{s'_n} + \left|F_k\right|^2 \sigma^2_{n_z}, \end{aligned} \tag{3.15}$$

where it is assumed that $\mathbb{E}\left[\left|N_k . S'^*_k\right|\right] = 0$ and $\sigma^2_{s'_n}$ denotes the average power of the MM symbols.

When MM is employed, note that (3.15) depends only on the transmitted MM symbol S'_k, and not on the original S_k; in fact, the MMSE tries to cancel only the distortion introduced by the channel. Therefore, the MM distortion d_n is independent of the channel impairment, and

similar reasoning to that for the AWGN channel can be followed, with the BER probability for the time-dispersive channel of an M-PSK system performing MM resulting directly from (3.8), thus

$$\bar{P}_e^{\mathrm{MM}}(\gamma) \simeq \frac{2}{\log_2(M)} Q\left(\sqrt{\frac{2\bar{m}^2 E_s}{\sigma^2_{\mathrm{MSE}} + \alpha\sigma_d^2 \sin^2(\pi/M)}} \sin\left(\frac{\pi}{M}\right)\right). \tag{3.16}$$

Performance Results

A comparison between the BER results obtained by simulation and the analytical expression (3.16) is presented next. M-PSK transmitters performing MM in the same way as the ones used in section 3.2.1 are tested, considering SC block-based transmission with $N_{block} = 1024$, over a severe time-dispersive channel with 32 symbol-spaced multipath components with uncorrelated Rayleigh fading. MMSE equalisation is applied at the reception assuming perfect synchronisation and channel estimation.

Fig. 3.9 gives the BER results for several cases using the correction factor α obtained from (3.10). They show that (3.16) is very accurate for all M-PSK cases considered, depending only on the size of the constellation and the KL divergence between the PDF of MM factors and the Gaussian PDF model.

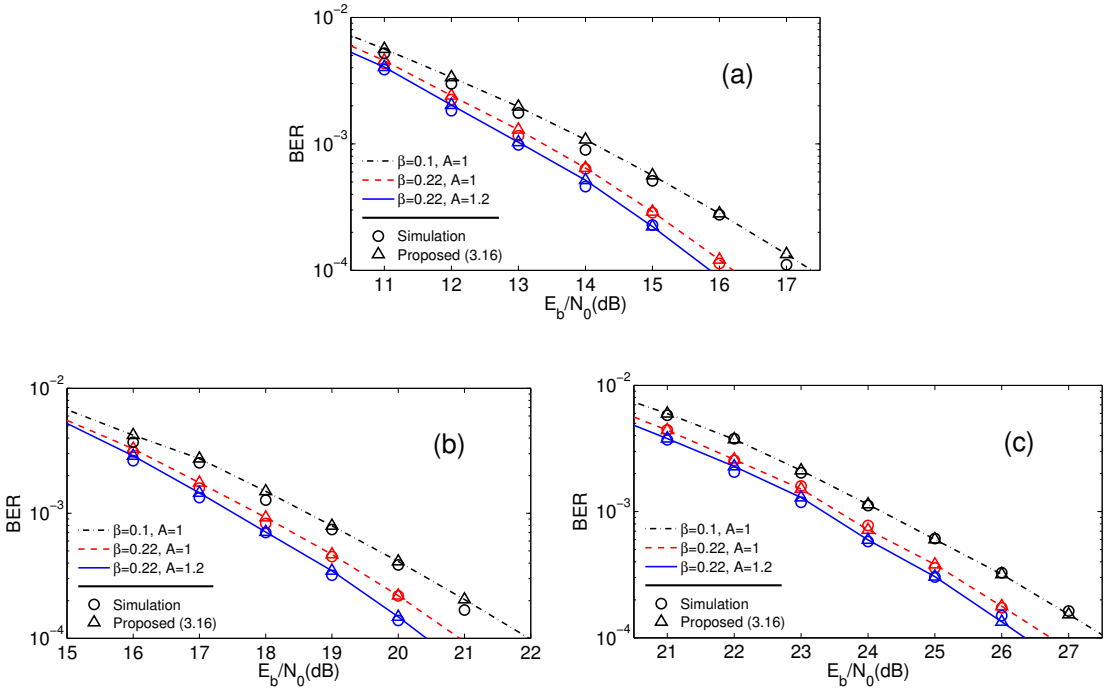

Figure 3.9 BER of (a) QPSK, (b) 8-PSK and (c) 16-PSK on a time-dispersive channel when using MM, 1-stage MPMM, different roll-off and MM maximum admissible amplitude values.

In conclusion, results show that the new proposed simplified BER expression for the analytical evaluation of systems performing MM with M-PSK constellations is quite accurate for both AWGN and time-dispersive channels and for different system parameters, such as MM maximum admissible amplitude and roll-off of the pulse shaping filter, depending only on the constellation size and the KL divergence between the PDF of MM factors and the Gaussian PDF model. The proposed BER expression makes the fast assessment of the performance M-PSK signals with MM possible in a straightforward manner, without having to perform extensive Monte Carlo simulations. This expression can be very useful on the design and evaluation of the proposed multilayer architecture.

3.3 Decomposition of multilevel constellations

Conventional SC signals still require quasi-linear amplifiers, even when envelope control techniques are employed. To allow the use of NLAs, one needs constant or almost constant envelope signals. They can be obtained by using OQPSK type schemes [75]. For larger constellations, one could write the signals as the sum of constant envelope PSK-type components (e.g. BPSK or OQPSK) [14, 15] that can be separately amplified without distortion (or with reduced distortion) by different NLAs [16], which can be particularly interesting for mmWave frequencies, while combined with BF and/or SM.

Offset modulations have the quadrature component shifted relative to the in-phase component, resulting in reduced envelope fluctuations and reduced dynamic range of the bandwidth limited signals (after pulse shaping) which simplifies amplification. This reduction occurs because OQPSK modulation does not have zero crossings while QPSK has, as can be seen in Fig. 3.10. This feature makes offset constellations of particular interest, and fortunately, any regular M-ary constellation can be regarded as a linear combination of OQPSK components.

3.3.1 Mapping rule

Let's consider a generic M-ary Quadrature Amplitude Modulation (M-QAM) or M-ary Offset Quadrature Amplitude Modulation (M-OQAM)[4], with the set of constellations symbols being denoted by $\mathfrak{G}$ and where M denotes the number of constellation points. Each symbol s_n of this con-

[4] An M-OQAM constellation can be obtained by delaying the quadrature component by $T_s/2$ with respect to the in-phase component of the correspondent M-QAM constellation, with T_s being the symbol's duration.

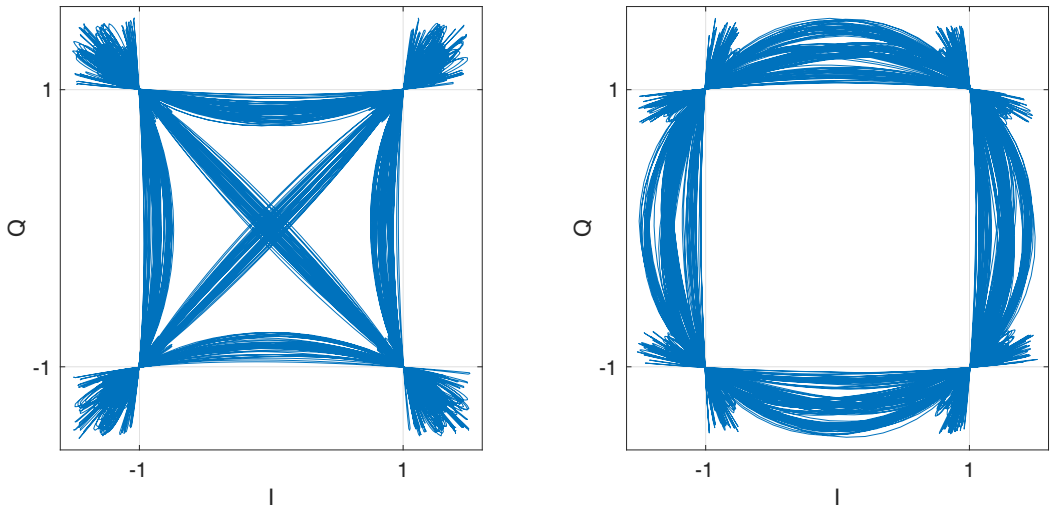

Figure 3.10 Comparison of transitions in a (a) QPSK modulation scheme and an (b) OQPSK modulation scheme.

stellation can be represented by its binary form $s_n \leftrightarrow \{\beta_n^0, \beta_n^1, \ldots, \beta_n^{\mu-1}\}$, with $\mu = log_2(M)$ bits, or in a equivalent polar form $s_n \leftrightarrow \{b_n^0, b_n^1, \ldots, b_n^{\mu-1}\}$, where $b_n^m = (-1)^{\beta_n^m}$, for $m = 0, \ldots, \mu-1$. The alphabet $\mathfrak{G}$ can be seen as the Cartesian product of two subsets $\mathfrak{G}^I$ and $j\mathfrak{G}^Q$, that disregarding the imaginary number are equal and for a square constellation[5] are composed by

$$\mathfrak{G}^I = \mathfrak{G}^Q = \{\pm 1, \pm 3, \cdots, \pm(\sqrt{M}-1)\}. \tag{3.17}$$

Thus, a symbol of a generic M-QAM or an M-OQAM, constellation can be represented as

$$s_n = s_n^{(I)} + j s_n^{(Q)}, \tag{3.18}$$

where $s_n^{(I)} \in \mathfrak{G}^{(I)}$ and $s_n^{(Q)} \in \mathfrak{G}^{(Q)}$ are the in-phase and the quadrature symbol's components, respectively. From (3.18), it is possible to see that both M-QAM and M-OQAM constellations can be represented as the combination of two $\sqrt{M}$-ary Pulse Amplitude Modulation (PAM) constellations with $\mu_p = log_2(\sqrt{M})$ bits per symbol. Moreover, each one of this $\sqrt{M}$-PAM constellations can be seen as the sum of N_p polar components with different powers [76].

[5]For matter of simplicity, and as it is the common case, consider that constellations are square, i.e. $\log_2(M)$ is even, and that the bit-mapping along in-phase and quadrature axis is the same.

Polar representation of $\sqrt{M}$-PAM

In fact, it is possible to express each symbol of the $\sqrt{M}$-PAM constellation as a linear function of the corresponding bits, i.e.,

$$\begin{aligned} s_{n_p} &= g_0 + g_1 b_{n_p}^{(0)} + g_2 b_{n_p}^{(1)} + g_3 b_{n_p}^{(0)} b_{n_p}^{(1)} + \\ &\quad + g_4 b_{n_p}^{(2)} + (\dots) + g_{\sqrt{M}-1} \prod_{m=0}^{\mu_p - 1} b_{n_p}^{(m)} = \\ &= \sum_{i=0}^{\sqrt{M}-1} g_i \prod_{m=0}^{\mu_p - 1} \left(b_{n_p}^{(m)} \right)^{\gamma_{m,i}} = \sum_{i=0}^{\sqrt{M}-1} g_i b_{n_p}^{eq(i)}, \end{aligned} \tag{3.19}$$

where s_{n_p} denotes the n_p-th symbol of the constellation, with $n_p = 0, \dots, \sqrt{M} - 1$, and g_i, with $i = 0, \dots, \sqrt{M}$ are the set of coefficients that rules the linear combination.

Also in (3.19), $(\gamma_{\mu_p - 1,i}, \gamma_{\mu_p - 2,i}, \dots, \gamma_{1,i}, \gamma_{0,i})$, corresponds to the binary representation of i, i.e., $i = \sum_{m=0}^{\mu_p - 1} 2^m \gamma_{m,i}$, and $b_{n_p}^{eq(i)} = \prod_{m=0}^{\mu_p - 1} \left(b_{n_p}^{(m)} \right)^{\gamma_{m,i}}$ to the i-th polar component of s_{n_p}.

Example. To have a better understanding, let's consider an example of an 8-PAM, meaning that $\mu_p = 3$. Therefore, $\gamma_{m,i}$ and $g_i b_{n_p}^{eq(i)}$ can assume the following values presented in table 3.2,

Table 3.2 Binary representation of i, i.e., $\gamma_{m,i}$, and $g_i b_{n_p}^{eq(i)}$ for an 8-PAM.

	$\gamma_{m,i}$			
i	**m=2**	**m=1**	**m=0**	$\mathbf{g_i b_{n_p}^{eq(i)}}$
0	0	0	0	$g_0 \cdot 1$
1	0	0	1	$g_1 \cdot b_{n_p}^{(0)}$
2	0	1	0	$g_2 \cdot b_{n_p}^{(1)}$
3	0	1	1	$g_3 \cdot b_{n_p}^{(1)} b_{n_p}^{(0)}$
4	1	0	0	$g_4 \cdot b_{n_p}^{(2)}$
5	1	0	1	$g_5 \cdot b_{n_p}^{(2)} b_{n_p}^{(0)}$
6	1	1	0	$g_6 \cdot b_{n_p}^{(2)} b_{n_p}^{(1)}$
7	1	1	1	$g_7 \cdot b_{n_p}^{(2)} b_{n_p}^{(1)} b_{n_p}^{(0)}$

and (3.19) becomes

$$s_{n_p} = g_0 + g_1 b_{n_p}^{(0)} + g_2 b_{n_p}^{(1)} + g_3 b_{n_p}^{(1)} b_{n_p}^{(0)} + g_4 b_{n_p}^{(2)} + \\ + g_5 b_{n_p}^{(2)} b_{n_p}^{(0)} + g_6 b_{n_p}^{(2)} b_{n_p}^{(1)} + g_7 b_{n_p}^{(2)} b_{n_p}^{(1)} b_{n_p}^{(0)}. \tag{3.20}$$

■

Returning to the general case, since there are $\sqrt{M}$ constellation symbols as well as $\sqrt{M}$ coefficients g_i, based on (3.19), it is possible to write a system of $\sqrt{M}$ equations for $n_p = 0, \ldots, \sqrt{M}-1$ to obtain the set of coefficients g_i. This system can be expressed in matrix form by

$$\mathbf{s} = \mathbf{W}\mathbf{g}, \tag{3.21}$$

where $\mathbf{s}$=$[s_0 \;\; s_1 \;\; \ldots \;\; s_{\sqrt{M}-1}]^T$ and $\mathbf{g}$=$[g_0 \;\; g_1 \;\; \ldots \;\; g_{\sqrt{M}-1}]^T$. It is shown in [76] that $\mathbf{W}$ results to be an Hadamard matrix with dimensions $\sqrt{M} \times \sqrt{M}$, and the coefficients g_i can be obtained from the inverse Hadamard transform of the vector of constellation points. In practice, $g_0 = 0$, since it is the centre of mass of the constellation; moreover, several other g_i can also be 0 [15] depending on the chose mapping between the μ_p-bit tuples and the symbols of the constellation. Denoting N_p as the number of nonzero g_i coefficients, then it is clear that a given constellation can be decomposed as the sum of $N_p \leq \sqrt{M}$ polar components [76].

When considering an uniform $\sqrt{M}$-PAM constellation, (that is the case that will be considered from now on) the only non-zero coefficients are $g_1, g_2, g_4, \cdots, g_{\sqrt{M}/2}$ (i.e., the coefficients $g_{2^m}, m = 0, 1, \cdots, \mu_p - 1$). Moreover, for a natural binary mapping, $g_{2^m} = 2^m$, with (3.19) becoming

$$s_{n_p} = \sum_{m=0}^{u_p-1} 2^m b_{n_p}^{(m)}. \tag{3.22}$$

While, to obtain a Gray mapping[6], (3.19) becomes

$$s_{n_p} = \sum_{i=0}^{\mu_p-1} 2^{\mu_p-1-i} \prod_{m=0}^{i-1} b_{n_p}^{(m)}. \tag{3.23}$$

Polar representation of M-QAM and M-OQAM

As M-QAM and M-OQAM constellations can be represented as the combination of two PAM constellations (since symbols are uniformly spaced along both in-phase and quadrature axis), their

[6]This is only one possibility to obtain a Gray mapping. There are others [76].

representation as sum of polar components results straightforward from combining (3.18) and (3.19). When the constellation is rectangular and the bit-mapping along in-phase and quadrature axis is the same, this results

$$\begin{aligned} s_n &= s_n^{(I)} + j s_n^{(Q)} \\ &= \sum_{i=0}^{\sqrt{M}-1} g_i \left(b_{n_p}^{eq(i,I)} + j b_{n_p}^{eq(i,Q)} \right). \end{aligned} \tag{3.24}$$

Each of the N_p polar components can thus be modulated as a BPSK signal [77], that can be seen as a serial representation of an OQPSK signal, enabling as so efficient implementations in m-MIMO context. The corresponding signals can then be separately amplified by N_p highly efficient, low-cost, strongly non-linear amplifiers before being transmitted by N_p antennas [16, 19].

However, offset signals with quasi-constant envelope (e.g., MSK or GMSK signals [47]) have poor spectral characteristics. Therefore, they should be specially designed to have acceptable trade-off between reduced envelope fluctuations and compact spectrum. Thus, while the use of RRC filtering (limiting the transmitted signal bandwidth towards the minimum Nyquist band) may cause an undesirable increase of signal's PAPR, MM can be combined with the decomposition of large constellation into OQPSK components to limit the envelope fluctuations of each band limited OQPSK component. Nonetheless, before combining these two techniques in mmWave m-MIMO schemes, there is the need of receivers that could equalise signals using offset constellations. This study will be done in chapter 5.

3.4 Transmitter structure

The decomposition of the signal associated to a given constellation in BPSK components and the possibility of having BPSK signals with reduced dynamic range [11, 12, 58, 59], together with compact spectrum by taking advantage of the relation between OQPSK signals in the serial format and BPSK signals [14, 15], are the key concepts behind our transmission architecture. Also, due to the small wave length of mmWave frequencies, we can have m-MIMO schemes with a large number of antennas packed in a relatively small space.

The transmitter structure is depicted in Fig. 3.11. The data bits are separated in N_u streams, each one is mapped in a given constellation which is the decomposed in $N_p \leq M$ polar com-

ponents. Each of the different polar components are then transmitted as an appropriate OQPSK signal in serial format, which is designed to have reduced envelope fluctuations and a small dynamic range, together with compact spectrum (e.g., as filtered MSK or GMSK signals). Due to the reduced envelope fluctuations, each of these components can be separately amplified with minimum distortion or even no distortion at all by a low complexity and high efficiency grossly non-linear amplifier.

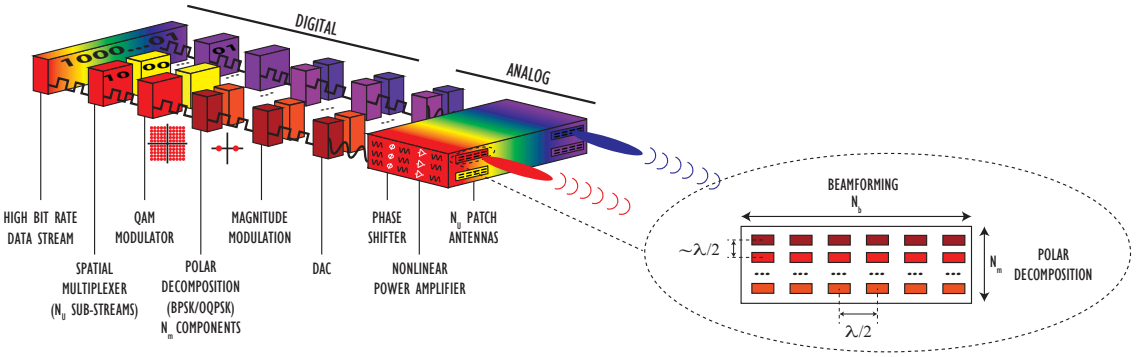

Figure 3.11 Generic block diagram of a multilayer m-MIMO transmitter for mmWave bands with high power and spectral efficiencies.

By combining the amplifier's outputs, we would obtain the signal associated to the intended constellation. However, combining these signals is not simple because we can have high combination losses and/or non-linearity problems at the combiner. To overcome this problem, we will send each of the N_p components of each of the N_u sub-streams to a different antenna. The set of N_p amplifiers, each one combined with a separate antenna performs some constellation shaping that is a function of the intended direction of radiation [78]. To avoid this shaping and simplify its compensation, the N_p antennas are placed vertically (where the direction of radiation is almost constant) and these antennas are assumed to be close to each other, with separation around $\lambda/2$ (with λ denoting the wavelength). The signals submitted to the N_p antennas associated to a given constellation symbol might have to be properly phase-shifted to allow the desirable constellation in a given direction [78].

The signal associated to each of the N_p BPSK/OQPSK components can be transmitted by N_b antennas instead of a single one, so as to allow BF effects. These N_b antennas are usually spaced by $\lambda/2$ and should be placed horizontally, since directive beams are usually intended to point to different azimuths (i.e., different horizontal directions). Therefore, we will have a transmitter with N_u sets of $N_p \times N_b$ antennas. These sets are separated by a distance much higher than

the wavelength so as to allow spacial multiplexing gains[7], as in a conventional Layered Space-Time (LST) scheme [8]. This means that we will have a massive antenna transmitter with a total of $N_T = N_u \times N_p \times N_b$ antennas divided in three different layers that employs saturated amplifiers and allows spacial multiplexing and BF gains.

For a better understanding, the transmission chain for each user is illustrated in Fig. 3.12. There, we can see the different stages of transmission: decomposition, envelope control and amplification. It also shown the combiner, that, desirably, will be the wireless channel, but can also be a physical one.

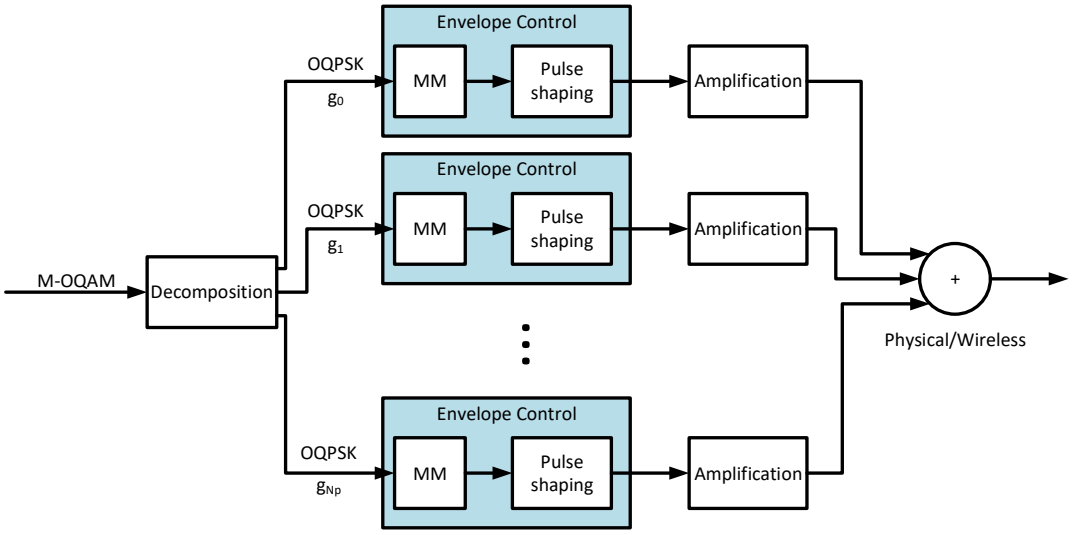

Figure 3.12 Transmission chain for a generic user of the proposed multilayer m-MIMO architecture at mmWave bands.

3.5 Receiver structure

At the receiver, we have $N_R = R_u \times R_b$ receiver antennas grouped in R_u sets of R_b antennas with the R_u sets separated by a distance much higher than the wavelength and the R_b BF antennas which, within each set, are typically separated by $\lambda/2$ (in general the number of BF antennas does not need to be the same at the transmitter and the receiver, although it is desirable to have at least as many sets of antennas at the receiver as the number of sets of $N_p \times N_b$ antennas used in the transmitter, i.e., $R_u \geq N_u$).

[7] Actually, the spacial multiplexing gain can be higher than the number of sets of $N_p \times N_b$ antennas, since we can have multiple beams, each one with the data symbols associated to a given user (provided the users can be spatially separated by the N_b BF antennas, naturally).

The basic receiver structure is depicted in Fig. 3.13. The equalisation and separation of the N_u data streams is performed by a frequency domain receiver based on the extension of the receiver proposed in [8] for general constellations [15]. However, this receiver needs to be appropriately modified taking into account the OQPSK nature of the transmitted signals, as proposed in [17]. The cyclic prefixes of the received blocks associated to each reception antenna are removed and the resulted blocks are submitted to DFT blocks, leading to a set of R_u frequency domain blocks $Y_k^{(r)}; k = 0,1,\ldots,N_{block}-1, r = 1,2,\ldots,N_R$. To detect the data symbols associated to a given data stream, these blocks are submitted to a set of N_R frequency domain feedforward filters $F_k^{(t,r)}; k = 0,1,...,N_{block}-1, t = 1,2,\ldots,N_T, r = 1,2,\ldots,N_R$. The data estimations associated to each data stream are used to compensate transmission imperfections (frequency offsets [79, 80], phase noise [81, 82], channel estimation errors [83], etc.) and to remove residual ISI and other interference through the set of N_T feedback coefficients $B_k^{(t,t)}; k = 0,1,...,N_{block}-1$, each one using the estimates of a given data stream from the previous iteration (more details could be found in [8]). These iterative receivers will be designed and adapted to mmWave channel characteristics and offset constellations in the following chapters.

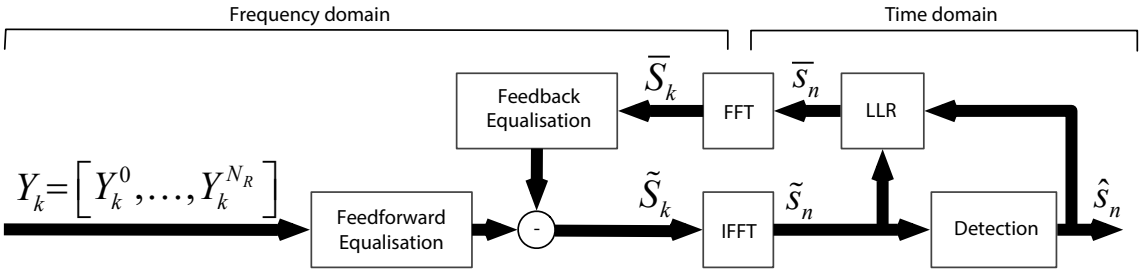

Figure 3.13 Generic block diagram of the iterative receivers to develop.

4

Iterative receivers for m-MIMO

The reception in m-MIMO schemes deals with multiple issues. These issues can result from multipath channels and/or multiple users in the system, which will cause interference between different replicas of the signal and/or different users, turning the signal separation one of the principal problems at the reception.

For optimal performance of the inter-antenna interference cancellation scheme, signal separation and equalisation should be performed together iteratively [7]. This fact is easily justified considering that to estimate a given signal, besides its equalisation, previous signals' estimations are also needed in order to produce an improved estimation through inter-antenna interference cancellation. In that sense, a MIMO equaliser should not only compensate the linear distortion caused by the channel frequency selectivity but also perform the signal separation.

A promising technique for SC-FDE schemes for the uplink MIMO channel is Iterative Block Decision Feedback Equalisation (IB-DFE) [7, 8, 74]. Receivers performing IB-DFE present an excellent performance, approaching the Matched Filter Bound (MFB) with only a few iterations [7, 8, 74]. However, one of the main challenges of multi-user m-MIMO schemes operating at

mmWave bands is the number of antennas that is feasible to use in a real m-MIMO system. Since the channel matrix dimensions grow with the number of antennas, conventional MIMO detection schemes such as IB-DFE can become too complex as the number of antennas is increased, namely due to the need to invert high dimension matrices for each subcarrier and each iteration. For this reason, m-MIMO schemes should employ simple equalisation techniques to separate data streams that avoid matrix inversions inherent to conventional MIMO receivers, while still able to achieve good performance. In that way, looking at section 2.6, where different linear equalisers for MIMO schemes have been presented, one could see that equalisers based on MRC and EGC concepts [50, 64] present significant gains when applied to scenarios with a large number of reception antennas (like the ones expected in m-MIMO schemes) without performing matrix inversions. However, their BER performance results are worse than ZF or MMSE. Therefore, in this chapter, an iterative approach similar to the one of the IB-DFE concept is applied to the receivers based on MRC and EGC concepts in order to improve their performance.

The chapter starts with a description of IB-DFE receivers for MIMO schemes that will serve as a basis for the iterative MRC and EGC receivers proposed in the next section. Then, a BER performance comparison of the different equalisation methods for multi-user m-MIMO schemes operating at mmWave bands, as well as, a complexity analysis are presented.

The work addressed in this chapter has resulted in one journal article [27] and another in an international conference [30]. This work has also been applied to multi carrier systems, giving rise to three articles in international conferences [31–33].

4.1 IB-DFE receiver

IB-DFE algorithms for multi-user/spatial multiplexing upon MIMO SC-FDE transmissions have been proposed and discussed in [7, 8, 74]. The main principle consists into the detection of each stream at a time while cancelling the interference from the already detected streams. The streams are ranked according to a quality measure, (e.g., the average received power) and detected from the best to worst ensuring that the stronger ones are not interfering when the weaker ones are being detected. This detection is done by performing iterative frequency domain equalisation with both feedback and feedforward filters, as shown in Fig. 4.1. Moreover, IB-DFE works on a per-block basis, meaning that the feedback's effectiveness to cancel all the interference is limited by the reliability of the detected data at previous iterations.

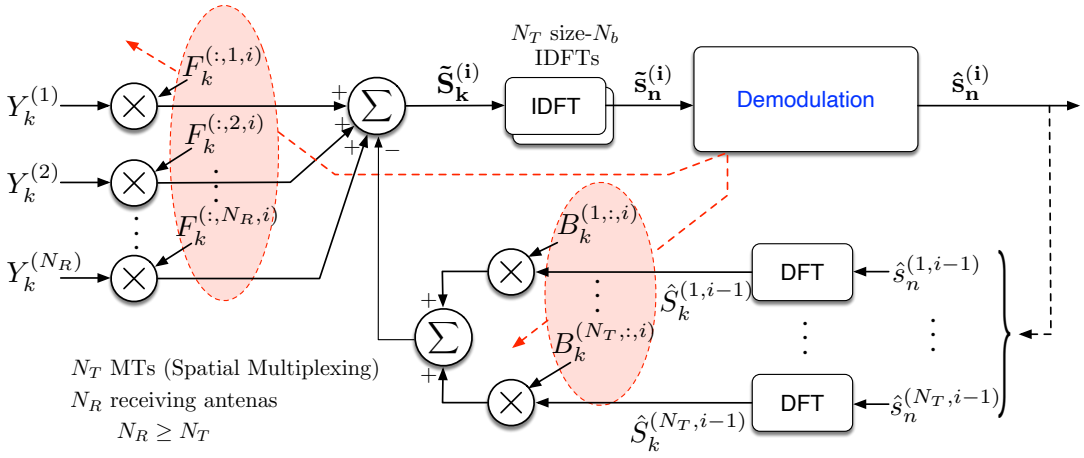

Figure 4.1 Generic block diagram of an IB-DFE receiver.

4.1.1 IB-DFE with hard decisions

Considering that the received signal at a given k frequency, $\mathbf{Y}_k$, is given by (2.5), the frequency domain estimations associated with the i-th iteration at the output of the equaliser are given by[1]

$$\widetilde{\mathbf{S}}_k^{(i)} = \mathbf{F}_k^{(i)}\mathbf{Y}_k - \mathbf{B}_k^{(i)}\hat{\mathbf{S}}_k^{(i-1)} \,, \tag{4.1}$$

where the feedforward and feedback matrices are

$$\mathbf{F}_k^{(i)} = \begin{bmatrix} F_k^{(1,1,i)} & \cdots & F_k^{(1,N_R,i)} \\ \vdots & \ddots & \vdots \\ F_k^{(N_T,1,i)} & \cdots & F_k^{(N_T,N_R,i)} \end{bmatrix} \tag{4.2}$$

and

$$\mathbf{B}_k^{(i)} = \begin{bmatrix} B_k^{(1,1,i)} & \cdots & B_k^{(1,N_T,i)} \\ \vdots & \ddots & \vdots \\ B_k^{(N_T,1,i)} & \cdots & B_k^{(N_T,N_T,i)} \end{bmatrix} , \tag{4.3}$$

respectively. $F_k^{(t,r,i)}$ and $B_k^{(t,t,i)}$ denote the feedforward and feedback filters coefficients at the i-th iteration and the vector $\hat{\mathbf{S}}_k^{(i-1)}$ contains the DFT of the hard-decision time domain blocks associated with the previous estimations for the transmitted symbols (for the first iteration those terms are zero, i.e., $\hat{\mathbf{S}}_k^{(0)} = \mathbf{0}_{N_T \times 1}$).

[1] In (2.30) and (2.32), it is obtained an estimation of the transmitted signal, $\widetilde{X}_k$, but here we want to retrieve the original symbols S_k before pulse shaping filter.

According to the Bussgang theorem [49], the hard-estimations $\hat{\mathbf{S}}_k^{(i-1)}$ can be seen as the sum of two uncorrelated components: one related to $\mathbf{S}_k$ and a distortion term. Hence, $\hat{\mathbf{S}}_k^{(i-1)}$ could be expressed as

$$\hat{\mathbf{S}}_k^{(i-1)} = \boldsymbol{\varrho}^{(i-1)}\mathbf{S}_k + \boldsymbol{\Delta}_k^{(i-1)}\ , \tag{4.4}$$

with

$$\boldsymbol{\Delta}_k^{(i-1)} = \left[\Delta_k^{(1,i-1)} \dots \Delta_k^{(N_T,i-1)}\right]^T, \tag{4.5}$$

where $\Delta_k^{(t,i-1)}$ represents the zero-mean quantisation error for the t-th transmitter at the iteration $(i-1)$, and

$$\boldsymbol{\varrho}^{(i-1)} = \text{diag}\left[\rho^{(1,i-1)} \dots \rho^{(N_T,i-1)}\right] \tag{4.6}$$

where $\rho^{(t,i-1)}$ is the correlation factor of the t-th transmitter at iteration $(i-1)$, which is expressed by

$$\rho^{(t,i-1)} = \frac{\mathbb{E}\left[S_k^{(t)}\left(\hat{S}_k^{(t,i-1)}\right)^*\right]}{\mathbb{E}\left[\left|S_k^{(t)}\right|^2\right]}. \tag{4.7}$$

The correlation factors supply a block-wise reliability measure of the estimates employed in the feedback loop, that is used to control the receiver's performance. This control is done taking into account the hard decisions for each block plus the overall block reliability, which reduces error propagation effects. Therefore, for the first iteration, the correlation factors are zero, i.e., $\boldsymbol{\varrho}^{(0)} = \mathbf{0}_{N_T \times N_T}$. Moreover, (4.6) is written as a diagonal matrix because it is assumed that the signals of the multiple transmitters are independent. This independence allied to $\mathbb{E}\left[\boldsymbol{\Delta}_k^{(i-1)}\right] = \mathbf{0}_{N_T \times 1}$, makes that from (4.4) results

$$\mathbb{E}\left[\left(\boldsymbol{\Delta}_k^{(i-1)}\right)\left(\boldsymbol{\Delta}_k^{(i-1)}\right)^H\right] \approx \left(\boldsymbol{I}_{N_T} - \left(\boldsymbol{\varrho}^{(i-1)}\right)^2\right)\mathbb{E}\left[\mathbf{S}_k\mathbf{S}_k^H\right], \tag{4.8}$$

with

$$\mathbb{E}\left[\mathbf{S}_k\mathbf{S}_k^H\right] = \sigma_{s_n}^2\boldsymbol{I}_{N_T}, \tag{4.9}$$

assuming that the transmitters are emitting the same power $\sigma_{s_n}^2$.

The feedback and the feedforward coefficients are chosen to minimise the MSE. For a generic MIMO system, the MSE of the t-th transmitter at iteration i and frequency k is given by

$$\Omega_k^{(t,i)} = \mathbb{E}\left[\left|\widetilde{S}_k^{(t,i)} - S_k^{(t)}\right|^2\right]. \tag{4.10}$$

Thus, to minimise the MSEs of all transmitters simultaneously, their sum should be minimised, i.e.,

$$\begin{aligned}\textbf{min}\ \ \boldsymbol{\Omega}_k^{(i)} &= \textbf{min}\ \ \sum_{t=1}^{N_T}\Omega_k^{(t,i)} = \\ &= \textbf{min}\ \ \sum_{t=1}^{N_T}\mathbb{E}\left[\left|\widetilde{S}_k^{(t,i)} - S_k^{(t)}\right|^2\right] = \\ &\overset{\text{(Prp. B)}}{=} \textbf{min}\ \ \mathbb{E}\left[\left(\widetilde{\mathbf{S}}_k^{(i)} - \mathbf{S}_k\right)^H\left(\widetilde{\mathbf{S}}_k^{(i)} - \mathbf{S}_k\right)\right],\end{aligned} \tag{4.11}$$

subject to

$$\frac{1}{N_{block}}\sum_{k=0}^{N_{block}-1}\sum_{r=1}^{N_R}F_k^{(t,r,i)}H_k^{(r,t)} = 1, \quad \text{with} \quad t = 1,\ldots,N_T, \tag{4.12}$$

in order to ensure the correct recovery of the transmitted signals. The set of constraints given by (4.12) can be grouped and written in matrix form as

$$\frac{1}{N_{block}}\sum_{k=0}^{N_{block}-1}\text{Tr}\left(\mathbf{F}_k^{(i)}\mathbf{H}_k\right) = N_T. \tag{4.13}$$

Using the method of Lagrange multipliers [84], it is possible to solve the problem defined in (4.11) and (4.13) as follows. We define the Lagrange function as

$$J_k^{(i)} = \mathbb{E}\left[\left(\widetilde{\mathbf{S}}_k^{(i)} - \mathbf{S}_k\right)^H\left(\widetilde{\mathbf{S}}_k^{(i)} - \mathbf{S}_k\right)\right] + \lambda_k^{(i)}\left(\frac{1}{N_{block}}\left(\sum_{k=0}^{N_{block}-1}\text{Tr}\left(\mathbf{F}_k^{(i)}\mathbf{H}_k\right)\right) - N_T\right), \tag{4.14}$$

where $\lambda_k^{(i)}$ corresponds to the Lagrange multiplier at iteration i and frequency k and the coefficients $\mathbf{F}_k^{(i)}$ and $\mathbf{B}_k^{(i)}$ that minimise the MSE could be obtained by solving the system of equations given by

$$\begin{cases}\nabla_{\mathbf{F}_k^{(i)}}(J_k^{(i)}) = \mathbf{0}_{N_T\times N_R} \\ \nabla_{\mathbf{B}_k^{(i)}}(J_k^{(i)}) = \mathbf{0}_{N_T\times N_T} \\ \nabla_{\lambda_k^{(i)}}(J_k^{(i)}) = 0\end{cases}. \tag{4.15}$$

After solving (4.15)[2], it is shown that the feedforward coefficients for iteration i are given by

$$\mathbf{F}_k^{(i)} = \boldsymbol{\kappa}\boldsymbol{\Lambda}_k^{(i)}{\mathbf{H}_k}^H, \tag{4.16}$$

[2]See appendix B for the full development of the optimisation problem.

where $\boldsymbol{\kappa}$ is a normalisation matrix[3] and $\boldsymbol{\Lambda}_k^{(i)}$ is given by

$$\boldsymbol{\Lambda}_k^{(i)} = \left(\frac{1}{\gamma} \left(\boldsymbol{I}_{N_T} - \left(\boldsymbol{\varrho}^{(i-1)} \right)^2 \right)^{-1} + \mathbf{H}_k^H \mathbf{H}_k \right)^{-1}, \tag{4.17}$$

with $\gamma = \sigma_{s_n}^2 / \sigma_{n_z}^2$ and

$$\sigma_{n_z}^2 = \mathbb{E}\left[\mathbf{N}_k^H \mathbf{N}_k \right]. \tag{4.18}$$

In its turn, the feedback coefficients for iteration i are given by

$$\mathbf{B}_k^{(i)} = \left(\mathbf{F}_k^{(i)} \mathbf{H}_k - \mathbf{I}_{N_T} \right) \boldsymbol{\varrho}^{(i-1)}. \tag{4.19}$$

Throughout the IB-DFE iterations, in general, the correlation coefficients in $\boldsymbol{\varrho}$ become higher while the deviations $\boldsymbol{\Delta}$ become lower, and the estimations are improved, enhancing the system BER performance. It must also be noted that at first IB-DFE iteration, (4.17) simplifies, corresponding to a linear MMSE-based equaliser.

4.1.2 IB-DFE with soft decisions

A way to improve the IB-DFE receiver is to use soft instead of hard decisions [15]. This improvement is achieved with the use of a different correlation factor for each symbol component instead of one factor that remains constant throughout the block. In this case, (4.1) becomes

$$\widetilde{\mathbf{S}}_k^{(i)} = \mathbf{F}_k^{(i)} \mathbf{Y}_k - \mathbf{B}_k^{(i)} \overline{\mathbf{S}}_k^{(i-1)}. \tag{4.20}$$

where $\overline{\mathbf{S}}_k^{(i-1)}$ denotes the average symbol values conditioned to the output of the equaliser at iteration $i-1$.

To obtain the values of $\overline{\mathbf{S}}_k^{(i-1)}$, one needs to demodulate the time domain estimations, $\tilde{\mathbf{s}}_n^{(i-1)}$, into the corresponding bits of each component. These bits[4] can be obtained by computing the Log-Likelihood Ratios (LLRs) associated with them. According to [15], the polar representation of the m-th estimated bit of the n-th transmitted symbol by the t-th transmitter at iteration $i-1$,

[3] Usually, $\boldsymbol{\kappa}$ is a diagonal matrix with size $N_T \times N_T$, with the values of position (t,t) given by the inverse of the Left Hand Side (LHS) of (4.12).

[4] Here, it will not be specified if these are in-phase or quadrature bits because the analysis is equal for both components. However, the reader should be aware that the formulas (4.21) to (4.26) refer only one component (i.e., the BPSK case), being applied to both the in-phase and quadrature components with their results being combined in (4.29).

$\bar{b}_n^{(t,m,i-1)}$, is related to the corresponding LLR, $\lambda_n^{(t,m,i-1)}$, by

$$\bar{b}_n^{(t,m,i-1)} = \tanh\left(\frac{\lambda_n^{(t,m,i-1)}}{2}\right), \tag{4.21}$$

with

$$\lambda_n^{(t,m,i-1)} = \ln\left(\frac{\Pr\left(\beta_n^{(t,m,i-1)}=1|\tilde{s}_n^{(t,i-1)}\right)}{\Pr\left(\beta_n^{(t,m,i-1)}=0|\tilde{s}_n^{(t,i-1)}\right)}\right) = \ln\left(\frac{\sum_{s\in\Psi_1^{(m)}} e^{\left(-\frac{|\tilde{s}_n^{(t,i-1)}-s|^2}{2\left(\sigma_{\text{LLR}}^{(i-1)}\right)^2}\right)}}{\sum_{s\in\Psi_0^{(m)}} e^{\left(-\frac{|\tilde{s}_n^{(t,i-1)}-s|^2}{2\left(\sigma_{\text{LLR}}^{(i-1)}\right)^2}\right)}}\right), \tag{4.22}$$

where $\beta_n^{(t,m,i-1)}$ denotes the binary representation of the m-th estimated bit of the n-th transmitted symbol by the t-th transmitter at iteration $i-1$, $\Psi_0^{(m)}$ and $\Psi_1^{(m)}$ are the subsets of $\mathfrak{S}$ containing a symbol s with $\beta_n^{(t,m,i-1)}=0$ or 1, respectively, and

$$\left(\sigma_{\text{LLR}}^{(i-1)}\right)^2 = \frac{1}{2}\mathbb{E}\left[|\tilde{s}_n^{(t,i-1)} - s_n^{(t)}|^2\right] \approx \frac{1}{2N_{block}}\sum_{n=0}^{N_{block}-1}|\tilde{s}_n^{(t,i-1)} - \hat{s}_n^{(t,i-1)}|^2, \tag{4.23}$$

where $\hat{s}_n^{(t,i-1)}$=IDFT$\left\{\hat{S}_k^{(t,i-1)}\right\}$.

Assuming uncorrelated bits and using (3.19), each of the components of the soft decision at iteration $i-1$ could be written as

$$\bar{s}_n^{(t,i-1)} = \sum_{i_p=0}^{\sqrt{M}-1} g_{i_p} \prod_{m=0}^{\mu_p-1}\left(\bar{b}_n^{(t,m,i-1)}\right)^{\gamma_{m,i_p}}, \tag{4.24}$$

where $\bar{s}_n^{(t,i-1)}$=IDFT$\left\{\bar{S}_k^{(t,i-1)}\right\}$ and $\bar{\mathbf{S}}_k^{(i-1)}$=$\left[\bar{S}_k^{(1,i-1)}\ldots\bar{S}_k^{(N_T,i-1)}\right]^T$.

Then, the reliability of each component of the estimates, either the in-phase and quadrature, to be used in the feedback loop at iteration $i-1$ is expressed by

$$\rho_n^{(t,i-1)} = \frac{\mathbb{E}\left[\bar{s}_n^{(t,i-1)}\left(s_n^{(t)}\right)^*\right]}{\mathbb{E}\left[\left|s_n^{(t)}\right|^2\right]} = \frac{\sum_{i_p=0}^{\sqrt{M}-1}|g_{i_p}|^2\prod_{m=0}^{\mu_p-1}\left(\rho_n^{(t,m,i-1)}\right)^{\gamma_{m,i_p}}}{\sum_{i_p=0}^{\sqrt{M}-1}|g_{i_p}|^2}, \tag{4.25}$$

where $\rho_n^{(t,m,i-1)}$ is the reliability of the m-th estimated bit of that component of the n-th transmitted

symbol by the t-th transmitter at iteration $i-1$, and it is given by

$$\rho_n^{(t,m,i-1)} = \tanh\left(\frac{|\lambda_n^{(t,m,i-1)}|}{2}\right). \tag{4.26}$$

When using soft decisions, the reliability is already included in $\overline{\mathbf{S}}_k^{(i-1)}$. Therefore, in this case, (4.19) does not need to include it in its calculation and becomes

$$\mathbf{B}_k^{(i)} = \mathbf{F}_k^{(i)}\mathbf{H}_k - \mathbf{I}_{N_T}. \tag{4.27}$$

On the other hand, the feedforward coefficients are still obtained by (4.16), but (4.17) becomes

$$\mathbf{\Lambda}_k^{(i)} = \left(\mathbf{H}_k\left(\boldsymbol{I}_{N_T} - \left(\overline{\boldsymbol{\varrho}}^{(i-1)}\right)^2\right)\mathbf{H}_k^H + \frac{1}{\gamma}\boldsymbol{I}_{N_R}\right)^{-1}, \tag{4.28}$$

where $\overline{\boldsymbol{\varrho}}^{(i-1)}$ denotes a diagonal matrix with each element given by

$$\overline{\rho}^{(t,i-1)} = \frac{1}{2N_{block}}\sum_{n=0}^{N_{block}-1}(\rho_n^{(I)} + \rho_n^{(Q)}), \tag{4.29}$$

with $\rho_n^{(I)}$ and $\rho_n^{(Q)}$ obtained using (4.25) applied to the in-phase and quadrature components, respectively[5].

4.2 Iterative MRC and EGC receivers

As matrix inversions could be a problem in m-MIMO schemes, receivers based on MRC and EGC concepts [50, 64] present lower complexity than ZF, MMSE or IB-DFE.

However, in section 2.6, it has been shown that, in both cases, linear equalisers present substantial residual interference levels, especially for moderate values of N_R/N_T. To overcome this problem, iterative receivers inspired by the IB-DFE concept are proposed in this section.

4.2.1 Motivation

The MRC and EGC techniques are appropriate when $N_R/N_T \gg 1$ (which is a reasonable approach for the uplink of m-MIMO systems) and the channels between different transmit and receive antennas have a small-to-medium correlation. In fact, for the next generation systems,

[5]Here, the superscripts $(t, i-1)$ have been omitted to lighten the notation.

these conditions can be verified, and MRC and EGC based receivers could be a low complexity solution for equalisation, presenting very good performance.

These low complexity approaches take advantage of the fact that the cross-correlation between the columns of the channel matrix is relatively low, which means that the corresponding Gramian matrix $\left(\mathbf{H}_{(k,l)}\right)^H \mathbf{H}_{(k,l)}$ is almost diagonal for MRC, as well as, the matrix $e^{j\arg\left(\mathbf{H}_{(k,l)}\right)}\mathbf{H}_{(k,l)}$ for EGC. Fig. 4.2 to 4.4 show colour maps of the absolute value of Gramian matrix $\left(\mathbf{H}_{(k,l)}\right)^H \mathbf{H}_{(k,l)}$ and the matrix $e^{j\arg\left(\mathbf{H}_{(k,l)}\right)}\mathbf{H}_{(k,l)}$ for different correlation values and two different systems with N_T=16 and N_R=$R_b \times R_u$=4 × 16=64 or N_R=$R_b \times R_u$=4×8=32.

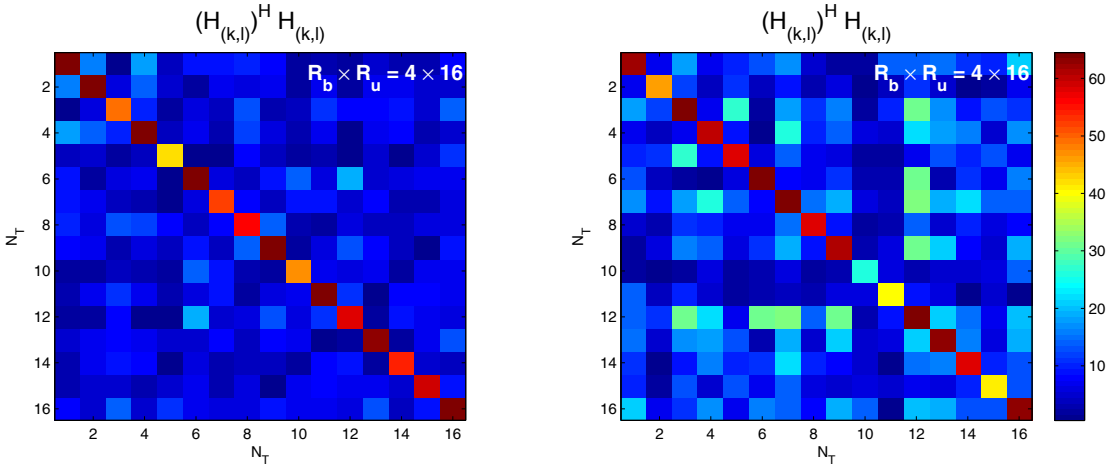

Figure 4.2 Colour map representing the magnitude of the absolute value of the Grammian matrix $\left(\mathbf{H}_{(k,l)}\right)^H \mathbf{H}_{(k,l)}$ in a system with $N_T = 16$ and $N_R = R_b \times R_u = 4 \times 16 = 64$ for (a) $\rho_u = 0.1$ and (b) $\rho_u = 0.9$.

In Fig. 4.2, it is shown that the most significant values are always in the main diagonal, with values outside the main diagonal increasing a little when the correlation becomes higher, showing that MRC principle is valid for low correlation. However, in this case, we are considering equal number of transmitters antennas and low correlated groups R_u with a ratio of N_R/N_T=64/16=4.

When the ratio is decreased, as for a system with $N_T = 16$ and $N_R = R_b \times R_u = 4 \times 8 = 32$, even for low correlation values, the difference between the main diagonal and the remaining values becomes reduced and for high correlation values, it is almost indistinguishable, as can be seen in Fig. 4.3. Therefore, to have better results with MRC, we should have at least the same number of low correlated antennas at the reception than at the transmission and to cope with scenarios with high correlation between reception antennas, their number should increase to fight this drawback.

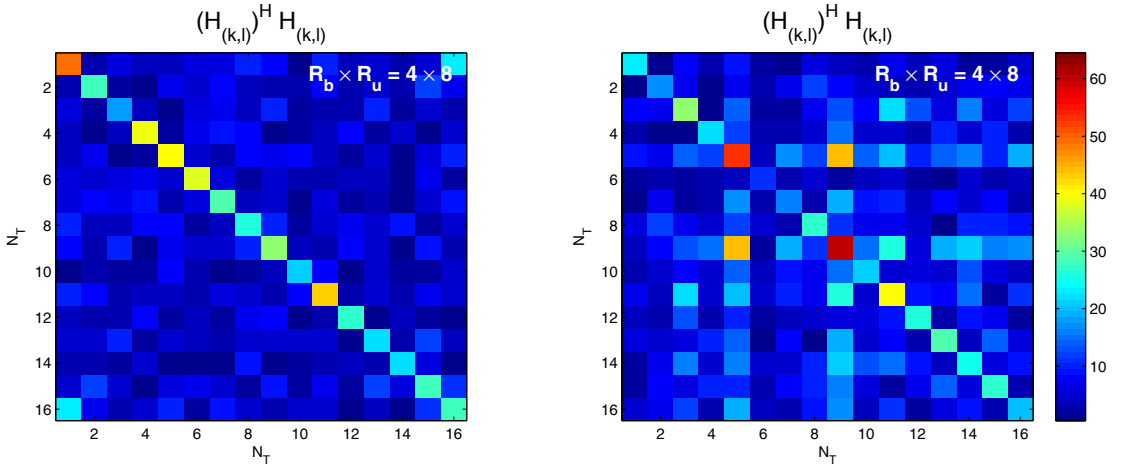

Figure 4.3 Colour map representing the magnitude of the absolute value of the Grammian matrix $\left(\mathbf{H}_{(k,l)}\right)^H \mathbf{H}_{(k,l)}$ in a system with $N_T = 16$ and $N_R = R_b \times R_u = 4 \times 8 = 32$ for (a) $\rho_u = 0.1$ and (b) $\rho_u = 0.9$.

At last, in Fig. 4.4, we see the matrix of $e^{j \arg\left(\mathbf{H}_{(k,l)}\right)} \mathbf{H}_{(k,l)}$, showing that the same conclusions taken for the MRC approach are also valid to EGC approach.

4.2.2 MRC and EGC Characterisation

It should be noted that, although the of-diagonal elements of the Gramian matrix converge to zero as we increase the number of receive antennas, the total power of them can still be similar to the power of the elements at the main diagonal when N_T is similar to N_R. For this reason, MRC or EGC receivers are only appropriate for the case when $N_T \ll N_R$. Since next generation communication systems can be designed to have high N_R/N_T ratios and many antennas that can be placed with distances of multiple wavelengths in a small space, especially for systems operating at mmWave frequencies, there will be conditions to use low complexity MRC and EGC based receivers. To adapt these receivers to offset signals, the iterative approach of IB-DFE can be employed using the block diagram of Fig. 4.1. Thus MRC and EGC receivers can also be iterative and can also use hard or soft decisions[6], with their output given by

$$\widetilde{\mathbf{S}}_k^{(i)} = \mathbf{F}_k \mathbf{Y}_k - \mathbf{B}_k \overline{\mathbf{S}}_k^{(i-1)} \,, \tag{4.30}$$

[6]Without loss of generality, in the remaining of the chapter, only soft decisions will be considered. The analysis for soft decisions is similar to the IB-DFE case and it follows the lines of subsection 4.1.2.

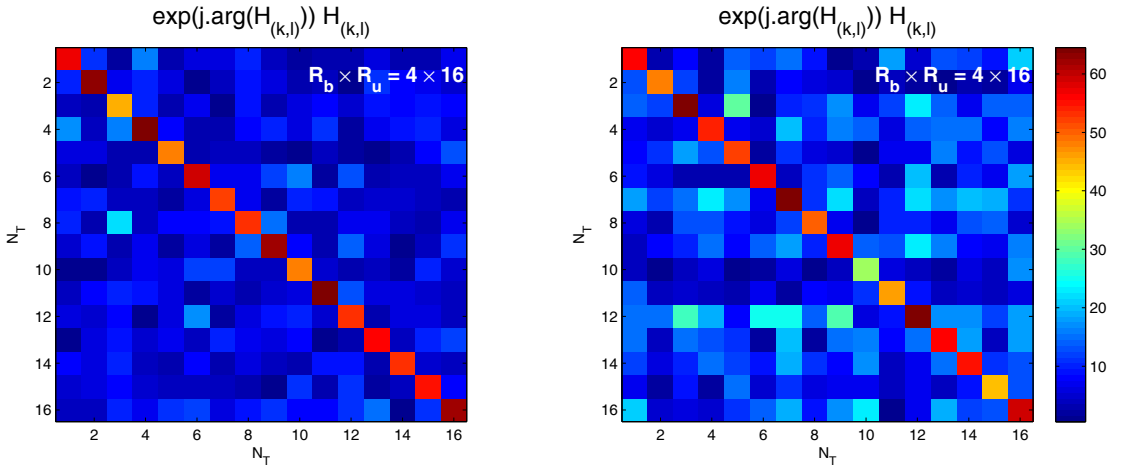

(a) (b)

Figure 4.4 Colour map representing the magnitude of the absolute value of the matrix $e^{j\arg\left(\mathbf{H}_{(k,l)}\right)}\mathbf{H}_{(k,l)}$ in a system with $N_T = 16$ and $N_R = R_b \times R_u = 4 \times 16 = 64$ for (a) $\rho_u = 0.1$ and (b) $\rho_u = 0.9$.

The main differences to the previous approach are that instead of obtaining the feedforward coefficients through (4.16) with the computation of high complexity equations (4.17) or (4.28), with the inversion of huge matrices for each frequency, MRC or EGC schemes use feedforward coefficients that are simpler to determine such as the Hermitian of the channel and the phase of the channel elements, respectively, and that do not depend on the iteration[7].

Hence, the feedfoward coefficients for the MRC receiver are given by

$$\mathbf{F}_k = \boldsymbol{\kappa}\mathbf{H}_k^H, \tag{4.31}$$

where $\boldsymbol{\kappa}$ denotes a normalisation diagonal matrix whose the (t,t)-th element is given by

$$\kappa^{(t,t)} = \left(\frac{1}{N_{block}} \sum_{k=0}^{N_{block}-1} \sum_{r=1}^{N_R} \left| H_k^{(r,t)} \right|^2 \right)^{-1}. \tag{4.32}$$

For the EGC receiver, it is considered

$$\mathbf{F}_k = \boldsymbol{\kappa}\mathbf{A}_k^H, \tag{4.33}$$

[7]It should be noted that, as in the MRC and EGC receiver of [64], the iterations are still required to cancel the residual inter-user interference levels, but feedforward and feedback filters are kept unchanged along the iterations.

with the elements of $\mathbf{A}_k$ given by (2.35) and $\boldsymbol{\kappa}$ denoting a normalisation diagonal matrix whose the (t,t)-th element is given by

$$\kappa^{(t,t)} = \left(\frac{1}{N_{block}} \sum_{k=0}^{N_{block}-1} \sum_{r=1}^{N_R} \left| H_k^{(r,t)} \right| \right)^{-1}. \tag{4.34}$$

Hereupon, it can easily be shown that the optimum values of $\mathbf{B}_k$ are still given by (4.27), but not depending on the iteration, becoming

$$\mathbf{B}_k = \mathbf{F}_k \mathbf{H}_k - \boldsymbol{I}_{N_T}. \tag{4.35}$$

The remaining process is equal to the one presented for the conventional IB-DFE. Therefore, iterative receivers based on MRC and EGC concepts are very similar to IB-DFE receivers but with the advantage of having fixed $\mathbf{F}_k$ and $\mathbf{B}_k$ matrices for the different iterations and not requiring complex matrix inversions, while obtaining almost the same BER performance for scenarios with $N_T \ll N_R$ and low correlation between antennas, as it will be shown in the next section.

4.3 BER Performance Evaluation

In this section, a BER performance comparison of the different receivers discussed in the previous sections is presented. This comparison is made using the channel model proposed in section 2.3.3. For the tests, 16 users with a single antenna are considered, each one producing 3 clusters with 4 rays, i.e., $N_{ray} = N_{ch\_clu} \times N_{ray\_clu} = 3 \times 4 = 12$, and it is also considered, without loss of generality, that the AoAs are uniformly distributed in $[0, 2\pi]$ (the extension to other cases is straightforward). Each antenna transmits 1000 blocks of $N_{block} = 256$ QPSK data symbols, and none coding technique is used. At the receiver, there is a total of 64 antennas, $N_R = 64$, that are arranged in three different ways:

- Scenario (A): all antennas belong to the same array, i.e., $R_b = 64$ and $R_u = 1$;
- Scenario (B): each group only contains one antenna, i.e., $R_b = 1$ and $R_u = 64$;
- Scenario (C): the antennas are grouped in arrays of 8 antennas, i.e., $R_b = 4$ and $R_u = 16$.

With these three scenarios, it is possible to infer the behaviour of each receiver in situations with different levels of correlation. The BER results are expressed as a function of E_b/N_0, with E_b

denoting the average bit energy for the set of N_R receive antennas (i.e., N_R times the bit energy for a single antenna), and N_0 denotes the unilateral power spectral density of the AWGN channel noise. The MFB performance is presented as a lower bound for the BER performance that can be attained, i.e., it represents the performance that one could obtain if the channel is perfectly equalised. When the AWGN channel is employed, MFB for a QPSK constellation is given by

$$P_b^{\text{MFB}} \approx Q\left(\sqrt{\frac{2E_b}{N_0}}\right). \tag{4.36}$$

The BER results for scenario A, where $R_u = 1$, are presented in Fig. 4.5. For iterative receivers, different iterations are presented. In this case, the antennas have a high correlation index, which is a drawback for MRC and EGC receivers. As expected, the residual interference levels (both ISI and the interference between different transmitted streams) are too high which causes an error floor, even in the 4-th iteration of MRC and EGC receivers. On the other hand, conventional IB-DFE receiver and ZF can reach a BER of 10^{-4}, with the first one being only 1.5 dB away of MFB after 4 iterations.

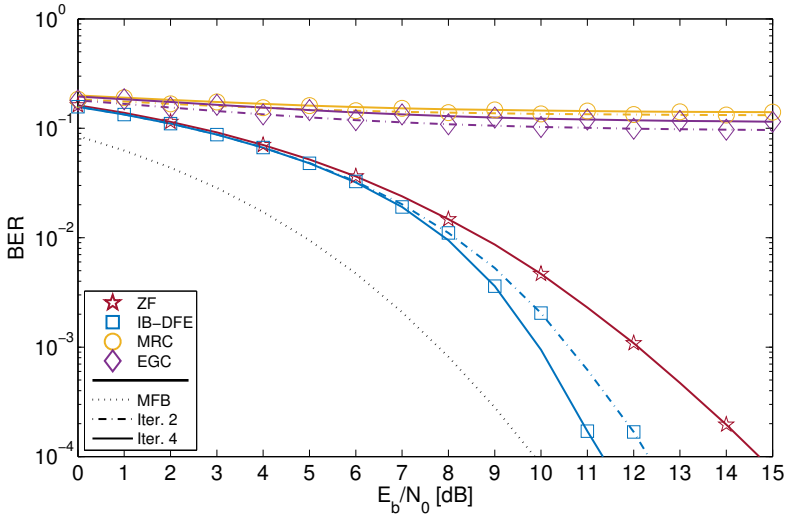

Figure 4.5 BER performance for several receivers in scenario (A) with $R_b = 64$ and $R_u = 1$.

For scenario B, where $R_b = 1$, the BF gain is wasted, and all antennas are sufficiently spaced to have low correlation. Although not envisioned as a desirable scenario in an m-MIMO implementation at mmWave, it allows the study of the behaviour of the receivers when they have lower correlation levels. Fig. 4.6 shows the BER curves of the receivers for two different levels of correlation between adjacent groups: one with low correlation, $\rho_u = 0.2$, and another with

high correlation $\rho_u = 0.8$. Here, only the 4-th iteration of conventional IB-DFE, MRC and EGC receivers is presented.

In this scenario, the correlation between each antenna pair is lower than in the previous one, even when $\rho_u = 0.8$, which is especially advantageous for MRC and EGC receivers. Therefore, all receivers have a similar BER performance, with MRC being able to approach the MFB after just 4 iterations. Also, it is shown that, without BF, the BER performance almost does not vary with ρ_u. This phenomenon is expected because the correlation between non-adjacent groups is much lower than 0.8 and for adjacent groups, only a pair of antennas is considered.

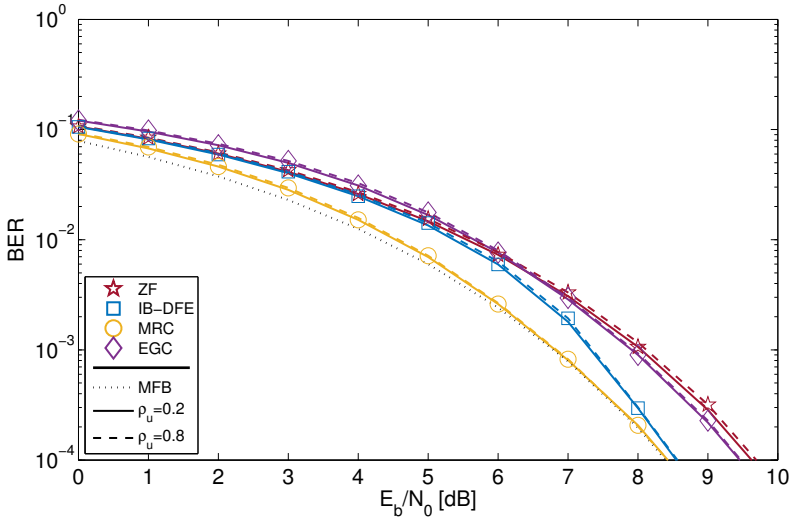

Figure 4.6 BER performance for several iterative receivers at the 4-th iteration and ZF in scenario (B) with $R_b = 1$ and $R_u = 64$ and different levels of correlation between adjacent groups.

On the other hand, when both layers of antennas are implemented as in scenario C, for each pair of adjacent groups, multiple pairs of antennas are involved, which results in more antennas with high correlation levels than in the previous case. Fig. 4.7 presents the results for $R_b = 4$ and $R_u = 16$. Once more, only the 4-th iteration of conventional IB-DFE, MRC and EGC receivers is presented. Now, three different levels of correlation, $\rho_u = [0.2, 0.5, 0.8]$, are used. Contrarily to the previous case, BER performance degrades as ρ_u increases, which is expected because the number of low correlation antennas becomes the same as the transmitters and BF antennas do not present a significant improvement. However, even for $\rho_u = 0.5$, these receivers present excellent performance, very close to the MFB. Only for the case of high correlation level, $\rho_u = 0.8$, MRC and EGC receivers have poor performance due to residual interference. The effects of these interference can be reduced with an increase in N_R/N_T relation as shown in section 2.6.

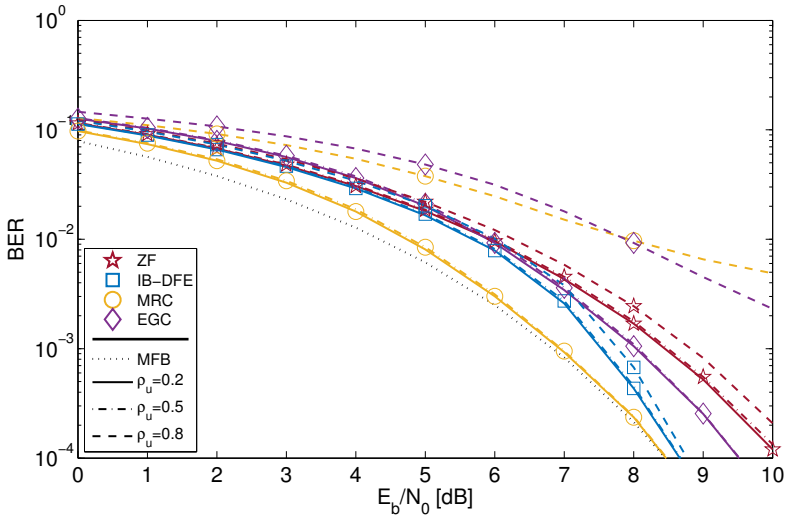

Figure 4.7 BER performance for several iterative receivers at the 4-th iteration and ZF in scenario (C) with $R_b = 4$ and $R_u = 16$ and different levels of correlation between adjacent groups.

Moreover, MRC receiver shows the best BER performance for the same number of iterations when the two layers of antennas are implemented, although the difference relative to the EGC is small. Therefore, these receivers are especially interesting for m-MIMO schemes since they do not require matrix inversions, presenting a lower complexity.

4.4 Complexity Analysis

In this section, a complexity analysis for the different equalisers presented in this chapter is performed. The equalisers here analysed are: ZF, conventional IB-DFE and iterative MRC and EGC. The analysis for conventional IB-DFE approach is only done for its linear part, that corresponds to an MMSE equaliser and is given by

$$\widetilde{\mathbf{S}}_k = \mathbf{F}_k \mathbf{Y}_k. \tag{4.37}$$

This decision resides in the fact that the iterative MRC and EGC with just 4 iterations present better results and much lower complexity (as it will be shown) than conventional IB-DFE approach, while performing very close to MFB. Therefore, it is not worthy to perform iterative conventional IB-DFE since results will be similar to the iterative MRC and EGC but with much higher complexity.

This analysis is performed per frequency k and the number of Floating-point Operations

(FLOPs) is used as comparison method. Only the calculus directly related to the MIMO equalisation procedure are included. We consider, as in [85], that the operations $+,-,\times,/$, and square root in the real domain require one FLOP. The number of required FLOPs for the remaining matrix and scalar operations used in this analysis are in Table 4.1. It is considered that c is a real scalar, w and z are complex numbers, **A**, **B** and **C** are arbitrary matrices of complex coefficients with dimensions $N\times P$, $P\times T$ and $P\times P$, respectively, **D** is a diagonal matrix of complex coefficients with dimensions $P\times P$, **I** is the $P\times P$ identity matrix and **v** is an arbitrary vector of complex coefficients with size $P\times 1$. $\mathbf{A}^H$ represents the Hermitian of the matrix **A**, whose calculus is considered that does not require any FLOP.

Table 4.1 Number of FLOPs - General Operations

Expression	FLOPs	Expression	FLOPs
$\mathbf{A}^H\mathbf{A}$	$4NP^2+4NP-P^2-P$	wz	6
$\mathbf{C}^{-1}$	$\frac{8}{3}P^3+\frac{19}{2}P^2-\frac{7}{6}P$	z^{-1}	5
AB	$8NPT-2NT$	$\lvert z\rvert$	4
DB	$6P$	$\lvert z\rvert^2$	3
$c\mathbf{A}$	$2NP$	$w\pm z$	2
$\mathbf{C}\pm\mathbf{I}$	P	$\frac{z}{w}$	11

The demonstration for the values present in Table 4.1 is straightforward, with the exception of the first two properties. The number of FLOPs to obtain the product of a matrix by its Hermitian, i.e. the Gramian matrix $\mathbf{A}^H\mathbf{A}$, follows from [86]. For the inversion of a matrix, it is considered the Gauss algorithm, with complexity presented in [87].

Table 4.2 presents the number of FLOPs of each algorithm stage[8], considering the equations presented in the previous sections. As this analysis is made per frequency k and the calculus of the normalisation diagonal matrix $\boldsymbol{\kappa}$ is equal for every frequency k, it only needs to be computed once and the calculus of its complexity is divided by N_{block}.

Note that for the iterative MRC and EGC equalisers, when estimating $\tilde{\mathbf{S}}_k$, the first iteration corresponds to the linear equaliser (4.37), and in the following iterations only the product $\mathbf{B}_k\tilde{\mathbf{S}}_k^{(i-1)}$ and its subtraction from the result of (4.37) has to be computed, since the matrices $\mathbf{F}_k$ and $\mathbf{B}_k$ are fixed; thus each additional iteration adds just a small computational burden.

Table 4.2 shows that there is an improvement in reducing the computational complexity of the

[8] See appendix D for the full development of the complexity analysis.

Table 4.2 Total number of FLOPs for each equaliser

Method		Equation(s)
ZF	$\boldsymbol{\kappa}$: $8N_TN_R$	LHS of (4.13)
	$\mathbf{F}_k$: $\frac{8}{3}N_T^3+12N_T^2N_R+\frac{17}{2}N_T^2+10N_TN_R+\frac{23}{6}N_T$	(2.29)
	$\widetilde{\mathbf{S}}_k$: $\frac{8}{3}N_T^3+12N_T^2N_R+\frac{17}{2}N_T^2+18N_TN_R+\frac{11}{6}N_T$	(4.37)
MMSE (1st iteration IB-DFE)	$\boldsymbol{\kappa}$: $8N_TN_R$	LHS of (4.13)
	$\mathbf{F}_k$: $\frac{8}{3}N_T^3+12N_T^2N_R+\frac{17}{2}N_T^2+10N_TN_R+\frac{35}{6}N_T$	(4.16)
	$\widetilde{\mathbf{S}}_k$: $\frac{8}{3}N_T^3+12N_T^2N_R+\frac{17}{2}N_T^2+18N_TN_R+\frac{23}{6}N_T$	(4.37)
MRC	$\boldsymbol{\kappa}$: $4N_TN_R$	(4.32)
	$\mathbf{F}_k$: $4N_TN_R+6N_T$	(4.31)
	$\mathbf{B}_k$: $8N_T^2N_R-2N_T^2+N_T$	(4.35)
	$\widetilde{\mathbf{S}}_k$ **(no iter.)**: $12N_TN_R+4N_T$ **($\mathbf{n_i}$>1 iter.)**: $8N_T^2N_R+(8n_i-10)N_T^2+12N_TN_R+5N_T$	(4.30)
EGC	$\boldsymbol{\kappa}$: $5N_TN_R$	(4.34)
	$\mathbf{F}_k$: $11N_TN_R+6N_T$	(4.33)
	$\mathbf{B}_k$: $8N_T^2N_R-2N_T^2+N_T$	(4.35)
	$\widetilde{\mathbf{S}}_k$ **(no iter.)**: $19N_TN_R+4N_T$ **($\mathbf{n_i}$>1 iter.)**: $8N_T^2N_R+(8n_i-10)N_T^2+19N_TN_R+5N_T$	(4.30)

overall system when employing the iterative MRC and EGC in comparison with ZF and the first iteration of conventional IB-DFE.

An important result that can be taken from Table 4.2 is the asymptotic complexity reduction when $N_R/N_T \gg 1$. From the table analysis, it can be concluded that ZF and MMSE present an asymptotic complexity of $(\frac{8}{3}+12(N_R/N_T))N_T^3$, while for the iterative MRC and EGC is $(8(N_R/N_T))N_T^3$. By performing the ratios of the asymptotic complexities, one gets

$$\frac{\text{FLOP}_{\text{MRC/EGC}}}{\text{FLOP}_{\text{ZF/MMSE}}} \underset{\frac{N_R}{N_T}\gg 1}{\approx} \frac{8(N_R/N_T)}{\frac{8}{3}+12(N_R/N_T)} \rightarrow \frac{2}{3} \quad , \tag{4.38}$$

which means that the complexity reduction converges asymptotically to 33%. Note that for moderate values of N_R and N_T, this may not seem a substantial reduction regarding the number of computed FLOPs. However, for m-MIMO scenarios, where it is necessary to deal with high dimension matrices, this reduction is noticeable, and it may correspond to the savings of hundreds

of thousands of FLOPs as shown in Table 4.3[9].

Table 4.3 Number of FLOPs for the different m-MIMO scenarios

$\mathbf{N_T \times R_b \times R_u}$	$\mathbf{16 \times 4 \times 16}$	$\mathbf{16 \times 4 \times 32}$	$\mathbf{16 \times 8 \times 32}$
ZF	228 168	443 208	873 288
MMSE	228 200	443 240	873 320
MRC	**1st iter**: 12 352 **2nd iter**: 132 624 **Following iterations**: 2048	**1st iter**: 24 640 **2nd iter**: 263 696 **Following iterations**: 2048	**1st iter**: 49 216 **2nd iter**: 525 840 **Following iterations**: 2048
	Total (for 4 iter.): 149 072	**Total (for 4 iter.)**: 292 432	**Total (for 4 iter.)**: 579 152
EGC	**1st iter**: 19 520 **2nd iter**: 132 624 **Following iterations**: 2048	**1st iter**: 38 976 **2nd iter**: 263 696 **Following iterations**: 2048	**1st iter**: 77 888 **2nd iter**: 525 840 **Following iterations**: 2048
	Total (for 4 iter.): 156 240	**Total (for 4 iter.)**: 306 768	**Total (for 4 iter.)**: 607 824
$\mathbf{N_R/N_T}$	1	2	2
Complexity Reduction (MMSE)	35%	34%	34%

4.5 Conclusion remarks

In this chapter, iterative receivers based on IB-DFE concept are studied in order to improve the BER performance when using m-MIMO schemes operating at mmWave bands and performing SC-FDE modulation. The BER curves of these techniques are evaluated using a general clustered channel model that emulates the effects of two different layers of antennas implemented in order to achieve BF and SM gains.

The results obtained using the proposed channel model show that iterative receivers based on MRC and EGC are suitable choices for m-MIMO schemes, presenting similar performance to the conventional IB-DFE receiver when the correlation factor is kept low, but without requiring matrix inversions. It also shown that the complexity reduction of iterative MRC and EGC relative to the linear ZF and MMSE equalisers will be at least 33% even using 4 iterations, that are sufficient for both receivers approach the MFB.

Finally, it should be noted note that, although these iterative receivers already perform multi-user detection, their implementation on systems that use offset constellations with SM is still an open issue. In this way, the next chapter will address the development of receivers able to cope with offset constellations.

[9]The ratio N_R/N_T in Table 4.3 only considers the number of R_u antennas since their correlation is the main factor that influences the performance of the receivers as we see in the previous sections.

5

m-MIMO with offset constellations

The multilayer m-MIMO scheme operating at mmWave bands and performing SC-FDE modulation presented in section 3.1 is based on the decomposition of multilevel constellations into OQPSK-type components in order to achieve high power and spectral efficiencies. Although these type of signals could ensure these efficiency criteria, their recovery at the receiver side is not trivial. The techniques previously mentioned are not designed to cope with offset constellations, and their performance is rather poor with offset constellations mainly due to the residual In-phase Quadrature Interference (IQI). To overcome this, the IB-DFE concept was modified for offset constellations [17, 24]. Although IB-DFE receivers were successfully extended to MIMO scenarios [8], as far as the authors know, the work on FDE receivers for offset signals in MIMO scenarios is limited.

Since offset signals are usually intended for strongly non-linear amplifiers, they are designed to have very low envelope fluctuations. In general, this means employing a pulse shape whose band is above the minimum Nyquist band, unless sophisticated techniques are employed to reduce the envelope's dynamic ranges such as magnitude filtering [11, 70].

In this chapter, we consider offset signals with reduced envelope fluctuations combined with MIMO schemes that are suitable to combine with strongly non-linear power amplifiers, and we design appropriate FDE receivers. Conventional IB-DFE receivers are changed to cope with offset signals in MIMO scenarios, while the pragmatic receivers presented in [17, 24] are also extended to these scenarios, leading to improvements of BER performance in comparison with conventional IB-DFE while reducing complexity. Notwithstanding their excellent performance, approaching the MFB with only few iterations, they become too complex for m-MIMO schemes due to the required inversion of very large channel matrices, for each subcarrier and each iteration.

Therefore, receivers that do not require matrix inversions must be used to reduce system complexity, while still able to achieve good performance. Iterative receivers based on MRC and EGC [18, 50, 64, 67] concepts are interesting because they do not require matrix inversions as previously explained. Although the residual interference levels (both interference between different transmitted streams and ISI) can be high with such low complexity receivers, they can achieve very good performance when $N_R \gg N_T$, which can be ensured in m-MIMO systems. Therefore, these receivers are also studied in this chapter and BER performance and complexity analyses of the mentioned receivers are performed to show the benefits of using low complexity receivers in offset scenarios.

Moreover, these equalisers should not only retrieve offset signals, but also cope with them when amplification is used. As we saw in chapter 3, offset signals ensure low envelope fluctuations, allowing the use of non-linear amplifiers. However, the efficiency of the power amplifier will depend on the pulse shaping filter, as well as, the spectral efficiency. Although bandwidth is not a concern at mmWave bands, the signal's band should be limited to the minimum possible. When applying more stringent pulse shaping filters, the envelope fluctuations will grow, decreasing the power efficiency of the system and/or the BER performance. In that sense, in this chapter, the different pulse shaping filters presented in section 2.4 are combined with offset signals passing trough the amplifier models presented in section 2.5.3.

This chapter starts with the study of the processing of M-OQAM signals. Next, the MIMO IB-DFE receiver previously presented is redefined for offset signals, followed by a pragmatic version that performs the pulse shaping matching separately in order to reduce the IQI. Then, the low complexity iterative receivers performing MRC and EGC concepts are adapted for offset signals. The BER performance of the different receivers is then evaluated, considering multiple constellations, several pulse shaping filters and different amplifier's models. At last, the complexity analysis

done in chapter 4 is performed again, but for offset scenarios.

The work addressed in this chapter has resulted in one journal article [25].

5.1 M-OQAM signal processing

In this chapter, we will consider the multilayer scheme presented in section 3.1, with a generic symbol s_n of an M-QAM or an M-OQAM constellation being obtained as described in section 3.3.

Although M-ary QAM and OQAM share a common polar decomposition in the discrete time domain, their continuous time counterpart signals differ considerably due to the half of symbol's period (i.e. $T_s/2$) time shift between the in-phase and quadrature components [47, 88], which ensures no zero crossings, reducing the envelope fluctuations and, consequently, improving the power efficiency. Thus, the complex equivalent baseband signal is for the QAM case given by

$$\begin{aligned} \breve{x}_\tau^{\text{QAM}} &= \sum_n \left(s_n^{(I)} + j s_n^{(Q)} \right) p_{\tau - nT_s} \\ &= \sum_n \sum_{i=0}^{\sqrt{M}-1} g_i \left(b_{n_p}^{eq(i,I)} + j b_{n_p}^{eq(i,Q)} \right) p_{\tau - nT_s}, \end{aligned} \tag{5.1}$$

while for the OQAM is

$$\begin{aligned} \breve{x}_\tau^{\text{OQAM}} &= \sum_n s_n^{(I)} p_{\tau - nT_s} + j s_n^{(Q)} p_{\tau - T_s/2 - nT_s} \\ &= \sum_n \sum_{i=0}^{\sqrt{M}-1} g_i \left(b_{n_p}^{eq(i,I)} p_{\tau - nT_s} + j b_{n_p}^{eq(i,Q)} p_{\tau - T_s/2 - nT_s} \right) \end{aligned} \tag{5.2}$$

where τ is the temporal index and p_τ is the Nyquist supporting pulse for bandwidth limited transmission, with the passband signal being given for both cases by

$$x_\tau = \Re \left\{ \breve{x}_\tau e^{j2\pi f_c \tau} \right\}, \tag{5.3}$$

with f_c denoting the carrier frequency.

Equation (5.2) shows that for the case of M-ary OQAM signal this can be seen as a serial representation of an OQPSK signals [77], that can be specially designed to have constant envelope or acceptable trade-off between reduced envelope fluctuations and compact spectrum upon proper choice of pulse shaping p_τ (e.g., a GMSK signal [47]). The N_p OQPSK components can

thus be separately amplified and transmitted by N_p antennas, with their combination to form the correspondent OQAM signal being performed on the air upon MIMO transmission [16, 19]. In addition, due to the controlled envelope nature of OQPSK signals, highly efficient, low-cost, strongly non-linear amplifiers can be employed in this case, making clear the advantages of using OQAM signals. This can be particularly interesting at mmWave where large aggregate antennas can be employed and signal's spectrum occupancy above the minimum Nyquist band is not a constraint.

5.1.1 Multirate processing of OQAM signals

Due to the time-shift between in-phase and quadrature components of offset signals, the digital processing of offset signals upon reception requires the use of sampling above the minimum Nyquist rate. Let $\breve{x}_{\tau}^{(t)}$ denote the baseband complex equivalent M-OQAM signal that is transmitted by the t-th antenna ($t = 1, \ldots, N_T$), and the corresponding sequence of transmitted M-OQAM symbols being $s_n^{(t)}$ as given by (3.24). Let $\breve{x}_{n'}^{(t)}$ denote the sequence resulting from sampling $\breve{x}_{\tau}^{(t)}$ at a rate L/T_s, with L being the oversampling factor above the Nyquist rate which is restricted to be even. According to (5.2) it is straightforward to prove that

$$\begin{aligned} \breve{x}_{n'}^{(t)} &= x_{\tau}^{(t)}\Big|_{\tau=n'\frac{T_s}{L}} \\ &= \left(\breve{s}_{n'}^{(t,I)} + j\breve{s}_{n'-L/2}^{(t,Q)}\right) * p_{n'}, \end{aligned} \tag{5.4}$$

where '$*$' denotes the discrete time convolution operation, $p_{n'}$ is the sampled version of the pulse shaping filter at the rate L/T_s, i.e.

$$p_{n'} = p_{\tau}|_{\tau=n'\frac{T_s}{L}}\,, \tag{5.5}$$

and $\breve{s}_{n'}^{(t,I)}$ and $\breve{s}_{n'}^{(t,Q)}$ are the upsampling rate expansion of the in-phase and quadrature components of the sequence of OQAM sent symbols $s_n^{(t)}$, respectively, with

$$\breve{s}_{n'}^{(t,j)} = \begin{cases} s_{\frac{n'}{L}}^{(t,j)}, & n' \bmod L = 0 \\ 0, & \text{otherwise} \end{cases} \quad \text{for } j \in \{I, Q\}\,. \tag{5.6}$$

Statement 1. For an SC-FDE transmission employing blocks of N_{block} symbols the DFT of sequences $\breve{s}_{n'}^{(t,j)}$ and $s_n^{(t,j)}$ can be related[a]. Let $S_k^{(t,j)}$=DFT$\{s_n^{(t,j)}; n=0,\ldots,N_{block}-1\}$, with

k=0,…, N_{block}−1, and $\breve{S}_{k'}^{(t,j)}$=DFT$\{\breve{s}_{n'}^{(t,j)}; n'$=0,…, $LN_{block}-1\}$, with k'=0,…, $LN_{block}-1$. Given the periodic nature of the DFT, these relate as

$$\breve{S}_{k'}^{(t,j)} = S_k^{(t,j)} \quad \text{for} \quad \begin{cases} k = k' \bmod N_{block} \\ j \in \{I, Q\} \end{cases}, \tag{5.7}$$

does meaning that the spectrum $S_k^{(t)}$ is repeated L times over $\breve{S}_{k'}^{(t)}$.

[a] For easy understanding, along the chapter, sample instant and frequency index are respectively denoted by n and k for processing at symbol rate $1/T_s$, and by n' and k' for processing at oversampling rate L/T_s.

Proof.

$$\begin{aligned} \breve{S}_{k'}^{(t)} &= \sum_{n'=0}^{LN_{block}-1} \breve{s}_{n'}^{(t)} e^{-jk\frac{2\pi}{LN_{block}}n'} = \sum_{\substack{n'=0 \\ n' \bmod L=0}}^{LN_{block}-1} s_{\frac{n'}{L}}^{(t)} \; e^{-jk\frac{2\pi}{LN_{block}}n'} \\ &\underset{n \mapsto \frac{n'}{L}}{=} \sum_{n=0}^{N_{block}-1} s_n^{(t)} \; e^{-jk\frac{2\pi}{N_{block}}n} = S_k^{(t)} \end{aligned}$$

■

An equivalent representation of symbol $s_n^{(t)}$ at oversampling rate L/T_s can thus be obtained based on (5.4), being given by

$$\breve{s}_{n'}^{(t)} = \breve{s}_{n'}^{(t,I)} + j\breve{s}_{n'-\frac{L}{2}}^{(t,Q)}. \tag{5.8}$$

It is important to note that $\breve{s}_{n'}^{(t)}$ embeds the physical nature of OQAM signals by having in-phase and quadrature components shifted by $L/2$ samples.

According to (5.7) and time-shifting property of the DFT, it results that the DFT of $\breve{s}_{n'}^{(t)}$ is given by

$$\begin{aligned} \breve{S}_{k'}^{(t)} &= \breve{S}_{k'}^{(t,I)} + je^{-j\pi\frac{k'}{N_{block}}} \breve{S}_{k'}^{(t,Q)} \\ &= S_k^{(t,I)} + j\Theta_{k'} S_k^{(t,Q)} \quad \text{for} \quad k = k' \bmod N_{block}, \end{aligned} \tag{5.9}$$

where

$$\Theta_{k'} = e^{-j\pi\frac{k'}{N_{block}}} = \begin{cases} e^{-j\pi\frac{k}{N_{block}}}, & k' = k + 2qN_{block} \\ -e^{-j\pi\frac{k}{N_{block}}}, & k' = k + (2q+1)N_{block} \end{cases} \tag{5.10}$$

with $q \in \mathbb{Z}$, meaning an alternation in the signal of the quadrature component of each replica.

Also, from (5.4) it results

$$\breve{X}_{k'}^{(t)} = P_{k'}\breve{S}_{k'}^{(t)}, \tag{5.11}$$

where $\breve{X}_{k'}^{(t)} = \text{DFT}\{\breve{x}_{n'}^{(t)}; n'=0,\ldots,LN_{block}-1\}$ and $P_{k'} = \text{DFT}\{p_{n'}; n'=0,\ldots,LN_{block}-1\}$.

Analysing (5.9) and (5.11) important conclusions can be drawn upon digital processing of OQAM signals. Although, according to (5.7), and considering (5.9) the block of OQAM transmitted symbols, $\{s_n; n=0,\ldots,N_{block}-1\}$, can be obtained from the first N_{block} samples of $\breve{X}_{k'}^{(t)}$ (which corresponds to process the signal at Nyquist rate), there is a sort of diversity effect that is created by processing the OQAM signal at a highest rate, where this information is repeated[1] every N_{block} samples of $\breve{X}_{k'}^{(t)}$. This can be very useful to improve the BER performance for linear equalisers when non-offset constellations are used, particularly for the case of low-envelope fluctuation offset signals. In this case, the pulse shape p_τ has typically a bandwidth considerable above the minimum Nyquist band. So, P'_k samples for $k' \geq N_{block}$ can have non-negligible values, and consequently the corresponding $\breve{X}_{k'}^{(t)}$ samples in equation (5.11) carry important information.

Statement 2. Considering $\breve{S}_{k'}^{(t)}$ given by (5.9), and $S_k^{(t)}=\text{DFT}\{s_n^{(t)}; n=0,\ldots,N_{block}-1\}$, to obtain $S_k^{(t)}$ from $\breve{S}_{k'}^{(t)}$, we can thus make an average over the L replicas, instead of considering only its first N_{block} values, as,

$$S_k^{(t)} = \frac{1}{L}\sum_{\substack{k'=0 \\ k' \bmod N_{block}=k}}^{LN_{block}-1} \breve{S}_{k'}^{(t)} + \frac{1}{L}\sum_{\substack{k'=0 \\ k' \bmod N_{block}=k}}^{LN_{block}-1} \frac{\breve{S}_{k'}^{(t)}}{\Theta_{k'}} \tag{5.12}$$

$$\underset{k' \mapsto k+lN_{block}}{=} \frac{1}{L}\sum_{l=0}^{L-1} \breve{S}_{k+lN_{block}}^{(t)} + \frac{1}{L}\sum_{l=0}^{L-1} \frac{\breve{S}_{k+lN_{block}}^{(t)}}{\Theta_{k+lN_{block}}}$$

$$\underset{k+lN_{block} \mapsto (k,l)}{=} \frac{1}{L}\sum_{l=0}^{L-1} \breve{S}_{(k,l)}^{(t)} + \frac{1}{L}\sum_{l=0}^{L-1} \frac{\breve{S}_{(k,l)}^{(t)}}{\Theta_{(k,l)}}\,, \tag{5.13}$$

where a new notation $\breve{S}_{(k,l)} = \breve{S}_{k+lN_{block}}$ have been adopted to refer the samples of $\breve{S}_{k'}$ related to S_k[a].

[a] Please note that, from this point forward, both notations $\breve{S}_{k'}$ and $\breve{S}_{(k,l)}$ will be used in an undifferentiated manner, with the choice of each one to be employed being driven by purposes of clarity of the presentation.

Proof. We will compute each of the average terms of the summation (5.13). By considering (5.9)

[1] In fact, this are not true replicas since they are affected by the phase shift factor $\Theta_{k'}$ given by (5.10) which is known, and can therefore be compensated.

the calculus of the left average term comes

$$\begin{aligned}\frac{1}{L}\sum_{l=0}^{L-1}\breve{S}_{(k,l)}^{(t)} &= \frac{1}{L}\sum_{l=0}^{L-1}S_k^{(t,I)} + j\frac{1}{L}\sum_{l=0}^{L-1}\Theta_{(k,l)}S_k^{(t,Q)} \\ &= S_k^{(t,I)} + jS_k^{(t,Q)}\frac{1}{L}\sum_{l=0}^{L-1}\Theta_{k+lN_{block}} \\ &\underset{\text{by (5.10)}}{=} S_k^{(t,I)}\end{aligned} \tag{5.14}$$

where last equality of (5.14) results from the fact that for consecutive values of l phase shifts are symmetric, i.e. $\Theta_{(k,l)} = -\Theta_{(k,l+1)}$, and the oversampling factor L has been restricted to be an even number.

Consider now the right average term of (5.13). Similarly, by using (5.9) and (5.10) it results,

$$\begin{aligned}\frac{1}{L}\sum_{l=0}^{L-1}\frac{\breve{S}_{(k,l)}^{(t)}}{\Theta_{(k,l)}} &= \frac{1}{L}\sum_{l=0}^{L-1}\frac{S_k^{(t,I)}}{\Theta_{(k,l)}} + j\frac{1}{L}\sum_{l=0}^{L-1}S_k^{(t,Q)} \\ &= S_k^{(t,I)}\frac{1}{L}\sum_{l=0}^{L-1}\Theta_{-k-lN_{block}} + jS_k^{(t,Q)} \\ &\underset{\text{by (5.10)}}{=} jS_k^{(t,Q)}.\end{aligned} \tag{5.15}$$

And so, it results from substituting (5.14) and (5.15) in (5.13) that

$$S_k^{(t)} = S_k^{(t,I)} + jS_k^{(t,Q)} = \text{DFT}\left\{s_n^{(t)}\right\}, \tag{5.16}$$

as it was wanted to be proved. ■

In order to simplify analysis that follows on the equalisation of OQAM signal under multirate signal processing, the average defined in (5.13) will be hereafter denoted as

$$S_k^{(t)} = \Upsilon\left(\breve{S}_{(k,l)}^{(t)}\right) = \frac{1}{L}\sum_{l=0}^{L-1}\breve{S}_{(k,l)}^{(t)} + \frac{1}{L}\sum_{l=0}^{L-1}\frac{\breve{S}_{(k,l)}^{(t)}}{\Theta_{(k,l)}}, \tag{5.17}$$

or in an equivalent manner, using (5.12), being denoted as

$$S_k^{(t)} = \Upsilon\left(\breve{S}_{k'}^{(t)}\right). \tag{5.18}$$

Linear frequency domain equalisation of OQAM signals upon multirate processing

Let's start by expressing (5.11) in an equivalent matrix as

$$\check{\mathbf{X}}_{k'} = P_{k'}\check{\mathbf{S}}_{k'}. \tag{5.19}$$

where $\check{\mathbf{X}}_{k'} = [\check{X}_{k'}^{(1)} \dots \check{X}_{k'}^{(N_T)}]^T$ and $\check{\mathbf{S}}_{k'} = [\check{S}_{k'}^{(1)} \dots \check{S}_{k'}^{(N_T)}]^T$.

For an m-MIMO system using SC-FDE with offset constellations, the received signals under multirate digital processing are given by

$$\begin{aligned} \mathbf{Y}_{k'} &= \mathbf{H}_{k'}\check{\mathbf{X}}_{k'} + \mathbf{N}_{k'} \\ &= P_{k'}\mathbf{H}_{k'}\check{\mathbf{S}}_{k'} + \mathbf{N}_{k'} \\ &= \mathbf{H}_{k'}^{eq}\check{\mathbf{S}}_{k'} + \mathbf{N}_{k'}, \end{aligned} \tag{5.20}$$

where $\mathbf{Y}_{k'} = [Y_{k'}^{(1)} \dots Y_{k'}^{(N_R)}]^T$ is the set of received signals, with $Y_{k'}^{(r)}$ denoting the signal received by the r-th antenna, $\mathbf{N}_{k'} = [N_{k'}^{(1)} \dots N_{k'}^{(N_R)}]^T$ is the AWGN component, and $\mathbf{H}_{k'}^{eq} = P_{k'}\mathbf{H}_{k'}$ is the equivalent MIMO channel frequency response to be equalised, which includes the channel frequency response and the pulse shaping filter, and where

$$\mathbf{H}_{k'} = \begin{bmatrix} H_{k'}^{(1,1)} & \cdots & H_{k'}^{(1,N_T)} \\ \vdots & \ddots & \vdots \\ H_{k'}^{(N_R,1)} & \cdots & H_{k'}^{(N_R,N_T)} \end{bmatrix}, \tag{5.21}$$

with $H_{k'}^{(r,t)}$ denoting the channel frequency response between the antenna pair (r,t).

At the receiver, one obtains an estimation of the oversampled transmitted symbol using the linear equaliser

$$\widetilde{\check{\mathbf{S}}}_{k'} = \mathbf{F}_{k'}\mathbf{Y}_{k'}. \tag{5.22}$$

where $\mathbf{F}_{k'}$ denotes the matrix of feedforward coefficients and the estimation of the block of OQAM transmitted symbols $\widetilde{\mathbf{S}}_k$ (i.e. at symbol rate) is obtained through averaging of all replicas for a given frequency k as defined in (5.17), i.e.

$$\widetilde{\mathbf{S}}_k = \Upsilon\left(\widetilde{\check{\mathbf{S}}}_{k'}\right) \tag{5.23}$$

Looking at (5.23), one can see that there is an average summation that does not exist for non-offset cases. Therefore, the already existent equalisers must be changed in accordance. Moreover,

in this chapter, it is also introduced the pulse shaping filter and the equalisation should also retrieve from it.

5.2 IB-DFE receiver for offset signals

In the previous chapter, it is seen that, although IB-DFE presents a high complexity, it approaches the MFB even in scenarios with high correlation between reception antennas. Nevertheless, it is still not able to cope with signals based in offset constellations. Thus, in this section, the IB-DFE equaliser will be derived for offset signals following the same approach used in section 4.1. Here, it is considered that the equaliser tries to reverse the pulse shaping filter and the channel frequency response simultaneously.

The new IB-DFE architecture is presented in Fig. 5.1. This architecture is similar to the one presented in Fig. 4.1, but here, when applying the feedforward filters, there are multiple layers that converge in the Υ function, increasing the complexity of the receiver and changing their optimum filters.

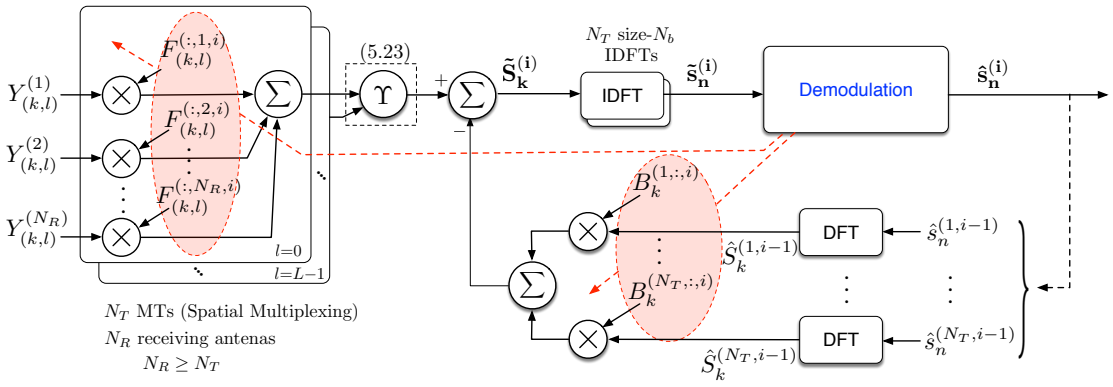

Figure 5.1 Generic block diagram of an IB-DFE receiver for offset constellations.

5.2.1 IB-DFE with hard decisions

The study of IB-DFE receivers with hard decisions for offset signals follows the same reasoning used in section 4.1.1. However, the frequency domain estimations associated with the i-th iteration at the output of the equaliser become

$$\widetilde{\mathbf{S}}^{(i)}_k = \Upsilon\left(\mathbf{F}^{(i)}_{(k,l)}\mathbf{Y}_{(k,l)}\right) - \mathbf{B}^{(i)}_k\hat{\mathbf{S}}^{(i-1)}_k \,, \tag{5.24}$$

where the oversampled feedforward and the feedback matrices are

$$\mathbf{F}_{(k,l)}^{(i)} = \begin{bmatrix} F_{(k,l)}^{(1,1,i)} & \cdots & F_{(k,l)}^{(1,N_R,i)} \\ \vdots & \ddots & \vdots \\ F_{(k,l)}^{(N_T,1,i)} & \cdots & F_{(k,l)}^{(N_T,N_R,i)} \end{bmatrix}. \tag{5.25}$$

and

$$\mathbf{B}_{k}^{(i)} = \begin{bmatrix} B_{k}^{(1,1,i)} & \cdots & B_{k}^{(1,N_T,i)} \\ \vdots & \ddots & \vdots \\ B_{k}^{(N_T,1,i)} & \cdots & B_{k}^{(N_T,N_T,i)} \end{bmatrix}, \tag{5.26}$$

respectively. $F_{(k,l)}^{(t,r,i)}$ and $B_{k}^{(t,t,i)}$ denote the feedforward and feedback filters coefficients at the i-th iteration and the vector $\hat{\mathbf{S}}_{k}^{(i-1)}$ contains the DFT of the hard-decision time domain blocks associated with the previous estimations for the transmitted symbols (for the first iteration those terms are zero, i.e., $\hat{\mathbf{S}}_{k}^{(0)} = \mathbf{0}_{N_T \times 1}$).

Although the feedforward filters are processed with oversampling, the hard-estimations $\hat{\mathbf{S}}_{k}^{(i-1)}$ are obtained at the original rate. Therefore, its relation with the original signal, the correlation factor and the quantisation error are still given by the set of equations (4.4)-(4.9).

Once more, the feedback and the feedforward coefficients are chosen to minimise the MSE. As we are still talking about an m-MIMO system, the MSE of the t-th transmitter at iteration i and frequency k is given by

$$\Omega_{k}^{(t,i)} = \mathbb{E}\left[\left|\widetilde{S}_{k}^{(t,i)} - S_{k}^{(t)}\right|^2\right]. \tag{5.27}$$

However, now $\widetilde{S}_{k}^{(t,i)}$ is given by (5.24), raising new challenges when solving the optimisation problem given by

$$\begin{aligned} \textbf{min}\ \ \boldsymbol{\Omega}_{k}^{(i)} &= \textbf{min}\ \ \sum_{t=1}^{N_T} \Omega_{k}^{(t,i)} = \\ &= \textbf{min}\ \ \sum_{t=1}^{N_T} \mathbb{E}\left[\left|\widetilde{S}_{k}^{(t,i)} - S_{k}^{(t)}\right|^2\right] = \\ &= \textbf{min}\ \ \mathbb{E}\left[\left(\widetilde{\mathbf{S}}_{k}^{(i)} - \mathbf{S}_{k}\right)^H \left(\widetilde{\mathbf{S}}_{k}^{(i)} - \mathbf{S}_{k}\right)\right], \end{aligned} \tag{5.28}$$

subject to

$$\frac{1}{LN_{block}} \sum_{k=0}^{N_{block}-1} \sum_{l=0}^{L-1} \mathrm{Tr}\left(\mathbf{F}_{(k,l)}^{(i)} \mathbf{H}_{(k,l)}^{eq}\right) = N_T. \tag{5.29}$$

The solution to this problem can be obtained using the method of Lagrange multipliers [84], defining the Lagrange function as

$$\begin{aligned} J_k^{(i)} = \mathbb{E}\left[\left(\widetilde{\mathbf{S}}_k^{(i)} - \mathbf{S}_k\right)^H \left(\widetilde{\mathbf{S}}_k^{(i)} - \mathbf{S}_k\right)\right] + \\ \lambda_k^{(i)} \left(\frac{1}{LN_{block}} \left(\sum_{k=0}^{N_{block}-1} \sum_{l=0}^{L-1} \mathrm{Tr}\left(\mathbf{F}_{(k,l)}^{(i)} \mathbf{H}_{(k,l)}^{eq}\right)\right) - N_T\right), \end{aligned} \tag{5.30}$$

where $\lambda_k^{(i)}$ corresponds to the Lagrange multiplier at iteration i and frequency k, and the coefficients $\mathbf{F}_{(k,l)}$ and $\mathbf{B}_k$ that minimise the MSE could be obtained by solving the system of equations given by

$$\begin{cases} \nabla_{\mathbf{F}_{(k,l)}^{(i)}}(J_k^{(i)}) = \mathbf{0}_{N_T \times N_R} \\ \nabla_{\mathbf{B}_k^{(i)}}(J_k^{(i)}) = \mathbf{0}_{N_T \times N_T} \\ \nabla_{\lambda_k^{(i)}}(J_k^{(i)}) = 0 \end{cases}. \tag{5.31}$$

After solving (5.31)[2], it is shown that the feedforward coefficients for iteration i are given by

$$\mathbf{F}_{(k,l)}^{(i)} = \boldsymbol{\kappa} \boldsymbol{\Lambda}_{(k,l)}^{(i)} \left(\mathbf{H}_{(k,l)}^{eq}\right)^H, \tag{5.32}$$

where $\boldsymbol{\kappa}$ is a normalisation matrix[3] and $\boldsymbol{\Lambda}_{(k,l)}^{(i)}$ is given by

$$\boldsymbol{\Lambda}_{(k,l)}^{(i)} = \left(\frac{1}{\gamma}\boldsymbol{I}_{N_T} + \left(\boldsymbol{I}_{N_T} - \left(\boldsymbol{\varrho}^{(i-1)}\right)^2\right) \left(\sum_{l=0}^{L-1} \left(\mathbf{H}_{(k,l)}^{eq}\right)^H \mathbf{H}_{(k,l)}^{eq}\right)\right)^{-1}. \tag{5.33}$$

In its turn, the feedback coefficients for iteration i are given by

$$\mathbf{B}_k^{(i)} = \left(\left(\frac{1}{L}\sum_{l=0}^{L-1} \mathbf{F}_{(k,l)}^{(i)} \mathbf{H}_{(k,l)}^{eq}\right) - \boldsymbol{I}_{N_T}\right) \boldsymbol{\varrho}^{(i-1)}. \tag{5.34}$$

This iterative process leads to improved estimations throughout iterations even for offset constellations despite their high IQI, and once more the first iterations corresponds to a linear MMSE-based equaliser.

[2] See appendix C for the full development of the optimisation problem.

[3] Usually, $\boldsymbol{\kappa}$ is a diagonal matrix with size $N_T \times N_T$, with the values of position (t,t) given by the inverse of the LHS of (5.29).

5.2.2 IB-DFE with soft decisions

As mentioned in chapter 4, IB-DFE receiver can be enhanced with the use of soft instead of hard decisions [15]. For offset constellations, it is also possible with (5.24) becoming

$$\widetilde{\mathbf{S}}_k^{(i)} = \Upsilon\left(\mathbf{F}_{(k,l)}^{(i)}\mathbf{Y}_{(k,l)}\right) - \mathbf{B}_k^{(i)}\overline{\mathbf{S}}_k^{(i-1)}\,, \tag{5.35}$$

where $\overline{\mathbf{S}}_k^{(i-1)}$ denotes the average symbol values conditioned to the output of the equaliser at iteration $i-1$.

Following the same steps presented in section 4.1.2, it is straightforward to obtain the feedback coefficients and they are given by

$$\mathbf{B}_k^{(i)} = \left(\frac{1}{L}\sum_{l=0}^{L-1}\mathbf{F}_{(k,l)}^{(i)}\mathbf{H}_{(k,l)}^{eq}\right) - \boldsymbol{I}_{N_T}. \tag{5.36}$$

On the other hand, the feedforward coefficients are still obtained by (5.32), but (5.33) becomes

$$\boldsymbol{\Lambda}_{(k,l)}^{(i)} = \left(\frac{1}{\gamma}\boldsymbol{I}_{N_T} + \left(\boldsymbol{I}_{N_T} - \left(\overline{\boldsymbol{\varrho}}^{(i-1)}\right)^2\right)\left(\sum_{l=0}^{L-1}\left(\mathbf{H}_{(k,l)}^{eq}\right)^H\mathbf{H}_{(k,l)}^{eq}\right)\right)^{-1}, \tag{5.37}$$

where $\overline{\boldsymbol{\varrho}}^{(i-1)}$ denotes a diagonal matrix with each element given by (4.29).

5.2.3 BER performance with IB-DFE for offset signals

In this subsection, the BER performance with IB-DFE for offset signals is evaluated. Although for the AWGN channel, OQPSK presents the same BER of the QPSK constellations [47], when dealing with time-dispersive channels, the in-phase and quadrature components can not maintain the initial offset, and at the sampling point in the receiver side, there will be IQI, compromising the BER performance.

In that sense, we considered the system presented in section 3.1 with $N_T = 16$ transmitters each one with one antenna, $N_R = R_b \times R_u = 4 \times 16 = 64$ reception antennas with the R_u groups uncorrelated (i.e., $\rho_u = 0$), and a clustered mmWave channel [18] (presented in section 2.3) with 4 clusters, each one with 3 rays each. The block size is $N_{block} = 256$ and the constellation 4-OQAM. Since we want to employ grossly non-linear amplifiers, requiring constant or almost constant envelope signals, a half-cosine arcade has been used as pulse shaping producing a MSK signal. This is not a problem at mmWave where there is huge bandwidth, allowing the relief of

the bandwidth constraint to obtain signals with constant envelope that could be amplified with non-linear amplifiers.

Fig. 5.2 present IB-DFE results at 1st and 4th iterations, where the MFB is given by an average of all the MFBs of each transmission antenna, i.e.,

$$\bar{P}_b^{\text{MFB}} \approx \mathbb{E}\left[P_{\text{MFB}}^{(t)}\right]. \tag{5.38}$$

with

$$P_{\text{MFB}}^{(t)} = 2\left(1-\frac{1}{\sqrt{M}}\right)\frac{2}{\log_2 M}Q\left(\frac{3\log_2 M}{(M-1)}\frac{E_b}{N_0}\frac{1}{LN_{block}}\sum_{k'=0}^{LN_{block}-1}\frac{\left|H_{k'}^{(:,t)}\right|^2}{N_R}\right). \tag{5.39}$$

It is possible to see that after 4 iterations the results are closer to the MFB, but for the linear FDE (i.e., when only one iteration is used), the performance of 4-OQAM is poor in comparison to 4-QAM due to the high IQI levels. In that sense, equalisers with better performance in the first iteration should be developed, ensuring that the receiver converges in few iterations and reducing its complexity. It can also be observed that the diversity effect created by oversampling, that enhances the results for the first iteration of QAM, almost vanish after a few iterations.

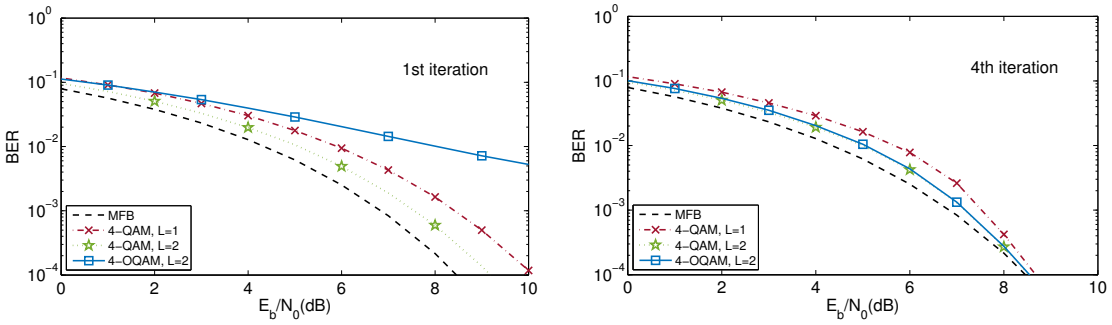

(a) (b)

Figure 5.2 BER performance comparison of the (a) 1st and (b) 4th iterations of IB-DFE with $N_T = 16$ transmitters each one with one antenna and a base-station with $N_R = R_b \times R_u = 4 \times 16 = 64$ reception antennas with the R_u uncorrelated antenna groups, i.e., $\rho_u = 0$.

5.3 Pragmatic receiver for offset signals

Since the problem of equalising offset signals resides on the IQI, ensuring a perfect match in the pulse shaping may be fundamental to minimise it. In conventional IB-DFE receiver design, pulse shaping effects are assumed to be together with the channel response, and they are estimated and recovered at the same time. As the pulse shaping is chosen to ensure the first Nyquist criterion, it is known *a priori*. Therefore, in [17], it was suggested a pragmatic approach for SISO where pulse shaping is assumed to be perfectly matched and the receiver only tries to equalise the channel response. Here, a receiver based on that concept is derived for MIMO and its BER performance is also evaluated.

The pragmatic receiver is also iterative and could also use hard or soft decisions[4]. However, instead of equalising and recovering the signal at the same time, i.e., taking into account the contribution of the multiple replicas of the signal created by the diversity effect introduced by oversampling, the pragmatic approach equalises the oversampled signals. Hence, the output of the equaliser is given by

$$\widetilde{\breve{\mathbf{S}}}^{(i)}_{(k,l)} = \mathbf{F}^{(i)}_{(k,l)}\mathbf{Y}_{(k,l)} - \mathbf{B}^{(i)}_{(k,l)}\bar{\breve{\mathbf{S}}}^{(i-1)}_{(k,l)} \tag{5.40}$$

with

$$\mathbf{F}^{(i)}_{(k,l)} = \mathbf{E}^{(i)}_{(k,l)}P^{*}_{(k,l)} \tag{5.41}$$

where the feedforward filter $\mathbf{F}^{(i)}_{(k,l)}$, at each iteration i, is pragmatically considered as the product of the pulse shaping matched filter $P^{*}_{(k,l)}$ and the filter $\mathbf{E}^{(i)}_{(k,l)}$ that tries to equalise the channel. This results in

$$\begin{aligned}\widetilde{\breve{\mathbf{S}}}^{(i)}_{(k,l)} &= \mathbf{E}^{(i)}_{(k,l)}P^{*}_{(k,l)}\left(P_{(k,l)}\mathbf{H}_{(k,l)}\breve{\mathbf{S}}_{(k,l)} + \mathbf{N}_{(k,l)}\right) - \mathbf{B}^{(i)}_{(k,l)}\bar{\breve{\mathbf{S}}}^{(i-1)}_{(k,l)} = \\ &= |P_{(k,l)}|^2\mathbf{E}^{(i)}_{(k,l)}\mathbf{H}_{(k,l)}\breve{\mathbf{S}}_{(k,l)} + \mathbf{E}^{(i)}_{(k,l)}P^{*}_{(k,l)}\mathbf{N}_{(k,l)} - \mathbf{B}^{(i)}_{(k,l)}\bar{\breve{\mathbf{S}}}^{(i-1)}_{(k,l)}.\end{aligned} \tag{5.42}$$

Only after the equalisation process, the signal is down sampled using (5.23), i.e. the estimated signal is given by

$$\widetilde{\mathbf{S}}^{(i)}_{k} = \Upsilon\left(\widetilde{\breve{\mathbf{S}}}^{(i)}_{(k,l)}\right). \tag{5.43}$$

Using an MMSE criterion like in the previous section, it can be shown that the feedforward

[4]Without loss of generality, from now on, only soft decisions will be considered. The analysis for soft decisions for the remaining equalisers is similar to the IB-DFE case and it follows the lines of subsection 4.1.2.

coefficients excluding the pulse shaping matched filter are given by

$$\mathbf{E}_{(k,l)}^{(i)} = \boldsymbol{\kappa}\boldsymbol{\Lambda}_{(k,l)}^{(i)} \left(\mathbf{H}_{(k,l)}\right)^{H}, \tag{5.44}$$

with

$$\boldsymbol{\Lambda}_{(k,l)}^{(i)} = \left(\frac{1}{\gamma}\boldsymbol{I}_{N_T} + \left(\boldsymbol{I}_{N_T} - \left(\boldsymbol{\varrho}^{(i-1)}\right)^2\right)\left(\mathbf{H}_{(k,l)}\right)^{H}\mathbf{H}_{(k,l)}\right)^{-1}. \tag{5.45}$$

and $\boldsymbol{\kappa}$ being a diagonal normalisation matrix ensuring

$$\frac{1}{LN_{block}}\sum_{k=0}^{N_{block}-1}\sum_{l=0}^{L-1}\mathrm{Tr}\left(\mathbf{E}_{(k,l)}^{(i)}\mathbf{H}_{(k,l)}\right) = N_T. \tag{5.46}$$

The feedback coefficients for iteration i are given by

$$\mathbf{B}_{(k,l)}^{(i)} = \mathbf{F}_{(k,l)}^{(i)}\mathbf{H}_{(k,l)} - \boldsymbol{I}_{N_T}. \tag{5.47}$$

5.3.1 BER performance with pragmatic receiver

In this subsection, the same system tested in section 5.2.3 is used. By observing Fig. 5.3, we can see that the first iteration of the pragmatic receiver presents a very good performance, with results closer to the MFB, contrarily to the IB-DFE first iteration that cannot converge. Clearly, the first iteration presents a good estimation and the second iteration the pragmatic receiver continues to be better than a conventional IB-DFE. However, in the fourth iteration the performance becomes similar for both.

Although the results are similar when using iterations and it is almost indifferent which receiver its used, when trying to reduce the complexity, using less iterations, the pragmatic is the best choice, presenting a good performance even in its linear form. Nevertheless, it still requires matrix inversions, requiring high complexity.

5.4 Low complexity receivers for offset signals

In chapter 4, we saw that receivers based on MRC and EGC concepts [50, 64] present lower complexity than conventional IB-DFE receivers or pragmatic approaches. In fact, they could be a low complexity solution for equalisation, presenting very good performance when $N_T \ll N_R$. Since next generation communication systems, such as the one presented in section 3.1, can be

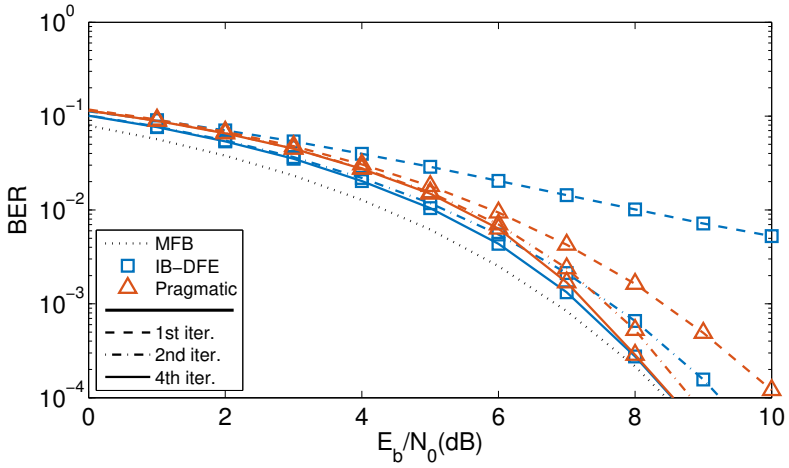

htb

Figure 5.3 BER performance comparison between IB-DFE and pragmatic receivers for a 4-OQAM constellation with $L = 2$, using multiple iterations with $N_T = 16$ transmitters each one with one antenna, $N_R = R_b \times R_u = 4 \times 16 = 64$ reception antennas with the R_u uncorrelated, i.e., $\rho_u = 0$.

designed to have high N_R/N_T ratios and that many antennas can be placed with distances of multiple wavelengths in a small space, especially for systems operating at mmWave frequencies, there will be conditions to use low complexity receivers that do not require matrix inversions. To adapt these receivers to offset signals, the pragmatic approach can be employed, equalising only the oversampled signal, instead of equalising and recover at the same time, and assuming pulse shaping perfect matching. Therefore, the output of the equaliser is given by

$$\widetilde{\breve{\mathbf{S}}}^{(i)}_{(k,l)} = \mathbf{F}_{(k,l)}\mathbf{Y}_{(k,l)} - \mathbf{B}_{(k,l)}\bar{\breve{\mathbf{S}}}^{(i-1)}_{(k,l)}\,, \tag{5.48}$$

followed by averaging according to (5.23), i.e., with result at the end of the i-th iteration being computed as in (5.43). The main differences to the previous approach are that instead of obtaining the feedforward coefficients through high complexity equations like (5.44) and (5.45), with the inversion of huge matrices for each frequency, MRC or EGC schemes use feedforward coefficients that are simpler to determine like the Hermitian of the channel and the phase of the channel elements, and that do not depend on the iteration[5].

Hence, the feedfoward coefficients for both equalisers are given by

$$\mathbf{F}_{(k,l)} = \mathbf{E}_{(k,l)}P^*_{(k,l)}, \tag{5.49}$$

[5]It should be noted that, as in the MRC and EGC receiver of [64], the iterations are still required to cancel the residual inter-user interference levels, but feedforward and feedback filters are kept unchanged along the iterations

with $\mathbf{E}_{(k,l)}$ varying accordingly the chosen method.

For the MRC equaliser, we have

$$\mathbf{E}_{(k,l)} = \boldsymbol{\kappa}\mathbf{H}^{H}_{(k,l)}, \tag{5.50}$$

where $\boldsymbol{\kappa}$ denotes a normalisation diagonal matrix whose the (t,t)-th element is given by

$$\kappa^{(t,t)} = \left(\frac{1}{LN_{block}} \sum_{l=0}^{L-1} \sum_{k=0}^{N_{block}-1} \sum_{r=1}^{N_R} \left| H^{(r,t)}_{(k,l)} \right|^2 \right)^{-1}. \tag{5.51}$$

For the EGC receiver, we have

$$\mathbf{E}_{(k,l)} = \boldsymbol{\kappa}\mathbf{A}^{H}_{(k,l)}, \tag{5.52}$$

with the elements of $\mathbf{A}_{(k,l)}$ given by

$$A^{(r,t)}_{(k,l)} = \frac{H^{(r,t)}_{(k,l)}}{|H^{(r,t)}_{(k,l)}|} = e^{j \arg\left(H^{(r,t)}_{(k,l)}\right)}, \tag{5.53}$$

and $\boldsymbol{\kappa}$ denoting a normalisation diagonal matrix whose the (t,t)-th element is given by

$$\kappa^{(t,t)} = \left(\frac{1}{LN_{block}} \sum_{l=0}^{L-1} \sum_{k=0}^{N_{block}-1} \sum_{r=1}^{N_R} \left| H^{(r,t)}_{(k,l)} \right| \right)^{-1}. \tag{5.54}$$

Hereupon, it can easily be shown that the optimum values of $\mathbf{B}_k$ are given by

$$\mathbf{B}_{(k,l)} = \mathbf{F}_{(k,l)}\mathbf{H}_{(k,l)} - \boldsymbol{I}_{N_T}. \tag{5.55}$$

The remaining process is equal to the one presented for the conventional IB-DFE or the pragmatic receivers. Therefore, iterative receivers based on MRC and EGC concepts are very similar to IB-DFE and pragmatic receivers but with the advantage of having fixed $\mathbf{F}_{(k,l)}$ and $\mathbf{B}_{(k,l)}$ matrices for the different iterations and not requiring complex matrix inversions, while obtaining almost the same BER performance for scenarios with $N_T \ll N_R$ and low correlation between antennas, as it will be shown in the next subsection.

5.4.1 BER performance analysis with low complexity receivers

In this subsection, the system presented in section 3.1 is used in a BER performance comparison for the receivers previously presented. We considered a system with $N_T = 16$ transmitters each one with one antenna and multiple configurations of the reception antennas. The mmWave channel described in section 2.3.3 was considered with $N_{ch\_clu} = 4$ clusters of $N_{ray\_clu} = 3$ rays each. The block size is $N_{block} = 256$ and different constellation sizes are tested. As previously, the pulse shaping is a half-cosine arcade.

We start to test the scenario with $N_R = R_b \times R_u = 4 \times 16 = 64$ reception antennas with the R_u groups uncorrelated, i.e., $\rho_u = 0$. These results are presented in Fig. 5.4. We can see that when using 4 iterations the low complexity receivers, especially the MRC, present a very good performance, close or even better than the IB-DFE and pragmatic approaches for 4-OQAM and 16-OQAM. This fact, allied to their low complexity, makes them a suitable choice for m-MIMO systems like the one herein described. However, for greater constellations such as 64-OQAM, their performance becomes poor. Since it was considered a scenario where the R_u were uncorrelated, the only way to improve the BER performance in 64-OQAM is to increase the number of reception antennas.

Therefore, we studied the BER performance when varying the correlation factor ρ_u for a given E_b/N_0 and for different number of reception antennas. The E_b/N_0 values chosen correspond to the MFB at 10^{-4} and are presented in table 5.1.

Table 5.1 E_b/N_0 at 10^{-4} of MFB for different constellations

	4-OQAM	**16-OQAM**	**64-OQAM**
E_b/N_0 @ 10^{-4}	8.6 dB	12.4 dB	16.7 dB

In Fig. 5.5, the BER results for the scenario previously presented with $N_R = R_b \times R_u = 4 \times 16 = 64$ reception antennas are depicted only for $\rho_u \geq 0.4$ because below this value there are no gains. It is shown that for 4-OQAM the BER is constant until the correlation reaches about 0.8 for all receivers. This limit is similar when considering 16-OQAM and 64-OQAM using IB-DFE or pragmatic receivers. However, as expected MRC and EGC are more sensible to the correlation factor, with MRC starting to be affected at $\rho_u = 0.5$ for 16-OQAM and with BER not being below 10^{-2} both of equalisers when using 64-OQAM.

On the other hand, when the number of antennas is increased to $N_R = R_b \times R_u = 4 \times 32 = 128$

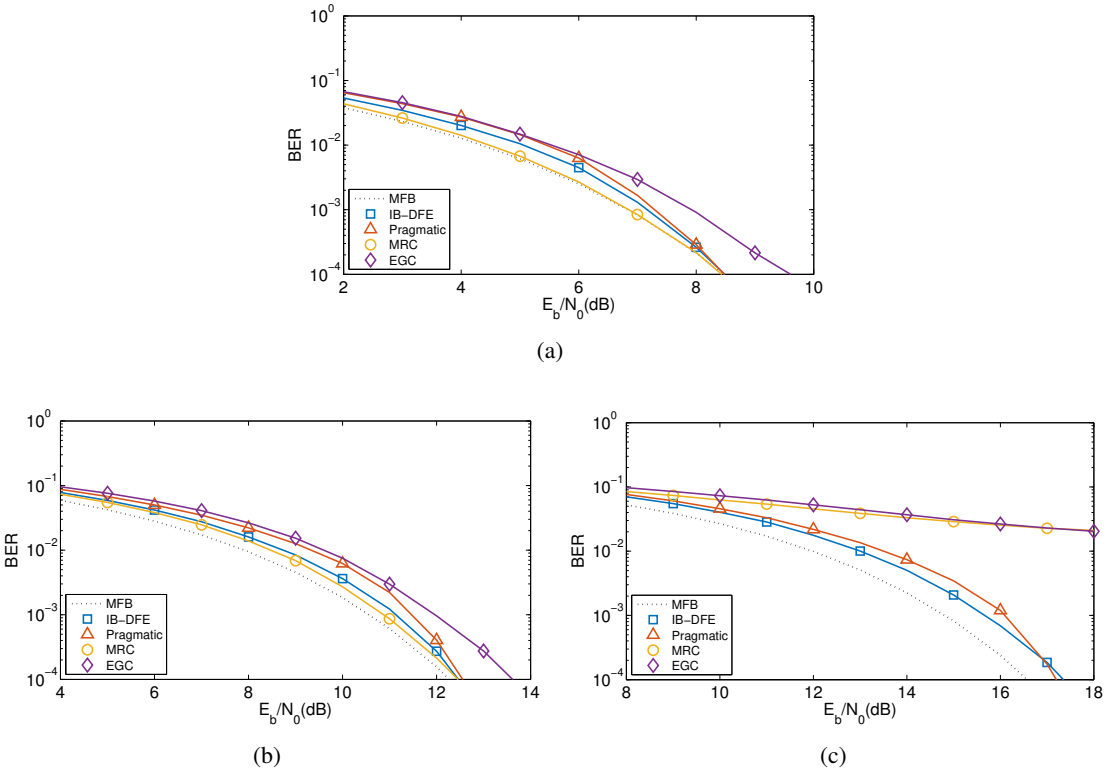

Figure 5.4 BER performance comparison of the 4th iteration of multiple receivers with $N_T = 16$ transmitters each one with one antenna, $N_R = R_b \times R_u = 4 \times 16 = 64$ reception antennas with the R_u groups uncorrelated, i.e., $\rho_u = 0$, for a) 4-OQAM, b) 16-OQAM and c) 64-OQAM constellations, with $L = 2$.

reception antennas, the performance of MRC and EGC improves substantially, even for 64-OQAM constellations, being only affected when $\rho_u \geq 0.8$ for the more complex methods as seen in Fig. 5.6. Therefore, once more it is shown that for an m-MIMO scenario at mmWaves, MRC is a low complexity alternative to other methods presenting the same or even better performance.

We have also performed simulations for an even harder case, where it was considered a system with $N_R = R_b \times R_u = 8 \times 32 = 256$ reception antennas and 64-OQAM. The results obtained were similar to the ones presented in Fig. 5.6(c), reinforcing the conclusions previously drawn, and for that reason they are not here presented. Simulation tests to study the impact of the diversity effect created by oversampling as also been conducted. It was also seen that, as long as $L \geq 2$, the diversity effect created by oversampling does not affect the BER performance when iterations are used and once more the results are not presented.

The hereby BER results show that low complexity receivers present performance very close to the MFB, with MRC being the best receiver tested, but they are more sensitive to correlation

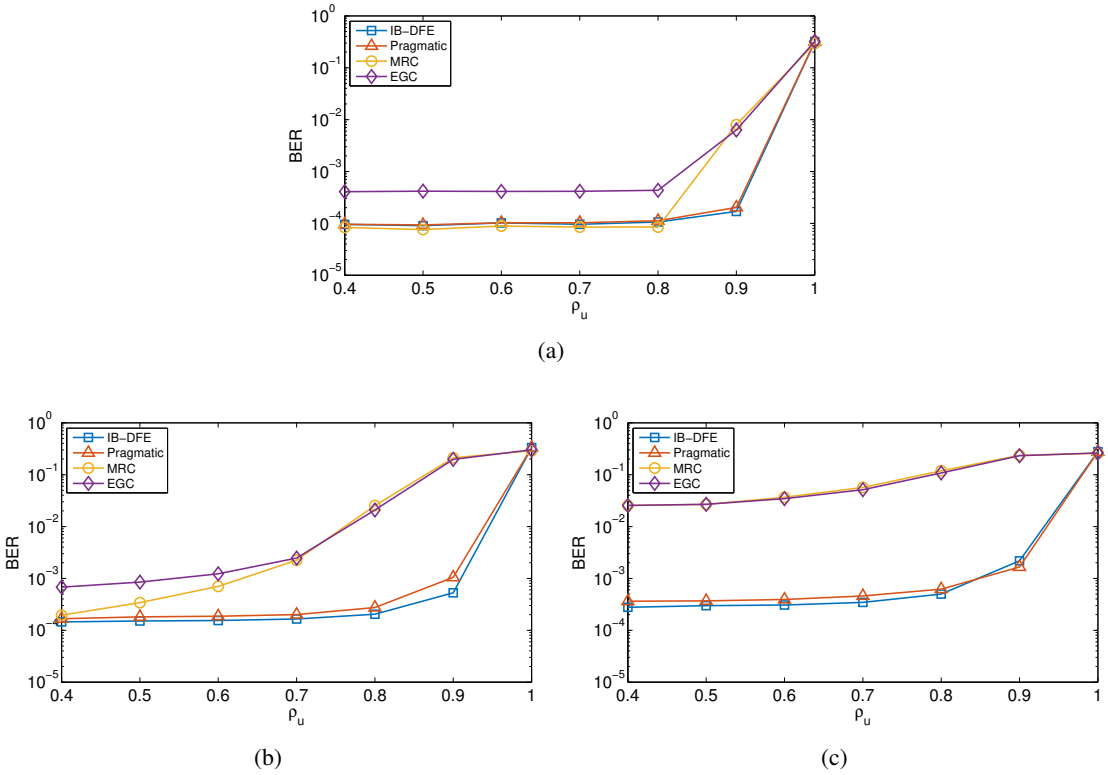

Figure 5.5 BER performance comparison at the 4th iteration of multiple receivers with $N_T = 16$ transmitters each one with one antenna, $N_R = R_b \times R_u = 4 \times 16 = 64$ reception antennas with variant correlation for a) 4-OQAM, b) 16-OQAM and c) 64-OQAM constellations with $L = 2$ using the E_b/N_0 values present in table 5.1.

between antennas. However, when under favourable conditions, i.e., for m-MIMO scenarios with hundreds of antennas, they present the same behaviour of IB-DFE or pragmatic approaches, only being affected for $\rho_u \geq 0.8$ values. Hence, considering their low complexity, as we will see at the end of the chapter, they are a suitable choice to use in the next generation communication systems.

5.5 BER Performance analysis using amplification

In the previous sections, we proposed and evaluated receivers for offset signals and we verified that the low complexity receivers present similar BER results to the IB-DFE ones. However, only half-cosine arcade has been used as pulse shaping and as we have seen in section 2.4, bandwidth is being wasted when using this kind of filters because they use bandwidth above the minimum Nyquist. To improve spectral efficiency, other kind of pulse shaping filters can be employed. Nonetheless, they will increase the envelope fluctuations in the time domain of the filtered signal,

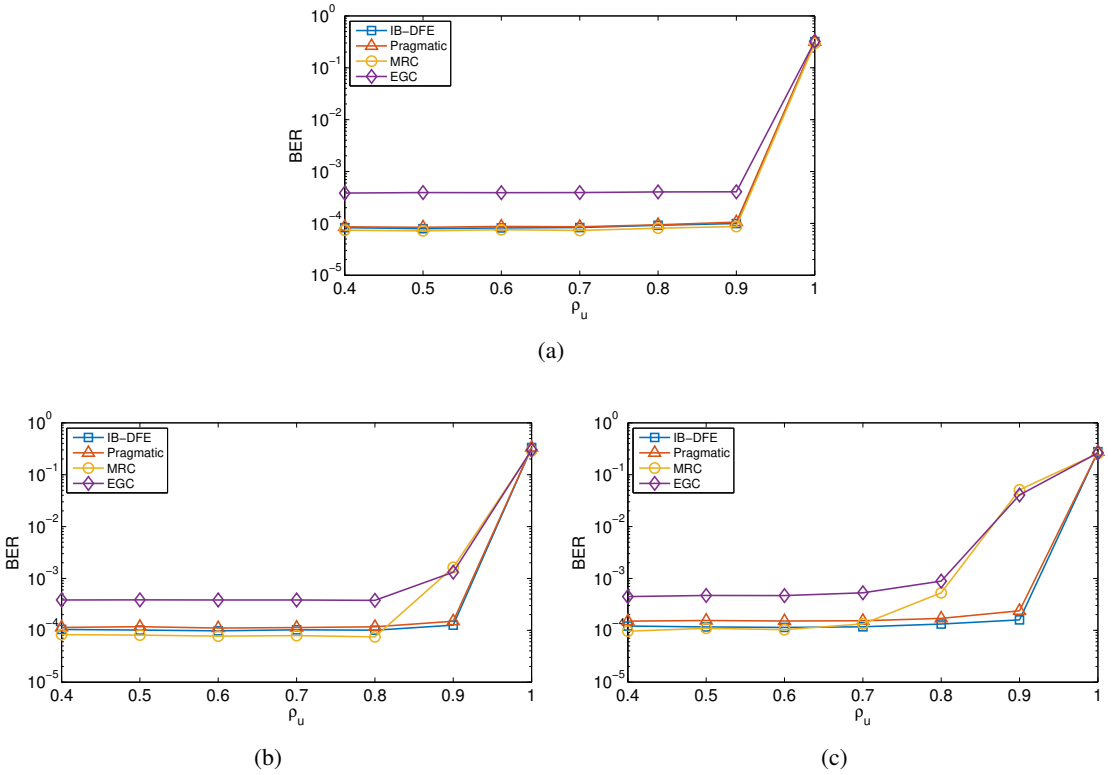

Figure 5.6 BER performance comparison at the 4th iteration of multiple receivers with $N_T = 16$ transmitters each one with one antenna, $N_R = R_b \times R_u = 4 \times 32 = 128$ reception antennas with variant correlation for a) 4-OQAM, b) 16-OQAM and c) 64-OQAM constellations with $L = 2$ using the E_b/N_0 values present in table 5.1.

reducing performance when amplification is used. In that sense, in this section, several pulse shaping filters are combined with different amplifier models when offset constellations are used.

In this section, we consider the same system used in the previous section with the addition of an amplification stage employing the SSPA or the hard limiter model. Moreover, only the hardest scenario is evaluated, i.e., 64-OQAM, because the interest of the system is to use large constellations to have high spectral efficiency and we saw in the previous sections that the increase of the constellation size is the bottleneck for the BER performance.

We start to combine the half-cosine arcade, previously used, with SSPA and hard limiter models. Here, we increase the number of groups R_u. Results are presented in Fig. 5.7, where we can see that there is no changes when employing amplification. This fact is easily explained because the signals present constant envelope, with the amplification not adding distortion. However, we already know that bandwidth is being wasted.

To improve the spectral efficiency without decreasing power efficiency, we employed a filtered

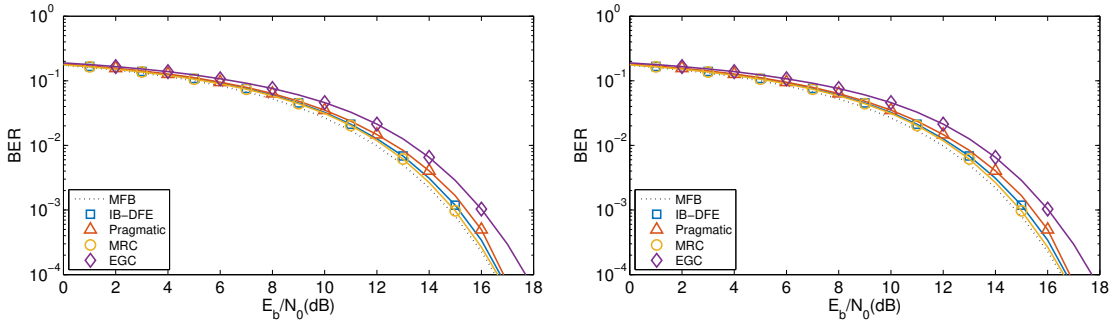

(a) (b)

Figure 5.7 BER performance comparison of the 4th iteration of multiple receivers with $N_T = 16$ transmitters each one with one antenna, $N_R = R_b \times R_u = 4 \times 32 = 128$ reception antennas with $\rho_u = 0.5$ for 64-OQAM constellations, with $L = 2$ and half-cosine pulse shaping filter, when using a) SSPA with $p_{amp} = 1$ and b) hard limiter models.

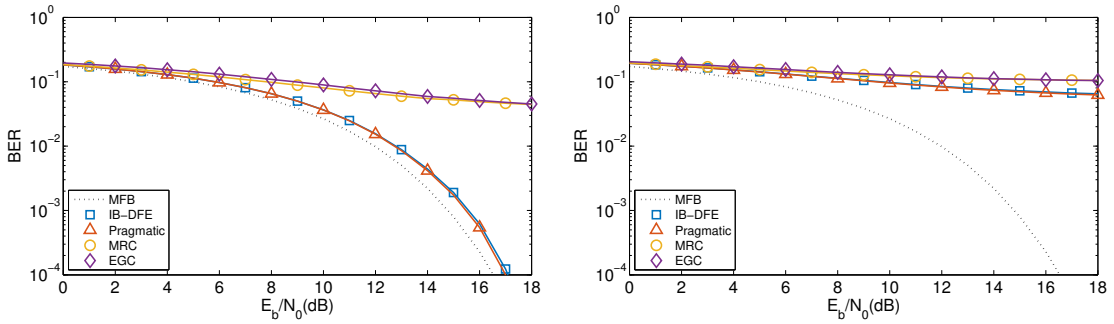

(a) (b)

Figure 5.8 BER performance comparison of the 4th iteration of multiple receivers with $N_T = 16$ transmitters each one with one antenna, $N_R = R_b \times R_u = 4 \times 32 = 128$ reception antennas with $\rho_u = 0.5$ for 64-OQAM constellations, with $L = 2$ and RC pulse shaping filter with $\beta = 0.22$, when using a) SSPA with $p_{amp} = 1$ and b) hard limiter models.

half-cosine pulse shaping filter obtaining the same results of Fig. 5.7 and for that reason they are not shown here. This fact is expected because the signal's envelope remains almost constant as we have seen in section 2.4.

To have further improvement in the limitation of the bandwidth, powerful pulse shaping filters should be used as RC or RRC. However, the signal's envelope will present some fluctuations which can present impact in the BER performance. In fact, when using an RC with $\beta = 0.22$ (the typical value used in LTE), BER suffers a large increase as we can see in Fig. 5.8. This increase only affects MRC and EGC when using SSPA model with $p_{amp} = 1$, but it is common to all equalisers when using the hard-limiter.

The same results of Fig. 5.8 are also obtained when using an RRC filter with the same roll-off. These results can be improved, with the use of more reception antennas as we see previously. Fig. 5.9 shows that in fact results are improved for the SSPA case, but there is still an error floor for hard limiter case, precluding the use of this kind of pulse shaping without envelope control techniques, even with very high N_R/N_T ratio.

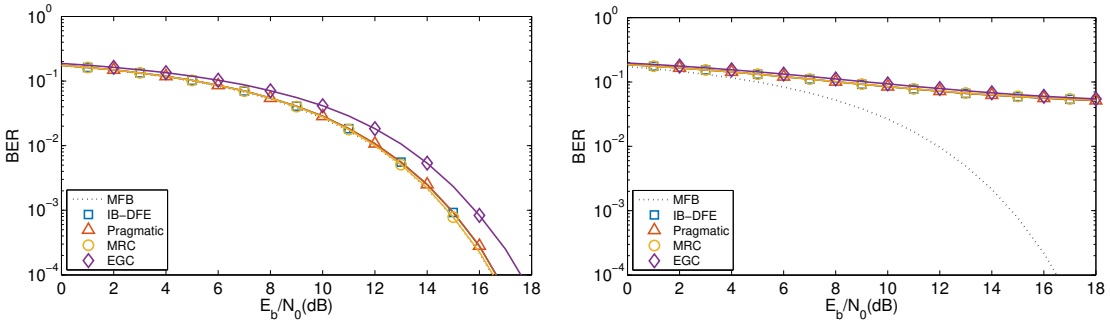

(a) (b)

Figure 5.9 BER performance comparison of the 4th iteration of multiple receivers with $N_T = 16$ transmitters each one with one antenna, $N_R = R_b \times R_u = 4 \times 128 = 512$ reception antennas with $\rho_u = 0.5$ for 64-OQAM constellations, with $L = 2$ and RRC pulse shaping filter with $\beta = 0.22$, when using a) SSPA with $p_{amp} = 1$ and b) hard limiter models.

Hence, the use of pulse shaping to limit the bandwidth, increasing the spectral efficiency of the communication systems, should be combined with control envelope techniques, such as MM, to reduce the signal's distortion and improve the BER performance.

5.6 Complexity Analysis

In this section, the complexity analysis for the different equalisers presented in this chapter is performed. This analysis is similar to the one presented in chapter 4, but now the equalisers analysed are: conventional IB-DFE, pragmatic and iterative MRC and EGC for offset signals. Once again, for conventional IB-DFE and pragmatic approaches, it is only done for its linear part, that in the case of IB-DFE corresponds to an MMSE equaliser.

This analysis is also performed per frequency k (i.e., at symbol rate $1/T_s$) to ensure a fair comparison when oversampling is used, since the various methods deal with it in different ways. Also, the number of FLOPs is used as comparison method and only the calculus directly related to the MIMO equalisation procedure are included. As in section 4.4, we consider that basic operations in the real domain require one FLOP. The number of required FLOPs for the remaining

matrix and scalar operations used in this analysis are in Table 4.1. Here, it is also considered the computational cost of $\Upsilon(\mathbf{v})$ function (where $\mathbf{v}$ is is an arbitrary vector of complex coefficients with size $P \times 1$ as defined in section 4.4 that is equal for all equalisers and corresponds to $15L$ FLOPs.

Table 5.2 presents the number of FLOPs of each algorithm stage, considering the equations presented in the previous sections. As this analysis is made per frequency k and the calculus of the normalisation diagonal matrix $\boldsymbol{\kappa}$ is equal for every frequency k, it only needs to be computed once and the calculus of its complexity is divided by N_{block}.

Note that for the iterative MRC and EGC equalisers, when estimating $\tilde{\mathbf{S}}_k$, the first iteration corresponds to the linear equaliser (5.22), and in the following iterations only the product $\mathbf{B}_{(k,l)}\bar{\mathbf{S}}_{(k,l)}^{(i-1)}$ and its subtraction from the result of (5.22) has to be computed, since the matrices $\mathbf{F}_{(k,l)}$ and $\mathbf{B}_{(k,l)}$ are fixed; thus each additional iteration adds just a small computational burden.

Table 5.2 shows that there is an improvement in reducing the computational complexity of the overall system when employing the iterative MRC and EGC in comparison with the first iteration of conventional IB-DFE and pragmatic receivers. Moreover, we see that conventional IB-DFE is more dependent on the oversampling factor, while the remaining methods only depend on it in the calculus of $\boldsymbol{\kappa}$ and when employing Υ function to recover the original symbols.

An important result that can be taken from Table 5.2 is the asymptotic complexity reduction when $N_R/N_T \gg 1$. From the table analysis, it can be concluded that MMSE and pragmatic present an asymptotic complexity of $(\frac{8}{3}+(4L+8)(N_R/N_T))N_T^3$ and $(\frac{8}{3}+12(N_R/N_T))N_T^3$, respectively, while for the iterative MRC and EGC is $(8(N_R/N_T))N_T^3$. By performing the ratios of the asymptotic complexities, one gets

$$\frac{\text{FLOPs}_{\text{MRC/EGC}}}{\text{FLOPs}_{\text{MMSE}}} \underset{\frac{N_R}{N_T}\gg 1}{\approx} \frac{8(N_R/N_T)}{\frac{8}{3}+(4L+8))(N_R/N_T)} \rightarrow \frac{8}{4L+8} \tag{5.56}$$

and

$$\frac{\text{FLOPs}_{\text{MRC/EGC}}}{\text{FLOPs}_{\text{Pragmatic}}} \underset{\frac{N_R}{N_T}\gg 1}{\approx} \frac{8(N_R/N_T)}{\frac{8}{3}+12(N_R/N_T)} \rightarrow \frac{2}{3} \quad , \tag{5.57}$$

which means that the complexity reduction converges asymptotically to 33% comparing with the pragmatic approach and, at least, 50% (considering L=2) when comparing with MMSE. Note that for moderate values of N_R and N_T, this may not seem a substantial reduction regarding the number of computed FLOPs. However, for m-MIMO scenarios, where it is necessary to deal with high dimension matrices, this reduction is noticeable, and it may correspond to the savings of

Table 5.2 Total number of FLOPs for each equaliser adapted for offset constellations

Method		**Equation(s)**
MMSE	$\boldsymbol{\kappa}$: $8LN_TN_R$	LHS of (5.29)
(1st iteration	$\mathbf{F}_{(k,l)}$: $\frac{8}{3}N_T^3+(4L+8)N_T^2N_R+\left(\frac{15}{2}+L\right)N_T^2+(12L-2)N_TN_R+\left(\frac{41}{6}-L\right)N_T$	(5.32)
IB-DFE)	$\widetilde{\mathbf{S}}_{(k,l)}$: $\frac{8}{3}N_T^3+(4L+8)N_T^2N_R+\left(\frac{15}{2}+L\right)N_T^2+(12L+6)N_TN_R+\left(\frac{29}{6}-L\right)N_T$	(5.22)
	$\widetilde{\mathbf{S}}_k$: $\frac{8}{3}N_T^3+(4L+8)N_T^2N_R+\left(\frac{15}{2}+L\right)N_T^2+(12L+6)N_TN_R+\left(\frac{29}{6}-L\right)N_T+15L$	(5.23)
Pragmatic	$\boldsymbol{\kappa}$: $8LN_TN_R$	LHS of (5.46)
(1st iteration)	$\mathbf{E}_{(k,l)}$: $\frac{8}{3}N_T^3+12N_T^2N_R+\frac{17}{2}N_T^2+2N_TN_R-\frac{1}{6}N_T$	(5.44)
	$\mathbf{F}_{(k,l)}$: $\frac{8}{3}N_T^3+12N_T^2N_R+\frac{17}{2}N_T^2+(8L+4)N_TN_R+\frac{35}{6}N_T$	(5.41)
	$\widetilde{\mathbf{S}}_{(k,l)}$: $\frac{8}{3}N_T^3+12N_T^2N_R+\frac{17}{2}N_T^2+(8L+12)N_TN_R+\frac{23}{6}N_T$	(5.22)
	$\widetilde{\mathbf{S}}_k$: $\frac{8}{3}N_T^3+12N_T^2N_R+\frac{17}{2}N_T^2+(8L+12)N_TN_R+\frac{23}{6}N_T+15L$	(5.23)
MRC	$\boldsymbol{\kappa}$: $4LN_TN_R$	(4.32)
	$\mathbf{E}_{(k,l)}$: $4LN_TN_R+6N_T$	(5.50)
	$\mathbf{F}_{(k,l)}$: $(4L+2)N_TN_R+6N_T$	(4.31)
	$\mathbf{B}_{(k,l)}$: $8N_T^2N_R-2N_T^2+N_T$	(5.55)
	$\widetilde{\mathbf{S}}_{(k,l)}$: $\underline{1^{st}\text{ iter}}$: $(4L+10)N_TN_R+4N_T$ $\underline{2^{nd}\text{ iter}}$: ($1^{st}$ iter) $+8N_T^2N_R+6N_T^2+N_T$ $\underline{n_i>2\text{ iter}}$: ($2^{nd}$ iter) $+(8n_i-16)N_T^2$	(5.48)
	$\widetilde{\mathbf{S}}_k$ **(no iter.)**: $(4L+10)N_TN_R+4N_T+15L$ **($\mathbf{n_i}$>1 iter.)**: $8N_T^2N_R+(8n_i-10)N_T^2+(4L+10)N_TN_R+5N_T+15L$	(5.23)
EGC	$\boldsymbol{\kappa}$: $5LN_TN_R$	(4.34)
	$\mathbf{E}_{(k,l)}$: $(5L+6)N_TN_R+6N_T$	(5.52)
	$\mathbf{F}_{(k,l)}$: $(5L+8)N_TN_R+6N_T$	(4.31)
	$\mathbf{B}_{(k,l)}$: $8N_T^2N_R-2N_T^2+N_T$	(5.55)
	$\widetilde{\mathbf{S}}_{(k,l)}$: $\underline{1^{st}\text{ iter}}$: $((5L+16)N_TN_R+4N_T$ $\underline{2^{nd}\text{ iter}}$: ($1^{st}$ iter) $+8N_T^2N_R+6N_T^2+N_T$ $\underline{n_i>2\text{ iter}}$: ($2^{nd}$ iter) $+(8n_i-16)N_T^2$	(5.48)
	$\widetilde{\mathbf{S}}_k$ **(no iter.)**: $(5L+16)N_TN_R+4N_T+15L$ **($\mathbf{n_i}$>1 iter.)**: $8N_T^2N_R+(8n_i-10)N_T^2+(5L+16)N_TN_R+5N_T+15L$	(5.23)

hundreds of thousands of FLOPs as shown in Table 5.3[6].

This complexity analysis shows that MRC and EGC receivers present even further complexity reduction than for non-offset signals and they are a valuable choice for the system proposed in section 3.1.

[6]The ratio N_R/N_T in Table 5.3 only considers the number of R_u antennas since their correlation is the main factor that influences the performance of the receivers as we see in chapter 4.

Table 5.3 Number of FLOPs for different m-MIMO scenarios using offset constellations

$N_T \times R_b \times R_u$	$16 \times 4 \times 16$	$16 \times 4 \times 32$	$16 \times 4 \times 128$
MMSE	306 294	599 158	2 356 342
Pragmatic	238 470	463 750	1 815 430
MRC	**1st iter**: 18 496 **2nd iter**: 132 624 **Following iterations**: 2048	**1st iter**: 36 928 **2nd iter**: 263 696 **Following iterations**: 2048	**1st iter**: 147 520 **2nd iter**: 1 050 128 **Following iterations**: 2048
	Total (for 4 iter.): 155 246	**Total (for 4 iter.)**: 304 750	**Total (for 4 iter.)**: 1 201 774
EGC	**1st iter**: 26 688 **2nd iter**: 132 624 **Following iterations**: 2048	**1st iter**: 53 312 **2nd iter**: 263 696 **Following iterations**: 2048	**1st iter**: 213 056 **2nd iter**: 1 050 128 **Following iterations**: 2048
	Total (for 4 iter.): 163 438	**Total (for 4 iter.)**: 321 134	**Total (for 4 iter.)**: 1 267 310
N_R/N_T	1	2	8
Complexity Reduction (MMSE)	49%	49%	49%
Complexity Reduction (Prag.)	35%	34%	34%

5.7 Conclusion remarks

In this chapter, we considered the use of offset constellations in m-MIMO systems operating at mmWave frequencies. The transmitted signals were designed to be compatible with strongly non-linear power amplifiers, since they either have an almost constant envelope (as in the OQPSK case) or can be decomposed as the sum of constant-envelope OQPSK components, making them compatible with strongly non-linear power amplifiers.

To equalise this type of signals, we proposed low complexity frequency domain receivers. In m-MIMO scenarios, it is shown that the proposed receivers can have performance close to the MFB, while achieving a complexity at least 33% lower than conventional methods that employ matrix inversions, making them particularly interesting for future wireless systems operating at mmWave bands.

Nonetheless, these receivers only work well when no amplification is employed or, if it is employed, when the pulse shaping has a bandwidth bigger than the minimum Nyquist band with the signals remaining with constant envelope. To use pulse shaping filters close to the minimum Nyquist band such as RC and RRC, signals should suffer some kind of envelope control to keep its envelope constant.

6

Conclusions and Future Work

6.1 Conclusions

This thesis proposed a new multilayer m-MIMO architecture at mmWave bands for the next generation wireless systems for uplink scenarios. This new architecture allows the achievement of high spectral and power efficiencies. The gains in spectral efficiency result from the use of high level constellations and spatial multiplexing which increases the overall system throughput. The gains in power efficiency result from the decomposition of these high level constellations into polar components with quasi-constant envelope (through the use of proper pulse shaping and/or MM techniques) transmitted over independent antennas, while using SC modulation and efficient non-linear amplification. The architecture use up to three layers of antennas at the transmitter enable to explore spatial multiplexing, beamforming and efficient amplification, and two layers at the receiver that explore spatial multiplexing and beamforming. This is made possible because of the small wavelengths at mmWave bands that allow the placement of hundreds of antennas in a small area.

Different features of this new architecture were studied and it was tested under a mmWave clustered channel model that was also proposed within the scope of this thesis. The main contributions to this new architecture can be summarised as:

- A simplified and accurate BER expression based on a Gaussian approximation has been proposed for systems performing MM with M-PSK constellations. This expression has proved to be suitable for both AWGN and time-dispersive channels within different system configurations, such as MM maximum admissible amplitude and the pulse shaping filter's roll-off, being dependent only on the constellation size and the KL divergence between the PDF of MM factors and the Gaussian PDF approximation. The proposed BER expression allows the fast assessment of the performance M-PSK signals with MM possible in a straightforward manner, without having to perform extensive Monte Carlo simulations.

- A new set of iterative low complexity equalisers based on the MRC and EGC principles have been proposed. These enable considerable savings on the computational burden when equalising m-MIMO signals employing block-based SC transmission with FDE. The gain of the proposed techniques results from not requiring the inversion of the channel matrix, as state of the art equalisers do.

- Low complexity frequency domain receivers to equalise OQPSK-type signals and to perform multi-user detection under m-MIMO scenarios were also proposed. This type of signals is very important in the development of the new proposed architecture since they have an almost constant envelope making them compatible with strongly non-linear power amplifiers enabling high power efficient transmission. In m-MIMO scenarios, it is shown that the proposed receivers can have performance close to the MFB, while achieving a complexity at least 33% lower than conventional methods that employ matrix inversions, making them particularly interesting for future wireless systems operating at mmWave bands.

6.2 Future Work

Although during this work we have produced 1 patent application, 3 journal articles and 10 articles in proceedings of international conferences, not all features of this new architecture have been addressed and there is still open issues to be solved in the future.

The development of the new multilayer m-MIMO at mmWave proposed in this thesis still present some challenges, mainly at the transmitter side. Fig. 6.1 recovers the transmitter chain per user presented in section 3.4. There, we can see that MM is not included in the system yet and the combination at wireless channel was not also performed.

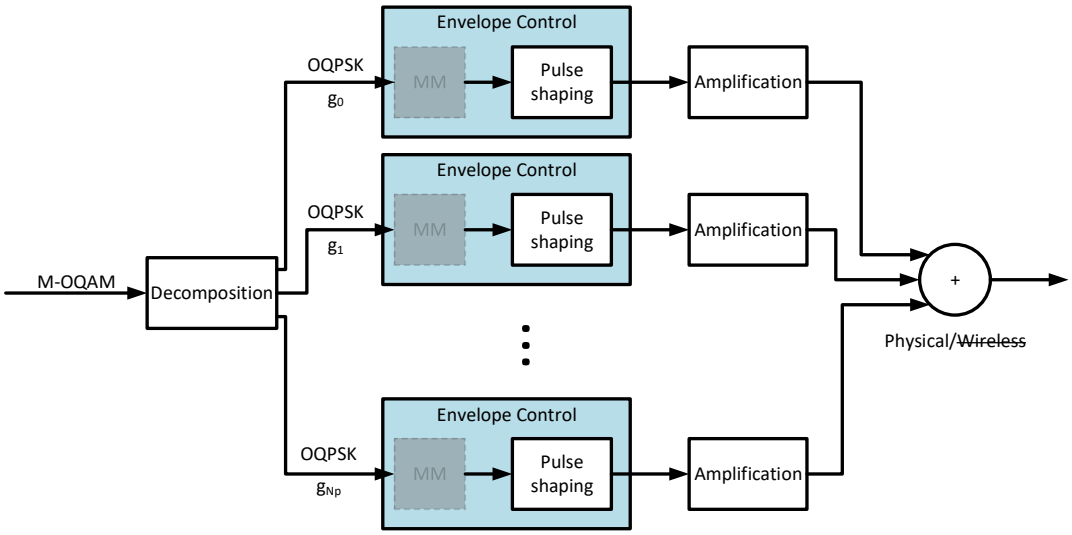

Figure 6.1 Current development status of the transmission chain of a generic user of the proposed multilayer m-MIMO architecture at mmWave bands.

Hence, one of the future challenges is to include an MM module in the transmitter system. This will allow the use of strongly non-linear amplifiers, but will require receivers able to retrieve MM signals. A possible approach to simplify receivers for MM signals is equalising only the channel impairments as we did in chapter 3. As we will consider OQPSK, each symbol is on a different quadrant and there is no zero crossings, which makes straightforward to obtain the original signals after equalising. Also, to improve the envelope control, MM techniques especially designed for OQPSK-type signals, such as Ring-type Magnitude Modulation (RMM) [28, 29, 70], can be employed.

Another future challenge is the use of the wireless channel as combiner for the polar components of a high level constellation. This will reduce the complexity at the transmitter side, but could raise some issues at the receiver side.

Beside these two topics that are only incremental to this thesis, there are other future possibilities of research, which are:

- The inclusion of the proposed architecture in a more complex system not only performing

uplink scenarios but also downlink scenarios, where probably will be used multi carrier modulations;

- The test of these techniques in the physical world, building a prototype, e.g. in software defined ratio platforms, to serve as proof of concept.

Bibliography

[1] A. Osseiran *et al.*, "Scenarios for 5G mobile and wireless communications: the vision of the METIS project," *IEEE Communications Magazine*, vol. 52, no. 5, pp. 26–35, May 2014.

[2] S. Rangan, T. Rappaport, and E. Erkip, "Millimeter-Wave Cellular Wireless Networks: Potentials and Challenges," *Proceedings of the IEEE*, vol. 102, no. 3, pp. 366–385, Mar 2014.

[3] F. Boccardi, R. Heath, A. Lozano, T. Marzetta, and P. Popovski, "Five disruptive technology directions for 5G," *Commun. Mag., IEEE*, vol. 52, no. 2, pp. 74–80, Feb 2014.

[4] S. Sun, T. Rappaport, R. Heath, A. Nix, and S. Rangan, "MIMO for millimeter-wave wireless communications: beamforming, spatial multiplexing, or both?" *Commun. Mag., IEEE*, vol. 52, no. 12, pp. 110–121, Dec 2014.

[5] E. Biglieri *et al.*, *MIMO Wireless Communications*. New York, NY, USA: Cambridge University Press, 2007.

[6] A. Alkhateeb, J. Mo, N. Gonzalez-Prelcic, and R. Heath, "MIMO Precoding and Combining Solutions for Millimeter-Wave Systems," *Commun. Mag., IEEE*, vol. 52, no. 12, pp. 122–131, Dec 2014.

[7] N. Benvenuto, R. Dinis, D. Falconer, and S. Tomasin, "Single Carrier Modulation With Nonlinear Frequency Domain Equalization: An Idea Whose Time Has Come Again," *Proceedings of the IEEE*, vol. 98, no. 1, pp. 69–96, Jan 2010.

[8] R. Dinis, R. Kalbasi, D. Falconer, and A. Banihashemi, "Iterative Layered Space-Time Receivers for Single-Carrier Transmission Over Severe Time-Dispersive Channels," *IEEE Comm. Letters*, vol. 39, no. 19, pp. 1144–1145, Sept 2004.

[9] R. Nee and R. Prasad, *OFDM for Wireless Multimedia Communications*. Artech House Publishers, 2000.

[10] U. S. Jha and R. Prasad, *OFDM Towards Fixed and Mobile Broadband Wireless Access*. Artech House Publishers, 2007.

[11] M. Gomes, V. Silva, F. Cercas, and M. Tomlinson, "Power efficient back-off reduction through polyphase filtering magnitude modulation," *Commun. Letters, IEEE*, vol. 13, no. 8, pp. 606–608, Aug 2009.

[12] M. Gomes, R. Dinis, V. Silva, F. Cercas, and M. Tomlinson, "Error rate analysis of M-PSK with magnitude modulation envelope control," *Electronics Letters*, vol. 49, no. 18, pp. 1184–1186, Aug 2013.

[13] A. Birafane, M. El-Asmar, A. Kouki, M. Helaoui, and F. Ghannouchi, "Analyzing LINC Systems," *Microwave Mag., IEEE*, vol. 11, no. 5, pp. 59–71, Aug 2010.

[14] J. Silva, R. Dinis, N. Souto, and P. Montezuma, "Single-carrier frequency domain equalisation with hierarchical constellations: an efficient transmission technique for broadcast and multicast systems," *Commun., IET*, vol. 6, no. 13, pp. 2065–2073, Sept 2012.

[15] R. Dinis, P. Montezuma, N. Souto, and J. Silva, "Iterative Frequency-Domain Equalization for general constellations," in *Sarnoff Symposium, 2010 IEEE*, Apr 2010, pp. 1–5.

[16] V. Astucia, R. Dinis, P. Montezuma, and M. Beko, "Efficient Amplification and Detection of Multilevel SC-FDE Signals Based on BPSK Components," in *Military Commun. Conf., MILCOM 2013 - 2013 IEEE*, Nov 2013, pp. 791–796.

[17] M. Luzio, R. Dinis, and P. Montezuma, "Pragmatic Frequency Domain Equalization for Single Carrier with Offset Modulations," *Wireless Commun., IEEE Transactions on*, vol. 12, no. 9, pp. 4496–4505, Sept 2013.

[18] P. Bento, A. Pereira, R. Dinis, M. Gomes, and V. Silva, "Frequency-Domain Detection without Matrix Inversions for mmWave Communications with Correlated Massive MIMO Channels," in *2017 IEEE 85th Vehicular Technology Conference (VTC Spring)*, June 2017, pp. 1–5.

[19] R. Dinis, P. Montezuma, P. Bento, M. Gomes, and V. Silva, "A multi-antenna technique for mm-wave communications with large constellations and strongly nonlinear amplifiers," in *Microwave Conf. (GeMiC), 2015 German*, Mar 2015, pp. 284–287.

[20] R. Dinis, P. Montezuma, P. Bento, M. Gomes, and V. Silva, "A Massive MIMO Architecture for Highly Efficient mm-Wave Communications with Saturated Amplifiers," in *International Conf. on Electronics, Information, and Communication*, Jan 2015.

[21] P. Bento, P. Carvalho, R. Dinis, M. Gomes, and V. Silva, "Transmission method with double directivity," USA PPP USPTO 15 330 968 (Pending), Jan, 2015.

[22] P. Bento, P. Carvalho, R. Dinis, M. Gomes, and V. Silva, "Método de Transmissão com dupla directividade," Portugal PPP PT 108 149A, Jan, 2015.

[23] P. Bento, A. Pereira, M. Gomes, R. Dinis, and V. Silva, "Simplified and accurate BER analysis of magnitude modulated M-PSK signals," *IET Communications*, vol. 13, pp. 1443–1448, June 2019.

[24] M. Luzio, R. Dinis, and P. Montezuma, "Sc-fde for offset modulations: An efficient transmission technique for broadband wireless systems," *IEEE Transactions on Communications*, vol. 60, no. 7, pp. 1851–1861, July 2012.

[25] P. Bento, A. Pereira, R. Dinis, M. Gomes, and V. Silva, "Low complexity equalisers for offset constellations in massive MIMO schemes," *IEEE Access*, June 2019.

[26] R. Dinis, P. Carvalho, P. Bento, M. Gomes, and V. Silva, "Linear Amplification with Multiple Amplifiers and Antennas," in *IASTED International Conf. on Modelling, Identification and Control - MIC*, vol. 1, February 2016, pp. 1–5.

[27] A. P. S. Silva, P. Bento, M. Gomes, R. Dinis, and V. Silva, "Complexity Analysis of FDE Receivers for Massive MIMO Block Transmission Systems," *IET Communications*, vol. 13, pp. 1762–1768, July 2019.

[28] A. Simões, P. Bento, M. A. C. Gomes, R. Dinis, and V. Silva, "Efficient LINC Amplification for 5G Through Ring-type Magnitude Modulation," in *IEEE GC 2015 Workshop on Mobile Commun. in Higher Frequency Bands (MCHFB) (GC'15 - Workshop - MCHFB)*, San Diego, USA, Dec. 2015.

[29] A. Simoes, P. Bento, M. Gomes, R. Dinis, and V. Silva, "Ring-Type Magnitude Modulation for OQPSK: Enabling NL-Amplification of Spectral Efficient Signals," in *2016 IEEE 83rd Vehicular Technology Conference (VTC Spring)*, May 2016, pp. 1–5.

[30] P. Bento, C. H. Antunes, M. Gomes, R. Dinis, and V. Silva, "Beamforming Optimization for Multiuser Wireless Systems Using Meta-Heuristics," in *2016 IEEE 84th Vehicular Technology Conference (VTC-Fall)*, Sep. 2016, pp. 1–5.

[31] A. Pereira, P. Bento, M. Gomes, R. Dinis, and V. Silva, "Iterative MRC and EGC Receivers for MIMO-OFDM Systems," in *2018 IEEE 87th Vehicular Technology Conference (VTC Spring)*, June 2018, pp. 1–4.

[32] A. Pereira, P. Bento, M. Gomes, R. Dinis, and V. Silva, "TIBWB-OFDM: A Promising Modulation Technique for MIMO 5G Transmissions," in *2018 IEEE 88th Vehicular Technology Conference (VTC-Fall)*, Aug 2018, pp. 1–5.

[33] A. Pereira, P. Bento, M. Gomes, R. Dinis, and V. Silva, "MIMO Time-Interleaved Block Windowed Burst OFDM with Iterative Frequency Domain Equalization," in *2018 15th International Symposium on Wireless Communication Systems (ISWCS)*, Aug 2018, pp. 1–6.

[34] G. PPP, "5G Vision," Brochure, Feb 2015. [Online]. Available: https://5g-ppp.eu/wp-content/uploads/2015/11/Vision-brochure.pdf

[35] T. Rappaport, R. Heath, R. Daniels, and J. Murdock, *Millimeter Wave Wireless Communications*. Pearson Education, 2014.

[36] "United States Frequency Allocation Chart." [Online]. Available: https://www.ntia.doc.gov/page/2011/united-states-frequency-allocation-chart

[37] "First Millimeter-wave Communication Experiments by J.C. Bose." [Online]. Available: http://ethw.org/Milestones:First_Millimeter-wave_Communication_Experiments_by_J.C._Bose

[38] A. Swindlehurst, E. Ayanoglu, P. Heydari, and F. Capolino, "Millimeter-wave massive MIMO: the next wireless revolution?" *Commun. Mag., IEEE*, vol. 52, no. 9, pp. 56–62, Sept 2014.

[39] G. Raleigh and J. Cioffi, "Spatio-temporal coding for wireless communications," in *Global Telecommunications Conf., 1996. GLOBECOM '96. 'Commun.: The Key to Global Prosperity*, vol. 3, Nov 1996, pp. 1809–1814 vol.3.

[40] R. Dinis and A. Gusmão, "A class of nonlinear signal-processing schemes for bandwidth-efficient OFDM transmission with low envelope fluctuation," *Commun., IEEE Transactions on*, vol. 52, no. 11, pp. 2009–2018, Nov 2004.

[41] G. J. Foschini, "Layered space-time architecture for wireless communication in a fading environment when using multi-element antennas," *Bell Labs Technical Journal*, vol. 1, no. 2, pp. 41–59, Autumn 1996.

[42] A. Carlson and P. Crilly, *Communication Systems*. McGraw-Hill, 2009.

[43] E. Castañeda, A. Silva, R. Robles, and A. Gameiro, "Low-Complexity User Selection for Rate Maximization in MIMO Broadcast Channels with Downlink Beamforming," *The Scientific World Journal*, vol. 2014, no. 1, pp. 1 – 13, Jan 2014.

[44] W. Hong, K.-H. Baek, Y. Lee, Y. Kim, and S.-T. Ko, "Study and prototyping of practically large-scale mmWave antenna systems for 5G cellular devices," *Commun. Mag., IEEE*, vol. 52, no. 9, pp. 63–69, Sept 2014.

[45] Y. Yu, P. Baltus, and A. van Roermund, *Integrated 60GHz RF Beamforming in CMOS*, ser. Analog Circuits and Signal Processing. Springer Netherlands, 2011.

[46] E. Björnson, J. Hoydis, and L. Sanguinetti, *Massive MIMO Networks: Spectral, Energy, and Hardware Efficiency*. Now Publishers Inc, 2017, vol. 11, no. 3-4. [Online]. Available: http://dx.doi.org/10.1561/2000000093

[47] S. Haykin, *Digital Communication Systems*. USA: Wiley, 2013.

[48] O. E. Ayach, S. Rajagopal, S. Abu-Surra, Z. Pi, and R. W. Heath, "Spatially Sparse Precoding in Millimeter Wave MIMO Systems," *IEEE Transactions on Wireless Communications*, vol. 13, no. 3, pp. 1499–1513, Mar 2014.

[49] A. Papoulis, *Probability, Random Variables, and Stochastic Processes*. Mcgraw-Hill, 1984.

[50] A. Goldsmith, *Wireless Communications*. New York, NY, USA: Cambridge University Press, 2005.

[51] E. A. Lee and D. G. Messerschmitt, *Digital Communication*. Norwell, MA, USA: Kluwer Academic Publishers, 1988.

[52] A. S. Sedra and K. C. Smith, *Microelectronic Circuits*, 6th ed. Oxford University Press, 2010.

[53] B. Razavi, *RF Microelectronics*, 2nd ed. Upper Saddle River, NJ, USA: Prentice Hall Press, 2011.

[54] S. Litsyn, *Peak Power Control in Multicarrier Communications*. Cambridge University Press, 2007.

[55] S. H. Han and J. H. Lee, "An Overview of Peak-to-Average Power Ratio Reduction Techniques for Multicarrier Transmission," *Wireless Commun., IEEE*, vol. 12, no. 2, pp. 56–65, Apr 2005.

[56] Y. Rahmatallah and S. Mohan, "Peak-To-Average Power Ratio Reduction in OFDM Systems: A Survey And Taxonomy," *Commun. Surveys Tutorials, IEEE*, vol. 15, no. 4, pp. 1567–1592, Fourth 2013.

[57] M. Gomes, "Magnitude modulation for peak power control in single carrier communication systems," Ph.D. dissertation, Universidade de Coimbra, Portugal, 2010.

[58] A. Tomlinson, A. Ambroze, and G. Wade, "Power and bandwidth efficient modulation and coding for small satellite communication terminals," in *2002 IEEE International Conf. on Communications. Conf. Proceedings. ICC 2002*, vol. 5, 2002, pp. 2943–2946.

[59] M. Gomes, R. Dinis, V. Silva, F. Cercas, and M. Tomlinson, "Iterative FDE Design for LDPC-coded Magnitude Modulation Schemes," in *ISWCS 2013; The Tenth International Symposium on Wireless Communication Systems*, Aug 2013, pp. 1–5.

[60] C. Rapp, "Effects of HPA-nonlinearity on a 4-DPSK/OFDM-signal for a digital sound broadcasting signal," in *Second European Conf. on Satellite Commun., Liége, Belgium*, vol. 332, Oct 1991, pp. 179–184.

[61] P. Silva and R. Dinis, *Frequency-Domain Multiuser Detection for CDMA Systems*. River Publishers, 2012.

[62] A. Katz, B. Eggleston, D. McGee, and J. MacDonald, "UHF GaN SSPA for space applications," in *Radio and Wireless Symposium (RWS), 2010 IEEE*, Jan 2010, pp. 108–111.

[63] F. Ribeiro, J. Guerreiro, R. Dinis, F. Cercas, and A. Silva, "Reduced complexity detection in MIMO systems with SC-FDE modulations and iterative DFE receivers," *Journal of Sensor and Actuator Networks*, vol. 7, p. 17, 04 2018.

[64] D. Borges, P. Montezuma, and R. Dinis, "Low complexity MRC and EGC Based Receivers for SC-FDE Modulations with Massive MIMO Schemes," in *IEEE GLOBALSIP'2016*, Dec 2016, pp. –.

[65] S. L. Miller and R. J. O'Dea, "Peak power and bandwidth efficient linear modulation," *IEEE Transactions on Communications*, vol. 46, no. 12, pp. 1639–1648, Dec 1998.

[66] H. G. Myung, J. Lim, and D. J. Goodman, "Single carrier FDMA for uplink wireless transmission," *IEEE Vehicular Technology Magazine*, vol. 1, no. 3, pp. 30–38, Sept 2006.

[67] R. Dinis and P. Montezuma, "Iterative receiver based on the EGC for massive MIMO schemes using SC-FDE modulations," *Electronics Letters*, vol. 52, no. 11, pp. 972–974, 2016.

[68] M. Beko and R. Dinis, "Designing Good Multi-Dimensional Constellations," *Wireless Commun. Letters, IEEE*, vol. 1, no. 3, pp. 221–224, Jun 2012.

[69] M. Gomes, F. Cercas, V. Silva, and M. Tomlinson, "Magnitude modulation for vsat's low back-off transmission," *Journal of Communications and Networks*, vol. 12, no. 6, pp. 544–557, Dec 2010.

[70] A. Simoes, M. Castanheira, M. Gomes, R. Dinis, and V. Silva, "Ring-type Magnitude Modulation for LINC: a pragmatic approach to the efficiency challenge," *IEEE Transactions on Communications*, vol. 65, no. 8, pp. 3302–3315, Aug. 2017.

[71] N. Souto, R. Dinis, and J. C. Silva, "Impact of channel estimation errors on sc-fde systems," *IEEE Transactions on Communications*, vol. 62, no. 5, pp. 1530–1540, May 2014.

[72] S. Kullback and R. A. Leibler, "On Information and Sufficiency," *Annals of Mathematical Statistics*, vol. 22, no. 1, pp. 79–86, March 1951.

[73] 3GPP, "Evolved Universal Terrestrial Radio Access (E-UTRA); User Equipment (UE) radio transmission and reception," 3rd Generation Partnership Project (3GPP), Technical Specification (TS) 36.101, 09 2017, version 15.0.0.

[74] F. Ribeiro, R. Dinis, F. Cercas, and A. Silva, "Receiver Design for the Uplink of Base Station Cooperation Systems employing SC-FDE Modulations," *EURASIP Journal on Wireless Commun. and Networking*, vol. 2015, no. 1, pp. 1–17, Jan 2015.

[75] A. Gusmão, V. Goncalves, and N. Esteves, "A novel approach to modeling of OQPSK-type digital transmission over nonlinear radio channels," *Selected Areas in Commun., IEEE Journal on*, vol. 15, no. 4, pp. 647–655, May 1997.

[76] P. Montezuma and A. Gusmão, "On analytically described trellis-coded modulation schemes," *IEEE 6th ISCTA'01*, 2001.

[77] F. Amoroso and J. Kivett, "Simplified MSK Signaling Technique," *IEEE Transactions on Communications*, vol. 25, no. 4, pp. 433–441, April 1977.

[78] P. Montezuma, D. Marques, V. Astucia, R. Dinis, and M. Beko, "Robust Frequency-Domain Receivers for a Transmission Technique with Directivity at the Constellation Level," in *2014 IEEE 80th Vehicular Technology Conference (VTC2014-Fall)*, Sep. 2014, pp. 1–7.

[79] R. Dinis, T. Araujo, P. Pedrosa, and F. Nunes, "Joint turbo equalisation and carrier synchronisation for SC-FDE schemes," *European Transactions on Telecommunications*, vol. 21, pp. 131–141, 03 2010.

[80] P. Pedrosa, R. Dinis, and F. Nunes, "Iterative Frequency Domain Equalization and Carrier Synchronization for Multi-Resolution Constellations," *IEEE Transactions on Broadcasting*, vol. 56, no. 4, pp. 551–557, Dec 2010.

[81] P. Pedrosa, R. Dinis, F. Nunes, and J. Bioucas-Dias, "Phase Drift Estimation and Symbol Detection in Digital Communications: A Stochastic Recursive Filtering Approach," *IEEE Communications Letters*, vol. 16, no. 6, pp. 854–857, June 2012.

[82] P. Pedrosa, R. Dinis, F. Nunes, and A. Rodrigues, "Joint equalization and Gaussian sums particle filtering phase noise estimation," in *2014 IEEE International Conference on Communications (ICC)*, June 2014, pp. 4378–4383.

[83] R. Dinis, C. Lam, and D. Falconer, "Joint Frequency-Domain Equalization and Channel Estimation Using Superimposed Pilots," in *2008 IEEE Wireless Communications and Networking Conference*, March 2008, pp. 447–452.

[84] S. Haykin, *Adaptive Filter Theory (3rd Ed.)*. Upper Saddle River, NJ, USA: Prentice-Hall, Inc., 1996.

[85] J. Ren and S. Yoon, "Soft-Output Signal Detectors: Performance Comparisons in Wireless MIMO Communication Systems," in *Future Control and Automation*, W. Deng, Ed. Berlin, Heidelberg: Springer Berlin Heidelberg, 2012, pp. 471–478.

[86] R. Hunger, "Floating point operations in matrix-vector calculus," Munich University of Technology, Tech. Rep. V1.3, 2007.

[87] R. W. Farebrother, *Linear least squares computations*. New York: Marcel Dekker Inc, 1988.

[88] R. Lopez-Valcarce, "Channel equalization with staggered modulation formats," in *2002 14th International Conference on Digital Signal Processing Proceedings. DSP 2002 (Cat. No.02TH8628)*, vol. 2, July 2002, pp. 769–772 vol.2.

[89] K. B. Petersen and M. S. Pedersen, "The Matrix Cookbook," nov 2012. [Online]. Available: http://www2.imm.dtu.dk/pubdb/p.php?3274

A

List of Properties

The properties hereby presented are based on [84, 89]. **A** and **B** stand for complex matrices, **a** stands for a complex vector and **I** is the identity matrix. X and Y stands for random variables, c stands for a constant and $f()$ stands for a function. s is a time domain signal and S_k its DFT.

$$\mathbf{A}\mathbf{A}^{-1} = \mathbf{A}^{-1}\mathbf{A} = \mathbf{I} \tag{Prp. A}$$

$$||\mathbf{a}||_2 = (|a_1|^2 + |a_2|^2 + ... + |a_n|^2)^{1/2} = (\mathbf{a}^H\mathbf{a})^{1/2} \tag{Prp. B}$$

$$\mathbf{A}^H = \mathbf{A}^{T*} \tag{Prp. C}$$

$$(\mathbf{A}+\mathbf{B})^H = \mathbf{A}^H + \mathbf{B}^H \tag{Prp. D}$$

$$(\mathbf{A}\mathbf{B})^H = \mathbf{B}^H\mathbf{A}^H \tag{Prp. E}$$

$$\mathbf{a}^H\mathbf{a} = \mathrm{Tr}(\mathbf{a}\mathbf{a}^H) \tag{Prp. F}$$

$$\mathrm{Tr}(\mathbf{A}+\mathbf{B}) = \mathrm{Tr}(\mathbf{A}) + \mathrm{Tr}(\mathbf{B}) \tag{Prp. G}$$

$$\mathbb{E}\{X+Y\} = \mathbb{E}\{X\} + \mathbb{E}\{Y\} \tag{Prp. H}$$

$$\mathbb{E}\{cX\} = c\mathbb{E}\{X\} \tag{Prp. I}$$

$$\partial(\mathbf{A}+\mathbf{B}) = \partial(\mathbf{A}) + \partial(\mathbf{B}) \tag{Prp. J}$$

$$\partial(\mathbf{AB}) = \partial(\mathbf{A})\mathbf{B} + \mathbf{A}\partial(\mathbf{B}) \tag{Prp. K}$$

$$\nabla_{\mathbf{A}} f(\mathbf{A},\mathbf{B}) = 2\frac{\partial f(\mathbf{A},\mathbf{B})}{\partial \mathbf{A}^*} = \frac{\partial f(\mathbf{A},\mathbf{B})}{\partial \Re\mathbf{A}} + j\frac{\partial f(\mathbf{A},\mathbf{B})}{\partial \Im\mathbf{A}} \tag{Prp. L}$$

$$\frac{\partial \mathrm{Tr}(\mathbf{AB}^H)}{\partial \mathbf{B}^*} = \mathbf{A} \tag{Prp. M}$$

$$\frac{\partial \mathbf{A}}{\partial \mathbf{A}^*} = \frac{\partial \mathbf{A}^*}{\partial \mathbf{A}} = \mathbf{0} \tag{Prp. N}$$

$$\partial(\mathbb{E}[\mathbf{A}]) = \mathbb{E}[\partial(\mathbf{A})] \tag{Prp. O}$$

$$s[n-n_o] \overset{DFT}{\rightarrow} e^{-j\frac{2\pi k}{N}n_o} S[k] \tag{Prp. P}$$

$$\begin{cases} a+b, & = e \\ c+d, & = f \end{cases} \Leftrightarrow a+b+c+d = e+f \tag{Prp. Q}$$

B

Minimisation of MSE in IB-DFE receivers for MIMO

In this appendix, it is shown the full development of the calculus of the feedforward and feedback coefficients that minimise the MSE in the IB-DFE receivers for MIMO presented in section 4.1. Although this problem has been addressed multiple times in the literature, there is no place where it is entirely developed for MIMO matrices. In this sense, this appendix represents the work on the understanding of such technique during this thesis, that has served as a basis on the development of the proposed receivers. Moreover, it intends to fulfil the gap of a full development on the literature and to serve as a tutorial for future studies on IB-DFE and the development of new techniques based on it.

Here, the expressions presented in section 4.1 will be fully developed, with indication of all the properties used and that are described in the List of Properties at appendix A. It should also be noted that as the development of the optimisation problem does not depend on the iteration number, the superscript (i) will be omitted to lighten the notation.

First, let's develop the sum of the MSEs:

$$\boldsymbol{\Omega}_k = \mathbb{E}\left[\left(\widetilde{\mathbf{S}}_k - \mathbf{S}_k\right)^H \left(\widetilde{\mathbf{S}}_k - \mathbf{S}_k\right)\right] \tag{B.1}$$

$$= \mathbb{E}\left[\mathrm{Tr}\left(\left(\widetilde{\mathbf{S}}_k - \mathbf{S}_k\right)\left(\widetilde{\mathbf{S}}_k - \mathbf{S}_k\right)^H\right)\right] \tag{B.2}$$

$$= \mathbb{E}\left[\mathrm{Tr}\left(\left(\mathbf{F}_k\mathbf{Y}_k - \mathbf{B}_k\hat{\mathbf{S}}_k - \mathbf{S}_k\right)\left(\mathbf{F}_k\mathbf{Y}_k - \mathbf{B}_k\hat{\mathbf{S}}_k - \mathbf{S}_k\right)^H\right)\right] \tag{B.3}$$

$$= \mathbb{E}\Bigg[\mathrm{Tr}\Big(\left(\mathbf{F}_k\left(\mathbf{H}_k\mathbf{S}_k + \mathbf{N}_k\right) - \mathbf{B}_k\left(\boldsymbol{\varrho}\mathbf{S}_k + \boldsymbol{\Delta}_k\right) - \mathbf{S}_k\right) \left(\mathbf{F}_k\left(\mathbf{H}_k\mathbf{S}_k + \mathbf{N}_k\right) - \mathbf{B}_k\left(\boldsymbol{\varrho}\mathbf{S}_k + \boldsymbol{\Delta}_k\right) - \mathbf{S}_k\right)^H\Big)\Bigg] \tag{B.4}$$

$$= \mathbb{E}\Bigg[\mathrm{Tr}\Big(\left(\mathbf{F}_k\mathbf{H}_k\mathbf{S}_k + \mathbf{F}_k\mathbf{N}_k - \mathbf{B}_k\boldsymbol{\varrho}\mathbf{S}_k - \mathbf{B}_k\boldsymbol{\Delta}_k - \mathbf{S}_k\right) \left(\mathbf{S}_k^H\mathbf{H}_k^H\mathbf{F}_k^H + \mathbf{N}_k^H\mathbf{F}_k^H - \mathbf{S}_k^H\boldsymbol{\varrho}^H\mathbf{B}_k^H - \boldsymbol{\Delta}_k^H\mathbf{B}_k^H - \mathbf{S}_k^H\right)\Big)\Bigg] \tag{B.5}$$

$$\begin{aligned}
= \mathbb{E}\Bigg[\mathrm{Tr}\Big(&\mathbf{F}_k\mathbf{H}_k\mathbf{S}_k\mathbf{S}_k^H\mathbf{H}_k^H\mathbf{F}_k^H + \mathbf{F}_k\mathbf{H}_k\mathbf{S}_k\mathbf{N}_k^H\mathbf{F}_k^H - \mathbf{F}_k\mathbf{H}_k\mathbf{S}_k\mathbf{S}_k^H\boldsymbol{\varrho}^H\mathbf{B}_k^H - \mathbf{F}_k\mathbf{H}_k\mathbf{S}_k\boldsymbol{\Delta}_k^H\mathbf{B}_k^H \\
&- \mathbf{F}_k\mathbf{H}_k\mathbf{S}_k\mathbf{S}_k^H + \mathbf{F}_k\mathbf{N}_k\mathbf{S}_k^H\mathbf{H}_k^H\mathbf{F}_k^H + \mathbf{F}_k\mathbf{N}_k\mathbf{N}_k^H\mathbf{F}_k^H - \mathbf{F}_k\mathbf{N}_k\mathbf{S}_k^H\boldsymbol{\varrho}^H\mathbf{B}_k^H - \mathbf{F}_k\mathbf{N}_k\boldsymbol{\Delta}_k^H\mathbf{B}_k^H \\
&- \mathbf{F}_k\mathbf{N}_k\mathbf{S}_k^H - \mathbf{B}_k\boldsymbol{\varrho}\mathbf{S}_k\mathbf{S}_k^H\mathbf{H}_k^H\mathbf{F}_k^H - \mathbf{B}_k\boldsymbol{\varrho}\mathbf{S}_k\mathbf{N}_k^H\mathbf{F}_k^H + \mathbf{B}_k\boldsymbol{\varrho}\mathbf{S}_k\mathbf{S}_k^H\boldsymbol{\varrho}^H\mathbf{B}_k^H + \mathbf{B}_k\boldsymbol{\varrho}\mathbf{S}_k\boldsymbol{\Delta}_k^H\mathbf{B}_k^H \\
&+ \mathbf{B}_k\boldsymbol{\varrho}\mathbf{S}_k\mathbf{S}_k^H - \mathbf{B}_k\boldsymbol{\Delta}_k\mathbf{S}_k^H\mathbf{H}_k^H\mathbf{F}_k^H - \mathbf{B}_k\boldsymbol{\Delta}_k\mathbf{N}_k^H\mathbf{F}_k^H + \mathbf{B}_k\boldsymbol{\Delta}_k\mathbf{S}_k^H\boldsymbol{\varrho}^H\mathbf{B}_k^H + \mathbf{B}_k\boldsymbol{\Delta}_k\boldsymbol{\Delta}_k^H\mathbf{B}_k^H \\
&+ \mathbf{B}_k\boldsymbol{\Delta}_k\mathbf{S}_k^H - \mathbf{S}_k\mathbf{S}_k^H\mathbf{H}_k^H\mathbf{F}_k^H - \mathbf{S}_k\mathbf{N}_k^H\mathbf{F}_k^H + \mathbf{S}_k\mathbf{S}_k^H\boldsymbol{\varrho}^H\mathbf{B}_k^H + \mathbf{S}_k\boldsymbol{\Delta}_k^H\mathbf{B}_k^H + \mathbf{S}_k\mathbf{S}_k^H\Big)\Bigg]
\end{aligned} \tag{B.6}$$

$$\begin{aligned}
= \mathbb{E}\Bigg[&\mathrm{Tr}\left(\mathbf{F}_k\mathbf{H}_k\mathbf{S}_k\mathbf{S}_k^H\mathbf{H}_k^H\mathbf{F}_k^H\right) + \mathrm{Tr}\left(\mathbf{F}_k\mathbf{H}_k\mathbf{S}_k\mathbf{N}_k^H\mathbf{F}_k^H\right) - \mathrm{Tr}\left(\mathbf{F}_k\mathbf{H}_k\mathbf{S}_k\mathbf{S}_k^H\boldsymbol{\varrho}^H\mathbf{B}_k^H\right) \\
&- \mathrm{Tr}\left(\mathbf{F}_k\mathbf{H}_k\mathbf{S}_k\boldsymbol{\Delta}_k^H\mathbf{B}_k^H\right) - \mathrm{Tr}\left(\mathbf{F}_k\mathbf{H}_k\mathbf{S}_k\mathbf{S}_k^H\right) + \mathrm{Tr}\left(\mathbf{F}_k\mathbf{N}_k\mathbf{S}_k^H\mathbf{H}_k^H\mathbf{F}_k^H\right) + \mathrm{Tr}\left(\mathbf{F}_k\mathbf{N}_k\mathbf{N}_k^H\mathbf{F}_k^H\right) \\
&- \mathrm{Tr}\left(\mathbf{F}_k\mathbf{N}_k\mathbf{S}_k^H\boldsymbol{\varrho}^H\mathbf{B}_k^H\right) - \mathrm{Tr}\left(\mathbf{F}_k\mathbf{N}_k\boldsymbol{\Delta}_k^H\mathbf{B}_k^H\right) - \mathrm{Tr}\left(\mathbf{F}_k\mathbf{N}_k\mathbf{S}_k^H\right) - \mathrm{Tr}\left(\mathbf{B}_k\boldsymbol{\varrho}\mathbf{S}_k\mathbf{S}_k^H\mathbf{H}_k^H\mathbf{F}_k^H\right) \\
&- \mathrm{Tr}\left(\mathbf{B}_k\boldsymbol{\varrho}\mathbf{S}_k\mathbf{N}_k^H\mathbf{F}_k^H\right) + \mathrm{Tr}\left(\mathbf{B}_k\boldsymbol{\varrho}\mathbf{S}_k\mathbf{S}_k^H\boldsymbol{\varrho}^H\mathbf{B}_k^H\right) + \mathrm{Tr}\left(\mathbf{B}_k\boldsymbol{\varrho}\mathbf{S}_k\boldsymbol{\Delta}_k^H\mathbf{B}_k^H\right) + \mathrm{Tr}\left(\mathbf{B}_k\boldsymbol{\varrho}\mathbf{S}_k\mathbf{S}_k^H\right) \\
&- \mathrm{Tr}\left(\mathbf{B}_k\boldsymbol{\Delta}_k\mathbf{S}_k^H\mathbf{H}_k^H\mathbf{F}_k^H\right) - \mathrm{Tr}\left(\mathbf{B}_k\boldsymbol{\Delta}_k\mathbf{N}_k^H\mathbf{F}_k^H\right) + \mathrm{Tr}\left(\mathbf{B}_k\boldsymbol{\Delta}_k\mathbf{S}_k^H\boldsymbol{\varrho}^H\mathbf{B}_k^H\right) + \mathrm{Tr}\left(\mathbf{B}_k\boldsymbol{\Delta}_k\boldsymbol{\Delta}_k^H\mathbf{B}_k^H\right) \\
&+ \mathrm{Tr}\left(\mathbf{B}_k\boldsymbol{\Delta}_k\mathbf{S}_k^H\right) - \mathrm{Tr}\left(\mathbf{S}_k\mathbf{S}_k^H\mathbf{H}_k^H\mathbf{F}_k^H\right) - \mathrm{Tr}\left(\mathbf{S}_k\mathbf{N}_k^H\mathbf{F}_k^H\right) + \mathrm{Tr}\left(\mathbf{S}_k\mathbf{S}_k^H\boldsymbol{\varrho}^H\mathbf{B}_k^H\right) \\
&+ \mathrm{Tr}\left(\mathbf{S}_k\boldsymbol{\Delta}_k^H\mathbf{B}_k^H\right) + \mathrm{Tr}\left(\mathbf{S}_k\mathbf{S}_k^H\right)\Bigg]
\end{aligned} \tag{B.7}$$

$$\begin{aligned}
= \mathbb{E}\Bigg[&\mathrm{Tr}\left(\mathbf{F}_k\mathbf{H}_k\mathbf{S}_k\mathbf{S}_k^H\mathbf{H}_k^H\mathbf{F}_k^H\right) - \mathrm{Tr}\left(\mathbf{F}_k\mathbf{H}_k\mathbf{S}_k\mathbf{S}_k^H\boldsymbol{\varrho}^H\mathbf{B}_k^H\right) - \mathrm{Tr}\left(\mathbf{F}_k\mathbf{H}_k\mathbf{S}_k\mathbf{S}_k^H\right) \\
&+ \mathrm{Tr}\left(\mathbf{F}_k\mathbf{N}_k\mathbf{N}_k^H\mathbf{F}_k^H\right) - \mathrm{Tr}\left(\mathbf{B}_k\boldsymbol{\varrho}\mathbf{S}_k\mathbf{S}_k^H\mathbf{H}_k^H\mathbf{F}_k^H\right) + \mathrm{Tr}\left(\mathbf{B}_k\boldsymbol{\varrho}\mathbf{S}_k\mathbf{S}_k^H\boldsymbol{\varrho}^H\mathbf{B}_k^H\right) + \mathrm{Tr}\left(\mathbf{B}_k\boldsymbol{\varrho}\mathbf{S}_k\mathbf{S}_k^H\right) \\
&+ \mathrm{Tr}\left(\mathbf{B}_k\boldsymbol{\Delta}_k\boldsymbol{\Delta}_k^H\mathbf{B}_k^H\right) - \mathrm{Tr}\left(\mathbf{S}_k\mathbf{S}_k^H\mathbf{H}_k^H\mathbf{F}_k^H\right) + \mathrm{Tr}\left(\mathbf{S}_k\mathbf{S}_k^H\boldsymbol{\varrho}^H\mathbf{B}_k^H\right) + \mathrm{Tr}\left(\mathbf{S}_k\mathbf{S}_k^H\right)\Bigg]
\end{aligned} \tag{B.8}$$

Next, it follows a description of the properties used to reach (B.8):

- From (B.1) to (B.2), it is used (Prp. F);
- From (B.2) to (B.3), it is used (4.1);
- From (B.3) to (B.4), it is used (2.4) and (4.4);
- From (B.4) to (B.5), it is used (Prp. E);
- From (B.6) to (B.7), it is used (Prp. G);
- From (B.7) to (B.8), it is assumed that $\mathbf{S}_k$, $\mathbf{N}_k$ and $\mathbf{\Delta}_k$ are independent between each other and $\mathbb{E}[\mathbf{N}_k] = \mathbb{E}[\mathbf{\Delta}_k] = 0$, resulting that $\mathbb{E}[\mathbf{S}_k\mathbf{N}_k] = \mathbb{E}[\mathbf{S}_k\mathbf{\Delta}_k] = \mathbb{E}[\mathbf{N}_k\mathbf{\Delta}_k] = 0$.

Now, one could solve the problem described by (4.15). Let's start with

$$\begin{aligned}
&\nabla_{\lambda_k}(J_k) = 0 \Leftrightarrow \\
\Leftrightarrow &\frac{\partial J_k}{\partial \lambda_k} = 0 \Leftrightarrow \\
\Leftrightarrow &\frac{1}{N_{block}} \sum_{k=0}^{N_{block}-1} \mathrm{Tr}\left(\mathbf{F}_k\mathbf{H}_k\right) - N_T = 0 \Leftrightarrow \\
\Leftrightarrow &\frac{1}{N_{block}} \sum_{k=0}^{N_{block}-1} \mathrm{Tr}\left(\mathbf{F}_k\mathbf{H}_k\right) = N_T
\end{aligned} \tag{B.9}$$

Then,

$$\begin{aligned}
&\nabla_{\mathbf{B}_k}(J_k) = \mathbf{0}_{N_T\times N_T} \Leftrightarrow \\
\overset{\text{(Prp. L)}}{\Leftrightarrow} &2\frac{\partial J_k}{\partial \mathbf{B}_k^*} = \mathbf{0}_{N_T\times N_T} \Leftrightarrow \\
\Leftrightarrow &\frac{\partial\left(\mathbb{E}\left[\left(\widetilde{\mathbf{S}}_k - \mathbf{S}_k\right)^H\left(\widetilde{\mathbf{S}}_k - \mathbf{S}_k\right)\right]\right)}{\partial \mathbf{B}_k^*} + \frac{\partial\left(\lambda_k\left(\frac{1}{N_{block}}\sum_{k=0}^{N_{block}-1}\mathrm{Tr}\left(\mathbf{F}_k\mathbf{H}_k\right) - N_T\right)\right)}{\partial \mathbf{B}_k^*} = \mathbf{0}_{N_T\times N_T} \Leftrightarrow \\
\Leftrightarrow &\frac{\partial\left(\mathbb{E}\left[\left(\widetilde{\mathbf{S}}_k - \mathbf{S}_k\right)^H\left(\widetilde{\mathbf{S}}_k - \mathbf{S}_k\right)\right]\right)}{\partial \mathbf{B}_k^*} = \mathbf{0}_{N_T\times N_T}
\end{aligned} \tag{B.10}$$

Replacing (B.8) in (B.10) and using the linearity properties of the expected value and the partial derivative given by (Prp. H) and (Prp. J), respectively, each term could be analysed separately. Hence,

$$\frac{\partial\left(\mathbb{E}\left[\mathrm{Tr}\left(\mathbf{F}_k\mathbf{H}_k\mathbf{S}_k\mathbf{S}_k^H\mathbf{H}_k^H\mathbf{F}_k^H\right)\right]\right)}{\partial \mathbf{B}_k^*} = \mathbf{0}_{N_T\times N_T} \tag{B.11}$$

$$\frac{\partial\left(\mathbb{E}\left[\mathrm{Tr}\left(\mathbf{F}_k\mathbf{H}_k\mathbf{S}_k\mathbf{S}_k^H\boldsymbol{\varrho}^H\mathbf{B}_k^H\right)\right]\right)}{\partial\mathbf{B}_k^*} \overset{\text{(Prp. O)}}{=} \mathbb{E}\left[\frac{\partial\left(\mathrm{Tr}\left(\mathbf{F}_k\mathbf{H}_k\mathbf{S}_k\mathbf{S}_k^H\boldsymbol{\varrho}^H\mathbf{B}_k^H\right)\right)}{\partial\mathbf{B}_k^*}\right]$$
$$\overset{\text{(Prp. M)}}{=} \mathbb{E}\left[\mathbf{F}_k\mathbf{H}_k\mathbf{S}_k\mathbf{S}_k^H\boldsymbol{\varrho}^H\right] = \mathbf{F}_k\mathbf{H}_k\mathbb{E}\left[\mathbf{S}_k\mathbf{S}_k^H\right]\boldsymbol{\varrho}^H \overset{(4.9)}{=} \sigma_{s_n}^2\mathbf{F}_k\mathbf{H}_k\boldsymbol{\varrho}^H \tag{B.12}$$

$$\frac{\partial\left(\mathbb{E}\left[\mathrm{Tr}\left(\mathbf{F}_k\mathbf{H}_k\mathbf{S}_k\mathbf{S}_k^H\right)\right]\right)}{\partial\mathbf{B}_k^*} = \mathbf{0}_{N_T\times N_T} \tag{B.13}$$

$$\frac{\partial\left(\mathbb{E}\left[\mathrm{Tr}\left(\mathbf{F}_k\mathbf{N}_k\mathbf{N}_k^H\mathbf{F}_k^H\right)\right]\right)}{\partial\mathbf{B}_k^*} = \mathbf{0}_{N_T\times N_T} \tag{B.14}$$

$$\frac{\partial\left(\mathbb{E}\left[\mathrm{Tr}\left(\mathbf{B}_k\boldsymbol{\varrho}\mathbf{S}_k\mathbf{S}_k^H\mathbf{H}_k^H\mathbf{F}_k^H\right)\right]\right)}{\partial\mathbf{B}_k^*} \overset{\text{(Prp. N)}}{=} \mathbf{0}_{N_T\times N_T} \tag{B.15}$$

$$\frac{\partial\left(\mathbb{E}\left[\mathrm{Tr}\left(\mathbf{B}_k\boldsymbol{\varrho}\mathbf{S}_k\mathbf{S}_k^H\boldsymbol{\varrho}^H\mathbf{B}_k^H\right)\right]\right)}{\partial\mathbf{B}_k^*} \overset{\text{(Prp. O)}}{=} \mathbb{E}\left[\frac{\partial\left(\mathrm{Tr}\left(\mathbf{B}_k\boldsymbol{\varrho}\mathbf{S}_k\mathbf{S}_k^H\boldsymbol{\varrho}^H\mathbf{B}_k^H\right)\right)}{\partial\mathbf{B}_k^*}\right]$$
$$\overset{\text{(Prp. M)}}{=} \mathbb{E}\left[\mathbf{B}_k\boldsymbol{\varrho}\mathbf{S}_k\mathbf{S}_k^H\boldsymbol{\varrho}^H\right] = \mathbf{B}_k\boldsymbol{\varrho}\mathbb{E}\left[\mathbf{S}_k\mathbf{S}_k^H\right]\boldsymbol{\varrho}^H \overset{(4.9)}{=} \sigma_{s_n}^2\mathbf{B}_k\boldsymbol{\varrho}\boldsymbol{\varrho}^H \tag{B.16}$$

$$\frac{\partial\left(\mathbb{E}\left[\mathrm{Tr}\left(\mathbf{B}_k\boldsymbol{\varrho}\mathbf{S}_k\mathbf{S}_k^H\right)\right]\right)}{\partial\mathbf{B}_k^*} \overset{\text{(Prp. N)}}{=} \mathbf{0}_{N_T\times N_T} \tag{B.17}$$

$$\frac{\partial\left(\mathbb{E}\left[\mathrm{Tr}\left(\mathbf{B}_k\boldsymbol{\Delta}_k\boldsymbol{\Delta}_k^H\mathbf{B}_k^H\right)\right]\right)}{\partial\mathbf{B}_k^*} \overset{\text{(Prp. O)}}{=} \mathbb{E}\left[\frac{\partial\left(\mathrm{Tr}\left(\mathbf{B}_k\boldsymbol{\Delta}_k\boldsymbol{\Delta}_k^H\mathbf{B}_k^H\right)\right)}{\partial\mathbf{B}_k^*}\right]$$
$$\overset{\text{(Prp. M)}}{=} \mathbb{E}\left[\mathbf{B}_k\boldsymbol{\Delta}_k\boldsymbol{\Delta}_k^H\right] = \mathbf{B}_k\mathbb{E}\left[\boldsymbol{\Delta}_k\boldsymbol{\Delta}_k^H\right] \overset{(4.8)}{=} \sigma_{s_n}^2\mathbf{B}_k\left(\boldsymbol{I}_{N_T}-\boldsymbol{\varrho}^2\right) \tag{B.18}$$

$$\frac{\partial\left(\mathbb{E}\left[\mathrm{Tr}\left(\mathbf{S}_k\mathbf{S}_k^H\mathbf{H}_k^H\mathbf{F}_k^H\right)\right]\right)}{\partial\mathbf{B}_k^*}=\mathbf{0}_{N_T\times N_T} \tag{B.19}$$

$$\begin{aligned}\frac{\partial\left(\mathbb{E}\left[\mathrm{Tr}\left(\mathbf{S}_k\mathbf{S}_k^H\boldsymbol{\varrho}^H\mathbf{B}_k^H\right)\right]\right)}{\partial\mathbf{B}_k^*} &\overset{\text{(Prp. O)}}{=}\mathbb{E}\left[\frac{\partial\left(\mathrm{Tr}\left(\mathbf{S}_k\mathbf{S}_k^H\boldsymbol{\varrho}^H\mathbf{B}_k^H\right)\right)}{\partial\mathbf{B}_k^*}\right]\\ &\overset{\text{(Prp. M)}}{=}\mathbb{E}\left[\mathbf{S}_k\mathbf{S}_k^H\boldsymbol{\varrho}^H\right]=\mathbb{E}\left[\mathbf{S}_k\mathbf{S}_k^H\right]\boldsymbol{\varrho}^H\overset{(4.9)}{=}\sigma_{s_n}^2\boldsymbol{\varrho}^H\end{aligned} \tag{B.20}$$

$$\frac{\partial\left(\mathbb{E}\left[\mathrm{Tr}\left(\mathbf{S}_k\mathbf{S}_k^H\right)\right]\right)}{\partial\mathbf{B}_k^*}=\mathbf{0}_{N_T\times N_T} \tag{B.21}$$

Putting (B.11) to (B.21) into (B.10), and taken into account that $\boldsymbol{\varrho}=\boldsymbol{\varrho}^H$ because $\boldsymbol{\varrho}$ is a diagonal matrix of real coefficients, one gets

$$\begin{aligned}&-\sigma_{s_n}^2\mathbf{F}_k\mathbf{H}_k\boldsymbol{\varrho}+\sigma_{s_n}^2\mathbf{B}_k\boldsymbol{\varrho}^2+\sigma_{s_n}^2\mathbf{B}_k\left(\boldsymbol{I}_{N_T}-\boldsymbol{\varrho}^2\right)+\sigma_{s_n}^2\boldsymbol{\varrho}=\mathbf{0}_{N_T\times N_T}\Leftrightarrow\\ \Leftrightarrow\ &\mathbf{B}_k\left(\boldsymbol{\varrho}^2+\boldsymbol{I}_{N_T}-\boldsymbol{\varrho}^2\right)=\left(\mathbf{F}_k\mathbf{H}_k-\boldsymbol{I}_{N_T}\right)\boldsymbol{\varrho}\Leftrightarrow\ \ \mathbf{B}_k=\left(\mathbf{F}_k\mathbf{H}_k-\boldsymbol{I}_{N_T}\right)\boldsymbol{\varrho}\end{aligned} \tag{B.22}$$

Finally,

$$\begin{aligned}&\nabla_{\mathbf{F}_k}(J_k)=\mathbf{0}_{N_T\times N_R}\Leftrightarrow\\ &\overset{\text{(Prp. L)}}{\Leftrightarrow}2\frac{\partial J_k}{\partial\mathbf{F}_k^*}=\mathbf{0}_{N_T\times N_R}\Leftrightarrow\\ &\Leftrightarrow\ \ \frac{\partial\left(\mathbb{E}\left[\left(\widetilde{\mathbf{S}}_k-\mathbf{S}_k\right)^H\left(\widetilde{\mathbf{S}}_k-\mathbf{S}_k\right)\right]\right)}{\partial\mathbf{F}_k^*}+\frac{\partial\left(\lambda_k\left(\frac{1}{N_{block}}\sum_{k=0}^{N_{block}-1}\mathrm{Tr}\left(\mathbf{F}_k\mathbf{H}_k\right)-N_T\right)\right)}{\partial\mathbf{F}_k^*}=\mathbf{0}_{N_T\times N_R}\Leftrightarrow\\ &\overset{\text{(Prp. N)}}{\Leftrightarrow}\frac{\partial\left(\mathbb{E}\left[\left(\widetilde{\mathbf{S}}_k-\mathbf{S}_k\right)^H\left(\widetilde{\mathbf{S}}_k-\mathbf{S}_k\right)\right]\right)}{\partial\mathbf{F}_k^*}=\mathbf{0}_{N_T\times N_R}\end{aligned} \tag{B.23}$$

Replacing (B.8) in (B.23) and using the linearity properties of the expected value and the partial derivative given by (Prp. H) and (Prp. J), respectively, each term could be analysed separately. Hence,

$$\frac{\partial\left(\mathbb{E}\left[\mathrm{Tr}\left(\mathbf{F}_k\mathbf{H}_k\mathbf{S}_k\mathbf{S}_k^H\mathbf{H}_k^H\mathbf{F}_k^H\right)\right]\right)}{\partial\mathbf{F}_k^*} \overset{\text{(Prp. O)}}{=} \mathbb{E}\left[\frac{\partial\left(\mathrm{Tr}\left(\mathbf{F}_k\mathbf{H}_k\mathbf{S}_k\mathbf{S}_k^H\mathbf{H}_k^H\mathbf{F}_k^H\right)\right)}{\partial\mathbf{F}_k^*}\right]$$
$$\overset{\text{(Prp. M)}}{=}\mathbb{E}\left[\mathbf{F}_k\mathbf{H}_k\mathbf{S}_k\mathbf{S}_k^H\mathbf{H}_k^H\right]=\mathbf{F}_k\mathbf{H}_k\mathbb{E}\left[\mathbf{S}_k\mathbf{S}_k^H\right]\mathbf{H}_k^H \overset{(4.9)}{=} \sigma_{s_n}^2\mathbf{F}_k\mathbf{H}_k\mathbf{H}_k^H \tag{B.24}$$

$$\frac{\partial\left(\mathbb{E}\left[\mathrm{Tr}\left(\mathbf{F}_k\mathbf{H}_k\mathbf{S}_k\mathbf{S}_k^H\boldsymbol{\varrho}^H\mathbf{B}_k^H\right)\right]\right)}{\partial\mathbf{F}_k^*} \overset{\text{(Prp. N)}}{=} \mathbf{0}_{N_T\times N_R} \tag{B.25}$$

$$\frac{\partial\left(\mathbb{E}\left[\mathrm{Tr}\left(\mathbf{F}_k\mathbf{H}_k\mathbf{S}_k\mathbf{S}_k^H\right)\right]\right)}{\partial\mathbf{F}_k^*} \overset{\text{(Prp. N)}}{=} \mathbf{0}_{N_T\times N_R} \tag{B.26}$$

$$\frac{\partial\left(\mathbb{E}\left[\mathrm{Tr}\left(\mathbf{F}_k\mathbf{N}_k\mathbf{N}_k^H\mathbf{F}_k^H\right)\right]\right)}{\partial\mathbf{F}_k^*} \overset{\text{(Prp. O)}}{=} \mathbb{E}\left[\frac{\partial\left(\mathrm{Tr}\left(\mathbf{F}_k\mathbf{N}_k\mathbf{N}_k^H\mathbf{F}_k^H\right)\right)}{\partial\mathbf{F}_k^*}\right]$$
$$\overset{\text{(Prp. M)}}{=}\mathbb{E}\left[\mathbf{F}_k\mathbf{N}_k\mathbf{N}_k^H\right]=\mathbf{F}_k\mathbb{E}\left[\mathbf{N}_k\mathbf{N}_k^H\right] \overset{(4.18)}{=} \sigma_{n_z}^2\mathbf{F}_k \tag{B.27}$$

$$\frac{\partial\left(\mathbb{E}\left[\mathrm{Tr}\left(\mathbf{B}_k\boldsymbol{\varrho}\mathbf{S}_k\mathbf{S}_k^H\mathbf{H}_k^H\mathbf{F}_k^H\right)\right]\right)}{\partial\mathbf{F}_k^*} \overset{\text{(Prp. O)}}{=} \mathbb{E}\left[\frac{\partial\left(\mathrm{Tr}\left(\mathbf{B}_k\boldsymbol{\varrho}\mathbf{S}_k\mathbf{S}_k^H\mathbf{H}_k^H\mathbf{F}_k^H\right)\right)}{\partial\mathbf{F}_k^*}\right]$$
$$\overset{\text{(Prp. M)}}{=}\mathbb{E}\left[\mathbf{B}_k\boldsymbol{\varrho}\mathbf{S}_k\mathbf{S}_k^H\mathbf{H}_k^H\right]=\mathbf{B}_k\boldsymbol{\varrho}\mathbb{E}\left[\mathbf{S}_k\mathbf{S}_k^H\right]\mathbf{H}_k^H \overset{(4.9)}{=} \sigma_{s_n}^2\mathbf{B}_k\boldsymbol{\varrho}\mathbf{H}_k^H \tag{B.28}$$

$$\frac{\partial\left(\mathbb{E}\left[\mathrm{Tr}\left(\mathbf{B}_k\boldsymbol{\varrho}\mathbf{S}_k\mathbf{S}_k^H\boldsymbol{\varrho}^H\mathbf{B}_k^H\right)\right]\right)}{\partial\mathbf{F}_k^*} = \mathbf{0}_{N_T\times N_R} \tag{B.29}$$

$$\frac{\partial\left(\mathbb{E}\left[\mathrm{Tr}\left(\mathbf{B}_k\boldsymbol{\varrho}\mathbf{S}_k\mathbf{S}_k^H\right)\right]\right)}{\partial\mathbf{F}_k^*} = \mathbf{0}_{N_T\times N_R} \tag{B.30}$$

$$\frac{\partial\left(\mathbb{E}\left[\mathrm{Tr}\left(\mathbf{B}_k\boldsymbol{\Delta}_k\boldsymbol{\Delta}_k^H\mathbf{B}_k^H\right)\right]\right)}{\partial\mathbf{F}_k^*}=\mathbf{0}_{N_T\times N_R} \tag{B.31}$$

$$\begin{aligned}\frac{\partial\left(\mathbb{E}\left[\mathrm{Tr}\left(\mathbf{S}_k\mathbf{S}_k^H\mathbf{H}_k^H\mathbf{F}_k^H\right)\right]\right)}{\partial\mathbf{F}_k^*} &\overset{\text{(Prp. O)}}{=} \mathbb{E}\left[\frac{\partial\left(\mathrm{Tr}\left(\mathbf{S}_k\mathbf{S}_k^H\mathbf{H}_k^H\mathbf{F}_k^H\right)\right)}{\partial\mathbf{F}_k^*}\right]\\ \overset{\text{(Prp. M)}}{=}\mathbb{E}\left[\mathbf{S}_k\mathbf{S}_k^H\mathbf{H}_k^H\right] &= \mathbb{E}\left[\mathbf{S}_k\mathbf{S}_k^H\right]\mathbf{H}_k^H \overset{(4.9)}{=} \sigma_{s_n}^2\mathbf{H}_k^H\end{aligned} \tag{B.32}$$

$$\frac{\partial\left(\mathbb{E}\left[\mathrm{Tr}\left(\mathbf{S}_k\mathbf{S}_k^H\boldsymbol{\varrho}^H\mathbf{B}_k^H\right)\right]\right)}{\partial\mathbf{F}_k^*}=\mathbf{0}_{N_T\times N_R} \tag{B.33}$$

$$\frac{\partial\left(\mathbb{E}\left[\mathrm{Tr}\left(\mathbf{S}_k\mathbf{S}_k^H\right)\right]\right)}{\partial\mathbf{F}_k^*}=\mathbf{0}_{N_T\times N_R} \tag{B.34}$$

Putting (B.24) to (B.34) into (B.23) and replacing $\mathbf{B}_k$ by (B.22), one gets

$$\begin{aligned}&\sigma_{s_n}^2\mathbf{F}_k\mathbf{H}_k\mathbf{H}_k^H+\sigma_{n_z}^2\mathbf{F}_k-\sigma_{s_n}^2\left(\mathbf{F}_k\mathbf{H}_k-\boldsymbol{I}_{N_T}\right)\boldsymbol{\varrho}^2\mathbf{H}_k^H-\sigma_{s_n}^2\mathbf{H}_k^H=\mathbf{0}_{N_T\times N_R}\Leftrightarrow\\ \Leftrightarrow\quad&\mathbf{F}_k\left(\mathbf{H}_k\mathbf{H}_k^H+\frac{1}{\gamma}\boldsymbol{I}_{N_R}-\mathbf{H}_k\boldsymbol{\varrho}^2\mathbf{H}_k^H\right)=\left(\boldsymbol{I}_{N_T}-\boldsymbol{\varrho}^2\right)\mathbf{H}_k^H\Leftrightarrow\\ \Leftrightarrow\quad&\mathbf{F}_k\left(\mathbf{H}_k\left(\boldsymbol{I}_{N_T}-\boldsymbol{\varrho}^2\right)\mathbf{H}_k^H+\frac{1}{\gamma}\boldsymbol{I}_{N_R}\right)=\left(\boldsymbol{I}_{N_T}-\boldsymbol{\varrho}^2\right)\mathbf{H}_k^H\Leftrightarrow\\ \overset{\text{(Prp. A)}}{\Leftrightarrow}\quad&\mathbf{F}_k=\left(\boldsymbol{I}_{N_T}-\boldsymbol{\varrho}^2\right)\mathbf{H}_k^H\left(\mathbf{H}_k\left(\boldsymbol{I}_{N_T}-\boldsymbol{\varrho}^2\right)\mathbf{H}_k^H+\frac{1}{\gamma}\boldsymbol{I}_{N_R}\right)^{-1}\Leftrightarrow \qquad\text{(B.35)}\\ \Leftrightarrow\quad&\mathbf{F}_k=\left(\frac{1}{\gamma}\left(\boldsymbol{I}_{N_T}-\boldsymbol{\varrho}^2\right)^{-1}+\mathbf{H}_k^H\mathbf{H}_k\right)^{-1}\mathbf{H}_k^H \qquad\text{(B.36)}\end{aligned}$$

The result ensuring that (B.35) is equivalent to (B.36) and it is given by equation (27) in [63]. This result makes possible to use a more advantageous expression accordingly the ratio N_R/N_T. If N_R/N_T>1, as in the uplink scenario considered in this work, (B.36) must be used. Otherwise, the choice should be (B.35).

C

Minimisation of MSE in IB-DFE receivers for MIMO using oversampled signals

In this appendix, it is shown the full development of the calculus of the feedforward and feedback coefficients that minimise the MSE in the IB-DFE receivers for MIMO using oversampled signals presented in section 5.2. This is a new problem that has not been addressed in the literature yet. The main difference to the problem presented in appendix B is the average in L given by

$$S_k^{(t)} = \Upsilon\left(\breve{S}_{(k,l)}^{(t)}\right) = \frac{1}{L}\sum_{l=0}^{L-1}\breve{S}_{(k,l)}^{(t)} + \frac{1}{L}\sum_{l=0}^{L-1}\frac{\breve{S}_{(k,l)}^{(t)}}{\Theta_{(k,l)}}\,, \tag{C.1}$$

Here, the expressions presented in section 5.2 will be fully developed, with a description of all the properties used and that are described in the List of Properties at the beginning of the thesis. It should also be noted that as the development of the optimisation problem does not depend on the iteration number, the superscript (i) will be omitted to lighten the notation.

First, let's develop the sum of the MSEs:

$$\boldsymbol{\Omega}_k = \mathbb{E}\left[\left(\widetilde{\mathbf{S}}_k - \mathbf{S}_k\right)^H \left(\widetilde{\mathbf{S}}_k - \mathbf{S}_k\right)\right] \tag{C.2}$$

$$= \mathbb{E}\left[\mathrm{Tr}\left(\left(\widetilde{\mathbf{S}}_k - \mathbf{S}_k\right)\left(\widetilde{\mathbf{S}}_k - \mathbf{S}_k\right)^H\right)\right] \tag{C.3}$$

$$= \mathbb{E}\left[\mathrm{Tr}\left(\left(\Upsilon\left(\mathbf{F}_{(k,l)}\mathbf{Y}_{(k,l)}\right) - \mathbf{B}_k\hat{\mathbf{S}}_k - \mathbf{S}_k\right)\left(\Upsilon\left(\mathbf{F}_{(k,l)}\mathbf{Y}_{(k,l)}\right) - \mathbf{B}_k\hat{\mathbf{S}}_k - \mathbf{S}_k\right)^H\right)\right] \tag{C.4}$$

$$= \mathbb{E}\Bigg[\mathrm{Tr}\Bigg(\left(\Upsilon\left(\mathbf{F}_{(k,l)}\left(\mathbf{H}^{eq}_{(k,l)}\mathbf{S}_{(k,l)} + \mathbf{N}_{(k,l)}\right)\right) - \mathbf{B}_k\left(\boldsymbol{\varrho}\mathbf{S}_k + \boldsymbol{\Delta}_k\right) - \mathbf{S}_k\right)$$
$$\left(\Upsilon\left(\mathbf{F}_{(k,l)}\left(\mathbf{H}^{eq}_{(k,l)}\mathbf{S}_{(k,l)} + \mathbf{N}_{(k,l)}\right)\right) - \mathbf{B}_k\left(\boldsymbol{\varrho}\mathbf{S}_k + \boldsymbol{\Delta}_k\right) - \mathbf{S}_k\right)^H\Bigg)\Bigg] \tag{C.5}$$

$$= \mathbb{E}\Bigg[\mathrm{Tr}\Bigg(\left(\Upsilon\left(\mathbf{F}_{(k,l)}\mathbf{H}^{eq}_{(k,l)}\mathbf{S}_{(k,l)}\right) + \Upsilon\left(\mathbf{F}_{(k,l)}\mathbf{N}_{(k,l)}\right) - \mathbf{B}_k\boldsymbol{\varrho}\mathbf{S}_k - \mathbf{B}_k\boldsymbol{\Delta}_k - \mathbf{S}_k\right)$$
$$\left(\Upsilon\left(\mathbf{S}^H_{(k,l)}\left(\mathbf{H}^{eq}_{(k,l)}\right)^H\mathbf{F}^H_{(k,l)}\right) + \Upsilon\left(\mathbf{N}^H_{(k,l)}\mathbf{F}^H_{(k,l)}\right) - \mathbf{S}^H_k\boldsymbol{\varrho}^H\mathbf{B}^H_k - \boldsymbol{\Delta}^H_k\mathbf{B}^H_k - \mathbf{S}^H_k\right)\Bigg)\Bigg] \tag{C.6}$$

$$= \mathbb{E}\Bigg[\mathrm{Tr}\left(\frac{1}{L^2}\left(\sum_{l=0}^{L-1}\mathbf{F}_{(k,l)}\mathbf{H}^{eq}_{(k,l)}\mathbf{S}_{(k,l)}\right)\left(\sum_{l=0}^{L-1}\mathbf{S}^H_{(k,l)}\left(\mathbf{H}^{eq}_{(k,l)}\right)^H\mathbf{F}^H_{(k,l)}\right)\right) +$$
$$+\mathrm{Tr}\left(\frac{1}{L^2}\left(\sum_{l=0}^{L-1}\mathbf{F}_{(k,l)}\mathbf{H}^{eq}_{(k,l)}\mathbf{S}_{(k,l)}\right)\left(\sum_{l=0}^{L-1}\frac{\mathbf{S}^H_{(k,l)}\left(\mathbf{H}^{eq}_{(k,l)}\right)^H\mathbf{F}^H_{(k,l)}}{\Theta^*_{(k,l)}}\right)\right) -$$
$$-\mathrm{Tr}\left(\left(\frac{1}{L}\sum_{l=0}^{L-1}\mathbf{F}_{(k,l)}\mathbf{H}^{eq}_{(k,l)}\mathbf{S}_{(k,l)}\right)\mathbf{S}^H_k\boldsymbol{\varrho}^H\mathbf{B}^H_k\right) - \mathrm{Tr}\left(\left(\frac{1}{L}\sum_{l=0}^{L-1}\mathbf{F}_{(k,l)}\mathbf{H}^{eq}_{(k,l)}\mathbf{S}_{(k,l)}\right)\mathbf{S}^H_k\right) +$$
$$+\mathrm{Tr}\left(\frac{1}{L^2}\left(\sum_{l=0}^{L-1}\frac{\mathbf{F}_{(k,l)}\mathbf{H}^{eq}_{(k,l)}\mathbf{S}_{(k,l)}}{\Theta_{(k,l)}}\right)\left(\sum_{l=0}^{L-1}\mathbf{S}^H_{(k,l)}\left(\mathbf{H}^{eq}_{(k,l)}\right)^H\mathbf{F}^H_{(k,l)}\right)\right) +$$
$$+\mathrm{Tr}\left(\frac{1}{L^2}\left(\sum_{l=0}^{L-1}\frac{\mathbf{F}_{(k,l)}\mathbf{H}^{eq}_{(k,l)}\mathbf{S}_{(k,l)}}{\Theta_{(k,l)}}\right)\left(\sum_{l=0}^{L-1}\frac{\mathbf{S}^H_{(k,l)}\left(\mathbf{H}^{eq}_{(k,l)}\right)^H\mathbf{F}^H_{(k,l)}}{\Theta^*_{(k,l)}}\right)\right) -$$
$$-\mathrm{Tr}\left(\frac{1}{L}\left(\sum_{l=0}^{L-1}\frac{\mathbf{F}_{(k,l)}\mathbf{H}^{eq}_{(k,l)}\mathbf{S}_{(k,l)}}{\Theta_{(k,l)}}\right)\mathbf{S}^H_k\boldsymbol{\varrho}^H\mathbf{B}^H_k\right) - \mathrm{Tr}\left(\frac{1}{L}\left(\sum_{l=0}^{L-1}\frac{\mathbf{F}_{(k,l)}\mathbf{H}^{eq}_{(k,l)}\mathbf{S}_{(k,l)}}{\Theta_{(k,l)}}\right)\mathbf{S}^H_k\right) +$$
$$+\mathrm{Tr}\left(\frac{1}{L^2}\left(\sum_{l=0}^{L-1}\mathbf{F}_{(k,l)}\mathbf{N}_{(k,l)}\right)\left(\sum_{l=0}^{L-1}\mathbf{N}^H_{(k,l)}\mathbf{F}^H_{(k,l)}\right)\right) +$$
$$+\mathrm{Tr}\left(\frac{1}{L^2}\left(\sum_{l=0}^{L-1}\mathbf{F}_{(k,l)}\mathbf{N}_{(k,l)}\right)\left(\sum_{l=0}^{L-1}\frac{\mathbf{N}^H_{(k,l)}\mathbf{F}^H_{(k,l)}}{\Theta^*_{(k,l)}}\right)\right) +$$
$$+\mathrm{Tr}\left(\frac{1}{L^2}\left(\sum_{l=0}^{L-1}\frac{\mathbf{F}_{(k,l)}\mathbf{N}_{(k,l)}}{\Theta_{(k,l)}}\right)\left(\sum_{l=0}^{L-1}\mathbf{N}^H_{(k,l)}\mathbf{F}^H_{(k,l)}\right)\right) +$$

$$
\begin{aligned}
&+\mathrm{Tr}\left(\frac{1}{L^2}\left(\sum_{l=0}^{L-1}\frac{\mathbf{F}_{(k,l)}\mathbf{N}_{(k,l)}}{\Theta_{(k,l)}}\right)\left(\sum_{l=0}^{L-1}\frac{\mathbf{N}_{(k,l)}^H\mathbf{F}_{(k,l)}^H}{\Theta_{(k,l)}^*}\right)\right)-\\
&-\mathrm{Tr}\left(\frac{1}{L}\mathbf{B}_k\boldsymbol{\varrho}\mathbf{S}_k\left(\sum_{l=0}^{L-1}\mathbf{S}_{(k,l)}^H\left(\mathbf{H}_{(k,l)}^{eq}\right)^H\mathbf{F}_{(k,l)}^H\right)\right)-\\
&-\mathrm{Tr}\left(\frac{1}{L}\mathbf{B}_k\boldsymbol{\varrho}\mathbf{S}_k\left(\sum_{l=0}^{L-1}\frac{\mathbf{S}_{(k,l)}^H\left(\mathbf{H}_{(k,l)}^{eq}\right)^H\mathbf{F}_{(k,l)}^H}{\Theta_{(k,l)}^*}\right)\right)+\mathrm{Tr}\left(\mathbf{B}_k\boldsymbol{\varrho}\mathbf{S}_k\mathbf{S}_k^H\boldsymbol{\varrho}^H\mathbf{B}_k^H\right)+\\
&+\mathrm{Tr}\left(\mathbf{B}_k\boldsymbol{\varrho}\mathbf{S}_k\mathbf{S}_k^H\right)+\mathrm{Tr}\left(\mathbf{B}_k\boldsymbol{\Delta}_k\boldsymbol{\Delta}_k^H\mathbf{B}_k^H\right)-\mathrm{Tr}\left(\frac{1}{L}\mathbf{S}_k\left(\sum_{l=0}^{L-1}\mathbf{S}_{(k,l)}^H\left(\mathbf{H}_{(k,l)}^{eq}\right)^H\mathbf{F}_{(k,l)}^H\right)\right)-\\
&-\mathrm{Tr}\left(\frac{1}{L}\mathbf{S}_k\left(\sum_{l=0}^{L-1}\frac{\mathbf{S}_{(k,l)}^H\left(\mathbf{H}_{(k,l)}^{eq}\right)^H\mathbf{F}_{(k,l)}^H}{\Theta_{(k,l)}^*}\right)\right)+\mathrm{Tr}\left(\mathbf{S}_k\mathbf{S}_k^H\boldsymbol{\varrho}^H\mathbf{B}_k^H\right)+\mathrm{Tr}\left(\mathbf{S}_k\mathbf{S}_k^H\right)\Big]
\end{aligned}
\tag{C.7}
$$

Next, it follows a description of the properties used to reach (C.7):

- From (C.2) to (C.3), it is used (Prp. F);
- From (C.3) to (C.4), it is used (5.24);
- From (C.4) to (C.5), it is used (5.20) and (4.4);
- From (C.5) to (C.6), it is used (Prp. D) and (Prp. E);
- From (C.6) to (C.7), it is used (Prp. G), (5.23) and it is assumed that $\mathbf{S}_k$, $\mathbf{N}_k$ and $\boldsymbol{\Delta}_k$ are independent between each other, with $\mathbb{E}[\mathbf{N}_k]=\mathbb{E}[\boldsymbol{\Delta}_k]=0$, resulting that $\mathbb{E}[\mathbf{S}_k\mathbf{N}_k]=\mathbb{E}[\mathbf{S}_k\boldsymbol{\Delta}_k]=\mathbb{E}[\mathbf{N}_k\boldsymbol{\Delta}_k]=0$.

Now, one could solve the problem described by (5.31). Let's start with

$$
\begin{aligned}
&\nabla_{\lambda_k}(J_k)=0\Leftrightarrow\\
\Leftrightarrow&\frac{\partial J_k}{\partial\lambda_k}=0\Leftrightarrow\\
\Leftrightarrow&\frac{1}{LN_{block}}\sum_{k=0}^{N_{block}-1}\sum_{l=0}^{L-1}\mathrm{Tr}\left(\mathbf{F}_{(k,l)}\mathbf{H}_{(k,l)}^{eq}\right)-N_T=0\Leftrightarrow\\
\Leftrightarrow&\frac{1}{LN_{block}}\sum_{k=0}^{N_{block}-1}\sum_{l=0}^{L-1}\mathrm{Tr}\left(\mathbf{F}_{(k,l)}\mathbf{H}_{(k,l)}^{eq}\right)=N_T
\end{aligned}
\tag{C.8}
$$

Then,

$$\begin{aligned}
&\nabla_{\mathbf{B}_k}(J_k) = \mathbf{0}_{N_T\times N_T} \Leftrightarrow \\
&\overset{\text{(Prp. L)}}{\Leftrightarrow} 2\frac{\partial J_k}{\partial \mathbf{B}_k^*} = \mathbf{0}_{N_T\times N_T} \Leftrightarrow \\
&\Leftrightarrow \frac{\partial\left(\mathbb{E}\left[\left(\widetilde{\mathbf{S}}_k-\mathbf{S}_k\right)^H\left(\widetilde{\mathbf{S}}_k-\mathbf{S}_k\right)\right]\right)}{\partial\mathbf{B}_k^*}+\frac{\partial\left(\lambda_k\left(\frac{1}{LN_{block}}\sum_{k=0}^{N_{block}-1}\sum_{l=0}^{L-1}\mathrm{Tr}\left(\mathbf{F}_{(k,l)}\mathbf{H}_{(k,l)}^{eq}\right)-N_T\right)\right)}{\partial\mathbf{B}_k^*}= \\
&\qquad\qquad = \mathbf{0}_{N_T\times N_T} \Leftrightarrow \\
&\Leftrightarrow \frac{\partial\left(\mathbb{E}\left[\left(\widetilde{\mathbf{S}}_k-\mathbf{S}_k\right)^H\left(\widetilde{\mathbf{S}}_k-\mathbf{S}_k\right)\right]\right)}{\partial\mathbf{B}_k^*} = \mathbf{0}_{N_T\times N_T} \qquad \text{(C.9)}
\end{aligned}$$

Replacing (C.7) in (C.9) and using the linearity properties of the expected value and the partial derivative given by (Prp. H) and (Prp. J), respectively, each term could be analysed separately. Hence,

$$\frac{\partial\left(\mathbb{E}\left[\mathrm{Tr}\left(\frac{1}{L^2}\left(\sum_{l=0}^{L-1}\mathbf{F}_{(k,l)}\mathbf{H}_{(k,l)}^{eq}\mathbf{S}_{(k,l)}\right)\left(\sum_{l=0}^{L-1}\mathbf{S}_{(k,l)}^H\left(\mathbf{H}_{(k,l)}^{eq}\right)^H\mathbf{F}_{(k,l)}^H\right)\right)\right]\right)}{\partial\mathbf{B}_k^*} = \mathbf{0}_{N_T\times N_T} \qquad \text{(C.10)}$$

$$\frac{\partial\left(\mathbb{E}\left[\mathrm{Tr}\left(\frac{1}{L^2}\left(\sum_{l=0}^{L-1}\mathbf{F}_{(k,l)}\mathbf{H}_{(k,l)}^{eq}\mathbf{S}_{(k,l)}\right)\left(\sum_{l=0}^{L-1}\frac{\mathbf{S}_{(k,l)}^H\left(\mathbf{H}_{(k,l)}^{eq}\right)^H\mathbf{F}_{(k,l)}^H}{\boldsymbol{\Theta}_{(k,l)}^*}\right)\right)\right]\right)}{\partial\mathbf{B}_k^*} = \mathbf{0}_{N_T\times N_T} \qquad \text{(C.11)}$$

$$\begin{aligned}
&\frac{\partial\left(\mathbb{E}\left[\mathrm{Tr}\left(\left(\frac{1}{L}\sum_{l=0}^{L-1}\mathbf{F}_{(k,l)}\mathbf{H}_{(k,l)}^{eq}\mathbf{S}_{(k,l)}\right)\mathbf{S}_k^H\boldsymbol{\varrho}^H\mathbf{B}_k^H\right)\right]\right)}{\partial\mathbf{B}_k^*} \\
&\overset{\text{(Prp. O)}}{=}\mathbb{E}\left[\frac{\partial\left(\mathrm{Tr}\left(\left(\frac{1}{L}\sum_{l=0}^{L-1}\mathbf{F}_{(k,l)}\mathbf{H}_{(k,l)}^{eq}\mathbf{S}_{(k,l)}\right)\mathbf{S}_k^H\boldsymbol{\varrho}^H\mathbf{B}_k^H\right)\right)}{\partial\mathbf{B}_k^*}\right] \\
&\overset{\text{(Prp. M)}}{=}\mathbb{E}\left[\left(\frac{1}{L}\sum_{l=0}^{L-1}\mathbf{F}_{(k,l)}\mathbf{H}_{(k,l)}^{eq}\mathbf{S}_{(k,l)}\right)\mathbf{S}_k^H\boldsymbol{\varrho}^H\right] \\
&\quad=\left(\frac{1}{L}\sum_{l=0}^{L-1}\mathbf{F}_{(k,l)}\mathbf{H}_{(k,l)}^{eq}\right)\mathbb{E}\left[\mathbf{S}_k\mathbf{S}_k^H\right]\boldsymbol{\varrho}^H\overset{(4.9)}{=}\sigma_{s_n}^2\left(\frac{1}{L}\sum_{l=0}^{L-1}\mathbf{F}_{(k,l)}\mathbf{H}_{(k,l)}^{eq}\right)\boldsymbol{\varrho}^H \qquad \text{(C.12)}
\end{aligned}$$

$$\frac{\partial\left(\mathbb{E}\left[\mathrm{Tr}\left(\left(\frac{1}{L}\sum_{l=0}^{L-1}\mathbf{F}_{(k,l)}\mathbf{H}_{(k,l)}^{eq}\mathbf{S}_{(k,l)}\right)\mathbf{S}_k^H\right)\right]\right)}{\partial\mathbf{B}_k^*}=\mathbf{0}_{N_T\times N_T} \tag{C.13}$$

$$\frac{\partial\left(\mathbb{E}\left[\mathrm{Tr}\left(\frac{1}{L^2}\left(\sum_{l=0}^{L-1}\frac{\mathbf{F}_{(k,l)}\mathbf{H}_{(k,l)}^{eq}\mathbf{S}_{(k,l)}}{\Theta_{(k,l)}}\right)\left(\sum_{l=0}^{L-1}\mathbf{S}_{(k,l)}^H\left(\mathbf{H}_{(k,l)}^{eq}\right)^H\mathbf{F}_{(k,l)}^H\right)\right)\right]\right)}{\partial\mathbf{B}_k^*}=\mathbf{0}_{N_T\times N_T} \tag{C.14}$$

$$\frac{\partial\left(\mathbb{E}\left[\mathrm{Tr}\left(\frac{1}{L^2}\left(\sum_{l=0}^{L-1}\frac{\mathbf{F}_{(k,l)}\mathbf{H}_{(k,l)}^{eq}\mathbf{S}_{(k,l)}}{\Theta_{(k,l)}}\right)\left(\sum_{l=0}^{L-1}\frac{\mathbf{S}_{(k,l)}^H\left(\mathbf{H}_{(k,l)}^{eq}\right)^H\mathbf{F}_{(k,l)}^H}{\Theta_{(k,l)}^*}\right)\right)\right]\right)}{\partial\mathbf{B}_k^*}=\mathbf{0}_{N_T\times N_T} \tag{C.15}$$

$$\begin{aligned}
&\frac{\partial\left(\mathbb{E}\left[\mathrm{Tr}\left(\left(\frac{1}{L}\sum_{l=0}^{L-1}\frac{\mathbf{F}_{(k,l)}\mathbf{H}_{(k,l)}^{eq}\mathbf{S}_{(k,l)}}{\Theta_{(k,l)}}\right)\mathbf{S}_k^H\boldsymbol{\varrho}^H\mathbf{B}_k^H\right)\right]\right)}{\partial\mathbf{B}_k^*}\\
&\overset{\text{(Prp. O)}}{=}\mathbb{E}\left[\frac{\partial\left(\mathrm{Tr}\left(\left(\frac{1}{L}\sum_{l=0}^{L-1}\frac{\mathbf{F}_{(k,l)}\mathbf{H}_{(k,l)}^{eq}\mathbf{S}_{(k,l)}}{\Theta_{(k,l)}}\right)\mathbf{S}_k^H\boldsymbol{\varrho}^H\mathbf{B}_k^H\right)\right)}{\partial\mathbf{B}_k^*}\right]\\
&\overset{\text{(Prp. M)}}{=}\mathbb{E}\left[\left(\frac{1}{L}\sum_{l=0}^{L-1}\frac{\mathbf{F}_{(k,l)}\mathbf{H}_{(k,l)}^{eq}\mathbf{S}_{(k,l)}}{\Theta_{(k,l)}}\right)\mathbf{S}_k^H\boldsymbol{\varrho}^H\right]\\
&\overset{(5.17)}{=}\left(\frac{1}{L}\sum_{l=0}^{L-1}\frac{\mathbf{F}_{(k,l)}\mathbf{H}_{(k,l)}^{eq}}{\Theta_{(k,l)}}\right)\mathbb{E}\left[\mathbf{S}_k\mathbf{S}_k^H\right]\boldsymbol{\varrho}^H\\
&\overset{(4.9)}{=}\sigma_{s_n}^2\left(\frac{1}{L}\sum_{l=0}^{L-1}\frac{\mathbf{F}_{(k,l)}\mathbf{H}_{(k,l)}^{eq}}{\Theta_{(k,l)}}\right)\boldsymbol{\varrho}^H\overset{(5.10)}{\approx}\mathbf{0}_{N_T\times N_T}
\end{aligned} \tag{C.16}$$

Although the product $\mathbf{F}_{(k,l)}\mathbf{H}_{(k,l)}^{eq}$ is not constant, in average it is equal to 1 and, as we see in (5.10), $\Theta_{(k,l)}$ coefficients over an average in L are symmetric. Therefore, the parcel of (C.16) will approximate 0.

$$\frac{\partial\left(\mathbb{E}\left[\mathrm{Tr}\left(\left(\frac{1}{L}\sum_{l=0}^{L-1}\frac{\mathbf{F}_{(k,l)}\mathbf{H}_{(k,l)}^{eq}\mathbf{S}_{(k,l)}}{\Theta_{(k,l)}}\right)\mathbf{S}_k^H\right)\right]\right)}{\partial\mathbf{B}_k^*}=\mathbf{0}_{N_T\times N_T} \tag{C.17}$$

$$\frac{\partial\left(\mathbb{E}\left[\mathrm{Tr}\left(\frac{1}{L^2}\left(\sum_{l=0}^{L-1}\mathbf{F}_{(k,l)}\mathbf{N}_{(k,l)}\right)\left(\sum_{l=0}^{L-1}\mathbf{N}_{(k,l)}^{H}\mathbf{F}_{(k,l)}^{H}\right)\right)\right]\right)}{\partial\mathbf{B}_k^*}=\mathbf{0}_{N_T\times N_T} \tag{C.18}$$

$$\frac{\partial\left(\mathbb{E}\left[\mathrm{Tr}\left(\frac{1}{L^2}\left(\sum_{l=0}^{L-1}\mathbf{F}_{(k,l)}\mathbf{N}_{(k,l)}\right)\left(\sum_{l=0}^{L-1}\frac{\mathbf{N}_{(k,l)}^{H}\mathbf{F}_{(k,l)}^{H}}{\Theta_{(k,l)}^{*}}\right)\right)\right]\right)}{\partial\mathbf{B}_k^*}=\mathbf{0}_{N_T\times N_T} \tag{C.19}$$

$$\frac{\partial\left(\mathbb{E}\left[\mathrm{Tr}\left(\frac{1}{L^2}\left(\sum_{l=0}^{L-1}\frac{\mathbf{F}_{(k,l)}\mathbf{N}_{(k,l)}}{\Theta_{(k,l)}}\right)\left(\sum_{l=0}^{L-1}\mathbf{N}_{(k,l)}^{H}\mathbf{F}_{(k,l)}^{H}\right)\right)\right]\right)}{\partial\mathbf{B}_k^*}=\mathbf{0}_{N_T\times N_T} \tag{C.20}$$

$$\frac{\partial\left(\mathbb{E}\left[\mathrm{Tr}\left(\frac{1}{L^2}\left(\sum_{l=0}^{L-1}\frac{\mathbf{F}_{(k,l)}\mathbf{N}_{(k,l)}}{\Theta_{(k,l)}}\right)\left(\sum_{l=0}^{L-1}\frac{\mathbf{N}_{(k,l)}^{H}\mathbf{F}_{(k,l)}^{H}}{\Theta_{(k,l)}^{*}}\right)\right)\right]\right)}{\partial\mathbf{B}_k^*}=\mathbf{0}_{N_T\times N_T} \tag{C.21}$$

$$\frac{\partial\left(\mathbb{E}\left[\mathrm{Tr}\left(\frac{1}{L}\mathbf{B}_k\boldsymbol{\varrho}\mathbf{S}_k\left(\sum_{l=0}^{L-1}\mathbf{S}_{(k,l)}^{H}\left(\mathbf{H}_{(k,l)}^{eq}\right)^{H}\mathbf{F}_{(k,l)}^{H}\right)\right)\right]\right)}{\partial\mathbf{B}_k^*}\overset{\text{(Prp. N)}}{=}\mathbf{0}_{N_T\times N_T} \tag{C.22}$$

$$\frac{\partial\left(\mathbb{E}\left[\mathrm{Tr}\left(\frac{1}{L}\mathbf{B}_k\boldsymbol{\varrho}\mathbf{S}_k\left(\sum_{l=0}^{L-1}\frac{\mathbf{S}_{(k,l)}^{H}\left(\mathbf{H}_{(k,l)}^{eq}\right)^{H}\mathbf{F}_{(k,l)}^{H}}{\Theta_{(k,l)}^{*}}\right)\right)\right]\right)}{\partial\mathbf{B}_k^*}\overset{\text{(Prp. N)}}{=}\mathbf{0}_{N_T\times N_T} \tag{C.23}$$

$$\begin{aligned}\frac{\partial\left(\mathbb{E}\left[\mathrm{Tr}\left(\mathbf{B}_k\boldsymbol{\varrho}\mathbf{S}_k\mathbf{S}_k^{H}\boldsymbol{\varrho}^{H}\mathbf{B}_k^{H}\right)\right]\right)}{\partial\mathbf{B}_k^*}&\overset{\text{(Prp. O)}}{=}\mathbb{E}\left[\frac{\partial\left(\mathrm{Tr}\left(\mathbf{B}_k\boldsymbol{\varrho}\mathbf{S}_k\mathbf{S}_k^{H}\boldsymbol{\varrho}^{H}\mathbf{B}_k^{H}\right)\right)}{\partial\mathbf{B}_k^*}\right]\\&\overset{\text{(Prp. M)}}{=}\mathbb{E}\left[\mathbf{B}_k\boldsymbol{\varrho}\mathbf{S}_k\mathbf{S}_k^{H}\boldsymbol{\varrho}^{H}\right]=\mathbf{B}_k\boldsymbol{\varrho}\mathbb{E}\left[\mathbf{S}_k\mathbf{S}_k^{H}\right]\boldsymbol{\varrho}^{H}\overset{(4.9)}{=}\sigma_{s_n}^2\mathbf{B}_k\boldsymbol{\varrho}\boldsymbol{\varrho}^{H}\end{aligned} \tag{C.24}$$

$$\frac{\partial\left(\mathbb{E}\left[\mathrm{Tr}\left(\mathbf{B}_k\boldsymbol{\varrho}\mathbf{S}_k\mathbf{S}_k^H\right)\right]\right)}{\partial\mathbf{B}_k^*} \overset{\text{(Prp. N)}}{=} \mathbf{0}_{N_T\times N_T} \tag{C.25}$$

$$\frac{\partial\left(\mathbb{E}\left[\mathrm{Tr}\left(\mathbf{B}_k\boldsymbol{\Delta}_k\boldsymbol{\Delta}_k^H\mathbf{B}_k^H\right)\right]\right)}{\partial\mathbf{B}_k^*} \overset{\text{(Prp. O)}}{=} \mathbb{E}\left[\frac{\partial\left(\mathrm{Tr}\left(\mathbf{B}_k\boldsymbol{\Delta}_k\boldsymbol{\Delta}_k^H\mathbf{B}_k^H\right)\right)}{\partial\mathbf{B}_k^*}\right]$$
$$\overset{\text{(Prp. M)}}{=}\mathbb{E}\left[\mathbf{B}_k\boldsymbol{\Delta}_k\boldsymbol{\Delta}_k^H\right] = \mathbf{B}_k\mathbb{E}\left[\boldsymbol{\Delta}_k\boldsymbol{\Delta}_k^H\right] \overset{(4.8)}{=} \sigma_{s_n}^2\mathbf{B}_k\left(\boldsymbol{I}_{N_T}-\boldsymbol{\varrho}^2\right) \tag{C.26}$$

$$\frac{\partial\left(\mathbb{E}\left[\mathrm{Tr}\left(\frac{1}{L}\mathbf{S}_k\left(\sum_{l=0}^{L-1}\mathbf{S}_{(k,l)}^H\left(\mathbf{H}_{(k,l)}^{eq}\right)^H\mathbf{F}_{(k,l)}^H\right)\right)\right]\right)}{\partial\mathbf{B}_k^*} = \mathbf{0}_{N_T\times N_T} \tag{C.27}$$

$$\frac{\partial\left(\mathbb{E}\left[\mathrm{Tr}\left(\frac{1}{L}\mathbf{S}_k\left(\sum_{l=0}^{L-1}\frac{\mathbf{S}_{(k,l)}^H\left(\mathbf{H}_{(k,l)}^{eq}\right)^H\mathbf{F}_{(k,l)}^H}{\Theta_{(k,l)}^*}\right)\right)\right]\right)}{\partial\mathbf{B}_k^*} = \mathbf{0}_{N_T\times N_T} \tag{C.28}$$

$$\frac{\partial\left(\mathbb{E}\left[\mathrm{Tr}\left(\mathbf{S}_k\mathbf{S}_k^H\boldsymbol{\varrho}^H\mathbf{B}_k^H\right)\right]\right)}{\partial\mathbf{B}_k^*} \overset{\text{(Prp. O)}}{=} \mathbb{E}\left[\frac{\partial\left(\mathrm{Tr}\left(\mathbf{S}_k\mathbf{S}_k^H\boldsymbol{\varrho}^H\mathbf{B}_k^H\right)\right)}{\partial\mathbf{B}_k^*}\right]$$
$$\overset{\text{(Prp. M)}}{=}\mathbb{E}\left[\mathbf{S}_k\mathbf{S}_k^H\boldsymbol{\varrho}^H\right] = \mathbb{E}\left[\mathbf{S}_k\mathbf{S}_k^H\right]\boldsymbol{\varrho}^H \overset{(4.9)}{=} \sigma_{s_n}^2\boldsymbol{\varrho}^H \tag{C.29}$$

$$\frac{\partial\left(\mathbb{E}\left[\mathrm{Tr}\left(\mathbf{S}_k\mathbf{S}_k^H\right)\right]\right)}{\partial\mathbf{B}_k^*} = \mathbf{0}_{N_T\times N_T} \tag{C.30}$$

Putting (C.10) to (C.30) into (C.9), and taken into account that $\boldsymbol{\varrho} = \boldsymbol{\varrho}^H$ because $\boldsymbol{\varrho}$ is a diagonal

matrix of real coefficients, one gets

$$
\begin{aligned}
&-\sigma_{s_n}^2\left(\frac{1}{L}\sum_{l=0}^{L-1}\mathbf{F}_{(k,l)}\mathbf{H}_{(k,l)}^{eq}\right)\boldsymbol{\varrho}+\sigma_{s_n}^2\mathbf{B}_k\boldsymbol{\varrho}^2+\sigma_{s_n}^2\mathbf{B}_k\left(\boldsymbol{I}_{N_T}-\boldsymbol{\varrho}^2\right)+\sigma_{s_n}^2\boldsymbol{\varrho}=\mathbf{0}_{N_T\times N_T}\Leftrightarrow\\
\Leftrightarrow\ &\mathbf{B}_k\left(\boldsymbol{\varrho}^2+\boldsymbol{I}_{N_T}-\boldsymbol{\varrho}^2\right)=\left(\left(\frac{1}{L}\sum_{l=0}^{L-1}\mathbf{F}_{(k,l)}\mathbf{H}_{(k,l)}^{eq}\right)-\boldsymbol{I}_{N_T}\right)\boldsymbol{\varrho}\\
\Leftrightarrow\ &\mathbf{B}_k=\left(\left(\frac{1}{L}\sum_{l=0}^{L-1}\mathbf{F}_{(k,l)}\mathbf{H}_{(k,l)}^{eq}\right)-\boldsymbol{I}_{N_T}\right)\boldsymbol{\varrho}
\end{aligned}
\tag{C.31}
$$

Finally,

$$
\begin{aligned}
&\nabla_{\mathbf{F}_{(k,l)}}(J_k)=\mathbf{0}_{N_T\times N_R}\Leftrightarrow\\
\overset{\text{(Prp. L)}}{\Leftrightarrow}\ &2\frac{\partial J_k}{\partial\mathbf{F}_{(k,l)}^*}=\mathbf{0}_{N_T\times N_R}\Leftrightarrow\\
\Leftrightarrow\ &\frac{\partial\left(\mathbb{E}\left[\left(\widetilde{\mathbf{S}}_k-\mathbf{S}_k\right)^H\left(\widetilde{\mathbf{S}}_k-\mathbf{S}_k\right)\right]\right)}{\partial\mathbf{F}_{(k,l)}^*}+\frac{\partial\left(\lambda_k\left(\frac{1}{LN_{block}}\sum_{k=0}^{N_{block}-1}\sum_{l=0}^{L-1}\mathrm{Tr}\left(\mathbf{F}_{(k,l)}\mathbf{H}_{(k,l)}^{eq}\right)-N_T\right)\right)}{\partial\mathbf{F}_{(k,l)}^*}=\\
&\qquad\qquad\qquad\qquad\qquad\qquad\qquad\qquad\qquad\qquad=\mathbf{0}_{N_T\times N_R}\Leftrightarrow\\
\overset{\text{(Prp. N)}}{\Leftrightarrow}\ &\frac{\partial\left(\mathbb{E}\left[\left(\widetilde{\mathbf{S}}_k-\mathbf{S}_k\right)^H\left(\widetilde{\mathbf{S}}_k-\mathbf{S}_k\right)\right]\right)}{\partial\mathbf{F}_{(k,l)}^*}=\mathbf{0}_{N_T\times N_R}
\end{aligned}
\tag{C.32}
$$

Replacing (C.7) in (C.32) and using the linearity properties of the expected value and the partial derivative given by (Prp. H) and (Prp. J), respectively, each term could be analysed separately. Hence,

$$
\begin{aligned}
&\frac{\partial\left(\mathbb{E}\left[\mathrm{Tr}\left(\frac{1}{L^2}\left(\sum_{l=0}^{L-1}\mathbf{F}_{(k,l)}\mathbf{H}_{(k,l)}^{eq}\mathbf{S}_{(k,l)}\right)\left(\sum_{l=0}^{L-1}\mathbf{S}_{(k,l)}^{H}\left(\mathbf{H}_{(k,l)}^{eq}\right)^{H}\mathbf{F}_{(k,l)}^{H}\right)\right)\right]\right)}{\partial\mathbf{F}_{(k,l)}^{*}}\\
&\overset{\text{(Prp. O)}}{=}\mathbb{E}\left[\frac{\partial\left(\mathrm{Tr}\left(\frac{1}{L^2}\left(\sum_{l=0}^{L-1}\mathbf{F}_{(k,l)}\mathbf{H}_{(k,l)}^{eq}\mathbf{S}_{(k,l)}\right)\left(\sum_{l=0}^{L-1}\mathbf{S}_{(k,l)}^{H}\left(\mathbf{H}_{(k,l)}^{eq}\right)^{H}\mathbf{F}_{(k,l)}^{H}\right)\right)\right)}{\partial\mathbf{F}_{(k,l)}^{*}}\right]\\
&\overset{\text{(Prp. M)}}{=}\mathbb{E}\left[\frac{1}{L^2}\left(\sum_{i=0}^{L-1}\mathbf{F}_{(k,i)}\mathbf{H}_{(k,i)}^{eq}\mathbf{S}_{(k,i)}\right)\mathbf{S}_{k}^{H}\left(\mathbf{H}_{(k,l)}^{eq}\right)^{H}\right]\\
&\quad=\frac{1}{L^2}\left(\sum_{i=0}^{L-1}\mathbf{F}_{(k,i)}\mathbf{H}_{(k,i)}^{eq}\right)\mathbb{E}\left[\mathbf{S}_{k}\mathbf{S}_{k}^{H}\right]\left(\mathbf{H}_{(k,l)}^{eq}\right)^{H}\overset{(4.9)}{=}\frac{\sigma_{s_n}^2}{L^2}\left(\sum_{i=0}^{L-1}\mathbf{F}_{(k,i)}\mathbf{H}_{(k,i)}^{eq}\right)\left(\mathbf{H}_{(k,l)}^{eq}\right)^{H}
\end{aligned}
\tag{C.33}
$$

$$
\begin{aligned}
&\frac{\partial\left(\mathbb{E}\left[\mathrm{Tr}\left(\frac{1}{L^2}\left(\sum_{l=0}^{L-1}\mathbf{F}_{(k,l)}\mathbf{H}_{(k,l)}^{eq}\mathbf{S}_{(k,l)}\right)\left(\sum_{l=0}^{L-1}\frac{\mathbf{S}_{(k,l)}^{H}\left(\mathbf{H}_{(k,l)}^{eq}\right)^{H}\mathbf{F}_{(k,l)}^{H}}{\mathbf{\Theta}_{(k,l)}^{*}}\right)\right)\right]\right)}{\partial\mathbf{F}_{(k,l)}^{*}}\\
&\overset{\text{(Prp. O)}}{=}\mathbb{E}\left[\frac{\partial\left(\mathrm{Tr}\left(\frac{1}{L^2}\left(\sum_{l=0}^{L-1}\mathbf{F}_{(k,l)}\mathbf{H}_{(k,l)}^{eq}\mathbf{S}_{(k,l)}\right)\left(\sum_{l=0}^{L-1}\frac{\mathbf{S}_{(k,l)}^{H}\left(\mathbf{H}_{(k,l)}^{eq}\right)^{H}\mathbf{F}_{(k,l)}^{H}}{\mathbf{\Theta}_{(k,l)}^{*}}\right)\right)\right)}{\partial\mathbf{F}_{(k,l)}^{*}}\right]\\
&\overset{\text{(Prp. M)}}{=}\mathbb{E}\left[\frac{1}{L^2}\left(\sum_{i=0}^{L-1}\mathbf{F}_{(k,i)}\mathbf{H}_{(k,i)}^{eq}\mathbf{S}_{(k,i)}\right)\frac{\mathbf{S}_{k}^{H}\left(\mathbf{H}_{(k,l)}^{eq}\right)^{H}}{\mathbf{\Theta}_{(k,l)}^{*}}\right]\\
&\quad=\frac{1}{L^2}\left(\sum_{i=0}^{L-1}\mathbf{F}_{(k,i)}\mathbf{H}_{(k,i)}^{eq}\right)\mathbb{E}\left[\mathbf{S}_{k}\mathbf{S}_{k}^{H}\right]\frac{\left(\mathbf{H}_{(k,l)}^{eq}\right)^{H}}{\mathbf{\Theta}_{(k,l)}^{*}}\overset{(4.9)}{=}\frac{\sigma_{s_n}^2}{L^2}\left(\sum_{i=0}^{L-1}\mathbf{F}_{(k,i)}\mathbf{H}_{(k,i)}^{eq}\right)\frac{\left(\mathbf{H}_{(k,l)}^{eq}\right)^{H}}{\mathbf{\Theta}_{(k,l)}^{*}}
\end{aligned}
\tag{C.34}
$$

$$
\frac{\partial\left(\mathbb{E}\left[\mathrm{Tr}\left(\left(\frac{1}{L}\sum_{l=0}^{L-1}\mathbf{F}_{(k,l)}\mathbf{H}_{(k,l)}^{eq}\mathbf{S}_{(k,l)}\right)\mathbf{S}_{k}^{H}\boldsymbol{\varrho}^{H}\mathbf{B}_{k}^{H}\right)\right]\right)}{\partial\mathbf{F}_{(k,l)}^{*}}\overset{\text{(Prp. N)}}{=}\mathbf{0}_{N_T\times N_R}
\tag{C.35}
$$

$$\frac{\partial\left(\mathbb{E}\left[\mathrm{Tr}\left(\left(\frac{1}{L}\sum_{l=0}^{L-1}\mathbf{F}_{(k,l)}\mathbf{H}_{(k,l)}^{eq}\mathbf{S}_{(k,l)}\right)\mathbf{S}_k^H\right)\right]\right)}{\partial\mathbf{F}_{(k,l)}^*} \overset{\text{(Prp. N)}}{=} \mathbf{0}_{N_T\times N_R} \tag{C.36}$$

$$\begin{aligned}
&\frac{\partial\left(\mathbb{E}\left[\mathrm{Tr}\left(\frac{1}{L^2}\left(\sum_{l=0}^{L-1}\frac{\mathbf{F}_{(k,l)}\mathbf{H}_{(k,l)}^{eq}\mathbf{S}_{(k,l)}}{\Theta_{(k,l)}}\right)\left(\sum_{l=0}^{L-1}\mathbf{S}_{(k,l)}^H\left(\mathbf{H}_{(k,l)}^{eq}\right)^H\mathbf{F}_{(k,l)}^H\right)\right)\right]\right)}{\partial\mathbf{F}_{(k,l)}^*}\\
&\overset{\text{(Prp. O)}}{=}\mathbb{E}\left[\frac{\partial\left(\mathrm{Tr}\left(\frac{1}{L^2}\left(\sum_{l=0}^{L-1}\frac{\mathbf{F}_{(k,l)}\mathbf{H}_{(k,l)}^{eq}\mathbf{S}_{(k,l)}}{\Theta_{(k,l)}}\right)\left(\sum_{l=0}^{L-1}\mathbf{S}_{(k,l)}^H\left(\mathbf{H}_{(k,l)}^{eq}\right)^H\mathbf{F}_{(k,l)}^H\right)\right)\right)}{\partial\mathbf{F}_{(k,l)}^*}\right]\\
&\overset{\text{(Prp. M)}}{=}\mathbb{E}\left[\frac{1}{L^2}\left(\sum_{i=0}^{L-1}\frac{\mathbf{F}_{(k,i)}\mathbf{H}_{(k,i)}^{eq}\mathbf{S}_{(k,i)}}{\Theta_{(k,i)}}\right)\mathbf{S}_k^H\left(\mathbf{H}_{(k,l)}^{eq}\right)^H\right]\\
&=\frac{1}{L^2}\left(\sum_{i=0}^{L-1}\frac{\mathbf{F}_{(k,i)}\mathbf{H}_{(k,i)}^{eq}}{\Theta_{(k,i)}}\right)\mathbb{E}\left[\mathbf{S}_k\mathbf{S}_k^H\right]\left(\mathbf{H}_{(k,l)}^{eq}\right)^H\\
&\overset{(4.9)}{=}\frac{\sigma_{s_n}^2}{L^2}\left(\sum_{i=0}^{L-1}\frac{\mathbf{F}_{(k,i)}\mathbf{H}_{(k,i)}^{eq}}{\Theta_{(k,i)}}\right)\left(\mathbf{H}_{(k,l)}^{eq}\right)^H\overset{(5.10)}{\approx}\mathbf{0}_{N_T\times N_R}
\end{aligned} \tag{C.37}$$

$$\begin{aligned}
&\frac{\partial\left(\mathbb{E}\left[\mathrm{Tr}\left(\frac{1}{L^2}\left(\sum_{l=0}^{L-1}\frac{\mathbf{F}_{(k,l)}\mathbf{H}_{(k,l)}^{eq}\mathbf{S}_{(k,l)}}{\Theta_{(k,l)}}\right)\left(\sum_{l=0}^{L-1}\frac{\mathbf{S}_{(k,l)}^H\left(\mathbf{H}_{(k,l)}^{eq}\right)^H\mathbf{F}_{(k,l)}^H}{\Theta_{(k,l)}^*}\right)\right)\right]\right)}{\partial\mathbf{F}_{(k,l)}^*}\\
&\overset{\text{(Prp. O)}}{=}\mathbb{E}\left[\frac{\partial\left(\mathrm{Tr}\left(\frac{1}{L^2}\left(\sum_{l=0}^{L-1}\frac{\mathbf{F}_{(k,l)}\mathbf{H}_{(k,l)}^{eq}\mathbf{S}_{(k,l)}}{\Theta_{(k,l)}}\right)\left(\sum_{l=0}^{L-1}\frac{\mathbf{S}_{(k,l)}^H\left(\mathbf{H}_{(k,l)}^{eq}\right)^H\mathbf{F}_{(k,l)}^H}{\Theta_{(k,l)}^*}\right)\right)\right)}{\partial\mathbf{F}_{(k,l)}^*}\right]\\
&\overset{\text{(Prp. M)}}{=}\mathbb{E}\left[\frac{1}{L^2}\left(\sum_{i=0}^{L-1}\frac{\mathbf{F}_{(k,i)}\mathbf{H}_{(k,i)}^{eq}\mathbf{S}_{(k,i)}}{\Theta_{(k,i)}}\right)\frac{\mathbf{S}_k^H\left(\mathbf{H}_{(k,l)}^{eq}\right)^H}{\Theta_{(k,l)}^*}\right]\\
&=\frac{1}{L^2}\left(\sum_{i=0}^{L-1}\frac{\mathbf{F}_{(k,i)}\mathbf{H}_{(k,i)}^{eq}}{\Theta_{(k,i)}}\right)\mathbb{E}\left[\mathbf{S}_k\mathbf{S}_k^H\right]\frac{\left(\mathbf{H}_{(k,l)}^{eq}\right)^H}{\Theta_{(k,l)}^*}\\
&\overset{(4.9)}{=}\frac{\sigma_{s_n}^2}{L^2}\left(\sum_{i=0}^{L-1}\frac{\mathbf{F}_{(k,i)}\mathbf{H}_{(k,i)}^{eq}}{\Theta_{(k,i)}}\right)\frac{\left(\mathbf{H}_{(k,l)}^{eq}\right)^H}{\Theta_{(k,l)}^*}\overset{(5.10)}{\approx}\mathbf{0}_{N_T\times N_R}
\end{aligned} \tag{C.38}$$

$$\frac{\partial\left(\mathbb{E}\left[\mathrm{Tr}\left(\left(\frac{1}{L}\sum_{l=0}^{L-1}\frac{\mathbf{F}_{(k,l)}\mathbf{H}_{(k,l)}^{eq}\mathbf{S}_{(k,l)}}{\Theta_{(k,l)}}\right)\mathbf{S}_k^H\boldsymbol{\varrho}^H\mathbf{B}_k^H\right)\right]\right)}{\partial\mathbf{F}_{(k,l)}^*}\overset{\text{(Prp. N)}}{=}\mathbf{0}_{N_T\times N_R} \tag{C.39}$$

$$\frac{\partial\left(\mathbb{E}\left[\mathrm{Tr}\left(\left(\frac{1}{L}\sum_{l=0}^{L-1}\frac{\mathbf{F}_{(k,l)}\mathbf{H}_{(k,l)}^{eq}\mathbf{S}_{(k,l)}}{\Theta_{(k,l)}}\right)\mathbf{S}_k^H\right)\right]\right)}{\partial\mathbf{F}_{(k,l)}^*}\overset{\text{(Prp. N)}}{=}\mathbf{0}_{N_T\times N_R} \tag{C.40}$$

$$\begin{aligned}
&\frac{\partial\left(\mathbb{E}\left[\mathrm{Tr}\left(\frac{1}{L^2}\left(\sum_{l=0}^{L-1}\mathbf{F}_{(k,l)}\mathbf{N}_{(k,l)}\right)\left(\sum_{l=0}^{L-1}\mathbf{N}_{(k,l)}^H\mathbf{F}_{(k,l)}^H\right)\right)\right]\right)}{\partial\mathbf{F}_{(k,l)}^*}\\
&\overset{\text{(Prp. O)}}{=}\mathbb{E}\left[\frac{\partial\left(\mathrm{Tr}\left(\frac{1}{L^2}\left(\sum_{l=0}^{L-1}\mathbf{F}_{(k,l)}\mathbf{N}_{(k,l)}\right)\left(\sum_{l=0}^{L-1}\mathbf{N}_{(k,l)}^H\mathbf{F}_{(k,l)}^H\right)\right)\right)}{\partial\mathbf{F}_{(k,l)}^*}\right]\\
&\overset{\text{(Prp. M)}}{=}\mathbb{E}\left[\frac{1}{L^2}\left(\sum_{\substack{i=0\\i\neq l}}^{L-1}\mathbf{F}_{(k,i)}\mathbf{N}_{(k,i)}\right)\mathbf{N}_{(k,l)}^H\right]+\frac{1}{L^2}\mathbf{F}_{(k,l)}\mathbb{E}\left[\mathbf{N}_{(k,l)}\mathbf{N}_{(k,l)}^H\right]\overset{(4.18)}{=}\frac{\sigma_{n_z}^2}{L^2}\mathbf{F}_{(k,l)}
\end{aligned} \tag{C.41}$$

Note that the noise components are independent with zero mean. Therefore, $\mathbb{E}\left[\mathbf{N}_{(k,i)}\mathbf{N}_{(k,l)}\right]=0\ \forall\ i\neq l$.

$$\begin{aligned}
&\frac{\partial\left(\mathbb{E}\left[\mathrm{Tr}\left(\frac{1}{L^2}\left(\sum_{l=0}^{L-1}\mathbf{F}_{(k,l)}\mathbf{N}_{(k,l)}\right)\left(\sum_{l=0}^{L-1}\frac{\mathbf{N}_{(k,l)}^H\mathbf{F}_{(k,l)}^H}{\Theta_{(k,l)}^*}\right)\right)\right]\right)}{\partial\mathbf{F}_{(k,l)}^*}\\
&\overset{\text{(Prp. O)}}{=}\mathbb{E}\left[\frac{\partial\left(\mathrm{Tr}\left(\frac{1}{L^2}\left(\sum_{l=0}^{L-1}\mathbf{F}_{(k,l)}\mathbf{N}_{(k,l)}\right)\left(\sum_{l=0}^{L-1}\frac{\mathbf{N}_{(k,l)}^H\mathbf{F}_{(k,l)}^H}{\Theta_{(k,l)}^*}\right)\right)\right)}{\partial\mathbf{F}_{(k,l)}^*}\right]\\
&\overset{\text{(Prp. M)}}{=}\mathbb{E}\left[\frac{1}{L^2}\left(\sum_{\substack{i=0\\i\neq l}}^{L-1}\mathbf{F}_{(k,i)}\mathbf{N}_{(k,i)}\right)\frac{\mathbf{N}_{(k,l)}^H}{\Theta_{(k,l)}^*}\right]+\frac{1}{L^2}\frac{\mathbf{F}_{(k,l)}}{\Theta_{(k,l)}^*}\mathbb{E}\left[\mathbf{N}_{(k,l)}\mathbf{N}_{(k,l)}^H\right]\overset{(4.18)}{=}\frac{\sigma_{n_z}^2}{L^2}\frac{\mathbf{F}_{(k,l)}}{\Theta_{(k,l)}^*}
\end{aligned} \tag{C.42}$$

$$\frac{\partial\left(\mathbb{E}\left[\mathrm{Tr}\left(\frac{1}{L^2}\left(\sum_{l=0}^{L-1}\frac{\mathbf{F}_{(k,l)}\mathbf{N}_{(k,l)}}{\Theta_{(k,l)}}\right)\left(\sum_{l=0}^{L-1}\mathbf{N}_{(k,l)}^{H}\mathbf{F}_{(k,l)}^{H}\right)\right)\right]\right)}{\partial\mathbf{F}_{(k,l)}^{*}}$$

$$\overset{\text{(Prp. O)}}{=}\mathbb{E}\left[\frac{\partial\left(\mathrm{Tr}\left(\frac{1}{L^2}\left(\sum_{l=0}^{L-1}\frac{\mathbf{F}_{(k,l)}\mathbf{N}_{(k,l)}}{\Theta_{(k,l)}}\right)\left(\sum_{l=0}^{L-1}\mathbf{N}_{(k,l)}^{H}\mathbf{F}_{(k,l)}^{H}\right)\right)\right)}{\partial\mathbf{F}_{(k,l)}^{*}}\right]$$

$$\overset{\text{(Prp. M)}}{=}\mathbb{E}\left[\frac{1}{L^2}\left(\sum_{\substack{i=0\\ i\neq l}}^{L-1}\frac{\mathbf{F}_{(k,i)}\mathbf{N}_{(k,i)}}{\Theta_{(k,i)}}\right)\mathbf{N}_{(k,l)}^{H}\right]+\frac{1}{L^2}\frac{\mathbf{F}_{(k,l)}}{\Theta_{(k,l)}}\mathbb{E}\left[\mathbf{N}_{(k,l)}\mathbf{N}_{(k,l)}^{H}\right]\overset{(4.18)}{=}\frac{\sigma_{n_z}^2}{L^2}\frac{\mathbf{F}_{(k,l)}}{\Theta_{(k,l)}} \tag{C.43}$$

$$\frac{\partial\left(\mathbb{E}\left[\mathrm{Tr}\left(\frac{1}{L^2}\left(\sum_{l=0}^{L-1}\frac{\mathbf{F}_{(k,l)}\mathbf{N}_{(k,l)}}{\Theta_{(k,l)}}\right)\left(\sum_{l=0}^{L-1}\frac{\mathbf{N}_{(k,l)}^{H}\mathbf{F}_{(k,l)}^{H}}{\Theta_{(k,l)}^{*}}\right)\right)\right]\right)}{\partial\mathbf{F}_{(k,l)}^{*}}$$

$$\overset{\text{(Prp. O)}}{=}\mathbb{E}\left[\frac{\partial\left(\mathrm{Tr}\left(\frac{1}{L^2}\left(\sum_{l=0}^{L-1}\frac{\mathbf{F}_{(k,l)}\mathbf{N}_{(k,l)}}{\Theta_{(k,l)}}\right)\left(\sum_{l=0}^{L-1}\frac{\mathbf{N}_{(k,l)}^{H}\mathbf{F}_{(k,l)}^{H}}{\Theta_{(k,l)}^{*}}\right)\right)\right)}{\partial\mathbf{F}_{(k,l)}^{*}}\right]$$

$$\overset{\text{(Prp. M)}}{=}\mathbb{E}\left[\frac{1}{L^2}\left(\sum_{\substack{i=0\\ i\neq l}}^{L-1}\frac{\mathbf{F}_{(k,i)}\mathbf{N}_{(k,i)}}{\Theta_{(k,i)}}\right)\frac{\mathbf{N}_{(k,l)}^{H}}{\Theta_{(k,l)}^{*}}\right]+\frac{1}{L^2}\frac{\mathbf{F}_{(k,l)}}{|\Theta_{(k,l)}|^2}\mathbb{E}\left[\mathbf{N}_{(k,l)}\mathbf{N}_{(k,l)}^{H}\right]\overset{(4.18)}{=}\frac{\sigma_{n_z}^2}{L^2}\frac{\mathbf{F}_{(k,l)}}{|\Theta_{(k,l)}|^2} \tag{C.44}$$

$$\frac{\partial\left(\mathbb{E}\left[\mathrm{Tr}\left(\frac{1}{L}\mathbf{B}_k\boldsymbol{\varrho}\mathbf{S}_k\left(\sum_{l=0}^{L-1}\mathbf{S}_{(k,l)}^{H}\left(\mathbf{H}_{(k,l)}^{eq}\right)^{H}\mathbf{F}_{(k,l)}^{H}\right)\right)\right]\right)}{\partial\mathbf{F}_{(k,l)}^{*}}$$

$$\overset{\text{(Prp. O)}}{=}\mathbb{E}\left[\frac{\partial\mathrm{Tr}\left(\frac{1}{L}\mathbf{B}_k\boldsymbol{\varrho}\mathbf{S}_k\left(\sum_{l=0}^{L-1}\mathbf{S}_{(k,l)}^{H}\left(\mathbf{H}_{(k,l)}^{eq}\right)^{H}\mathbf{F}_{(k,l)}^{H}\right)\right)}{\partial\mathbf{F}_{(k,l)}^{*}}\right]$$

$$\overset{\text{(Prp. M)}}{=}\mathbb{E}\left[\frac{1}{L}\mathbf{B}_k\boldsymbol{\varrho}\mathbf{S}_k\mathbf{S}_{(k,l)}^{H}\left(\mathbf{H}_{(k,l)}^{eq}\right)^{H}\right]=\frac{1}{L}\mathbf{B}_k\boldsymbol{\varrho}\mathbb{E}\left[\mathbf{S}_k\mathbf{S}_k^{H}\right]\left(\mathbf{H}_{(k,l)}^{eq}\right)^{H}\overset{(4.9)}{=}\frac{\sigma_{s_n}^2}{L}\mathbf{B}_k\boldsymbol{\varrho}\left(\mathbf{H}_{(k,l)}^{eq}\right)^{H} \tag{C.45}$$

$$\frac{\partial\left(\mathbb{E}\left[\mathrm{Tr}\left(\frac{1}{L}\mathbf{B}_k\boldsymbol{\varrho}\mathbf{S}_k\left(\sum_{l=0}^{L-1}\frac{\mathbf{S}_{(k,l)}^H\left(\mathbf{H}_{(k,l)}^{eq}\right)^H\mathbf{F}_{(k,l)}^H}{\Theta_{(k,l)}^*}\right)\right)\right]\right)}{\partial\mathbf{F}_{(k,l)}^*}$$

$$\overset{\text{(Prp. O)}}{=}\mathbb{E}\left[\frac{\partial\mathrm{Tr}\left(\frac{1}{L}\mathbf{B}_k\boldsymbol{\varrho}\mathbf{S}_k\left(\sum_{l=0}^{L-1}\frac{\mathbf{S}_{(k,l)}^H\left(\mathbf{H}_{(k,l)}^{eq}\right)^H\mathbf{F}_{(k,l)}^H}{\Theta_{(k,l)}^*}\right)\right)}{\partial\mathbf{F}_{(k,l)}^*}\right]$$

$$\overset{\text{(Prp. M)}}{=}\mathbb{E}\left[\frac{1}{L}\mathbf{B}_k\boldsymbol{\varrho}\mathbf{S}_k\frac{\mathbf{S}_{(k,l)}^H\left(\mathbf{H}_{(k,l)}^{eq}\right)^H}{\Theta_{(k,l)}^*}\right]=\frac{1}{L}\mathbf{B}_k\boldsymbol{\varrho}\mathbb{E}\left[\mathbf{S}_k\mathbf{S}_k^H\right]\frac{\left(\mathbf{H}_{(k,l)}^{eq}\right)^H}{\Theta_{(k,l)}^*}\overset{(4.9)}{=}\frac{\sigma_{s_n}^2}{L}\mathbf{B}_k\boldsymbol{\varrho}\frac{\left(\mathbf{H}_{(k,l)}^{eq}\right)^H}{\Theta_{(k,l)}^*} \tag{C.46}$$

$$\frac{\partial\left(\mathbb{E}\left[\mathrm{Tr}\left(\mathbf{B}_k\boldsymbol{\varrho}\mathbf{S}_k\mathbf{S}_k^H\boldsymbol{\varrho}^H\mathbf{B}_k^H\right)\right]\right)}{\partial\mathbf{F}_{(k,l)}^*}=\mathbf{0}_{N_T\times N_R} \tag{C.47}$$

$$\frac{\partial\left(\mathbb{E}\left[\mathrm{Tr}\left(\mathbf{B}_k\boldsymbol{\varrho}\mathbf{S}_k\mathbf{S}_k^H\right)\right]\right)}{\partial\mathbf{F}_{(k,l)}^*}=\mathbf{0}_{N_T\times N_R} \tag{C.48}$$

$$\frac{\partial\left(\mathbb{E}\left[\mathrm{Tr}\left(\mathbf{B}_k\boldsymbol{\Delta}_k\boldsymbol{\Delta}_k^H\mathbf{B}_k^H\right)\right]\right)}{\partial\mathbf{F}_{(k,l)}^*}=\mathbf{0}_{N_T\times N_R} \tag{C.49}$$

$$\frac{\partial\left(\mathbb{E}\left[\mathrm{Tr}\left(\frac{1}{L}\mathbf{S}_k\left(\sum_{l=0}^{L-1}\mathbf{S}_{(k,l)}^H\left(\mathbf{H}_{(k,l)}^{eq}\right)^H\mathbf{F}_{(k,l)}^H\right)\right)\right]\right)}{\partial\mathbf{F}_{(k,l)}^*}$$

$$\overset{\text{(Prp. O)}}{=}\mathbb{E}\left[\frac{\partial\left(\mathrm{Tr}\left(\frac{1}{L}\mathbf{S}_k\left(\sum_{l=0}^{L-1}\mathbf{S}_{(k,l)}^H\left(\mathbf{H}_{(k,l)}^{eq}\right)^H\mathbf{F}_{(k,l)}^H\right)\right)\right)}{\partial\mathbf{F}_{(k,l)}^*}\right]$$

$$\overset{\text{(Prp. M)}}{=}\mathbb{E}\left[\frac{1}{L}\mathbf{S}_k\mathbf{S}_{(k,l)}^H\left(\mathbf{H}_{(k,l)}^{eq}\right)^H\right]=\mathbb{E}\frac{1}{L}\left[\mathbf{S}_k\mathbf{S}_k^H\right]\left(\mathbf{H}_{(k,l)}^{eq}\right)^H\overset{(4.9)}{=}\frac{\sigma_{s_n}^2}{L}\left(\mathbf{H}_{(k,l)}^{eq}\right)^H \tag{C.50}$$

$$\frac{\partial\left(\mathbb{E}\left[\mathrm{Tr}\left(\frac{1}{L}\mathbf{S}_k\left(\sum_{l=0}^{L-1}\frac{\mathbf{S}_{(k,l)}^H\left(\mathbf{H}_{(k,l)}^{eq}\right)^H\mathbf{F}_{(k,l)}^H}{\mathbf{\Theta}_{(k,l)}^*}\right)\right)\right]\right)}{\partial\mathbf{F}_{(k,l)}^*}$$

$$\overset{\text{(Prp. O)}}{=}\mathbb{E}\left[\frac{\partial\left(\mathrm{Tr}\left(\frac{1}{L}\mathbf{S}_k\left(\sum_{l=0}^{L-1}\frac{\mathbf{S}_{(k,l)}^H\left(\mathbf{H}_{(k,l)}^{eq}\right)^H\mathbf{F}_{(k,l)}^H}{\mathbf{\Theta}_{(k,l)}^*}\right)\right)\right)}{\partial\mathbf{F}_{(k,l)}^*}\right]$$

$$\overset{\text{(Prp. M)}}{=}\mathbb{E}\left[\frac{1}{L}\mathbf{S}_k\frac{\mathbf{S}_{(k,l)}^H\left(\mathbf{H}_{(k,l)}^{eq}\right)^H}{\mathbf{\Theta}_{(k,l)}^*}\right]=\mathbb{E}\frac{1}{L}\left[\mathbf{S}_k\mathbf{S}_k^H\right]\frac{\left(\mathbf{H}_{(k,l)}^{eq}\right)^H}{\mathbf{\Theta}_{(k,l)}^*}\overset{(4.9)}{=}\frac{\sigma_{s_n}^2}{L}\frac{\left(\mathbf{H}_{(k,l)}^{eq}\right)^H}{\mathbf{\Theta}_{(k,l)}^*} \tag{C.51}$$

$$\frac{\partial\left(\mathbb{E}\left[\mathrm{Tr}\left(\mathbf{S}_k\mathbf{S}_k^H\boldsymbol{\varrho}^H\mathbf{B}_k^H\right)\right]\right)}{\partial\mathbf{F}_{(k,l)}^*}=\mathbf{0}_{N_T\times N_R} \tag{C.52}$$

$$\frac{\partial\left(\mathbb{E}\left[\mathrm{Tr}\left(\mathbf{S}_k\mathbf{S}_k^H\right)\right]\right)}{\partial\mathbf{F}_{(k,l)}^*}=\mathbf{0}_{N_T\times N_R} \tag{C.53}$$

Putting (C.33) to (C.53) into (C.32) and replacing $\mathbf{B}_k$ by (C.31), one gets

$$\frac{\sigma_{s_n}^2}{L^2}\left(\sum_{i=0}^{L-1}\mathbf{F}_{(k,i)}\mathbf{H}_{(k,i)}^{eq}\right)\left(\mathbf{H}_{(k,l)}^{eq}\right)^H+\frac{\sigma_{s_n}^2}{L^2}\left(\sum_{i=0}^{L-1}\mathbf{F}_{(k,i)}\mathbf{H}_{(k,i)}^{eq}\right)\frac{\left(\mathbf{H}_{(k,l)}^{eq}\right)^H}{\Theta_{(k,l)}^*}+\frac{\sigma_{n_z}^2}{L^2}\mathbf{F}_{(k,l)}$$
$$+\frac{\sigma_{n_z}^2}{L^2}\frac{\mathbf{F}_{(k,l)}}{\Theta_{(k,l)}^*}+\frac{\sigma_{n_z}^2}{L^2}\frac{\mathbf{F}_{(k,l)}}{\Theta_{(k,l)}}+\frac{\sigma_{n_z}^2}{L^2}\frac{\mathbf{F}_{(k,l)}}{|\Theta_{(k,l)}|^2}-\frac{\sigma_{s_n}^2}{L}\left(\left(\frac{1}{L}\sum_{i=0}^{L-1}\mathbf{F}_{(k,i)}\mathbf{H}_{(k,i)}^{eq}\right)-\boldsymbol{I}_{N_T}\right)\boldsymbol{\varrho}^2\left(\mathbf{H}_{(k,l)}^{eq}\right)^H$$
$$-\frac{\sigma_{s_n}^2}{L}\left(\left(\frac{1}{L}\sum_{i=0}^{L-1}\mathbf{F}_{(k,i)}\mathbf{H}_{(k,i)}^{eq}\right)-\boldsymbol{I}_{N_T}\right)\boldsymbol{\varrho}^2\frac{\left(\mathbf{H}_{(k,l)}^{eq}\right)^H}{\Theta_{(k,l)}^*}-\frac{\sigma_{s_n}^2}{L}\left(\mathbf{H}_{(k,l)}^{eq}\right)^H-\frac{\sigma_{s_n}^2}{L}\frac{\left(\mathbf{H}_{(k,l)}^{eq}\right)^H}{\Theta_{(k,l)}^*}$$
$$=\mathbf{0}_{N_T\times N_R}\Leftrightarrow$$

$$\Leftrightarrow\quad\frac{\sigma_{n_z}^2}{L^2}\mathbf{F}_{(k,l)}\left(1+\frac{1}{|\Theta_{(k,l)}|^2}+\frac{1}{\Theta_{(k,l)}^*}+\frac{1}{\Theta_{(k,l)}}\right)+\frac{\sigma_{s_n}^2}{L^2}\left(\sum_{i=0}^{L-1}\mathbf{F}_{(k,i)}\mathbf{H}_{(k,i)}^{eq}\right)\left(\mathbf{H}_{(k,l)}^{eq}\right)^H\left(1+\frac{1}{\Theta_{(k,l)}^*}\right)$$
$$-\frac{\sigma_{s_n}^2}{L}\left(\left(\frac{1}{L}\sum_{i=0}^{L-1}\mathbf{F}_{(k,i)}\mathbf{H}_{(k,i)}^{eq}\right)-\boldsymbol{I}_{N_T}\right)\boldsymbol{\varrho}^2\left(\mathbf{H}_{(k,l)}^{eq}\right)^H\left(1+\frac{1}{\Theta_{(k,l)}^*}\right)$$
$$-\frac{\sigma_{s_n}^2}{L}\left(\mathbf{H}_{(k,l)}^{eq}\right)^H\left(1+\frac{1}{\Theta_{(k,l)}^*}\right)=\mathbf{0}_{N_T\times N_R}\Leftrightarrow$$

$$\Leftrightarrow\quad\frac{1}{\gamma}\mathbf{F}_{(k,l)}\left(1+\frac{1}{|\Theta_{(k,l)}|^2}+\frac{1}{\Theta_{(k,l)}^*}+\frac{1}{\Theta_{(k,l)}}\right)+\left(\left(\sum_{i=0}^{L-1}\mathbf{F}_{(k,i)}\mathbf{H}_{(k,i)}^{eq}\right)\left(\mathbf{H}_{(k,l)}^{eq}\right)^H\right.$$
$$\left.-L\left(\left(\frac{1}{L}\sum_{i=0}^{L-1}\mathbf{F}_{(k,i)}\mathbf{H}_{(k,i)}^{eq}\right)-\boldsymbol{I}_{N_T}\right)\boldsymbol{\varrho}^2\left(\mathbf{H}_{(k,l)}^{eq}\right)^H-L\left(\mathbf{H}_{(k,l)}^{eq}\right)^H\right)\left(1+\frac{1}{\Theta_{(k,l)}^*}\right)$$
$$=\mathbf{0}_{N_T\times N_R}\Leftrightarrow$$

$$\Leftrightarrow\quad\frac{1}{\gamma}\mathbf{F}_{(k,l)}\left(1+\frac{1}{|\Theta_{(k,l)}|^2}+\frac{1}{\Theta_{(k,l)}^*}+\frac{1}{\Theta_{(k,l)}}\right)+\left(\left(\sum_{i=0}^{L-1}\mathbf{F}_{(k,i)}\mathbf{H}_{(k,i)}^{eq}\right)(\boldsymbol{I}_{N_T}-\boldsymbol{\varrho}^2)\left(\mathbf{H}_{(k,l)}^{eq}\right)^H+\right.$$
$$\left.+L\left(\boldsymbol{\varrho}^2-\boldsymbol{I}_{N_T}\right)\left(\mathbf{H}_{(k,l)}^{eq}\right)^H\right)\left(1+\frac{1}{\Theta_{(k,l)}^*}\right)=\mathbf{0}_{N_T\times N_R}\Leftrightarrow$$

$$\Leftrightarrow\quad\frac{1}{\gamma}\mathbf{F}_{(k,l)}\left(1+\frac{1}{|\Theta_{(k,l)}|^2}+\frac{1}{\Theta_{(k,l)}^*}+\frac{1}{\Theta_{(k,l)}}\right)$$
$$+\left(\sum_{i=0}^{L-1}\mathbf{F}_{(k,i)}\mathbf{H}_{(k,i)}^{eq}\right)(\boldsymbol{I}_{N_T}-\boldsymbol{\varrho}^2)\left(\mathbf{H}_{(k,l)}^{eq}\right)^H\left(1+\frac{1}{\Theta_{(k,l)}^*}\right)=$$
$$=L(\boldsymbol{I}_{N_T}-\boldsymbol{\varrho}^2)\left(\mathbf{H}_{(k,l)}^{eq}\right)^H\left(1+\frac{1}{\Theta_{(k,l)}^*}\right)\quad\text{(C.54)}$$

To remove the summation with $\mathbf{F}_{(k,i)}$, let's do some mathematical manipulation. Multiplying all terms by $\mathbf{H}_{(k,l)}^{eq}$ and using (Prp. Q) to sum the equations for all l values, (C.54) becomes

$$\frac{1}{\gamma}\left(\sum_{l=0}^{L-1}\mathbf{F}_{(k,l)}\mathbf{H}_{(k,l)}^{eq}\right)+\underbrace{\frac{1}{\gamma}\left(\sum_{l=0}^{L-1}\mathbf{F}_{(k,l)}\mathbf{H}_{(k,l)}^{eq}\left(\frac{1}{|\Theta_{(k,l)}|^2}+\frac{1}{\Theta_{(k,l)}^*}+\frac{1}{\Theta_{(k,l)}}\right)\right)}_{\approx 0}+$$

$$+\left(\sum_{l=0}^{L-1}\left(\sum_{i=0}^{L-1}\mathbf{F}_{(k,i)}\mathbf{H}_{(k,i)}^{eq}\right)(\boldsymbol{I}_{N_T}-\boldsymbol{\varrho}^2)\left(\mathbf{H}_{(k,l)}^{eq}\right)^H\mathbf{H}_{(k,l)}^{eq}\right)+$$

$$+\underbrace{\left(\sum_{l=0}^{L-1}\left(\sum_{i=0}^{L-1}\mathbf{F}_{(k,i)}\mathbf{H}_{(k,i)}^{eq}\right)(\boldsymbol{I}_{N_T}-\boldsymbol{\varrho}^2)\left(\mathbf{H}_{(k,l)}^{eq}\right)^H\mathbf{H}_{(k,l)}^{eq}\frac{1}{\Theta_{(k,l)}^*}\right)}_{\approx 0}=$$

$$=\left(\sum_{l=0}^{L-1}L(\boldsymbol{I}_{N_T}-\boldsymbol{\varrho}^2)\left(\mathbf{H}_{(k,l)}^{eq}\right)^H\mathbf{H}_{(k,l)}^{eq}\right)+\underbrace{\left(\sum_{l=0}^{L-1}L(\boldsymbol{I}_{N_T}-\boldsymbol{\varrho}^2)\left(\mathbf{H}_{(k,l)}^{eq}\right)^H\mathbf{H}_{(k,l)}^{eq}\frac{1}{\Theta_{(k,l)}^*}\right)}_{\approx 0}\Leftrightarrow$$

$$\Leftrightarrow\frac{1}{\gamma}\underbrace{\left(\sum_{l=0}^{L-1}\mathbf{F}_{(k,l)}\mathbf{H}_{(k,l)}^{eq}\right)}_{\text{A}}+\underbrace{\left(\sum_{i=0}^{L-1}\mathbf{F}_{(k,i)}\mathbf{H}_{(k,i)}^{eq}\right)}_{\text{B}}(\boldsymbol{I}_{N_T}-\boldsymbol{\varrho}^2)\left(\sum_{l=0}^{L-1}\left(\mathbf{H}_{(k,l)}^{eq}\right)^H\mathbf{H}_{(k,l)}^{eq}\right)=$$

$$=L(\boldsymbol{I}_{N_T}-\boldsymbol{\varrho}^2)\left(\sum_{l=0}^{L-1}\left(\mathbf{H}_{(k,l)}^{eq}\right)^H\mathbf{H}_{(k,l)}^{eq}\right)\Leftrightarrow$$

$$\overset{A=B}{\Leftrightarrow}\left(\sum_{i=0}^{L-1}\mathbf{F}_{(k,i)}\mathbf{H}_{(k,i)}^{eq}\right)\left(\frac{1}{\gamma}\boldsymbol{I}_{N_T}+(\boldsymbol{I}_{N_T}-\boldsymbol{\varrho}^2)\left(\sum_{l=0}^{L-1}\left(\mathbf{H}_{(k,l)}^{eq}\right)^H\mathbf{H}_{(k,l)}^{eq}\right)\right)=$$

$$=L(\boldsymbol{I}_{N_T}-\boldsymbol{\varrho}^2)\left(\sum_{l=0}^{L-1}\left(\mathbf{H}_{(k,l)}^{eq}\right)^H\mathbf{H}_{(k,l)}^{eq}\right)\Leftrightarrow$$

$$\overset{\text{(Prp. A)}}{\Leftrightarrow}\left(\sum_{i=0}^{L-1}\mathbf{F}_{(k,i)}\mathbf{H}_{(k,i)}^{eq}\right)=$$

$$=L(\boldsymbol{I}_{N_T}-\boldsymbol{\varrho}^2)\left(\sum_{l=0}^{L-1}\left(\mathbf{H}_{(k,l)}^{eq}\right)^H\mathbf{H}_{(k,l)}^{eq}\right)\left(\frac{1}{\gamma}\boldsymbol{I}_{N_T}+(\boldsymbol{I}_{N_T}-\boldsymbol{\varrho}^2)\left(\sum_{l=0}^{L-1}\left(\mathbf{H}_{(k,l)}^{eq}\right)^H\mathbf{H}_{(k,l)}^{eq}\right)\right)^{-1}$$

(C.55)

Replacing (C.55) into (C.54) and considering that in average $\frac{1}{\Theta_{(k,l)}}\approx 0$, $\frac{1}{\Theta^{*}_{(k,l)}}\approx 0$ and $\frac{1}{|\Theta_{(k,l)}|^2}\approx 1$

$$
\begin{aligned}
&\frac{1}{\gamma}\mathbf{F}_{(k,l)}+ \\
&+L(\boldsymbol{I}_{N_T}-\boldsymbol{\varrho}^2)\left(\sum_{l=0}^{L-1}\left(\mathbf{H}^{eq}_{(k,l)}\right)^H\mathbf{H}^{eq}_{(k,l)}\right)\left(\frac{1}{\gamma}\boldsymbol{I}_{N_T}+(\boldsymbol{I}_{N_T}-\boldsymbol{\varrho}^2)\left(\sum_{l=0}^{L-1}\left(\mathbf{H}^{eq}_{(k,l)}\right)^H\mathbf{H}^{eq}_{(k,l)}\right)\right)^{-1} \\
&(\boldsymbol{I}_{N_T}-\boldsymbol{\varrho}^2)\left(\mathbf{H}^{eq}_{(k,l)}\right)^H = L(\boldsymbol{I}_{N_T}-\boldsymbol{\varrho}^2)\left(\mathbf{H}^{eq}_{(k,l)}\right)^H \Leftrightarrow \\
&\Leftrightarrow \frac{1}{\gamma}\mathbf{F}_{(k,l)} = \left(\boldsymbol{I}_{N_T}-(\boldsymbol{I}_{N_T}-\boldsymbol{\varrho}^2)\left(\sum_{l=0}^{L-1}\left(\mathbf{H}^{eq}_{(k,l)}\right)^H\mathbf{H}^{eq}_{(k,l)}\right)\right. \\
&\left.\left(\frac{1}{\gamma}\boldsymbol{I}_{N_T}+(\boldsymbol{I}_{N_T}-\boldsymbol{\varrho}^2)\left(\sum_{l=0}^{L-1}\left(\mathbf{H}^{eq}_{(k,l)}\right)^H\mathbf{H}^{eq}_{(k,l)}\right)\right)^{-1}\right)L(\boldsymbol{I}_{N_T}-\boldsymbol{\varrho}^2)\left(\mathbf{H}^{eq}_{(k,l)}\right)^H \Leftrightarrow \\
&\Leftrightarrow \mathbf{F}_{(k,l)} = \gamma\left(\left(\frac{1}{\gamma}\boldsymbol{I}_{N_T}+(\boldsymbol{I}_{N_T}-\boldsymbol{\varrho}^2)\left(\sum_{l=0}^{L-1}\left(\mathbf{H}^{eq}_{(k,l)}\right)^H\mathbf{H}^{eq}_{(k,l)}\right)\right)\right. \\
&\left(\frac{1}{\gamma}\boldsymbol{I}_{N_T}+(\boldsymbol{I}_{N_T}-\boldsymbol{\varrho}^2)\left(\sum_{l=0}^{L-1}\left(\mathbf{H}^{eq}_{(k,l)}\right)^H\mathbf{H}^{eq}_{(k,l)}\right)\right)^{-1} - (\boldsymbol{I}_{N_T}-\boldsymbol{\varrho}^2)\left(\sum_{l=0}^{L-1}\left(\mathbf{H}^{eq}_{(k,l)}\right)^H\mathbf{H}^{eq}_{(k,l)}\right) \\
&\left.\left(\frac{1}{\gamma}\boldsymbol{I}_{N_T}+(\boldsymbol{I}_{N_T}-\boldsymbol{\varrho}^2)\left(\sum_{l=0}^{L-1}\left(\mathbf{H}^{eq}_{(k,l)}\right)^H\mathbf{H}^{eq}_{(k,l)}\right)\right)^{-1}\right)L(\boldsymbol{I}_{N_T}-\boldsymbol{\varrho}^2)\left(\mathbf{H}^{eq}_{(k,l)}\right)^H \Leftrightarrow \\
&\Leftrightarrow \mathbf{F}_{(k,l)} = \left(\frac{1}{\gamma}\boldsymbol{I}_{N_T}+(\boldsymbol{I}_{N_T}-\boldsymbol{\varrho}^2)\left(\sum_{l=0}^{L-1}\left(\mathbf{H}^{eq}_{(k,l)}\right)^H\mathbf{H}^{eq}_{(k,l)}\right)\right)^{-1}L(\boldsymbol{I}_{N_T}-\boldsymbol{\varrho}^2)\left(\mathbf{H}^{eq}_{(k,l)}\right)^H \qquad \text{(C.56)}
\end{aligned}
$$

D

Complexity Analysis for MIMO equalisers

In this appendix, the complexity analysis for the different equalisers presented in this thesis is detailed step by step. In the next sections, the complexity of each equaliser is derived.

D.1 ZF equaliser's complexity

The output of the ZF equaliser is given by

$$\widetilde{\mathbf{S}}_k = \Upsilon\left(\widetilde{\check{\mathbf{S}}}_{(k,l)}\right) = \frac{1}{L}\sum_{l=0}^{L-1}\widetilde{\check{\mathbf{S}}}_{(k,l)} + \frac{1}{L}\sum_{l=0}^{L-1}\frac{\widetilde{\check{\mathbf{S}}}_{(k,l)}}{\Theta_{(k,l)}} \tag{D.1}$$

where

$$\widetilde{\check{\mathbf{S}}}_{(k,l)} = \mathbf{F}_{(k,l)}\mathbf{Y}_{(k,l)} \tag{D.2}$$

with

$$\mathbf{F}_{(k,l)} = \boldsymbol{\kappa}\left(\mathbf{H}^H_{(k,l)}\mathbf{H}_{(k,l)}\right)^{-1}\mathbf{H}^H_{(k,l)}. \tag{D.3}$$

Thus, to obtain the number of FLOPs associated with this equaliser, we should determine its

computational cost step by step. We start with the normalisation factor $\boldsymbol{\kappa}$ given by

$$\boldsymbol{\kappa} = \text{diag}\left[\kappa^{(1,1)} \dots \kappa^{(N_T,N_T)}\right] \tag{D.4}$$

where

$$\kappa^{(t,t)} = \left(\frac{1}{LN_{block}} \sum_{l=0}^{L-1} \sum_{k=0}^{N_{block}-1} \sum_{r=1}^{N_R} F_{(k,l)}^{(t,r)} H_{(k,l)}^{(r,t)}\right)^{-1}. \tag{D.5}$$

This factor is equal for all frequencies k. Therefore, it only needs to be calculated once and its computational cost is divided by the number of frequencies in each block, i.e. N_{block}. We start to determine the number of FLOPs used to obtain each diagonal element and, step by step, it is given by

$$F_{(k,l)}^{(t,r)} H_{(k,l)}^{(r,t)} \Rightarrow 6 \tag{D.6}$$

$$\sum_{r=1}^{N_R} F_{(k,l)}^{(t,r)} H_{(k,l)}^{(r,t)} \Rightarrow N_R \times \text{(D.6)} + 2(N_R - 1) \tag{D.7}$$

$$\sum_{k=0}^{N_{block}-1} \sum_{r=1}^{N_R} F_{(k,l)}^{(t,r)} H_{(k,l)}^{(r,t)} \Rightarrow N_{block} \times \text{(D.7)} + 2(N_{block} - 1) \tag{D.8}$$

$$\sum_{l=0}^{L-1} \sum_{k=0}^{N_{block}-1} \sum_{r=1}^{N_R} F_{(k,l)}^{(t,r)} H_{(k,l)}^{(r,t)} \Rightarrow L \times \text{(D.8)} + 2(L - 1) \tag{D.9}$$

Here, the cost of obtaining LN_{block} is not considered because it is needed for all approaches and it could be saved in a constant variable.

$$\frac{1}{LN_{block}} \sum_{l=0}^{L-1} \sum_{k=0}^{N_{block}-1} \sum_{r=1}^{N_R} F_{(k,l)}^{(t,r)} H_{(k,l)}^{(r,t)} \Rightarrow \text{(D.9)} + 2 \tag{D.10}$$

$$\kappa^{(t,t)} = \left(\frac{1}{LN_{block}} \sum_{l=0}^{L-1} \sum_{k=0}^{N_{block}-1} \sum_{r=1}^{N_R} F_{(k,l)}^{(t,r)} H_{(k,l)}^{(r,t)}\right)^{-1} \Rightarrow \text{(D.10)} + 5 = 8LN_{block}N_R + 5 \tag{D.11}$$

The number of FLOPs to obtain the entire diagonal normalisation matrix is given by

$$\boldsymbol{\kappa} \Rightarrow \frac{N_T}{N_{block}} \times \text{(D.11)} = 8LN_TN_R + 5\frac{N_T}{N_{block}} \approx 8LN_TN_R \tag{D.12}$$

Following, the computational cost to obtain feedforward coefficients in ZF using expression (D.3) is

$$\mathbf{H}_{(k,l)}^{H}\mathbf{H}_{(k,l)} \Rightarrow 4N_R N_T^2 + 4N_R N_T - N_T^2 - N_T \tag{D.13}$$

$$\left(\mathbf{H}_{(k,l)}^{H}\mathbf{H}_{(k,l)}\right)^{-1} \Rightarrow (\text{D.13}) + \frac{8}{3}N_T^3 + \frac{19}{2}N_T^2 - \frac{7}{6}N_T \tag{D.14}$$

$$\left(\mathbf{H}_{(k,l)}^{H}\mathbf{H}_{(k,l)}\right)^{-1}\mathbf{H}_{(k,l)}^{H} \Rightarrow (\text{D.14}) + 8N_T^2 N_R - 2N_T N_R \tag{D.15}$$

$$\begin{aligned}\mathbf{F}_{(k,l)} = \boldsymbol{\kappa}\left(\mathbf{H}_{(k,l)}^{H}\mathbf{H}_{(k,l)}\right)^{-1}\mathbf{H}_{(k,l)}^{H} \Rightarrow (\text{D.12}) + (\text{D.15}) + 6N_T = \\ = \frac{8}{3}N_T^3 + 12N_T^2 N_R + \frac{17}{2}N_T^2 + (8L+2)N_T N_R + \frac{23}{6}N_T\end{aligned} \tag{D.16}$$

At last and using the previous results, the total number of FLOPs needed to obtain the estimated transmitted symbol $\widetilde{\mathbf{S}}_k$ is given by

$$\widetilde{\widetilde{\mathbf{S}}}_{(k,l)} = \mathbf{F}_{(k,l)}\mathbf{Y}_{(k,l)} \Rightarrow (\text{D.16}) + 8N_T N_R - 2N_T \tag{D.17}$$

$$\begin{aligned}\widetilde{\mathbf{S}}_k = \Upsilon\left(\widetilde{\widetilde{\mathbf{S}}}_{(k,l)}\right) \Rightarrow (\text{D.17}) + 2(L-1) + 2 + 11L + 2(L-1) + 2 = \\ = \frac{8}{3}N_T^3 + 12N_T^2 N_R + \frac{17}{2}N_T^2 + (8L+10)N_T N_R + \frac{11}{6}N_T + 15L\end{aligned} \tag{D.18}$$

D.2 Linear conventional IB-DFE equaliser's complexity

The linear conventional IB-DFE, i.e its first iteration, is equivalent to the MMSE equaliser. Its output is given by

$$\widetilde{\mathbf{S}}_k = \Upsilon\left(\mathbf{F}_{(k,l)}\mathbf{Y}_{(k,l)}\right) \tag{D.19}$$

with

$$\mathbf{F}_{(k,l)} = \boldsymbol{\kappa}\left(\frac{1}{\gamma}\boldsymbol{I}_{N_T} + \sum_{l=0}^{L-1}\left(\mathbf{H}_{(k,l)}^{eq}\right)^{H}\mathbf{H}_{(k,l)}^{eq}\right)^{-1}\left(\mathbf{H}_{(k,l)}^{eq}\right)^{H} \tag{D.20}$$

As we can see, (D.1) and (D.19) are equivalents. However, this only occurs because we are considering the linear conventional IB-DFE. When using iterations, only the feedforward net is affected by the Υ function, with the feedback loop being performed without oversampling. In

that sense, we have the non-oversampled symbol $\widetilde{\mathbf{S}}_k$ at the output of the equaliser, instead of the removing the oversampling after the output of the equaliser as in the next equalisers.

In this case, $\boldsymbol{\kappa}$ is obtained as in ZF approach, needing the same number of FLOPs described by (D.12), and following a similar step by step approach as previously, the computational cost to obtain $\mathbf{F}_{(k,l)}$ using (D.20) is given by

$$\left(\mathbf{H}^{eq}_{(k,l)}\right)^H \mathbf{H}^{eq}_{(k,l)} \Rightarrow 4N_T^2N_R + 4N_TN_R - N_T^2 - N_T \tag{D.21}$$

$$\sum_{l=0}^{L-1}\left(\mathbf{H}^{eq}_{(k,l)}\right)^H \mathbf{H}^{eq}_{(k,l)} \Rightarrow L \times \underbrace{(\text{D.21})}_{\text{multiplications}} + (L-1)\underbrace{(2N_T^2)}_{\text{sums}} \tag{D.22}$$

Here, $1/\gamma$ is considered to be a constant that is saved to be used by multiple methods and its computational cost is ignored.

$$\frac{1}{\gamma}\boldsymbol{I}_{N_T} \Rightarrow N_T \tag{D.23}$$

$$\frac{1}{\gamma}\boldsymbol{I}_{N_T} + \sum_{l=0}^{L-1}\left(\mathbf{H}^{eq}_{(k,l)}\right)^H \mathbf{H}^{eq}_{(k,l)} \Rightarrow (\text{D.22}) + (\text{D.23}) + N_T \tag{D.24}$$

$$\left(\frac{1}{\gamma}\boldsymbol{I}_{N_T} + \sum_{l=0}^{L-1}\left(\mathbf{H}^{eq}_{(k,l)}\right)^H \mathbf{H}^{eq}_{(k,l)}\right)^{-1} \Rightarrow (\text{D.24}) + \frac{8}{3}N_T^3 + \frac{19}{2}N_T^2 - \frac{7}{6}N_T \tag{D.25}$$

$$\begin{aligned}\left(\frac{1}{\gamma}\boldsymbol{I}_{N_T} + \sum_{l=0}^{L-1}\left(\mathbf{H}^{eq}_{(k,l)}\right)^H \mathbf{H}^{eq}_{(k,l)}\right)^{-1}\left(\mathbf{H}^{eq}_{(k,l)}\right)^H &\Rightarrow (\text{D.25}) + 8N_T^2N_R - 2N_TN_R = \\ = \frac{8}{3}N_T^3 + (4L+8)N_T^2N_R + \left(\frac{15}{2}+L\right)N_T^2 + (4L-2)N_TN_R + \left(\frac{5}{6}-L\right)N_T &\end{aligned} \tag{D.26}$$

$$\begin{aligned}\mathbf{F}_{(k,l)} = \boldsymbol{\kappa}\left(\frac{1}{\gamma}\boldsymbol{I}_{N_T} + \sum_{l=0}^{L-1}\left(\mathbf{H}^{eq}_{(k,l)}\right)^H \mathbf{H}^{eq}_{(k,l)}\right)^{-1}\left(\mathbf{H}^{eq}_{(k,l)}\right)^H &\Rightarrow (\text{D.12}) + (\text{D.26}) + 6N_T = \\ = \frac{8}{3}N_T^3 + (4L+8)N_T^2N_R + \left(\frac{15}{2}+L\right)N_T^2 + (12L-2)N_TN_R + \left(\frac{41}{6}-L\right)N_T &\end{aligned} \tag{D.27}$$

Finally, the total number of FLOPs needed to obtain the estimated transmitted symbol $\widetilde{\mathbf{S}}_k$ is given by

$$\mathbf{F}_{(k,l)}\mathbf{Y}_{(k,l)} \Rightarrow (\text{D.27}) + 8N_TN_R - 2N_T \tag{D.28}$$

$$\widetilde{\mathbf{S}}_k = \Upsilon\left(\widetilde{\mathbf{S}}_{(k,l)}\right) \Rightarrow \text{(D.28)} + 2(L-1) + 2 + 11L + 2(L-1) + 2 =$$
$$= \frac{8}{3}N_T^3 + (4L+8)N_T^2 N_R + \left(\frac{15}{2}+L\right)N_T^2 + (12L+6)N_T N_R + \left(\frac{29}{6}-L\right)N_T + 15L \quad \text{(D.29)}$$

D.3 Linear pragmatic equaliser's complexity

Contrarily to the conventional IB-DFE, the output of the pragmatic equaliser contains oversampling, only being removed after equalisation. Therefore, for its linear version, the output and the non-oversampling symbols are given by (D.1) and (D.2), respectively. However, in this equaliser, pulse shaping is not equalised, assuming perfect matching. Therefore, the feddfoward coefficients are given by

$$\mathbf{F}_{(k,l)} = \mathbf{E}_{(k,l)} P^*_{(k,l)} \quad \text{(D.30)}$$

with

$$\mathbf{E}_{(k,l)} = \boldsymbol{\kappa}\left(\frac{1}{\gamma}\boldsymbol{I}_{N_T} + \mathbf{H}^H_{(k,l)}\mathbf{H}_{(k,l)}\right)^{-1}\mathbf{H}^H_{(k,l)}. \quad \text{(D.31)}$$

Once more, the calculus of $\boldsymbol{\kappa}$ is equal to the ZF case and the step by step analysis for the feedforward coefficients becomes

$$\mathbf{H}^H_{(k,l)}\mathbf{H}_{(k,l)} \Rightarrow \text{(D.21)} \quad \text{(D.32)}$$

$$\frac{1}{\gamma}\boldsymbol{I}_{N_T} \Rightarrow \text{(D.23)} \quad \text{(D.33)}$$

$$\frac{1}{\gamma}\boldsymbol{I}_{N_T} + \mathbf{H}^H_{(k,l)}\mathbf{H}_{(k,l)} \Rightarrow \text{(D.32)} + \text{(D.33)} + N_T \quad \text{(D.34)}$$

$$\left(\frac{1}{\gamma}\boldsymbol{I}_{N_T} + \mathbf{H}^H_{(k,l)}\mathbf{H}_{(k,l)}\right)^{-1} \Rightarrow \text{(D.34)} + \frac{8}{3}N_T^3 + \frac{19}{2}N_T^2 - \frac{7}{6}N_T \quad \text{(D.35)}$$

$$\left(\frac{1}{\gamma}\boldsymbol{I}_{N_T} + \mathbf{H}^H_{(k,l)}\mathbf{H}_{(k,l)}\right)^{-1}\mathbf{H}^H_{(k,l)} \Rightarrow \text{(D.35)} + 8N_T^2 N_R - 2N_T N_R =$$
$$= \frac{8}{3}N_T^3 + 12N_T^2 N_R + \frac{17}{2}N_T^2 + 2N_T N_R - \frac{1}{6}N_T \quad \text{(D.36)}$$

$$\mathbf{E}_{(k,l)} = \boldsymbol{\kappa}\left(\frac{1}{\gamma}\boldsymbol{I}_{N_T}+\mathbf{H}^H_{(k,l)}\mathbf{H}_{(k,l)}\right)^{-1}\mathbf{H}^H_{(k,l)} \Rightarrow (\text{D.12})+(\text{D.36})+6N_T \tag{D.37}$$

$$= \frac{8}{3}N_T^3+12N_T^2N_R+\frac{17}{2}N_T^2+(8L+2)N_TN_R+\frac{35}{6}N_T \tag{D.38}$$

$$\mathbf{F}_{(k,l)} = \mathbf{E}_{(k,l)}P^*_{(k,l)} \Rightarrow (\text{D.38})+2N_TN_R = \frac{8}{3}N_T^3+12N_T^2N_R+\frac{17}{2}N_T^2+(8L+4)N_TN_R+\frac{35}{6}N_T \tag{D.39}$$

With these results, it is possible to obtain the total number of FLOPs needed to obtain the estimated transmitted symbol $\widetilde{\mathbf{S}}_k$, which is given by

$$\widetilde{\widetilde{\mathbf{S}}}_{(k,l)} = \mathbf{F}_{(k,l)}\mathbf{Y}_{(k,l)} \Rightarrow (\text{D.39})+8N_TN_R-2N_T \tag{D.40}$$

$$\widetilde{\mathbf{S}}_k = \Upsilon\left(\widetilde{\widetilde{\mathbf{S}}}_{(k,l)}\right) \Rightarrow (\text{D.40})+15L =$$
$$= \frac{8}{3}N_T^3+12N_T^2N_R+\frac{17}{2}N_T^2+(8L+12)N_TN_R+\frac{23}{6}N_T+15L \tag{D.41}$$

D.4 Iterative MRC equaliser's complexity

The iterative MRC equaliser is based on the pragmatic. Thus, its output is also obtained with oversampling, that needs to be removed using (D.1), and it is given by

$$\widetilde{\widetilde{\mathbf{S}}}^{(i)}_{(k,l)} = \mathbf{F}_{(k,l)}\mathbf{Y}_{(k,l)}-\mathbf{B}_{(k,l)}\bar{\bar{\mathbf{S}}}^{(i-1)}_{(k,l)} \tag{D.42}$$

where

$$\mathbf{B}_{(k,l)} = \mathbf{F}_{(k,l)}\mathbf{H}_{(k,l)}-\boldsymbol{I}_{N_T} \tag{D.43}$$

and

$$\mathbf{F}_{(k,l)} = \mathbf{E}_{(k,l)}P^*_{(k,l)} \tag{D.44}$$

with

$$\mathbf{E}_{(k,l)} = \boldsymbol{\kappa}\mathbf{H}^H_{(k,l)}. \tag{D.45}$$

Note that this is an iterative method, with a feedback loop, but neither the feedforward nor the feedback coefficients depend on the iteration, remaining constant through iterations and decreasing

complexity.

For the MRC equaliser, the normalisation factor is also given by the diagonal matrix expressed in (D.4). However, its elements are given by

$$\kappa^{(t,t)} = \left(\frac{1}{LN_{block}} \sum_{l=0}^{L-1} \sum_{k=0}^{N_{block}-1} \sum_{r=1}^{N_R} \left| H_{(k,l)}^{(r,t)} \right|^2 \right)^{-1}. \tag{D.46}$$

Doing the previously step by step analysis, the calculus of the normalisation factor needs the following number of FLOPs:

$$\left| H_{(k,l)}^{(r,t)} \right|^2 \Rightarrow 3 \tag{D.47}$$

$$\sum_{r=1}^{N_R} \left| H_{(k,l)}^{(r,t)} \right|^2 \Rightarrow N_R \times (\text{D.47}) + N_R - 1 \tag{D.48}$$

$$\sum_{k=0}^{N_{block}-1} \sum_{r=1}^{N_R} \left| H_{(k,l)}^{(r,t)} \right|^2 \Rightarrow N_{block} \times (\text{D.48}) + N_{block} - 1 \tag{D.49}$$

$$\sum_{l=0}^{L-1} \sum_{k=0}^{N_{block}-1} \sum_{r=1}^{N_R} \left| H_{(k,l)}^{(r,t)} \right|^2 \Rightarrow L \times (\text{D.49}) + L - 1 \tag{D.50}$$

$$\frac{1}{LN_{block}} \sum_{l=0}^{L-1} \sum_{k=0}^{N_{block}-1} \sum_{r=1}^{N_R} \left| H_{(k,l)}^{(r,t)} \right|^2 \Rightarrow (\text{D.50}) + 1 \tag{D.51}$$

$$\kappa^{(t,t)} = \left(\frac{1}{LN_{block}} \sum_{l=0}^{L-1} \sum_{k=0}^{N_{block}-1} \sum_{r=1}^{N_R} \left| H_{(k,l)}^{(r,t)} \right|^2 \right)^{-1} \Rightarrow (\text{D.51}) + 1 = 4LN_{block}N_R + 1 \tag{D.52}$$

The number of FLOPs to obtain the entire diagonal normalisation matrix is given by

$$\boldsymbol{\kappa} \Rightarrow \frac{N_T}{N_{block}} \times (\text{D.52}) = 4LN_TN_R + 1\frac{N_T}{N_{block}} \approx 4LN_TN_R \tag{D.53}$$

The total number of FLOPs to obtain the feedforward coeficcients is given by

$$\mathbf{H}_{(k,l)}^H \Rightarrow 0 \tag{D.54}$$

$$\mathbf{E}_{(k,l)} = \boldsymbol{\kappa}\mathbf{H}_{(k,l)}^H \Rightarrow (\text{D.53}) + (\text{D.54}) + 6N_T = 4LN_TN_R + 6N_T \tag{D.55}$$

$$\mathbf{F}_{(k,l)} = \mathbf{E}_{(k,l)} P^{*}_{(k,l)} \Rightarrow (\text{D.55}) + 2N_T N_R = (4L+2)N_T N_R + 6N_T. \tag{D.56}$$

Note that we assumed that there is no cost to compute the Hermitian matrix.

With the calculus of $\mathbf{F}_{(k,l)}$ is possible to obtain the feedback coefficients. Ignoring the computational cost to obtain $\mathbf{F}_{(k,l)}$ because this operation only needs to be counted once, the number of FLOPs to obtain $\mathbf{B}_{(k,l)}$ are given by

$$\mathbf{F}_{(k,l)}\mathbf{H}_{(k,l)} \Rightarrow 8N_T^2 N_R - 2N_T^2 \tag{D.57}$$

$$\mathbf{B}_{(k,l)} = \mathbf{F}_{(k,l)}\mathbf{H}_{(k,l)} - \boldsymbol{I}_{N_T} \Rightarrow (\text{D.57}) + N_T = 8N_T^2 N_R - 2N_T^2 + N_T \tag{D.58}$$

At last, we need to determine the computational cost of obtaining the transmitted symbols $\widetilde{\mathbf{S}}_k^{(1)}$. This cost will depend on the number of iterations. For the first iteration, it is given by

$$\widetilde{\breve{\mathbf{S}}}_{(k,l)}^{(1)} = \mathbf{F}_{(k,l)}\mathbf{Y}_{(k,l)} \Rightarrow (\text{D.56}) + 8N_T N_R - 2N_T = (4L+10)N_T N_R + 4N_T \tag{D.59}$$

$$\begin{aligned}\widetilde{\mathbf{S}}_k^{(1)} = \Upsilon\left(\widetilde{\breve{\mathbf{S}}}_{(k,l)}^{(1)}\right) &\Rightarrow (\text{D.59}) + 2(L-1) + 2 + 11L + 2(L-1) + 2 = \\ &= (4L+10)N_T N_R + 4N_T + 15L.\end{aligned} \tag{D.60}$$

For the second iteration, the computational cost becomes

$$\mathbf{B}_{(k,l)}\bar{\breve{\mathbf{S}}}_{(k,l)}^{(1)} \Rightarrow (\text{D.58}) + 8N_T^2 - 2N_T = 8N_T^2 N_R + 6N_T^2 - N_T \tag{D.61}$$

$$\begin{aligned}\widetilde{\breve{\mathbf{S}}}_{(k,l)}^{(2)} &= \mathbf{F}_{(k,l)}\mathbf{Y}_{(k,l)} - \mathbf{B}_{(k,l)}\bar{\breve{\mathbf{S}}}_{(k,l)}^{(1)} \Rightarrow (\text{D.59}) + (\text{D.61}) + 2N_T \\ &= 8N_T^2 N_R + 6N_T^2 + (4L+10)N_T N_R + 5N_T\end{aligned} \tag{D.62}$$

$$\widetilde{\mathbf{S}}_k^{(2)} = \Upsilon\left(\widetilde{\breve{\mathbf{S}}}_{(k,l)}^{(2)}\right) \Rightarrow (\text{D.62}) + 15L. \tag{D.63}$$

At last, for the remaining iterations, the total cost is given by

$$\mathbf{B}_{(k,l)}\tilde{\tilde{\mathbf{S}}}_{(k,l)}^{(i-1)} \Rightarrow 8N_T^2 - 2N_T \tag{D.64}$$

$$\begin{aligned}\widetilde{\tilde{\mathbf{S}}}_{(k,l)}^{(i)} &= \mathbf{F}_{(k,l)}\mathbf{Y}_{(k,l)} - \mathbf{B}_{(k,l)}\tilde{\tilde{\mathbf{S}}}_{(k,l)}^{(i-1)} \Rightarrow \text{(D.62)} + (i-2)\times\text{(D.64)} + (i-2)\times 2N_T = \\ &= 8N_T^2N_R + (8i-10)N_T^2 + (4L+10)N_TN_R + 5N_T\end{aligned} \tag{D.65}$$

$$\widetilde{\mathbf{S}}_k^{(i)} = \Upsilon\left(\widetilde{\tilde{\mathbf{S}}}_{(k,l)}^{(i)}\right) \Rightarrow \text{(D.65)} + 15L. \tag{D.66}$$

Note that when $i > 2$ the feedback coefficients $\mathbf{B}_{(k,l)}$ are already determined, and only their multiplication by the estimations and the subtraction of their result to the feedforward loop need to be done again, saving lots of operations.

D.5 Iterative EGC equaliser's complexity

The iterative EGC equaliser is very similar to the MRC, resulting in an analysis close to the previous one. The main difference is that $\mathbf{E}_{(k,l)}$ is given by

$$\mathbf{E}_{(k,l)} = \boldsymbol{\kappa}\mathbf{A}_{(k,l)}^H, \tag{D.67}$$

with the elements of $\mathbf{A}_k$ given by

$$A_{(k,l)}^{(r,t)} = \frac{H_{(k,l)}^{(r,t)}}{|H_{(k,l)}^{(r,t)}|}, \tag{D.68}$$

resulting in different normalisation factors.

Therefore, the computation cost to obtain $\boldsymbol{\kappa}$ when using EGC equalisers is given by

$$\kappa^{(t,t)} = \left(\frac{1}{LN_{block}}\sum_{l=0}^{L-1}\sum_{k=0}^{N_{block}-1}\sum_{r=1}^{N_R}\left|H_{(k,l)}^{(r,t)}\right|\right)^{-1}. \tag{D.69}$$

$$\left|H_{(k,l)}^{(r,t)}\right| \Rightarrow 4 \tag{D.70}$$

$$\sum_{r=1}^{N_R} \left| H_{(k,l)}^{(r,t)} \right| \Rightarrow N_R \times (\text{D.70}) + N_R - 1 \tag{D.71}$$

$$\sum_{k=0}^{N_{block}-1} \sum_{r=1}^{N_R} \left| H_{(k,l)}^{(r,t)} \right| \Rightarrow N_{block} \times (\text{D.71}) + N_{block} - 1 \tag{D.72}$$

$$\sum_{l=0}^{L-1} \sum_{k=0}^{N_{block}-1} \sum_{r=1}^{N_R} \left| H_{(k,l)}^{(r,t)} \right| \Rightarrow L \times (\text{D.72}) + L - 1 \tag{D.73}$$

$$\frac{1}{LN_{block}} \sum_{l=0}^{L-1} \sum_{k=0}^{N_{block}-1} \sum_{r=1}^{N_R} \left| H_{(k,l)}^{(r,t)} \right| \Rightarrow (\text{D.73}) + 1 \tag{D.74}$$

$$\kappa^{(t,t)} = \left(\frac{1}{LN_{block}} \sum_{l=0}^{L-1} \sum_{k=0}^{N_{block}-1} \sum_{r=1}^{N_R} \left| H_{(k,l)}^{(r,t)} \right| \right)^{-1} \Rightarrow (\text{D.74}) + 1 = 5LN_{block}N_R + 1 \tag{D.75}$$

$$\boldsymbol{\kappa} \Rightarrow \frac{N_T}{N_{block}} \times (\text{D.75}) = 5LN_TN_R + 1\frac{N_T}{N_{block}} \approx 5LN_TN_R \tag{D.76}$$

Contrarily, to the MRC case, $\mathbf{E}_{(k,l)}$ has some computational cost, and the number of FLOPs to obtain the feedforward coefficients becomes

$$|H_{(k,l)}^{(r,t)}| \Rightarrow 4 \tag{D.77}$$

$$\frac{H_{(k,l)}^{(r,t)}}{|H_{(k,l)}^{(r,t)}|} \Rightarrow (\text{D.77}) + 2 = 6 \tag{D.78}$$

$$\mathbf{A}_{(k,l)}^{H} \Rightarrow (\text{D.78}) \times N_TN_R = 6N_TN_R \tag{D.79}$$

$$\mathbf{E}_{(k,l)} = \boldsymbol{\kappa}\mathbf{A}_{(k,l)}^{H} \Rightarrow (\text{D.76}) + (\text{D.79}) + 6N_T = (5L+6)N_TN_R + 6N_T \tag{D.80}$$

$$\mathbf{F}_{(k,l)} = \mathbf{E}_{(k,l)}P_{(k,l)}^{*} \Rightarrow (\text{D.80}) + 2N_TN_R = (5L+8)N_TN_R + 6N_T \tag{D.81}$$

Here, the cost to obtain the feedback coefficients is also given by (D.58) and the computational

cost to obtain the transmitted symbols $\widetilde{\mathbf{S}}_k^{(1)}$ in the first iteration is given by

$$\widetilde{\breve{\mathbf{S}}}_{(k,l)}^{(1)} = \mathbf{F}_{(k,l)}\mathbf{Y}_{(k,l)} \Rightarrow (\text{D.81}) + 8N_TN_R - 2N_T = (5L+16)N_TN_R + 4N_T \tag{D.82}$$

$$\begin{aligned}\widetilde{\mathbf{S}}_k^{(1)} = \Upsilon\left(\widetilde{\breve{\mathbf{S}}}_{(k,l)}^{(1)}\right) \Rightarrow (\text{D.82}) + 2(L-1) + 2 + 11L + 2(L-1) + 2 = \\ = (5L+16)N_TN_R + 4N_T + 15L\end{aligned} \tag{D.83}$$

For the second iteration, the computational cost becomes

$$\mathbf{B}_{(k,l)}\bar{\breve{\mathbf{S}}}_{(k,l)}^{(1)} \Rightarrow (\text{D.58}) + 8N_T^2 - 2N_T = 8N_T^2N_R + 6N_T^2 - N_T \tag{D.84}$$

$$\begin{aligned}\widetilde{\breve{\mathbf{S}}}_{(k,l)}^{(2)} &= \mathbf{F}_{(k,l)}\mathbf{Y}_{(k,l)} - \mathbf{B}_{(k,l)}\bar{\breve{\mathbf{S}}}_{(k,l)}^{(1)} \Rightarrow (\text{D.82}) + (\text{D.84}) + 2N_T \\ &= 8N_T^2N_R + 6N_T^2 + (5L+16)N_TN_R + 5N_T\end{aligned} \tag{D.85}$$

$$\widetilde{\mathbf{S}}_k^{(2)} = \Upsilon\left(\widetilde{\breve{\mathbf{S}}}_{(k,l)}^{(2)}\right) \Rightarrow (\text{D.62}) + 15L \tag{D.86}$$

At last, for the remaining iterations, the total cost is given by

$$\mathbf{B}_{(k,l)}\bar{\breve{\mathbf{S}}}_{(k,l)}^{(i-1)} \Rightarrow 8N_T^2 - 2N_T \tag{D.87}$$

$$\begin{aligned}\widetilde{\breve{\mathbf{S}}}_{(k,l)}^{(i)} = \mathbf{F}_{(k,l)}\mathbf{Y}_{(k,l)} - \mathbf{B}_{(k,l)}\bar{\breve{\mathbf{S}}}_{(k,l)}^{(i-1)} \Rightarrow (\text{D.85}) + (i-2)\times(\text{D.87}) + (i-2)\times 2N_T = \\ = 8N_T^2N_R + (8i-10)N_T^2 + (5L+16)N_TN_R + 5N_T\end{aligned} \tag{D.88}$$

$$\widetilde{\mathbf{S}}_k^{(i)} = \Upsilon\left(\widetilde{\breve{\mathbf{S}}}_{(k,l)}^{(i)}\right) \Rightarrow (\text{D.88}) + 15L \tag{D.89}$$